δ^{13}C of mid-Pacific carbonate sediments around the time of Ocean Anoxic Event 2

by

Kalila Morsink
B.A., Columbia University, 2019

A Thesis Submitted in Partial Fulfillment of the
Requirements for the Degree of

MASTER OF SCIENCE

in the School of Earth and Ocean Sciences

We acknowledge and respect the Lək´ʷəŋən (Songhees and Esquimalt) Peoples on whose territory the university stands, and the Lək´ʷəŋən and W̱SÁNEĆ Peoples whose historical relationships with the land continue to this day.

δ^{13}C of mid-Pacific carbonate sediments around the time of Ocean Anoxic Event 2

by

Kalila Morsink
B.A., Columbia University, 2019

Supervisory Committee

Dr. L.A. Coogan, Supervisor
(School of Earth and Ocean Sciences, University of Victoria)

Dr. B. Dyer, Supervisor
(School of Earth and Ocean Sciences, University of Victoria)

Dr. A.S. Ahm, Departmental Member
(School of Earth and Ocean Sciences, University of Victoria)

ABSTRACT

The $\delta^{13}C$ of marine carbonates is commonly used as a proxy for the global burial fraction of carbonate vs. organic carbon. At the same time, carbonate $\delta^{13}C$ is understood to vary locally from the global ocean average due to coeval spatial variation in seawater geochemistry, especially in shallow marine settings, and/or post-depositional alteration of sediments. In Cretaceous-age shallow marine sections, Ocean Anoxic Event 2 (OAE2) is identified by a positive $\delta^{13}C$ excursion near the Cenomanian-Turonian boundary (∼93.9 Ma). However, there are currently no OAE2 $\delta^{13}C$ records from the Pacific basin, which at the time was ∼65% of ocean area and included most of the world's deep ocean. Here I present new (n = 255) and previously published (n = 13) bulk carbonate $\delta^{13}C$ and $\delta^{18}O$ data from 10 mid-Pacific sites, measured in sediments recovered by the Deep Sea Drilling Program, which I use to test the hypothesis that there was a global change in the $\delta^{13}C_{DIC}$ of seawater at the time of OAE2. I use existing biostratigraphic data to target sediments of Cenomanian and Turonian age. Between sites, I compare $\delta^{13}C_{carbonate}$ and $\delta^{18}O_{carbonate}$ values associated with the same planktonic foraminifera species. My Pacific $\delta^{13}C_{carbonate}$ values range from 0.88‰ to 4.20‰ VPDB (excluding 3 samples within a 7-cm interval with -2.7‰ to -2.5‰ VPDB). They are generally lower than shallow marine bulk carbonate $\delta^{13}C$ values where the OAE2 positive $\delta^{13}C$ excursion has been identified, e.g., the well-known Eastbourne, UK section where Cenomanian and Turonian $\delta^{13}C$ values range from 2.6 to 5.4‰ VPDB. To explain $\delta^{13}C_{carbonate}$ values within the Pacific, I invoke both factors local to the sites, such as proximity to a shallow semi-restricted carbonate platform in the case of the site with the shallowest paleodepth, and changes in global ocean $\delta^{13}C_{DIC}$ over time. An OAE2 positive $\delta^{13}C_{carbonate}$ excursion is not observed at most Pacific sites in this thesis, which has two possible explanations. One possible explanation is that a global ocean OAE2 $\delta^{13}C$ excursion did occur, but that some process largely prevented its deposition, preservation, or recovery in the mid-Pacific. Another possible explanation is that the OAE2 $\delta^{13}C$ excursion occurred only in the shallow epicontinental basins and continental slope environments where it is observed (including the Atlantic, Western Tethys, Neotethys, and Western Interior Seaway of North America) because organic carbon burial within these relatively restricted water masses changed their $\delta^{13}C_{DIC}$s but did not affect $\delta^{13}C_{DIC}$ in the mid-Pacific.

Contents

List of Tables

List of Figures

ACKNOWLEDGEMENTS

Thanks to my advisors **Blake Dyer** and **Laurence Coogan**, from whom I have learned a lot.

Thanks to **Stacey Edmonsond**, who taught me how to run a mass spectrometer and answered many basic questions about carbonates, and also added five of my samples to one of her mass spectrometer runs. Thanks also to **Jon Husson** for his help operating the mass spectrometer and understanding its output, and for sharing his insight into carbonate sediments across geologic time.

Thanks to **Hannah Robutka**, for traveling to the Gulf Coast Repository with me and spending long hours sampling cores, not to mention providing applesauce and sympathy after I got food poisoning on the flight. Thanks to the **Geological Society of America** for providing the Graduate Student Research Grant that funded the trip.

Thanks to **Katie Jamson**, for providing me lots of downloaded Neptune Sandbox Berlin data which I would not otherwise have been able to access, and for multiple meetings explaining biostratigraphy to me. Thanks also to **Andy Fraass** for consulting on biostratigraphic age models.

Thanks to the **organizers of the 2022 TIDE Seminar on Racism, Colonialism, and Extraction in the Geosciences** at MIT, and to University of Victoria Indigenous Resurgence Coordinator **Lydia Toorenburgh**, for teaching me how to question the way research is conducted in my field.

Thanks to **members of the UVic Earth History group past and present** including **Connor van Wieren**, **Matthew Stephens**, **Olivia Wren**, and **Jerry Lei**. Thanks to **members of the Fall 2022 EOS 525 cohort**, including **Xi Wang** for putting the University of Victoria's official territory acknowledgement into LaTeX. Thanks to **Katie Withrow** and **Xin Qiao** for many kindnesses.

Thanks to **Marisa Borreggine**, **Linda Pan**, **Schmitty Thompson**, **Natasha Valencic**, and **Ariana Castillo**, who helped me learn how to make it through graduate

school. Thanks to **Kara Hartig** and **Roger Creel** for being role models as scientists and friends. Thanks to **Natalie Tawil** and **Willow Hayes** for feeding me while I wrote. Thanks to **Chaim Spaulding** and **Akari Goda-Maurezzutt** for being on the phone, and thanks to **Pia Deshpande**, **Dorothy Manevich**, and **Wesley Brown** for being in the group chat.

This research used samples and data provided by the **International Ocean Discovery Program (IODP)**. I acknowledge the support of the **Natural Sciences and Engineering Research Council of Canada (NSERC)**.

Stone has been formed from flowing water...by the deposition from it, in its course, of something which adheres to the surface of its bed and (then) petrifies...in the course of ages the limits of which history has not preserved.
Ibn Sinā (c. 980-1037) in the Kitāb al-shifā', tr. Al-Rawi (2002)

Introduction

The long-term carbon cycle of the Earth, i.e. the system of transfers of carbon in and out of the solid Earth (Section 1.1) that sets atmospheric CO_2, is important to climate. Because adding CO_2 to the atmosphere increases the surface temperature of the Earth (Foote, 1856) via the greenhouse effect (Broecker, 1975), release of carbon from the solid Earth warms global climate. For example, ongoing anthropogenic perturbation of the carbon cycle via burning of fossil fuels has long been known to cause global warming (Arrhenius, 1896). Research into variations in the carbon cycle over geologic time may yield information relevant to this ongoing anthropogenic perturbation (e.g. Keller et al., 2018; Hollis et al., 2019; McClymont et al., 2020). One past variation in the carbon cycle, Ocean Anoxic Event 2, is studied here. In this thesis I test the hypothesis that there was a global increase in organic carbon burial at the time of this event.

1.1 Earth's carbon cycle

In the long-term carbon cycle (on time scales of millions of years), carbon is transferred between the solid Earth and the surficial reservoir, consisting of the ocean, atmosphere, and biosphere (e.g. Berner, 2004). The ocean holds most of the carbon in the surficial reservoir. The transfer of carbon between the solid Earth and surficial reservoir and its partitioning within the surficial reservoir impact climate because carbon in the atmosphere as carbon dioxide (CO_2) warms the surface of the Earth via the greenhouse effect. Carbon is mixed between the ocean, atmosphere, and biosphere on short time scales relative to transfer with the solid Earth, so I consider the surficial reservoir as one reservoir when discussing the long-term carbon cycle. Understanding the long-term carbon cycle, specifically the amount of carbon in the ocean and atmosphere, can help us understand why Earth has remained in a habitable temperature range through much of its geologic past (Berner and Caldeira, 1997; Kump et al., 2000).

In the long term, the amount of carbon in the surficial reservoir is set by a balance of inputs and outputs (Figure 1.1A). Carbon enters the surficial reservoir via volcanoes, and exits the ocean and atmosphere via incorporation into sediments and authigenic carbonate minerals in the upper ocean crust. Specifically, in sediments, carbon may enter carbonate minerals or organic matter. The weathering of silicate minerals is required to remove carbon from the ocean-atmosphere reservoir into carbonate sediments. A reaction from the work of Urey (1952) shows that the reactants CO_2 and calcium (or magnesium) silicate are consumed to produce calcium (or magnesium) carbonate minerals and silica:

$$CaSiO_3 + 2\,CO_2 + H_2O \longrightarrow CaCO_3 + SiO_2 + CO_2 + H_2O \tag{1.1}$$

On long time scales, the weathering of carbonate minerals is thought to be largely balanced by the precipitation of carbonate minerals in the oceans and therefore thought not to change the amount of CO_2 in the surficial reservoir. Carbon enters organic matter via photosynthesis and enters sediments when the organic matter becomes lithified after the death of the organism. Before burial, carbon in sediments may return to the ocean and atmosphere. For example, carbonate minerals may be weathered or dissolved, or organic matter in sediments may be weathered or decomposed. (The latter process is sometimes called "remineralization.")

Carbonate minerals are more soluble under conditions of greater pressure and lower temperature, and as a consequence dissolve at the "carbonate compensation depth" (CCD) and below (Broecker, 2003). In the modern ocean, carbonate sediments accumulate on shallow areas of the ocean floor such as mid-ocean ridges and continental shelves, but do not accumulate in the deep ocean (Taft, 1967; Broecker, 2003). Most of the carbonate sediments studied here were initially deposited in the open ocean above the CCD (Section 3.2). I next introduce the framework under which the isotopic composition of carbonate sediments is interpreted.

1.2 The $\delta^{13}C$ of carbonate sediments

The carbon isotopic composition of marine carbonate sediments has been used as a proxy for the global burial fraction of carbonate vs. organic matter sediments at the time of deposition of those carbonate sediments (e.g. Kump and Arthur, 1999). For this proxy, it is conventional to describe carbon isotope composition using the

carbon isotope ratio $\delta^{13}C$, which is a measure of the relative amounts of the two stable isotopes of carbon (^{13}C and ^{12}C) in a material. The quantity δ is calculated relative to a standard reference material:

$$\delta = \left(\frac{R_{sample}}{R_{standard}} - 1 \right) \times 1000‰ \tag{1.2}$$

where R is the ratio of the heavier isotope to the lighter isotope (e.g. $^{13}C/^{12}C$) in either the sample or the standard. The quantity δ is reported in permil (‰). The Vienna PeeDee Belemnite (VPDB) is the primary standard reference for stable carbon and oxygen isotope measurements in carbonates (Brand et al., 2014; Hoffman and Rasmussen, 2022). All $\delta^{13}C$ and $\delta^{18}O$ values in this thesis are reported relative to this standard (‰ VPDB).

To relate the $\delta^{13}C$ of carbonate sediments to the long-term carbon cycle, it is assumed that the influx and outflux of carbon from the ocean-atmosphere reservoir are balanced in the long term (over millions of years). In other words, all of the carbon that enters the ocean and atmosphere is eventually buried as carbonate sediment or organic sediment. Similarly, the isotopic composition of the carbon that enters the ocean and atmosphere must be equal to the combined isotopic composition of carbonate and organic sediment. This mass balance can be expressed as an equation:

$$\delta^{13}C_{\text{total}} = \delta^{13}C_{\text{carbonate}} f_{\text{carbonate}} + \delta^{13}C_{\text{organic}} f_{\text{organic}} \tag{1.3}$$

where the term $\delta^{13}C_{\text{total}}$ is the $\delta^{13}C$ of the total influx from the surficial reservoir (carbonate and organic matter sediments combined); the term $\delta^{13}C_{\text{carbonate}}$ is the $\delta^{13}C$ of carbonate sediments; the term $\delta^{13}C_{\text{organic}}$ is the $\delta^{13}C$ of organic matter; and $f_{\text{carbonate}}$ and f_{organic} are the fractions of the total outflux in carbonate and organic matter sediments respectively. Importantly, these two fractions are assumed in this simple model to equal 1:

$$f_{\text{carbonate}} + f_{\text{organic}} = 1 \tag{1.4}$$

Also, the lighter isotope of carbon (^{12}C) is preferentially incorporated into organic matter during photosynthesis, offsetting the $\delta^{13}C$ of the organic matter to a lower value:

$$\delta^{13}C_{\text{organic}} = \delta^{13}C_{\text{carbonate}} - \varepsilon \tag{1.5}$$

where ε is the difference between $\delta^{13}C_{carbonate}$ and $\delta^{13}C_{organic}$. In the simple carbon cycle described by Equations 1.3 - 1.5, the $\delta^{13}C$ of carbonate is controlled by the relative outfluxes of carbon from the surficial reservoir in carbonate vs. organic sediments ($f_{carbonate}$ vs. $f_{organic}$), the average carbon isotopic fractionation of organic matter (ε), and the isotopic composition of carbon entering the surficial reservoir ($\delta^{13}C_{total}$). Generally, it is assumed that ε and $\delta^{13}C_{total}$ play a smaller role than $f_{carbonate}$ vs. $f_{organic}$. If this model broadly described nature, a time of globally increased organic carbon burial would lead to higher $\delta^{13}C$ values in carbonate sediments and in organic matter deposited during that time (Figure 1.1B). If ε is -28‰, a change of 0.1 in the global burial fraction of organic carbon is required to produce an increase of 2.8‰ in the $\delta^{13}C$ of carbonate sediments.

Models like the one just described have been used to interpret marine $\delta^{13}C_{carbonate}$ values of both deep open-ocean (e.g. Scholle and Arthur, 1980; Berger and Vincent, 1986) and shallow (e.g. Ferreri et al., 1997) carbonate sediments. Some such interpretations assume that the $\delta^{13}C$ of newly forming carbonate sediments (and the $\delta^{13}C$ of newly forming organic matter) is the same everywhere in the ocean, i.e. that the global ocean is well-mixed and precipitates carbonate sediments with $\delta^{13}C$ equal to the $\delta^{13}C$ of dissolved inorganic carbon (DIC) in the water. Interpretation of $\delta^{13}C_{carbonate}$ values in this thesis will involve dismantling this assumption. Therefore I introduce a number of considerations that complicate this assumption:

1. $\delta^{13}C_{DIC}$ varies with depth in the ocean.

2. The carbonate minerals calcite and aragonite have different carbon isotope fractionation between the mineral and seawater.

3. Carbon isotope fractionation occurs during biogenic precipitation of carbonate ("vital effects").

4. It is possible that carbonate sediments formed from a restricted water mass.

5. Carbonate sediments may be altered by diagenesis.

In the following sections I explain each of these considerations, including their implications for the interpretation of bulk $\delta^{13}C_{carbonate}$ values.

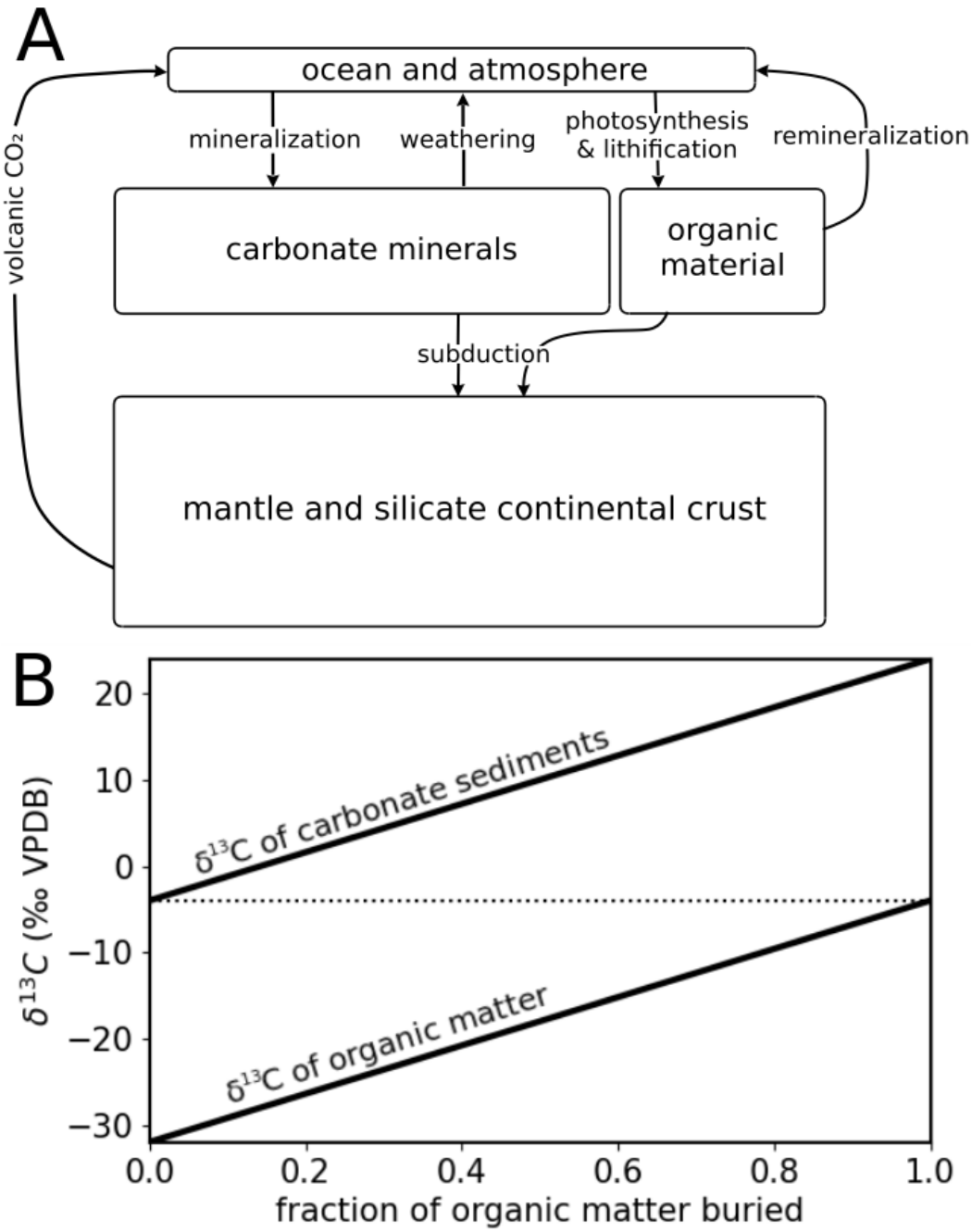

Figure 1.1: (A) A simple box model of Earth's long-term carbon cycle, modified from Figure 7.1 in Sharp (2017). The carbonate minerals and organic material reservoirs pictured are both sedimentary reservoirs. (B) δ^{13}C of carbonate sediments and organic matter plotted against the fraction of organic matter that is buried, assuming that the δ^{13}C of outflux from the surficial reservoir is -4‰ (shown by the dotted line) and there is a constant offset ε of -28‰ between carbonate carbon and organic matter carbon.

1.2.1 Variation of $\delta^{13}C_{DIC}$ with depth in the ocean

The $\delta^{13}C_{DIC}$ varies with depth in the open ocean due to the "biologic pump". In the modern mid-Pacific $\delta^{13}C_{DIC}$ has its maximum of about 1.5‰ at the surface and decreases with depth to its minimum of about 0‰ between 1000 and 2000 mbsl (Schmittner et al., 2013). Typically, $\delta^{13}C_{DIC}$ is highest in the surface ocean because photosynthesizers living there preferentially take up ^{12}C into organic matter they produce, leaving relatively more ^{13}C in the water. Respirators remineralize organic matter everywhere in the ocean, returning ^{12}C into the water, and circulation of deepwater derived directly from the surface ocean slightly increases $\delta^{13}C_{DIC}$ values at depth, such that the $\delta^{13}C_{DIC}$ minimum is at mid-depth. Therefore the $\delta^{13}C$ value of carbonate sediment depends partially on where it formed in the water column. Much carbonate sediment is biogenic, produced as the tests either of organisms dwelling in the photic zone or of organisms dwelling upon or within seafloor sediments (Lowenstam and Epstein, 1954; Schlager, 2003). Carbonate can also be inorganically precipitated, including from pore water within seafloor sediments. Overall, in the open ocean, carbonate minerals are produced throughout the entire water column and in seafloor sediments, with the highest production rates at the top of the water column. Open-ocean ("pelagic") bulk carbonate is likely to include components from surface water (where $\delta^{13}C_{DIC}$ is highest), from bottom water (where $\delta^{13}C_{DIC}$ is lower), and from carbonate formed within seafloor sediments (where $\delta^{13}C_{DIC}$ is heterogeneous; McCorkle and Emerson, 1988), and the proportions of these components may vary in different locations and/or through time.

1.2.2 Carbon isotope fractionation of calcite vs. aragonite with respect to seawater

The most common carbonate minerals are calcite and aragonite, and at equilibrium these minerals have different $\delta^{13}C$ values. When inorganic calcite is precipitated in laboratory experiments, its $\delta^{13}C$ is higher than that of dissolved bicarbonate (HCO_3^-, the dominant species of carbon in seawater) by about 1‰, whereas the $\delta^{13}C$ of aragonite is higher by about 2.7‰ (Rubinson and Clayton, 1969; Romanek et al., 1992). The carbon isotope fractionation of these minerals relative to HCO_3^- does not appear to depend on precipitation rate or on temperature in the range 10-40°C (Romanek et al., 1992). Differing proportions of calcite and aragonite are a possible source of variation (up to 1.7‰) in the $\delta^{13}C$ of bulk carbonate samples.

Both calcite and aragonite are produced by many groups of marine organisms (including foraminifera, bivalves, serpulid worms, molluscs, algae, gastropods, pteropods, corals, etc.; Lowenstam and Epstein, 1954; Romanek et al., 1992; Conci et al., 2021). In the modern open ocean, biogenically produced calcite dominates carbonate sediments, while in shallow areas such as continental shelves, carbonate sediments are largely composed of aragonite and metastable high-Mg calcite (Milliman and Droxler, 1996; Iglesias-Rodriguez et al., 2002). In the past the ocean has undergone periods in which the deposition of aragonite was inhibited, and one such time period (a "calcite sea") occurred between about 175 and about 35 Ma (Stanley and Hardie, 1998). The carbonate sediments studied here were deposited during this time.

As most carbonate sediment in this thesis was likely initially deposited in the open ocean in a calcite sea, it was likely dominantly composed of calcite. Some carbonate sediments studied here may have been initially deposited in shallow environments (Sections 3.2 and 3.3). As these sediments were deposited in a calcite sea, they may also have been dominated by calcite but could have included aragonite.

1.2.3 Variation in carbon isotope fractionation during biogenic precipitation of carbonate ("vital effects")

Bulk carbonate sediments like those in this thesis generally include biogenic components from calcifying organisms. Many such organisms precipitate carbonate out of carbon isotope equilibrium with the water in which they form (Weiner and Dove, 2003). This "vital effect" (Urey et al., 1951), meaning here the extent to which the $\delta^{13}C$ value of biogenic carbonate material is out of equilibrium with the $\delta^{13}C_{DIC}$ of the water in which it forms, varies between species and may even vary by specimen (Weiner and Dove, 2003; Hoogakker et al., 2024). Generally, vital effects in coccolithophores and foraminifera, the major biogenic components of open-ocean carbonate sediments, may increase, decrease, or not change the $\delta^{13}C$ value of the biogenic carbonate test (Anderson and Arthur, 1983; Sharp, 2017). In some foraminifera, especially planktonic foraminifera, vital effects may differ depending on the growth stage of the organism (Friedrich et al., 2006; Hoogakker et al., 2024). As for benthic foraminifera, although some species of benthic foraminifera are noted for having negligible vital effects on $\delta^{13}C_{carbonate}$, it is important to note that benthic foraminifera often have non-negligible vital effects (Schmittner et al., 2017; Dubicka et al., 2018; Hoogakker et al., 2024). In individual benthic foraminifera recovered alive from the modern con-

tinental margin of the Pacific Ocean, vital effects are found to lower $\delta^{13}C_{carbonate}$ by 0-4‰ for a majority of specimens and up to 10‰ for some specimens, relative to the $\delta^{13}C_{DIC}$ of the water in which the tests form (Ishimura et al., 2012; Hoogakker et al., 2024).

One category of vital effects is called "microhabitat" effects. Organisms' $\delta^{13}C_{carbonate}$ values may record $\delta^{13}C_{DIC}$ differences between their habitats across short (centimeter-scale) vertical distances (Corliss, 1985; Hoogakker et al., 2024). Microhabitat effects are noted particularly for benthic foraminifera living just above the sediment-water interface vs. living within the sediment, as the pore water within the sediments may have lower $\delta^{13}C_{DIC}$ than bottom water due to oxidation of organic carbon (Friedrich et al., 2006; Hoogakker et al., 2024). The benthic foraminifera species with $\delta^{13}C_{carbonate}$ values reported in this thesis dwell in a range of sediment depths from the sediment-water interface to centimeters below it (Appendix A.27). The magnitude of benthic foraminiferal microhabitat effects is typically 0-2‰ (Rathburn et al., 1996; Mackensen and Licari, 2003).

As vital effects are imperfectly understood and are not known for all taxa, it is difficult to control for their effect on $\delta^{13}C_{carbonate}$ values, especially $\delta^{13}C$ values of bulk carbonate sediments like the majority of sediments examined in this thesis. At the same time, vital effects may be negligible, or if vital effects are similar for all carbonate sediments at one site, they may not be an important factor in explaining $\delta^{13}C_{carbonate}$ variation.

1.2.4 Possibility that carbonate sediments formed from a restricted water mass

A water mass that mixes more slowly with other water masses will be more affected by local processes than a water mass that mixes more quickly with other water masses. Local $\delta^{13}C_{DIC}$ may differ from the global average in restricted basins that are not well mixed with the rest of the ocean, particularly epicontinental seas (e.g. Immenhauser et al., 2008). A distinct balance of carbon fluxes for such a basin, including a low-$\delta^{13}C$ flux derived from the oxidation of terrestrial plant organic matter (e.g. Panchuk et al., 2005) or a high-$\delta^{13}C$ flux from high productivity in shallow areas of the basin (e.g. Fanton and Holmden, 2007), may contribute to a distinct $\delta^{13}C_{DIC}$ of the basin. Carbonate sediments from past restricted basins may have $\delta^{13}C_{carbonate}$ variations that only occur there, not in carbonate sediments deposited in the global ocean at

the same time (e.g. Simo et al., 2003).

1.2.5 Diagenetic alteration of carbonate sediments

Post-depositional processes ("diagenesis") may change the $\delta^{13}C$ of carbonate sediments (Brand and Veizer, 1981; Banner and Hanson, 1990; Higgins et al., 2018; Ahm et al., 2018). Carbonate minerals in sediments react with diagenetic fluids derived from seawater, which themselves change chemically over time due to ongoing physical mixing with seawater and reactions with sediments. Diagenesis occurs in the shallow subsurface soon after initial deposition ("early marine diagenesis;" Bathurst, 1983; Mullins et al., 1985; Higgins et al., 2018; Ahm et al., 2018), as well as deep below the seafloor where new seawater is unlikely to reach sediments ("burial diagenesis;" Scholle and Halley, 1985; Swart, 2015). If marine carbonates move out of the ocean, they may react with diagenetic fluids derived from freshwater ("meteoric diagenesis"). Meteoric diagenesis can occur along continental margins while the sediments are still below sea level, at or near where they were deposited.

During diagenesis of carbonate sediments, metastable carbonate minerals such as aragonite and high-Mg calcite convert to more stable replacive carbonate minerals such as low-Mg calcite and dolomite. Cements also precipitate in pore spaces within sediments. Generally, the amount of diagenetic carbonate minerals in sediments increases with time and reduces pore space (Bathurst, 1972). If replacive carbonate minerals or cements precipitate from diagenetic fluid that has a different $\delta^{13}C$ than the $\delta^{13}C$ of the initial carbonate minerals, the $\delta^{13}C$ of the bulk carbonate sediment changes. When the flow rate of the diagenetic fluid is higher and/or the diagenetic fluid $\delta^{13}C$ is farther from the $\delta^{13}C$ of the initial carbonate minerals, the $\delta^{13}C$ of the bulk carbonate sediment changes more (Brand and Veizer, 1981; Banner and Hanson, 1990; Higgins et al., 2018; Ahm et al., 2018).

Diagenesis is generally expected to lower $\delta^{13}C_{carbonate}$ because many sources of carbon in diagenetic fluid have $\delta^{13}C$ lower than seawater, notably decomposing organic matter (e.g. Malone et al., 2001). Meteoric fluids such as rainwater and groundwater generally have low $\delta^{13}C$ (e.g. Allan and Matthews, 1990) because they have interacted with organic carbon. An exception would be diagenetic fluid with high $\delta^{13}C_{DIC}$ as a result of methane production preferentially taking up ^{12}C and leaving the fluid with high $\delta^{13}C_{DIC}$ values (Gautier and Claypool, 1984; Heuer et al., 2009; Meister and Reyes, 2019). It is also possible for diagenesis to have negligible effect on $\delta^{13}C_{carbonate}$

values, e.g. in the absence of extensive organic matter oxidation during marine diagenesis, or if carbonate sediments do not have prolonged contact with freshwater during meteoric diagenesis, or most simply if the fluid is unmodified seawater.

1.3 The δ^{18}O of carbonate sediments

There is a temperature-dependent equilibrium oxygen isotope fractionation between water and carbonate minerals. Although most calcite formed on Earth's surface is subject to kinetic oxygen isotope effects and likely does not truly precipitate at equilibrium (Daëron et al., 2019), marine $\delta^{18}O_{carbonate}$ values vary depending on temperature under many conditions. Because of this temperature dependence and because continental ice sheets remove low-δ^{18}O water from the ocean, $\delta^{18}O_{carbonate}$ values have been used as a proxy for both planetary ice volume and temperature in the geologic past (e.g. Shackleton, 1974; Chappell and Shackleton, 1986; Waelbroeck et al., 2002; Westerhold et al., 2020). As Earth had no ice sheets during the Cretaceous (Shackleton and Kennett, 1975; MacLeod et al., 2013), Cretaceous $\delta^{18}O_{carbonate}$ values have been used as a proxy for past temperatures in benthic and planktonic foraminifera (e.g. Barron, 1983; Miller et al., 1999) as well as bulk carbonate sediments (e.g. Stoll and Schrag, 1996, 2000).

Because the equilibrium δ^{18}O fractionation between water and carbonate minerals is higher at lower temperatures, higher $\delta^{18}O_{carbonate}$ values correspond to colder paleotemperatures. Experimental calibrations have determined the temperatures corresponding to $\delta^{18}O_{carbonate}$ values for calcite precipitated biogenically (e.g. Erez and Luz, 1983; Shackleton, 1974) and inorganically (O'Neil et al., 1969; Kim and O'Neil, 1997). The equation of Kim and O'Neil (1997) for inorganically precipitated calcite is:

$$1000 \ln(\alpha) = \frac{18.03 \times 10^3}{T} - 32.42 \tag{1.6}$$

where α is the fractionation factor between calcite and water and T is the temperature in Kelvin. For the temperature range and likely δ^{18}O of seawater of the time examined in this thesis, Equation 1.6 relates an increase of about 0.2‰ in the $\delta^{18}O_{carbonate}$ value of calcite to a decrease in temperature of about 1 K (equivalent to 1°C), and other experimental calibrations are similar (Figure A.1).

Vital effects on $\delta^{18}O_{carbonate}$ are conceptually similar to vital effects on $\delta^{13}C_{carbonate}$,

although organic carbon does not play a role in $\delta^{18}O_{carbonate}$ vital effects. One example of a microhabitat vital effect in the open ocean is that the $\delta^{18}O_{carbonate}$ of benthic foraminifera living just above the sediment-water interface is typically lower than the $\delta^{18}O_{carbonate}$ of benthic foraminifera living within the sediment (Theodor et al., 2016). The mechanism for this effect is disputed (Hoogakker et al., 2024). Vital effects on $\delta^{18}O_{carbonate}$ are negligible in some species of benthic foraminifera and non-negligible in others (Schmittner et al., 2017; Dubicka et al., 2018; Hoogakker et al., 2024). One taxon of benthic foraminifera considered in this thesis (*Praebulimina sp.*) has $\delta^{18}O_{carbonate}$ found to be in near-equilibrium with bottom water (Dubicka et al., 2018).

The $\delta^{18}O$ of carbonate minerals can also be altered by diagenesis. The diagenesis of carbonate sediments is more prone to reset $\delta^{18}O_{carbonate}$ values than $\delta^{13}C_{carbonate}$ values, first because the ratio of oxygen in diagenetic fluid to oxygen in carbonate sediments is high (as H_2O contains high amounts of oxygen), and comparatively the ratio of carbon in diagenetic fluid to carbon in carbonate sediments is low. Second, even if the diagenetic fluid has an oxygen isotope composition similar to the fluid from which the carbonate mineral formed, temperature-dependent oxygen isotope fractionation lowers $\delta^{18}O_{carbonate}$ values when diagenesis takes place at high temperatures. Another generally small effect is that silicate minerals contain much more oxygen than carbon, so in the case that silicate minerals are present, chemical reactions with those minerals in the subsurface can change the $\delta^{18}O$ of diagenetic fluid. For example, the weathering of basalts to clay minerals lowers the $\delta^{18}O$ of pore fluids during basalt alteration (Lawrence et al., 1975).

1.4 Background on Ocean Anoxic Events and Ocean Anoxic Event 2 (OAE2)

1.4.1 Ocean Anoxic Events (OAEs)

In the 1970s, it was observed that sediments of mid-Cretaceous age that are rich in organic carbon are present in multiple ocean basins and outcrops worldwide (Lancelot et al., 1972; Kaneps, 1976; Jackson and Schlanger, 1976; Schlanger and Jenkyns, 1976; Ryan and Cita, 1977; Thiede and Van Andel, 1977). Schlanger and Jenkyns (1976) hypothesized that these organic-rich sediments attest to the development of oxygen-

minimum zones throughout the global ocean during episodes that they named Ocean Anoxic Events (OAEs). Although it was recognized that events of deposition of organic-rich sediments had occurred throughout the Cretaceous, initially two OAEs were identified as "major" (i.e. suggested to be global in extent) in the Aptian and Cenomanian-Turonian stages respectively (today usually called OAE1a and OAE2; Schlanger and Jenkyns, 1976; Jenkyns, 2010). OAE2 was studied as an exemplar OAE with a large carbon isotope excursion (Figure 1.2; Arthur et al., 1990), and is studied in this thesis.

Because black shale deposition may vary locally depending on availability of nutrients and other factors affecting productivity, as well as sedimentation rates and other factors affecting preservation, it is more likely to occur in some parts of the ocean, such as continental shelves (Lowery et al., 2017). During an OAE, black shale deposition would not be expected across the entire ocean floor (Okhouchi et al., 2015). Therefore, OAEs are now identified by positive excursions in $\delta^{13}C_{carbonate}$ (Figure 1.2) and $\delta^{13}C_{organic}$, on the grounds that $\delta^{13}C_{carbonate}$ records relative change in global burial flux of organic vs. carbonate carbon (Section 1.2; Figure 1.1; Jenkyns, 2010; Lowery et al., 2017).

At least 9 OAEs are suggested in the Phanerozoic, with the earliest in the Toarcian stage and the latest at the Paleocene-Eocene boundary (i.e. the Paleocene-Eocene Thermal Maximum may be characterized as an OAE; Jenkyns, 2010). Most OAEs occurred during the Cretaceous period between the Valanginian stage and the Santonian stage (Figure 1.2). The durations of positive $\delta^{13}C_{carbonate}$ excursions associated with OAEs are usually estimated at hundreds of thousands of years based on cyclostratigraphy and biostratigraphy (e.g. Suan et al., 2008 for the Toarcian OAE; Jenkyns, 2010). For some OAEs, there is active debate regarding whether or not they were global in extent (e.g. Reolid et al., 2021 regarding the Toarcian OAE, Westermann et al., 2010 regarding the Late Valanginian OAE, Grasby et al., 2024 regarding OAE3). Four "major" OAEs (OAE1a, OAE1b in the Aptian-Albian stages, OAE2, and a Paleozoic OAE in the early Toarcian stage) have geographically widespread records of positive $\delta^{13}C_{carbonate}$ excursions and are consequently suggested to be global in extent (Jenkyns, 2010).

Besides positive $\delta^{13}C_{carbonate}$ excursions, other geochemical fingerprints have been interpreted in conjunction with OAEs. Jenkyns (2010) reviews records interpreted as proxies for paleotemperature ($\delta^{18}O$, Mg/Ca, TEX_{86}), marine redox states (biomarker compounds produced by sulfate-reducing bacteria, concentrations in marine sediments

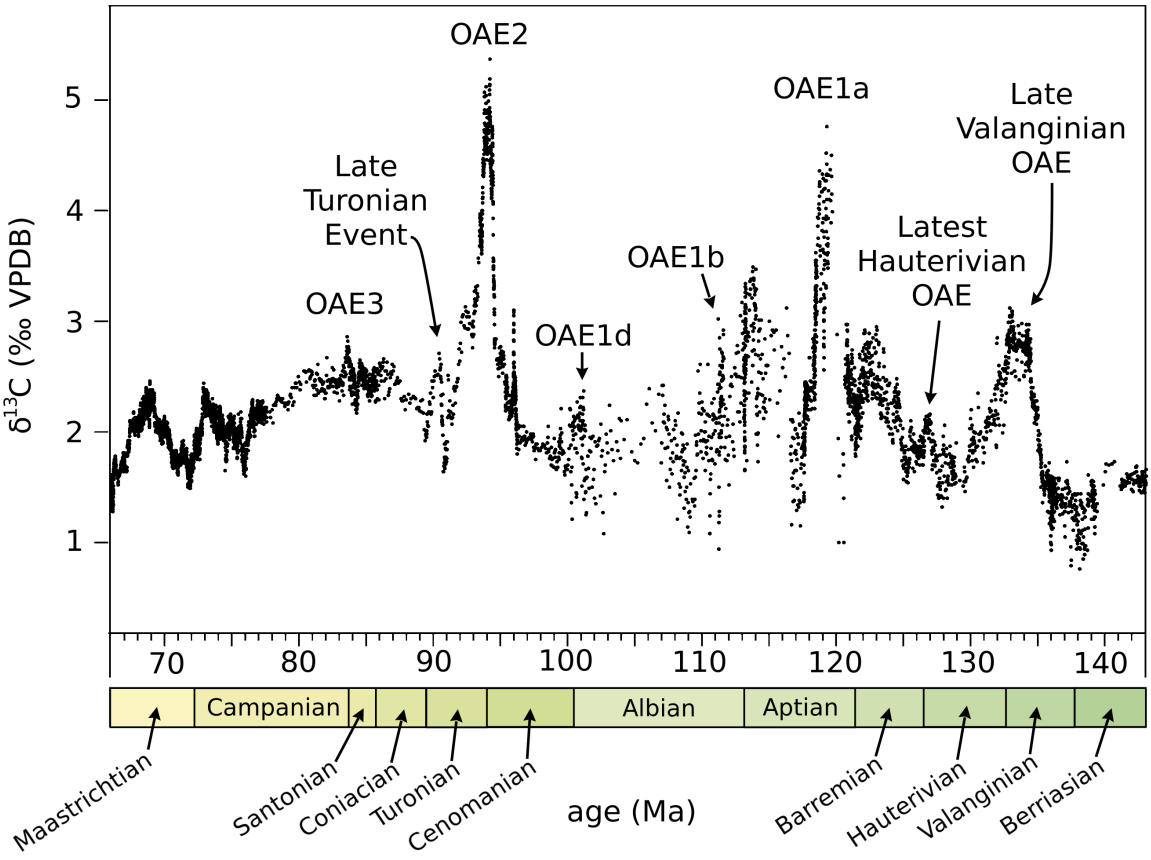

Figure 1.2: Bulk $\delta^{13}C_{carbonate}$ values from the Cretaceous compiled by Cramer and Jarvis (2020) and modified from their Figure 11.12, with positive $\delta^{13}C_{carbonate}$ excursions thought to correspond to Cretaceous OAEs labeled following the time scale from Jenkyns (2010). The Late Turonian Event (Gale et al., 2020) is not thought to correspond to an OAE.

of trace metals such as Mo that are thought to increase when there are euxinic conditions below the seafloor or in the water column, isotope ratios in marine sediments such as $\delta^{34}S$ that are likewise thought to be redox-sensitive), and continental weathering (isotope ratios in marine sediments such as $^{87}Sr/^{86}Sr$ and $^{187}Os/^{188}Os$ for which the radiogenic isotope is thought to be concentrated in continental crust). The latter is also interpreted as a proxy for volcanic activity (as the unradiogenic isotope is concentrated in the mantle). Jenkyns (2010) concludes that OAEs are forced by rising temperatures and that they are accompanied by oceanic anoxia and euxinia (particularly in more restricted areas of the ocean) as well as increased continental weathering.

Organic-rich sediments, positive $\delta^{13}C_{carbonate}$ excursions (and $\delta^{13}C_{organic}$ excur-

sions), and other geochemical fingerprints have been incorporated into a general, constantly refining hypothesis describing what occurs during an OAE. In this hypothesis, an OAE occurs when marine deoxygenation limits the transfer of carbon from organic matter to the ocean facilitated by respirating organisms, and/or enhanced productivity in the surface ocean increases rain rates of organic matter and overwhelms respirating organisms, leading to anoxia or euxinia in some areas of the ocean. Organic carbon is buried more efficiently, producing a sedimentary layer with elevated organic carbon content and a positive $\delta^{13}C_{carbonate}$ excursion. A warming climate is considered to be the trigger for marine deoxygenation (e.g. Schlanger and Jenkyns, 1976; Jenkyns, 2003) as it is suggested to accelerate the hydrological cycle, increasing continental weathering and therefore increasing nutrient fluxes to the ocean (e.g. Hochuli et al., 1999). A warming climate in turn may be triggered by release of CO_2 during the emplacement of a large igneous province (LIP; Larson and Erba, 1999; Jenkyns, 2010).

1.4.2 Ocean Anoxic Event 2 (OAE2)

The focus of this thesis is Ocean Anoxic Event 2 (OAE2), a prominent mid-Cretaceous OAE dated to the uppermost Cenomanian stage or Cenomanian-Turonian boundary, at 93.9 Ma (Cramer and Jarvis, 2020; Gale et al., 2020). Consistent with the general OAE hypothesis, OAE2 is associated with black shale deposition (Figure 1.3; Schlanger et al., 1987; Arthur et al., 1987; Okhouchi et al., 2015; Owens et al., 2018) and positive $\delta^{13}C_{carbonate}$ excursions (Figure 1.2). OAE2 is commonly identified as a positive excursion of the correct age, normally based on biostratigraphy, in $\delta^{13}C_{carbonate}$ (e.g. Falzoni et al., 2018) and/or $\delta^{13}C_{organic}$ (e.g. Arthur et al., 1988), including occasionally in the $\delta^{13}C$ of terrestrial organic matter (Hasegawa et al., 2013). Regarding the geographic distribution of evidence for OAE2, sites with elevated organic matter content ($\geq$ 2 wt.%) in sediments of the correct age are located mostly on continental margins or former shallow epicontinental seas such as the Western Interior Seaway of North America (Figure 1.3).

The geographic distribution of sites with positive $\delta^{13}C$ excursions from around the time of OAE2 is relevant to this thesis, as the new data in this thesis are $\delta^{13}C_{carbonate}$ records from around the time of OAE2. Most, although not all, OAE2 $\delta^{13}C$ records are from sediments deposited on continental margins or in shallow basins (Figure 1.4; Owens et al., 2018). Owens et al. (2018) compiled 40 sites worldwide where a positive

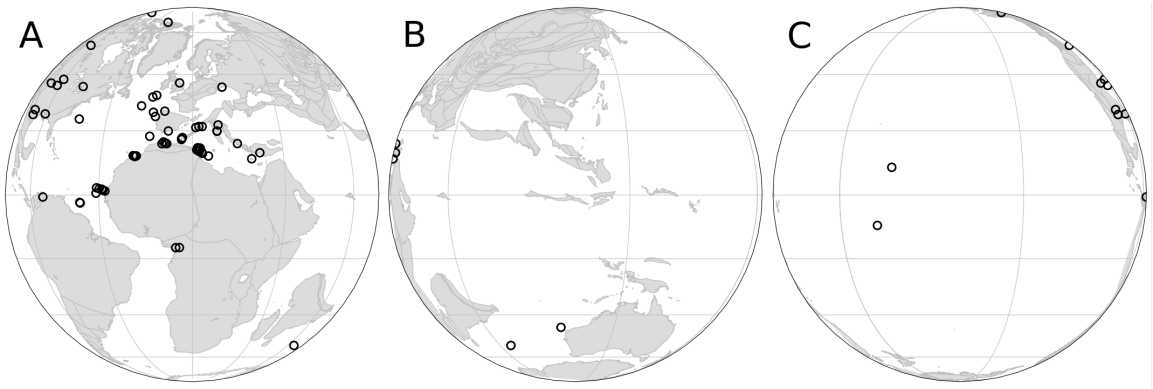

Figure 1.3: Paleomaps at 93.9 Ma with central longitudes of (A) 0°(B) 103°E and (C) 140°W showing sites where organic-rich sediment ($\geq$ 2 wt.%) of OAE2 age has been identified, compiled by Owens et al. (2018). The mid-Pacific sites are DSDP 32-305 (north) and DSDP 89-585 (south). Paleogeography from Müller et al. (2019).

$\delta^{13}C_{carbonate}$ and/or $\delta^{13}C_{organic}$ excursion is identified (Figure 1.4).

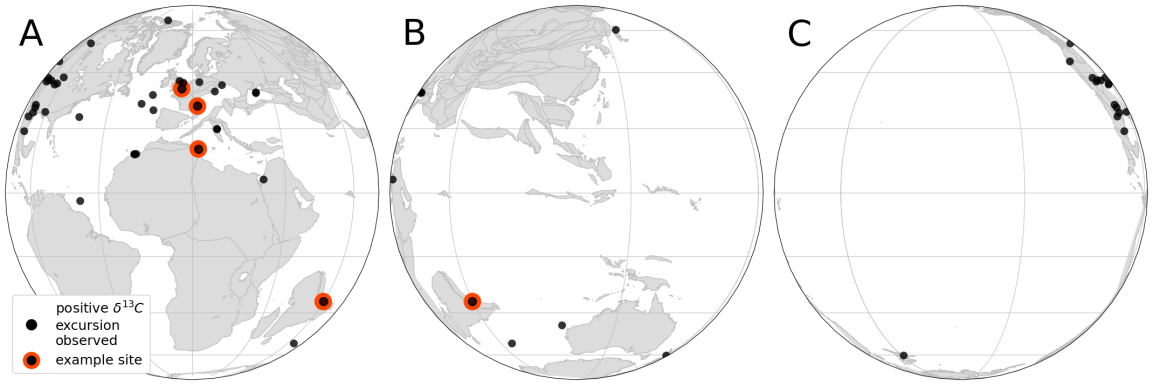

Figure 1.4: Paleomaps at 93.9 Ma with central longitudes of (A) 0°(B) 103°E and (C) 140°W showing sites where $\delta^{13}C_{carbonate}$ and/or $\delta^{13}C_{organic}$ has been measured in sediments of OAE2 age and a positive excursion observed (Owens et al., 2018; Falzoni et al., 2018). Five sites with positive $\delta^{13}C_{carbonate}$ excursions discussed in this thesis are circled in red (2 of these sites in present-day France are so close to each other they appear as one marker). At the site on the southern Pacific margin the $\delta^{13}C$ of terrestrial organic matter was measured in sediments by Hasegawa et al. (2013). Paleogeography from Müller et al. (2019).

Among records where an OAE2 positive $\delta^{13}C$ excursion is present, excursions have a range of magnitudes and sometimes have multiple peaks. Magnitudes range from about 1.1‰ to about 6.25‰, most commonly 2-3‰ (Owens et al., 2018). Regarding the number of peaks, in some sections, the positive $\delta^{13}C_{carbonate}$ excursion interpreted as OAE2 has been described as having three peaks (Caron et al., 2006; Grosheny

et al., 2006; Jarvis et al., 2006, 2011; Falzoni et al., 2016; Eldrett et al., 2015; Falzoni et al., 2018) and a possible fourth peak (Voigt et al., 2007, 2008), or alternatively one peak and one plateau separated by a trough (Pratt and Threlkeld, 1984; Gale et al., 2020).

OAE2 has also been linked to many geochemical records interpreted as proxies of environmental perturbation. For example, planktonic foraminiferal $\delta^{18}O$ and TEX_{86} paleotemperature proxy records are interpreted to indicate warming of sea surface temperatures during OAE2 and subsequently during the Turonian (Figure 1.5; Forster et al., 2007; MacLeod et al., 2013; O'Brien et al., 2017; Robinson et al., 2019), although at some sites a period of cooling (the "Plenus Cold Event") is indicated during OAE2 (Jefferies, 1961; Sinninghe Damsté et al., 2010; Jenkyns et al., 2017; O'Connor et al., 2020). Generally, Cretaceous sea surface paleotemperatures have a wide range because temperature is highly correlated with paleolatitude (Figure 1.5), because the planktonic foraminiferal $\delta^{18}O$ and TEX_{86} proxies may record temperatures at different depths in the water column, and because planktonic foraminiferal $\delta^{18}O$ may also be affected by local salinity and carbonate ion concentration (O'Brien et al., 2017). Decreases of 0.4 - 0.8 in $^{187}Os/^{188}Os$ at the onset of OAE2 $\delta^{13}C_{organic}$ excursions have been attributed to an input of low-$^{187}Os/^{188}Os$ osmium from the hydrothermal alteration of young ocean crust, and interpreted to indicate a pulse of massive magmatic activity that may have triggered OAE2 (Turgeon and Creaser, 2008; Du Vivier et al., 2014; Percival et al., 2020; Jones et al., 2021). It has been suggested that OAE2 was triggered by emplacement of LIPs with apparently coincident timing including the Caribbean-Colombian Plateau, High Arctic LIP, Ontong-Java Plateau, and Madagascar flood basalts (Kerr, 1998; Kuroda et al., 2007).

In this thesis, I compare newly collected Pacific bulk $\delta^{13}C_{carbonate}$ values to five outcrop $\delta^{13}C_{carbonate}$ records with sediments dated to have formed during OAE2: Eastbourne, England; Clot Chevalier, France; Pont d'Issole, France; wadi Bahloul, Tunisia; and Gongzha, Tibet (Tsikos et al., 2004; Falzoni et al., 2016; Jarvis et al., 2011; Caron et al., 2006; Bomou et al., 2013). These sites were selected because detailed planktonic foraminiferal biostratigraphy and correlated $\delta^{13}C_{carbonate}$ data have been published for each site (Falzoni et al., 2018). At these sites, the size of the OAE2 positive $\delta^{13}C_{carbonate}$ excursion is between about 1.5‰ and 3‰. At Eastbourne, Clot Chevalier, Pont d'Issole, and possibly at Gongzha, the baseline $\delta^{13}C_{carbonate}$ values after the excursion are about 0.5‰ higher than the baseline $\delta^{13}C_{carbonate}$ values before the excursion, while at wadi Bahloul the $\delta^{13}C_{carbonate}$ values return to the original

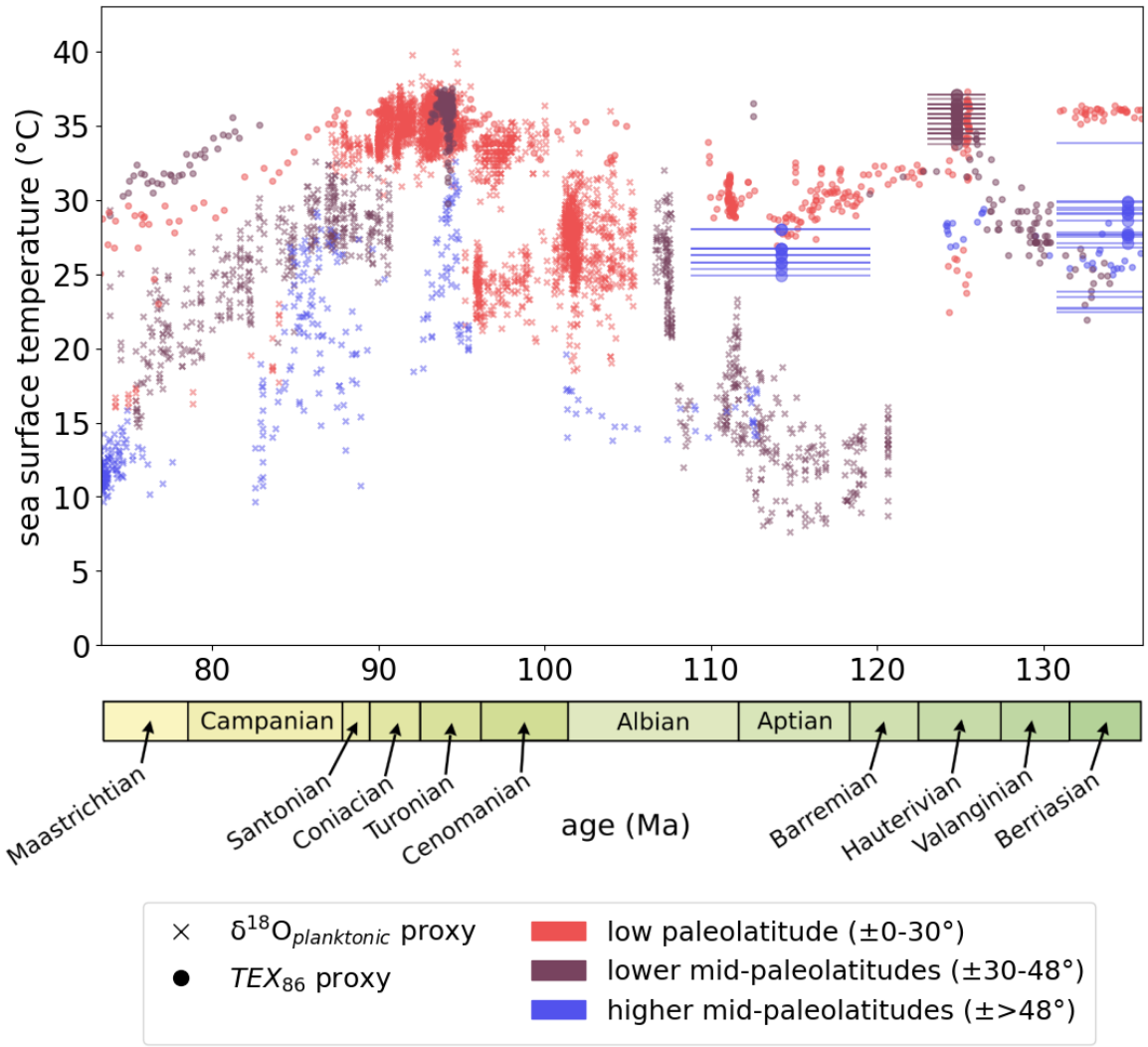

Figure 1.5: Cretaceous sea surface paleotemperatures based on planktonic foraminiferal $\delta^{18}O$ and TEX_{86} data, compiled and interpreted as paleotemperature proxies by O'Brien et al. (2017) following Bemis et al. (1998) for planktonic foraminiferal $\delta^{18}O$ and the $TEX_{86}{}^{H}$ calibration of Kim et al. (2010) for TEX_{86}. Ages are as reported by original authors, including some TEX_{86} with large age uncertainties (horizontal bars). Following O'Brien et al. (2017), data are categorized by paleolatitude: low paleolatitude (±0-30°) data are red, lower mid-paleolatitudes (±30-48°) data are purple, and higher mid-paleolatitudes (± >48°) data are blue.

baseline (Table 1.1, Figure 1.6). At each site, three peaks have been identified, although for some sections authors differ on the stratigraphic height of a peak (Figure 1.6).

In this thesis, the $\delta^{13}C_{carbonate}$ records from the aforementioned 5 sites will be compared to $\delta^{13}C_{carbonate}$ records from Pacific sites (Section 5.2.1). Differences between

Site	$\delta^{13}C_{carbonate}$ value before excursion (‰VPDB)	$\delta^{13}C_{carbonate}$ value at peak of excursion (‰VPDB)	$\delta^{13}C_{carbonate}$ value after excursion (‰VPDB)
Eastbourne, England	about 3	5.4	about 3.5
Clot Chevalier, France	about 2.5	4.4	about 3
Pont d'Issole, France	about 2.5	4.4	about 3
wadi Bahloul, Tunisia	about 2	3.7	about 2
Gongzha, Tibet	about 1-2	3.6	if section includes return to baseline, about 2.5

Table 1.1: For each of 5 outcrop sections with sediments biostratigraphically dated to have formed during OAE2, all of which have positive $\delta^{13}C_{carbonate}$ excursions: the $\delta^{13}C_{carbonate}$ value before, at the peak of, and after the excursion.

$\delta^{13}C_{carbonate}$ records between different sites may exist for many reasons, including differences in paleogeography and ocean dynamics between sites. It is therefore important to understand the paleogeographic context of the Pacific and non-Pacific sites, including the relative size and depth of the ocean basins where they were located at the time of OAE2.

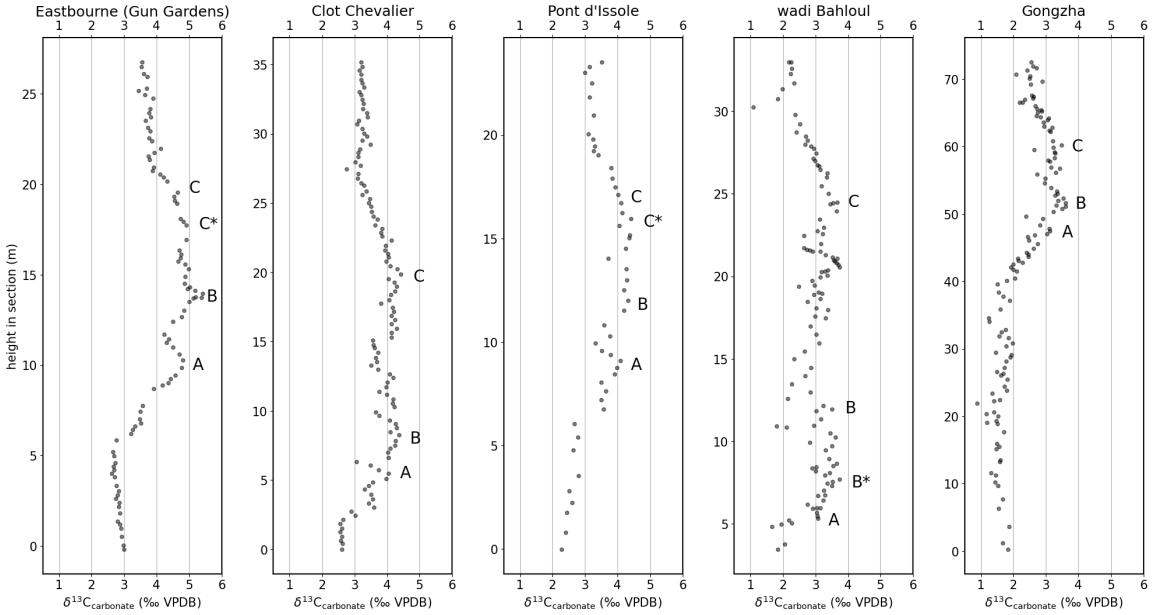

Figure 1.6: Bulk $\delta^{13}C_{carbonate}$ values at outcrop sites in sediments dated to the Cenomanian and Turonian. The y-axis differs between plots. Sources of the $\delta^{13}C_{carbonate}$ values from left to right are Tsikos et al. (2004); Falzoni et al. (2016); Jarvis et al. (2011); Caron et al. (2006); Bomou et al. (2013). Peaks are labeled after the sources of the $\delta^{13}C_{carbonate}$ values, except Eastbourne A, B, and C are after Jarvis et al. (2006), Eastbourne C* is after Voigt et al. (2008), and Pont d'Issole C* and wadi Bahloul B* are after Falzoni et al. (2018).

1.5 Paleogeography in OAE2 time

Figure 1.7 shows the names used in this thesis for the regions of the ocean at the time of OAE2. In this thesis the focus will be on sites in the Pacific, and sites in the Atlantic, Western Tethys, and Neotethys will also be considered. At the time of OAE2 the majority of the ocean by mass was the Pacific Ocean. The Pacific was deep, with deepwater production likely occurring throughout the Cretaceous in the high-latitude Northern Pacific as well as the high-latitude Southern Pacific at least up to the time of OAE2 (Murphy and Thomas, 2012; Hague et al., 2012; Donnadieu et al., 2016). Also, Pacific surface area was large: the Pacific Ocean accounted for more than 60% of ocean area at the time of OAE2 (Takashima et al., 2011), as opposed to about 45% today.

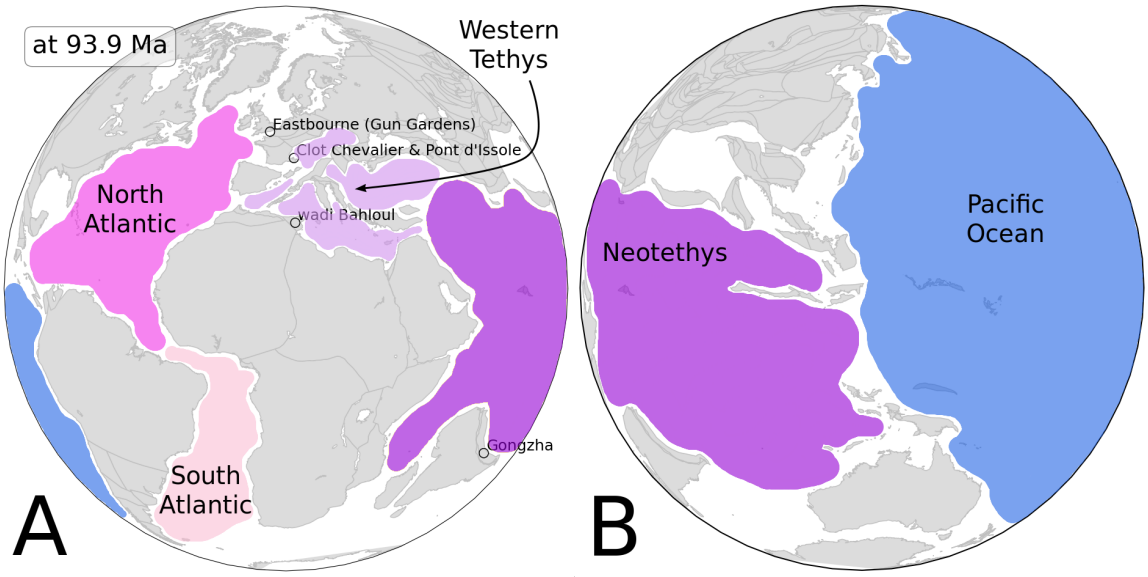

Figure 1.7: Paleomaps at 93.9 Ma with central longitudes of (A) 0°and (B) 115°E. Ocean regions are labeled with the names used in this text: North Atlantic (dark pink), South Atlantic (light pink), Western Tethys (light purple), Neotethys (dark purple), and Pacific (blue). Paleogeography from Müller et al. (2019). Five sites discussed in this thesis with positive $\delta^{13}C_{carbonate}$ excursions are shown.

The Atlantic Ocean was much narrower and shallower at the time of OAE2. As the connection between the North and South Atlantic only occurred several million years before OAE2 (estimated at 112 Ma by Eagles, 2007 and Moulin et al., 2010; 103 Ma by Heine et al., 2013; 95 Ma by Granot and Dyment, 2015), the Atlantic was likely not well-connected to the global deep ocean at the time of OAE2. Even in models in which

the North and South Atlantic become connected at 112 Ma, deepwater connection between the North and South Atlantic is not thought to have started until 100 Ma at the earliest (Eagles, 2007). It has been argued that the formation and circulation of North Atlantic deepwater did not begin until much later, during the latest Cretaceous (69 Ma; MacLeod et al., 2011; Voigt et al., 2013).

The ocean between Eurasia, India, and Australia, connecting the Atlantic and Pacific (Dilek and Furnes, 2018) and bordered to the south by the passive continental margin of the Indian continent (Willems et al., 1996), can be considered as two realms at the time of OAE2, with the extent of the connection to the global ocean differing between these realms. In this thesis, the western part of this ocean is called the Western Tethys, while the rest of this ocean is called the Neotethys (Figure 1.7). The Western Tethys at the time of OAE2 was likely poorly connected to the global deep ocean as it was characterized by multiple small basins, whose formation was enabled by the many microplates and continental fragments in that region (Schettino and Turco, 2011; Dilek and Furnes, 2018). Shallow marine carbonate depositional environments developed in these basins. For example, during Cenomanian-Turonian time in present-day southern Jordan, a carbonate shelf formed (Powell and Moh'd, 2011) In Cenomanian time, in the present-day Apennines of Italy, basins formed between shallow-water carbonate platforms (Carrannante et al., 2009). By contrast, the Neotethys was likely much better connected to the global deep ocean, as it was not divided into small basins: Neotethys crust was mostly produced by a single spreading ridge, which is thought to have been subducted under Eurasia during the Cenomanian at 100 Ma (Zhang et al., 2023). In the Cenomanian and Turonian, the Neotethys was connected to the Pacific via the area of the ocean between Australia and Eurasia (Hall, 2012).

It is possible that $\delta^{13}C$ records from deeper, less restricted regions of the global ocean such as the Pacific and potentially the Neotethys would better represent global ocean $\delta^{13}C$ than $\delta^{13}C$ records from shallower, more restricted regions of the global ocean. In this thesis, I consider this possibility when I compare bulk $\delta^{13}C_{carbonate}$ records from the time of OAE2 at study sites in the Pacific to similar records at study sites in other ocean basins, notably the Western Tethys and Neotethys.

1.6 Motivation for this thesis

It is foundational to the current understanding of OAEs that positive $\delta^{13}C_{carbonate}$ excursions observed at the time of OAE2 are interpreted to represent a perturbation to the global carbon cycle. The interpretation of OAE2 as a global event is suggested by many authors (e.g. Tsikos et al., 2004; Caron et al., 2006; Li et al., 2006; Jarvis et al., 2011; Bomou et al., 2013; Lowery et al., 2017; Percival et al., 2020; Falzoni and Petrizzo, 2020), and the OAE2 positive $\delta^{13}C_{carbonate}$ excursion has been used as a chronostratigraphic tool to correlate sections at geographically distant sites (e.g. Falzoni et al., 2018). However, the magnitude of the OAE2 positive $\delta^{13}C_{carbonate}$ excursion is not consistent between sites (Section 1.4), and most $\delta^{13}C_{carbonate}$ records from OAE2 time are from the North Atlantic, Western Tethys, and North America (which had an epicontinental sea in OAE2 time). Records from the Pacific are lacking, which is important because the Pacific at the time of OAE2 accounted for the majority of the mass of the ocean (Section 1.5) and therefore contained the majority of the carbon in Earth's ocean-atmosphere reservoir.

In this thesis I test the hypothesis that there was a global change in the $\delta^{13}C_{DIC}$ of seawater at the time of OAE2, as is predicted by a model of a substantial increase in organic carbon burial. I measured $\delta^{13}C_{carbonate}$ values of open-ocean Pacific sediments, recovered from the seafloor by drilling, that are dated to the Cenomanian and Turonian stages using microfossil biostratigraphy. I also correlate these sediments to sediments at selected non-Pacific sites using planktonic foraminiferal biostratigraphic data. Finally, I discuss whether the Pacific $\delta^{13}C_{carbonate}$ record is consistent with a global positive excursion in $\delta^{13}C_{DIC}$ at the time of OAE2. I argue that these Pacific $\delta^{13}C_{carbonate}$ values are consistent with either a global ocean OAE2 $\delta^{13}C$ excursion occurring alongside a process that largely prevented its deposition, preservation, or recovery in the mid-Pacific, or that an excursion in $\delta^{13}C$ did not occur in the Pacific at the time of OAE2 but did occur and is recorded outside it (Section 5.3).

Methods

2.1 Scientific ocean drilling

Sediments and many other lithologies have been recovered from the seafloor by a series of scientific ocean drilling programs: the Deep Sea Drilling Project (DSDP) from 1968-1983, the Ocean Drilling Program (ODP) from 1984-2003, the Integrated Ocean Drilling Program (IODP) from 2003-2013, and since 2013 the International Ocean Discovery Program (also IODP) (National Research Council, 2011). Conventions from these programs are used for sample names, depth calculations, etc., as sedimentary samples in this thesis were collected between 1971 and 1982 by the Deep Sea Drilling Project (DSDP).

A scientific ocean drilling voyage is called a "leg" or "expedition." During the expedition drilling is conducted at several sites. Expeditions and sites are both numbered beginning with DSDP's Leg 1 Site 1 and continuing through the International Ocean Discovery Program (IODP) Expedition 403 Site 1624 in August of 2024 (Lucchi et al., 2024). Sites are referred to by their expedition and site numbers, e.g. Leg 89 Site 585 is 89-585. Per DSDP convention, the first hole drilled at the site has no suffix (e.g. 89-585), but if a second hole is drilled at a site, it receives the suffix A (e.g. 89-585A). For this thesis, samples from 10 holes were collected (17-167, 17-169, 17-170, 17-171, 30-288A, 32-305, 32-310A, 62-463, 89-585, 89-585A), and two of those holes (89-585 and 89-585A) are from the same site. Table 2.1 shows the references corresponding to the DSDP Initial Reports for each of these holes. Holes at the same site can be up to 1800 meters away from each other (Thiede et al., 1981; Baltuck et al., 1986). During Leg 89, successive holes were at least 100 meters away from each other (Baltuck et al., 1986). In this thesis 89-585 and 89-585A are sometimes referred to as two "sites" *sensu lato*.

The sediments sampled for this thesis were drilled using punch-core rotary drilling, in which the drilling assembly penetrates the sediment or rock, rotating around a barrel in which material is collected. Drilling fluid (seawater or mud slurry) is pumped

Site and hole	Reference
17-167	Shipboard Scientific Party (1973b)
17-169	Shipboard Scientific Party (1973c)
17-170	Shipboard Scientific Party (1973d)
17-171	Shipboard Scientific Party (1973e)
30-288A	Shipboard Scientific Party (1975a)
32-305	Shipboard Scientific Party (1975c)
32-310A	Shipboard Scientific Party (1975e)
62-463	Shipboard Scientific Party (1981b)
89-585	Shipboard Scientific Party (1986)
89-585A	Shipboard Scientific Party (1986) (same as 89-585)

Table 2.1: References for the Deep Sea Drilling Project Initial Report corresponding to each of the Pacific sites in this study.

through the drilling assembly and carries away the material cut by the drill bit, while material from the center of the hole enters the barrel. If sediments are sufficiently soft and scientists do not wish to retrieve them, they can be intentionally "washed" by high-pressure drilling fluid that disaggregates them and carries them away (Moberly et al., 1975). Material from the hole is retrieved in metal barrels 9.1-9.5 meters long, lined with plastic (Winterer, 1973; Moberly et al., 1975; Thiede et al., 1981; Baltuck et al., 1986). The material in one such barrel is called a "core" and while it is pulled up to the drilling vessel, it is prevented from falling out of the barrel by a "core catcher," which may contain up to 20-25 cm of core (Leg 17 Introduction, Leg 32 Introduction, Leg 62 Introduction, Leg 89 Introduction).

If the material recovered is equal in length to the depth interval cored (usually ∼9.5 m but occasionally shorter; Thiede et al., 1981; Baltuck et al., 1986), "recovery" is 100%. It is common for recovery to be less than 100%. Recovery is often poor in cherty sections of carbonate like many of the Pacific cores sampled in this thesis. Unpredictable alternation of hard chert with soft carbonate sediments makes it very difficult to achieve the balance between downward speed of the drilling assembly, rotation speed of the drilling assembly, and pressure of the drilling fluid that is required for good recovery (Moberly et al., 1975). In this situation carbonate sediments are often accidentally washed. The presence of chert in sediments is often cited as a

reason for poor recovery in the cores studied herein (e.g. Shipboard Scientific Party, 1973b,c,d,e, 1975c,e, 1981b, 1986)and the presence of other hard rocks (such as basalt) in relatively soft sediments can have a similar effect (e.g. Shipboard Scientific Party, 1973d).

Once a core is on the deck of the drilling vessel, it is cut into 150-cm "sections," which are numbered beginning with the uppermost section in which there is core material (Winterer, 1973). Material in the core catcher is retained separately. If recovery is 100% there will be 7 sections, one <150 cm in length, in addition to the core catcher. A sample is designated by the distance between the top of the section and the sample in centimeters, usually to the top and bottom of the sample, e.g. 96-97 cm. The full designation for a sample also includes the associated expedition, site, hole, core, and section, e.g. 89-585A-7-3-96/97. Samples from the core catcher are designated with the abbreviation "CC," e.g. 89-585A-8-CC-15/16. Some core catchers studied herein are archived as loose material in plastic tubs, and in this case there is no information about the distance to the top and bottom of the sample, e.g. 17-171-29-CC (Figure 2.1). Also, cores are split longitudinally, into an "archive" half ("A") which is preserved and a "working" half ("W") from which samples are taken. The sample designation can be written to include information on the type of coring ("rotary" for all samples collected in this thesis; see above) and the core half ("working" for all samples collected in this thesis), e.g. 89-585A-7R-3W-96/97.

2.2 Depths of samples

For all samples in this thesis, depth is calculated according to the CSF-A depth convention and reported in meters below sea floor (mbsl). The CSF-A depth is the sum of the depth to the top of the cored interval in the hole, the curated length(s) of the section(s) above the section of the sample, and the distance from the top of the section to the sample (IODP-MI, 2011; Baltuck et al., 1986). Curated lengths of sections can be obtained from the Janus database (`iodp.tamu.edu/database`, Mithal and Becker, 2006).[1] CSF-A depths are used in this thesis at high precision to visualize data (in stratigraphic columns, $\delta^{13}C_{carbonate}$ vs. depth plots, etc.). The relative depths of samples collected by the same author from the same section of core are known at centimeter-level precision in most cases. However, the distances between samples from

[1]Depths reported in visual core descriptions (VCDs) generally agree with depths reported in Janus except for 17-169. In this thesis CSF-A depths according to Janus are used for 17-169.

Figure 2.1: A plastic tub containing the core catcher of core 29 of hole 17-171 (17-171-29-CC), which contains hyaloclastite (one large chunk) and carbonate (very friable and broken into smaller pieces; Shipboard Scientific Party, 1973e). The footprint of the tub is about 10 cm x 10 cm.

different sections and sometimes even the relative order of samples (superposition) are uncertain for two main reasons.

First, the depth to the top of the cored interval in the hole is measured along the "drill string" (the pipe connecting the vessel to the drilling assembly). The heave of the drilling vessel and extension or compression of drill string joints may affect the measurement of this depth (Winterer, 1973; Moberly et al., 1975). Also, generally each core can be considered stratigraphically deeper than the core taken before it because cores are retrieved sequentially from drilling deeper into the hole, but in some cases "cavings" from the hole are retrieved in deeper cores. Caved material may be identified by the recognition of younger fossils (e.g. few Neogene and Turonian foraminifera found among many Cenomanian foraminifera in Core 17 of Hole 32-310A; Shipboard Scientific Party, 1975e).

Second, in the CSF-A depth calculation, it is assumed that all the recovered material came from the top of the cored interval (Winterer, 1973), but it is unknown where in the depth interval the material originated. During core retrieval, the core material slides to one end of the core and stacks there, except in rare cases where void is preserved within a section of the retrieved core barrel. If recovery of core material is less than 100%, uncertainty up to the length of the void interval is added. Also, superpo-

sition cannot always be assumed if sediment is disturbed by the drilling process, and pieces are substantially smaller than the 6-cm width of the core and can move past one another. In soft sediment, signs of mechanical disturbance include contortion of layers that may originally have been flat (particularly if they are concave downward across the width of the core), mixing of lumps of rock with different lithologies, and sediments which were water-saturated when retrieved (Moberly et al., 1975; Baltuck et al., 1986). (Sediments in archives do not remain water-saturated and become more unconsolidated after they dry out.) Finally, the locations of samples can change over time due to shifting of the core when it is handled (Winterer, 1973).

Of the 62-463 sediments sampled for this thesis, several core intervals were "soupy" (water-saturated) when retrieved (Shipboard Scientific Party, 1981b), which is classified as the most extreme form of drilling disturbance as the original bedding has been destroyed and material may be entirely mixed within soupy interval of the core (Thiede et al., 1981). Superposition is unlikely in intervals like these. Within the soupy interval it should not be assumed that change in depth is change in time. Therefore, for some entirely soupy intervals I took only one sample (e.g. cores 31, 35, 44; see 262.2 mbsf, 300.3 mbsf, 386.3 mbsf on Figure 4.5), while for others I took a few to test whether they had very similar bulk $\delta^{13}C_{carbonate}$ and $\delta^{18}O_{carbonate}$ values (e.g. core 38 section 1 26-58 cm; see 328.8-329.1 mbsf on Figure 4.5). From one soupy interval (Core 43) I took 21 samples which I used as a set of replicates to assess precision of $\delta^{13}C_{carbonate}$ and $\delta^{18}O_{carbonate}$ measurements (Section 2.6.5).

2.3 Ages of samples

In this thesis, biostratigraphic zonation schemes for the mid-Cretaceous based on microfossils (e.g. Sliter, 1989; Bralower et al., 1995) are used. Pacific sediments examined in this thesis have been assigned to geologic stages based on planktonic foraminiferal, radiolarian, and nannofossil biostratigraphy (references in Table 2.1). In this thesis, the shallowest (or deepest) depth I assign to a stage at a Pacific site is the depth at the top of the youngest (or bottom of the oldest) core that is assigned to the stage by shipboard scientists. Figures in this thesis (Figures 4.3 - 4.13) show the depth of the base of the Cenomanian and the depth of the top of the Turonian according to this rule. The Cenomanian-Turonian boundary depth at a Pacific site is determined as the depth of the top of the Cenomanian and bottom of the Turonian, and other geologic stage boundaries are determined in the same way. For some Pacific sites in

this thesis, the Cenomanian-Turonian boundary has been assigned to a depth range rather than a single depth because:

1. There are gaps between the depth ranges assigned to cores, so the depth of the shallowest Cenomanian differs from the depth of the deepest Turonian. In these cases these different depths are the bottom and top of the depth range assigned to the Cenomanian-Turonian boundary.

2. A core of uncertain stage (e.g. labeled "?") is between cores assigned to different stages, or a core was labeled as belonging to more than one stage without specifying a boundary. In these cases the core was treated as though it could have belonged to either of the stages of the cores immediately adjacent (i.e. either the Cenomanian or the Turonian, so the entire core would be included in the depth range assigned to the Cenomanian-Turonian boundary).

These circumstances did not arise for any other geologic stage boundaries noted on figures in this thesis (Figures 4.3 - 4.13). Note that when the Cenomanian-Turonian boundary depth is used in estimating the paleodepth of deposition of sediments (Section 2.4), the depth of the Cenomanian-Turonian boundary is assumed to be the average of the range.

To compare sediments at non-Pacific sites to the Pacific sediments studied (Section 5.2), I used planktonic foraminifera. Biostratigraphy based on planktonic foraminifera is used because abundant planktonic foraminifera occurrence data are available in these sediments. Also, planktonic foraminifera are generally good biostratigraphic tools because they are abundant, widely geographically distributed, and usually well preserved, and they have high rates of species turnover (Kimoto, 2015; Huber et al., 2016). Existing planktonic foraminiferal biostratigraphic zonation schemes are widely used for the Mesozoic (Huber et al., 2016), including the Cenomanian and Turonian specifically (Caron et al., 2006). Previous workers have logged planktonic foraminifera occurrences at the species level in samples throughout the cores I sampled (Table 2.2; Douglas, 1973; Caron, 1975; Michael, 1975; Boersma, 1981; Premoli Silva and Sliter, 1986; Sliter, 1992). Previous workers have also logged species-level planktonic foraminifera occurrences in other sections outside of the Pacific, including selected sites considered in this thesis (Table 2.2; Section 3.3 and Section 5.2). Only positive species-level identifications were used (e.g. "*Whiteinella sp. aff. W. aprica*" indicates the specimen varies from the species description and was therefore not treated as an identification of *Whiteinella aprica*).

Work on taxonomic organization of Cretaceous planktonic foraminifera is ongoing and made available through online databases such as pforams@mikrotax (`www.mikrotax.org/pforams/`, Huber et al., 2016; Young et al., 2019) and the World Register of Marine Species (WoRMS; `www.marinespecies.org`, WoRMS Editorial Board, 2024). When complete, the Neptune Sandbox Berlin (NSB) database project will standardize and digitize existing biostratigraphic data from the DSDP through the IODP (Lazarus, 1994; Spencer-Cervato, 1999; Renaudie et al., 2020). Because taxon names and identification criteria are continuously revised, an important part of standardizing biostratigraphic data is ensuring that the same taxon names are used to refer to the same species, a process which I here call "resolving" species names. For some of the DSDP sites in this thesis (17-170, 17-171, 32-305, and 62-463), all DSDP planktonic foraminifera occurrence data has already been entered into the NSB database and the taxon names have been resolved. For other sites in this thesis (17-169, 30-288A, 32-310A, 89-585, 89-585A), I digitized the planktonic foraminifera occurrence data and resolved the taxon names. Although 17-167 is present in the NSB database, planktonic foraminiferal occurrence data are only available in the cores I studied from a non-DSDP publication (Sliter, 1992), so I resolved the taxon names for 17-167 also. The NSB database retains the original and the resolved taxon name for all planktonic foraminifera occurrence data, so for any names that matched NSB original names, I used the same resolved names as the NSB database. Where a name was used that was not already in the NSB database, I used the aforementioned taxonomic organization databases such as pforams@mikrotax to determine whether the name could be resolved to an NSB resolved name (Table A.1) or if the name could be treated as resolved name (Table A.2).

Table 2.2: The sources of species-level planktonic foraminifera occurrence data consulted in this thesis. If synonymous names of taxa were resolved by NSB, then the database contained all planktonic foraminifera occurrence data with both original and updated taxon names. If synonymous names of taxa were resolved by this thesis, the NSB database did not contain the planktonic foraminifera occurrence data for the site, and I used the NSB database along with pforams@mikrotax to determine which species names would be treated as synonymous. See Table A.1.

Site	Source(s) for planktonic foraminiferal biostratigraphy	Synonymous names of taxa resolved by	Source for bulk $\delta^{13}C_{carbonate}$ values
17-167	Sliter (1992)	this thesis	this thesis; Douglas and Savin (1973); Coplen and Schlanger (1973)
17-169	Douglas (1973), Table 8	this thesis	this thesis
17-170	Douglas (1973), Table 9	NSB**	this thesis
17-171	Douglas (1973), Table 12	NSB**	this thesis
30-288A	Michael (1975)	this thesis	this thesis
32-305	Caron (1975), Figure 1	NSB**	this thesis; Price et al. (1998)
32-310A	Caron (1975), Figure 2	this thesis	this thesis
62-463	Boersma (1981), Figure 3	NSB**	this thesis; Price et al. (1998)

Site	Source(s) for planktonic foraminiferal biostratigraphy	Synonymous names of taxa resolved by	Source for bulk $\delta^{13}C_{carbonate}$ values
89-585	Premoli Silva and Sliter (1986), Figure 3	this thesis	this thesis
89-585A	Premoli Silva and Sliter (1986), Figure 3	this thesis	this thesis
Eastbourne (Gun Gardens)*	Falzoni and Petrizzo (2020), Appendix A	this thesis	Tsikos et al. (2004), Figure 2
Clot Chevalier*	Falzoni et al. (2016), Figure 3	this thesis	Falzoni et al. (2016), Figure 2
Pont d'Issole*	Grosheny et al. (2006), Figure 3	this thesis	Jarvis et al. (2011), via Falzoni et al. (2018) supplementary Figure B
wadi Bahloul*	Caron et al. (2006), Figure 8	this thesis	Caron et al. (2006), Figure 9
Gongzha*	Bomou et al. (2013), Figure 3	this thesis	Bomou et al. (2013), Figure 5

* These sites are compiled in Falzoni et al. (2018).

** Accessed the NSB database prior to 14 March 2022.

2.4 Paleodepth estimation

To estimate the depth of deposition of the sediments studied, I follow Stein and Stein (1992). Stein and Stein (1992) model the subsidence of old lithosphere (≥20 Myr) using a standard plate model. Conceptually, the lithosphere is modeled to have an isothermal boundary at its base, and therefore its depth approaches an asymptote, increasing more slowly with age. Stein and Stein (1992) publish an approximation which accurately reproduces the results of their model:

$$d = 2600 + 365\sqrt{t} \qquad \text{if } t < 20\text{Myr} \tag{2.1}$$

$$d = d_r + d_s \times \left(1 - \tfrac{8}{\pi^2} e^{-0.0278t}\right) \quad \text{if } t \geq 20\text{Myr} \tag{2.2}$$

where t is age (in Myr), d is depth of igneous basement (in mbsl), d_r is the depth of the ridge axis (in mbsl), and d_s is the asymptotic igneous basement depth approached by old lithosphere (in mbsl). For their approximation, Stein and Stein (1992) use d_r of about 2500 m and d_s of 5651 mbsl in Equation 2.2. In my approach:

1. I calculate the asymptotic igneous basement depth d_s approached by old lithosphere as the present-day igneous basement depth below sea level of each Pacific site. Specifically, I add together the present-day seafloor depth and the present-day igneous basement depth below the seafloor to get the present-day igneous basement depth below the sea surface (in mbsl). I do this because at all Pacific sites examined in this thesis the crust is sufficiently old that its depth is more than 95% of the way to the asymptotic igneous basement depth (Table 2.3). This approach may underestimate d_s by a few hundred meters (e.g. for a d_s of 5651 mbsl, there is a difference of 225 m between the igneous basement depth and the asymptotic depth at the 95% mark; Figure A.2).

2. I shift the subsidence curve for crust ≥20 Myr (generated by Equation 2.2) so that the curve intersects present-day igneous basement depth. (Mathematically, this is the same as changing d_r). I then shift the subsidence curve for crust <20 Myr (generated by Equation 2.1) so that the overall subsidence curve is continuous.

Because Stein and Stein (1992) empirically fitted their model using data from crust loaded by sediment, I do not account separately for the effect of sediment

accumulation on igneous basement depth. My modifications yield the equation:

$$d = (d_{sf} + d_{ib}) \times \left(1 - \frac{8}{\pi^2} e^{-0.0278 t_e}\right) \tag{2.3}$$

where t_e is the time elapsed since igneous basement formation (in Myr), d is the igneous basement depth at time t_e (in mbsl), d_{sf} is the present-day seafloor depth (in mbsl) and d_{ib} is present-day igneous basement depth below the seafloor (in mbsf). t_e is different than t in Equations 2.1 and 2.2 because t is measured from the present and t_e is measured from the time of crustal formation. To determine the igneous basement depth d at the time of sediment deposition, I input the time elapsed between the time of igneous basement formation (t_0 in Ma) and the time of sediment deposition (t_{sed} in Ma) as t_e into Equation 2.3.

Site and hole	How close is the present-day crustal depth to asymptotic crustal depth? (%)
17-167	97.9
17-169	98.7
17-170	98.7
17-171	95.6
30-288A	97.5
32-305	98.2
32-310A	95.7
62-463	98.4
89-585	98.9
89-585A	98.9 (same as 89-585)

Table 2.3: Closeness of the present-day crustal depth to the asymptotic crustal depth, expressed as a percentage of the depth between the crust at the time of crustal formation and the asymptotic depth, at each Pacific site in this thesis.

To determine the depth of the sediment at the time of deposition, I subtract[2] the thickness of sediment at the time of deposition from the depth of igneous basement at the time of deposition. The thickness of the sediment at the time of deposition is calculated as the distance between the sediment being deposited and the igneous

[2]because depth is a positive quantity

basement ($d_{ib} - d_{sed}$), which I assume to be the same in the present-day as at the time of deposition (i.e. I neglect compaction). Therefore, in summary, I calculate the depth of deposition of the sediments studied (d_{dep}, in mbsl) using the equation:

$$d_{dep} = (d_{sf} + d_{ib}) \times \left(1 - \frac{8}{\pi^2} e^{-0.0278(t_0 - t_{sed})}\right) - (d_{ib} - d_{sed}) \tag{2.4}$$

where d_{dep} is the depth of deposition of the sediment (in mbsl),

d_{sf} is the present-day seafloor depth below sea level (in mbsl),

d_{ib} is present-day igneous basement depth below the seafloor (in mbsf),

t_0 is the time elapsed since the formation of the igneous basement (in Myr),

t_{sed} is the time elapsed since the deposition of the sediment (in Myr), and

d_{sed} is the present-day depth of the sediment below the seafloor (in mbsf).

The present-day seafloor depth below sea level (d_{sf}, in mbsl) are from GeoMapApp (`www.geomapapp.org`). The ages of the crust underlying the sites (t_0, in Myr) are also from GeoMapApp.

Present-day igneous basement depth (d_{ib}, in mbsf) is treated as synonymous with modern sediment thickness, i.e. it is the depth below the seafloor where the top of the basement is reached. For this value, measurements are available at 4 sites (17-167, 17-169, 17-170, and 17-171) where the holes reached basement. For holes that did not reach basement, I used the reanalysis dataset CRUST1.0, which incorporates drilling and surface wave velocity data to produce sediment thickness estimates on a global 1°× 1°grid (accessed through GeoMapApp, described at `igppweb.ucsd.edu/~gabi/crust1.html` and in Laske et al., 2013). At 3 sites (30-288A, 32-305, and 32-310A) the CRUST1.0 grid point nearest the site gave a sediment thickness greater than the maximum penetration depth of the DSDP expedition at that site, so I used this sediment thickness as the present-day crustal depth for that site.

For the remaining sites (62-463, 89-585, and 89-585A), an estimate of present-day igneous basement depth was unavailable. The CRUST1.0 sediment thickness was less than the thickness of sediment penetrated by the DSDP expedition at that site. Sediment thicknesses nearest these sites from another reanalysis dataset, GlobSed, were also unphysically shallow (accessed through GeoMapApp, described at `www.ngdc.noaa.gov/mgg/sedthick` and in Divins, 2003; Straume et al., 2019). Therefore at 62-463, 89-585, and 89-585A, the depth of maximum drilling penetration is used as the present-day igneous basement depth for the calculation of the

depositional depth. As the subsidence curve is constrained to intersect present-day igneous basement depth in my paleodepth estimation approach, a deeper present-day igneous basement depth input yields a deeper depositional paleodepth. The present-day igneous basement depth may be deeper at 62-463, 89-585, and 89-585A: across the globe, the sediment thickness in mid-basinal open ocean areas is generally less than 2 km (`igppweb.ucsd.edu/~gabi/crust1.html`, Laske et al., 2013), which is 1 km deeper than the present-day igneous basement depth inputs used for 62-463, 89-585, and 89-585A, and therefore lowers depositional depth estimates by ∼1 km. The calculated paleodepth at 62-463, 89-585, and 89-585A is treated as a minimum depth for the Cenomanian-Turonian (Table 3.1, Figure 3.2).

For the age and depth of the sediment in question (t_{sed}, in Myr; d_{sed}, in mbsl), I determined the depth of the oldest Cenomanian, Cenomanian-Turonian boundary, and youngest Turonian sediments using biostratigraphic stage assignments in the visual core descriptions of the DSDP Initial Reports (Section 2.3), as these are the best available. I then assigned ages corresponding to the beginning of the Cenomanian (100.5 Ma), the Cenomanian-Turonian boundary (93.9 Ma), and the end of the Turonian (89.8 Ma) as determined by the International Commission on Stratigraphy (Cohen et al., 2024).

2.5 Sampling procedure

Samples (n = 305) including powder residues of samples prepared by previous workers (n = 44) were collected from the International Ocean Discovery Program Gulf Coast Repository (IODP-GCR). First, I selected intervals of core to be sampled using color photographs of cores from the Janus database (`iodp.tamu.edu/database`, Mithal and Becker, 2006) and Visual Core Descriptions (VCDs; references in Table 2.1). I prioritized intervals of core that looked likely to preserve superposition, specifically continuous pieces of core that spanned the width of the core and/or were longer than the width of the core and were therefore unlikely to have rotated within the core liner. I also prioritized intervals of core likely to have high carbonate content, based on smear slide measurements and measurements of the gas generated when a sediment sample is reacted with hydrochloric acid in a "carbonate bomb" apparatus (references in Table 2.1).

I remotely requested some samples from 89-585 and 89-585A (n = 36), and visited the IODP-GCR with an assistant in order to observe the cores firsthand and take the

rest of the samples (n = 269; Table 2.4). I directly observed and described the core sections from which most samples (n = 242) were taken, except for powder residues (Table 2.4) and some of the samples taken by IODP-GCR staff (n = 25 from 89-585 and 89-585A). Sample volumes were 3-5 cc. Samples were examined under a microscope and described (Appendix A.21).

Hole	Core length sampled (m)	Depth range sampled (mbsl)	Cores and sections observed	Total # of samples	# of powder residue samples
17-167	12.04	841.9 - 853.94	Core 60 section 1 – core 61 section 2	18	0
17-169	72.5	154.5 - 227.0	Core 7 section 1	21	8
17-170	176.9	10.1 - 187.0	Core 12 core catcher	33	32
17-171	100.98	307.37 - 408.35	Core 24 section 1 – core 32 core catcher	62	2
30-288A	96.14	818.35 - 914.49	Core 19 section 1 – core 26 core catcher	57	0
32-305	186.71	252.4 - 439.11	Core 28 section 1 – core 43 section 2	9	2
32-310A	147.0	198.0 - 345.0	Core 4 core catcher – core 18 core catcher	9	0
62-463	161.47	243.54 - 405.01	Core 29 section 1 – core 47 core catcher	48	0
89-585	46.49	513.18 - 559.67	Core 32 section 3 (archive half observed)	21	0
89-585A	48.72	504.56 - 553.28	Core 7 section 3	27	0

Table 2.4: From each hole, the core length and depth range sampled, the cores and sections I observed and described, and the number of samples including the number of powder residues. Core catchers that were not found in the repository were not among the cores and sections that were observed.

2.6 δ^{13}C and δ^{18}O measurements

2.6.1 Procedure to measure δ^{13}C, δ^{18}O, and beam area

Newly taken samples were powdered either by grinding in an agate mortar and pestle, if the sample crumbled when handled, or by micro-drilling with a carbide burr, if the sample was indurated enough not to crumble when handled. Visually identifiable indications of alteration such as veins and manganese dendrites were avoided. Powder residues of samples taken by previous workers were ground in an agate mortar and pestle to ensure they were as fine as the newly produced powders. About 0.1 to 1.8 cc of homogenized powder was produced from each sample, and aliquots of these powders were weighed on a microbalance and used for carbon and oxygen isotope analyses. In one sample (17-167-60-2-41/42), different powders collected deliberately from two visually distinct zones of the same sample were analyzed (Section 4.2). A total of 357 analyses of natural samples were performed.

First analyses of all powders used aliquots of 0.752 mg to 1.888 mg. For each analysis, the aliquot was placed into a borosilicate glass vial and heated to 90°C for ≥12 hours in order to eliminate adsorbed water and other highly volatile contaminants. Vials were then placed in a GasBox II preparation device at 85°C and flushed with helium. Phosphoric acid (8-15 drops of 100% H_3PO_4) was injected into all vials, and the reaction was allowed to proceed for ≥40 minutes to produce CO2 from the carbon in the samples. Analyses were then conducted on a Sercon 20-22 continuous flow isotope ratio mass spectrometer (CF-IRMS) at the University of Victoria. In each aliquot, isotopologues of CO_2 ($^{16}O^{12}C^{16}O$ with mass 44 amu; $^{16}O^{13}C^{16}O$, $^{17}O^{12}C^{16}O$, $^{16}O^{12}C^{17}O$ with mass 45 amu; $^{17}O^{13}C^{16}O$, $^{16}O^{13}C^{17}O$, $^{17}O^{12}C^{17}O$, $^{18}O^{12}C^{16}O$, $^{16}O^{12}C^{18}O$ with mass 46 amu) were ionized, imparting a different mass-to-charge ratio to each mass such that they separated when accelerated through a magnetic field. The abundances of the isotopologues were measured simultaneously as voltages in a Faraday-cup collector array (Systems Engineer, 2018), and δ^{13}C and δ^{18}O were calculated from the abundances following Craig (1957) (Skrzypek and Dunn, 2020). During each mass spectrometer run, the samples were measured out of stratigraphic order so that instrumental drift could not be mistaken for monotonic change over time. Replicate analyses of aliquots of standards were conducted bracketing analyses of natural samples (Table 2.5; Figure 2.2).

Because the mass spectrometer measures beams of ionized particles formed from

Name of standard	Material	Number of analyses of natural powders between replicate analyses of the standard	Accepted δ^{13}C of standard ± uncertainty if available (‰VPDB)	Accepted δ^{18}O of standard ± uncertainty if available (‰VPDB)
IAEA-603	natural marble	22 - 55	2.46 ± 0.01	-2.37 ± 0.04
IAEA-CO8	natural carbonatite	22 - 55	-5.764 ± 0.032	-22.7 ± 0.2
VTS	natural marble	2 - 5	-1.48	-8.54
UVIC-1	pure calcite	2 - 5	0.63	-9.80
UVIC-3	pure calcite	2 - 5	-4.90	-25.00

Table 2.5: Standard reference materials analyzed during mass spectrometer runs. IAEA standards are international standards supplied by the International Atomic Energy Agency. The uncertainty associated with IAEA-603 is the combined standard uncertainty from multiple independently assessed components of uncertainty (1σ-level combined standard uncertainty using a coverage factor k = 1; Fajgelj and Assonov, 2016; Working Group 1 of the Joint Committee for Guides in Metrology, 2008), and the uncertainty associated with IAEA-CO8 is the standard deviation (n = 12 for δ^{13}C and n = 13 for δ^{18}O; Stichler, 2008). UVIC-1 and UVIC-3 are standards developed at the University of Victoria and only used there. VTS was developed at Princeton University and is used there as well as at the University of Victoria.

the ionization of sample material (Harvey, 2005), the "beam area" associated with a measurement is proportional to the amount of carbonate in the aliquot that has been converted to CO_2. Beam areas in this thesis are reported as calculated by the Sercon HS20-22 Callisto software (Systems Engineer, 2018). The ratio of the beam area to the total mass of the aliquot before dissolution (beam area / sample mass ratio, in units of Coulombs per milligram or C·mg^{-1}) is used as a proxy for the sample's carbonate content.

Values of δ^{13}C and δ^{18}O were corrected for drift using the Sercon HS20-22 Callisto software (Systems Engineer, 2018) with UVIC-1 as the reference standard. Then values of δ^{13}C and δ^{18}O were normalized to the VPDB scale using a two-point calibration

(Coplen et al., 2006; Paul and Skrzypek, 2007), which requires two standards. UVIC-1 was used as the first standard and UVIC-3 was used as the second. Specifically, each isotope ratio was calculated following Equation 17 in Paul et al. (2007):

$$\delta^T = \frac{\delta_1^T - \delta_2^T}{\delta_1^M - \delta_2^M} \times \left(\delta^M - \delta_2^M\right) + \delta_2^T \tag{2.5}$$

where δ_1^T and δ_2^T are the accepted values of the first and second standard (Table 2.5), δ_1^M and δ_2^M are the average measured values of the first and second standard for the mass spectrometer run, δ^M is the measured value of the aliquot being analyzed, and δ^T is the accepted value of the aliquot being analyzed. To validate this two-point calibration, values of VTS, IAEA-603, and IAEA-CO8 were calculated as unknowns δ^T using Equation 2.5 and compared to accepted values (Section 2.6.3). All δ^{13}C and δ^{18}O values measured in this thesis are reported herein as δ^T determined according to Equation 2.5.

2.6.2 Exclusion of certain δ^{13}C and δ^{18}O analyses

During initial setup of the mass spectrometer, a range of differently sized aliquots of IAEA-603 were measured repeatedly. At beam areas $\leq 2.5 \times 10^{-8}$ C·mg^{-1}, a clear drop-off in precision and accuracy (relative to the accepted δ^{13}C and δ^{18}O values of IAEA-603; Table 2.5) was noted. Low beam area (i.e. below this "cutoff" of 2.5×10^{-8} C·mg^{-1}) may indicate low carbonate content or a leaky vial. In this thesis, analyses of standards with beam areas below this cutoff were not used to calculate or monitor δ^{13}C and δ^{18}O values. Analyses of natural samples with low beam area (n = 61) were excluded from consideration in this thesis. Larger aliquots were used for reanalysis of the sample in cases when the beam area / mass ratio of the first analysis indicated the powder had a low carbonate content, and in some cases the reanalysis had a beam area above the cutoff (n = 26).

Three analyses were excluded even though they had beam areas $\geq 2.5 \times 10^{-8}$ C·mg^{-1}, two because of concern about instrument stability immediately following analysis of a sample very rich in labile organic carbon, and one because the δ^{13}C and δ^{18}O values of the monitoring standard (VTS) at the end of the run diverged noticeably from the accepted values, so the final block of samples was excluded. This one sample was the only sample in the final block with a beam area above the cutoff (Appendix A.22). Standards associated with these two incidents were also not used to calculate or monitor δ^{13}C and δ^{18}O values of natural samples.

2.6.3 Accuracy and precision assessed using monitoring standards

Measurements of the monitoring standards VTS, IAEA-603, and IAEA-CO8 as unknowns (Figure 2.2) are compared to the accepted δ^{13}C and δ^{18}O values to assess data accuracy and precision. I also compare measured and accepted values of UVIC-3, although as UVIC-3 is the second standard used in the two-point calibration (Equation 2.5), its measured values will differ from its accepted value only as far as they differed from the average measured mean UVIC-3 value for the mass spectrometer run. Therefore UVIC-3 can be used to assess precision but not accuracy. [3] Each mass spectrometer run began with an analysis of VTS but these are excluded because they were run before the drift monitor and therefore are not corrected for drift.

Across the monitoring standards, all measured δ^{13}C values are within 0.72‰ of the accepted value, and all measured δ^{18}O values are within 1.25‰ of the accepted value (Figure 2.2). Most measured δ^{13}C and δ^{18}O values are much closer to the accepted value than this. Standard deviations of the measured δ^{13}C values are < 0.20‰ for all standards, and for each standard, the accepted δ^{13}C value is within one standard deviation of the mean measured δ^{13}C value (Table 2.6). As for δ^{18}O values, measured δ^{18}O values are less precise than measured δ^{13}C values with standard deviations of the measured δ^{18}O values between 0.20‰ and 0.41‰ (Table 2.6). However, the accuracy of measured δ^{18}O values is similar to the accuracy of measured δ^{13}C values in that for each standard, the accepted δ^{18}O value is within one standard deviation of the mean measured δ^{18}O value (Table 2.6).

[3] As UVIC-1 was the first primary standard used to correct for drift and calculate δ^{13}C and δ^{18}O values, its "measured" value always exactly matched its accepted value.

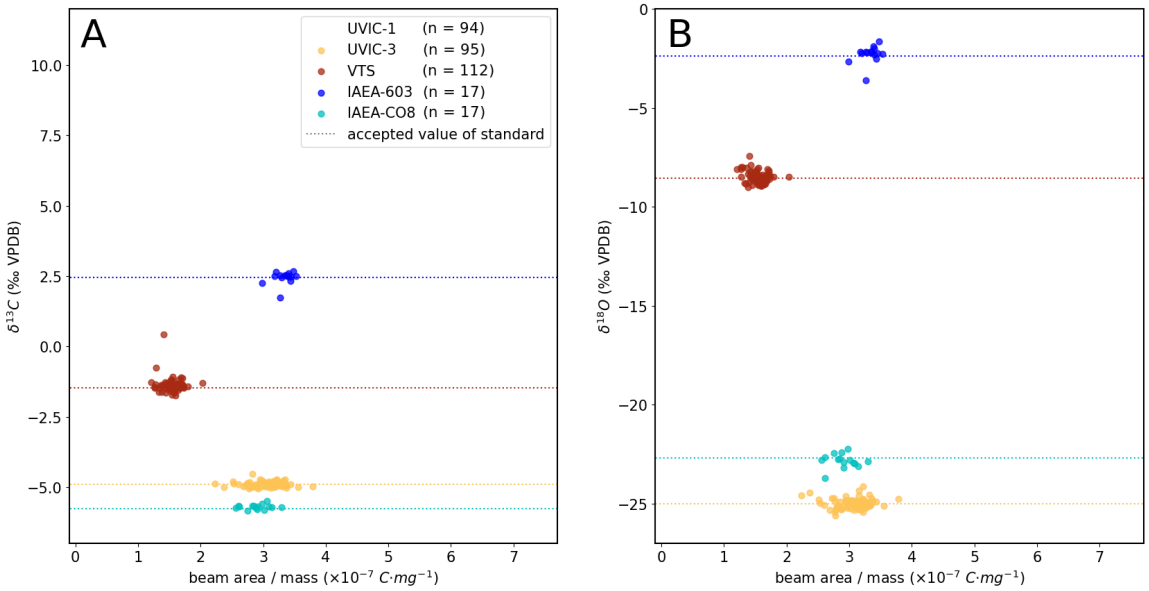

Figure 2.2: (A) Measured δ^{13}C values plotted against beam area / mass ratios of standards, with accepted δ^{13}C value of each standard plotted as a dotted line. Values of UVIC-1 are not shown because UVIC-1 was the first primary standard used to correct for drift and calculate δ^{13}C (and δ^{18}O) values, so its value was assumed to be its accepted value (see text). (B) Same for δ^{18}O.

Monitoring standard	Number of measurements	Mean measured δ^{13}C ± standard deviation (‰ VPDB)	Accepted δ^{13}C ± uncertainty if available (‰ VPDB)	Mean measured δ^{18}O ± standard deviation (‰ VPDB)	Accepted δ^{18}O ± uncertainty if available (‰ VPDB)
UVIC-3	95	-4.90 ± 0.08	-4.90	-24.99 ± 0.23	-25.00
VTS	103	-1.41 ± 0.11	-1.48	-8.57 ± 0.20	-8.54
IAEA-603	17	2.46 ± 0.20	2.46 ± 0.01	-2.25 ± 0.41	-2.37 ± 0.04
IAEA-CO8	17	-5.72 ± 0.09	-5.764 ± 0.032	-22.80 ± 0.32	-22.7 ± 0.2

Table 2.6: Measured δ^{13}C and δ^{18}O across all mass spectrometer runs in this thesis compared to accepted δ^{13}C and δ^{18}O, for UVIC-3 (the second standard used in the two-point calibration) and for monitoring standards VTS, IAEA-603, and IAEA-CO8. The uncertainty associated with IAEA-603 is the combined standard uncertainty from multiple independently assessed components of uncertainty (1σ-level combined standard uncertainty using a coverage factor k = 1; Fajgelj and Assonov, 2016; Working Group 1 of the Joint Committee for Guides in Metrology, 2008), and the uncertainty associated with IAEA-CO8 is the standard deviation (n = 12 for δ^{13}C and n = 13 for δ^{18}O; Stichler, 2008).

Of the monitoring standards, VTS was measured most frequently during each mass spectrometer run. Its measured mean δ^{13}C value is about 0.1‰ higher than the accepted δ^{13}C value for all runs except the 12 June 2023 run, for which the measured δ^{13}C value is about 0.2‰ lower than the accepted δ^{13}C value (Figure 2.3). As for δ^{18}O values, the measured mean δ^{18}O value of VTS is within 0.2‰ of the accepted δ^{18}O value for all runs except the 12 June 2023 run (Figure 2.3). The anomalous 12 June 2023 only generated 15 natural samples measurements, all from 89-585 (Appendix A.23).

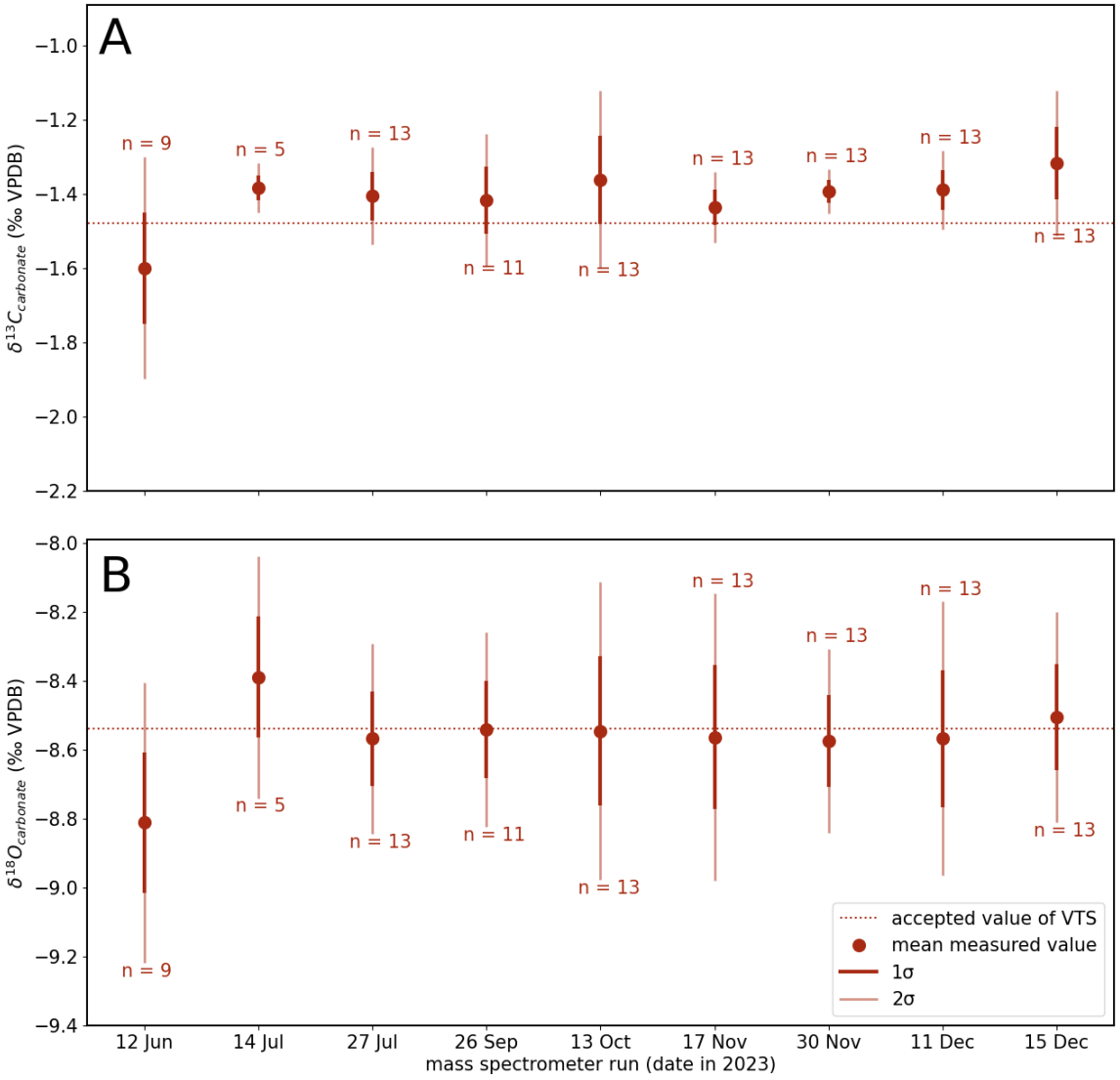

Figure 2.3: (A) For monitoring standard VTS, mean δ^{13}C value for each mass spectrometer run, with error bars showing one and two standard deviations. Dotted line shows accepted δ^{13}C value of VTS. (B) Same for δ^{18}O.

2.6.4 Precision assessed using repeated measurements of samples

Repeated measurements of natural samples were also assessed for precision. 16 natural samples were analyzed in duplicate and 1 natural sample (89-585A-7-3-96/97) was analyzed in triplicate. Here I compare 19 pairs of replicate measurements, accounting for 3 pairs from the sample with three replicates (Figure 2.4). Of the 19 pairs of replicate measurements, 17 are aliquots measured during different mass spectrometer runs, and 2 of the pairs are aliquots measured during the same mass spectrometer run as each other (17-171-29-CC, and 89-585A-7-3-96/97). Comparison of these replicates allows precision to be assessed for measurements of materials that are not pure carbonate, unlike the standards UVIC-1 and UVIC-3 (Section 2.6.2).

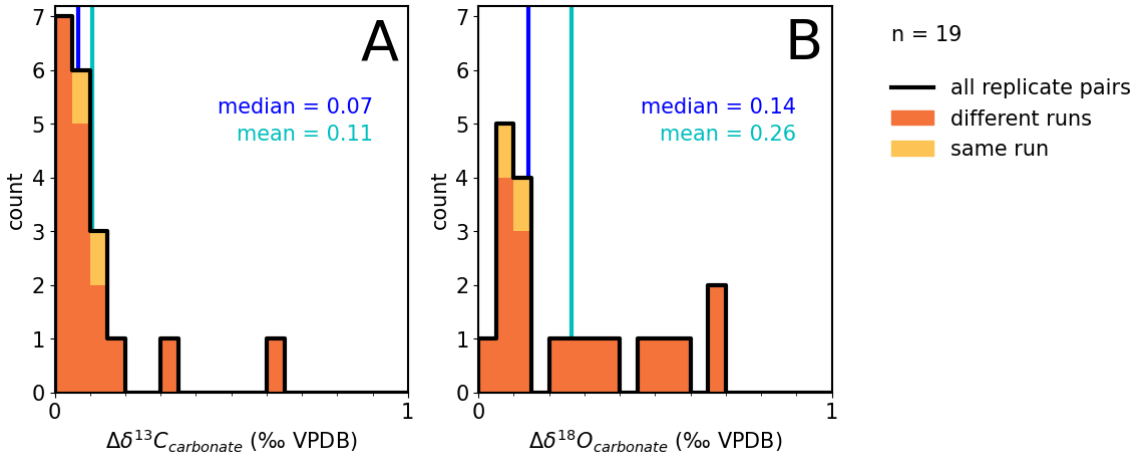

Figure 2.4: Distribution, median, and mean of differences between pairs of replicate measurements of (A) δ^{13}C ($\Delta\delta^{13}C_{carbonate}$) and (B) δ^{18}O ($\Delta\delta^{18}O_{carbonate}$) for all natural samples with replicate analyses. For the sample with three replicates, each of the three possible pairs is compared.

Overall, powders analyzed on different mass spectrometer runs yield larger differences in isotopic composition than those run on the same day. The mean difference between replicate analyses of the same natural sample for $\delta^{13}C_{carbonate}$ is 0.07‰ and for $\delta^{18}O_{carbonate}$ is 0.14‰. The median difference between replicate analyses of the same natural sample for $\delta^{13}C_{carbonate}$ is 0.11‰ and for $\delta^{18}O_{carbonate}$ is 0.26‰. The maximum difference between replicate analyses of the same natural sample for $\delta^{13}C_{carbonate}$ is 0.63‰ and for $\delta^{18}O_{carbonate}$ is 0.70‰. To calculate a standard deviation characteristic of replicate analyses for $\delta^{13}C_{carbonate}$ and $\delta^{18}O_{carbonate}$, I take the

difference between the mean value and the individual replicate value for each analysis, then take the standard deviation of these normalized replicate $\delta^{13}C_{carbonate}$ and $\delta^{18}O_{carbonate}$ values. The standard deviation of replicate analyses of natural samples for $\delta^{13}C_{carbonate}$ is 0.07‰ and for $\delta^{18}O_{carbonate}$ is 0.11‰.

2.6.5 Precision assessed using measurements from core 43 of 62-463

Material in Core 43 from 62-463 was well mixed by drilling disturbance, so $\delta^{13}C_{carbonate}$ and $\delta^{18}O_{carbonate}$ values from this core can be considered as a set of replicates and used to assess precision. Core 43 was entirely soupy when recovered (Shipboard Scientific Party, 1981b), and its archived sediment is unconsolidated and homogeneous. Subcentimeter angular fragments of chert throughout this core also indicate a high level of drilling disturbance. I took 21 samples from Core 43 which was made possible by its high recovery (68%; Figure 4.5). The $\delta^{13}C_{carbonate}$ values range from 1.75‰ to 2.03‰ with a standard deviation of 0.07‰, and the $\delta^{18}O_{carbonate}$ values range from -1.92‰ to -1.21‰ with a standard deviation of 0.15‰ (see 376.2-382.1 mbsf on Figure 4.5). The standard deviations are similar to those noted for replicate analyses in Section 2.6.4, 0.07‰ for $\delta^{13}C_{carbonate}$ and for 0.11‰ for $\delta^{18}O_{carbonate}$.

2.6.6 Summary of accuracy and precision assessments

In summary, the accuracy of $\delta^{13}C_{carbonate}$ and $\delta^{18}O_{carbonate}$ measurements in this thesis, as characterized by standards, is within 0.20‰ for most $\delta^{13}C_{carbonate}$ measurements and within 0.41‰ for most $\delta^{18}O_{carbonate}$ measurements. At its worst, accuracy is within 0.72‰ for $\delta^{13}C_{carbonate}$ and within 1.25‰ for $\delta^{18}O_{carbonate}$ (Section 2.6.3).

The precision of $\delta^{13}C_{carbonate}$ and $\delta^{18}O_{carbonate}$ measurements in this thesis is considered in terms of standard deviations of replicate measurements. Replicate $\delta^{13}C_{carbonate}$ measurements have standard deviations of 0.08 - 0.20‰ among standards, depending on the standard (Section 2.6.3), 0.07‰ among normalized replicates of samples (Section 2.6.4), and 0.07‰ among samples from Core 43 of 62-463 (Section 2.6.5). Replicate $\delta^{18}O_{carbonate}$ measurements have standard deviations of 0.20 - 0.41‰ for the standards (Section 2.6.3), 0.11‰ for samples (Section 2.6.4), and 0.15‰ for Core 43 of 62-463 (Section 2.6.5). If the $\delta^{13}C_{carbonate}$ and $\delta^{18}O_{carbonate}$ measurements in all these populations are normalized to the mean of the sample from

which they were taken (as in Section 2.6.4), the aggregate population (n = 288) has a $\delta^{13}C_{carbonate}$ standard deviation of 0.08‰ and a $\delta^{18}O_{carbonate}$ standard deviation of 0.16‰.

Study sites

3.1 Selection of sites

Carbonaceous sediments of OAE2 age, deposited in the open-ocean Pacific, can be used to test the hypothesis that there was a global change in the $\delta^{13}C_{DIC}$ of seawater at OAE2 time (Section 1.6). Of all scientific ocean drilling holes through IODP Expedition 312, 283 holes drilled in the Pacific are located on crust estimated to be near OAE2 age (compilation accessed through GeoMapApp; `www.geomapapp.org`). Although OAE2 occurred at ∼93.9 Ma (Cramer and Jarvis, 2020; Gale et al., 2020), I investigated all holes on crust of estimated age 93 Ma or older in case of uncertainty in the crustal age model used in GeoMapApp. Of these 283 holes, 29 have sediments dated to the Cenomanian and/or Turonian. I decided not to consider sampling 9 of these 29 holes due to uncertain biostratigraphy and/or a low proportion or absence of carbonate content (Table A.3).

The remaining 19 holes were ranked based on recovery rate, carbonate content, detail of the biostratigraphy, reports of black shale at or near the Cenomanian-Turonian boundary, and/or inclusion in previous literature on OAE2 (Thiede et al., 1982; Schlanger et al., 1987; Owens et al., 2018). I sampled sediments from the 10 top holes from this ranking and they are the focus of this thesis (Figure 3.1).

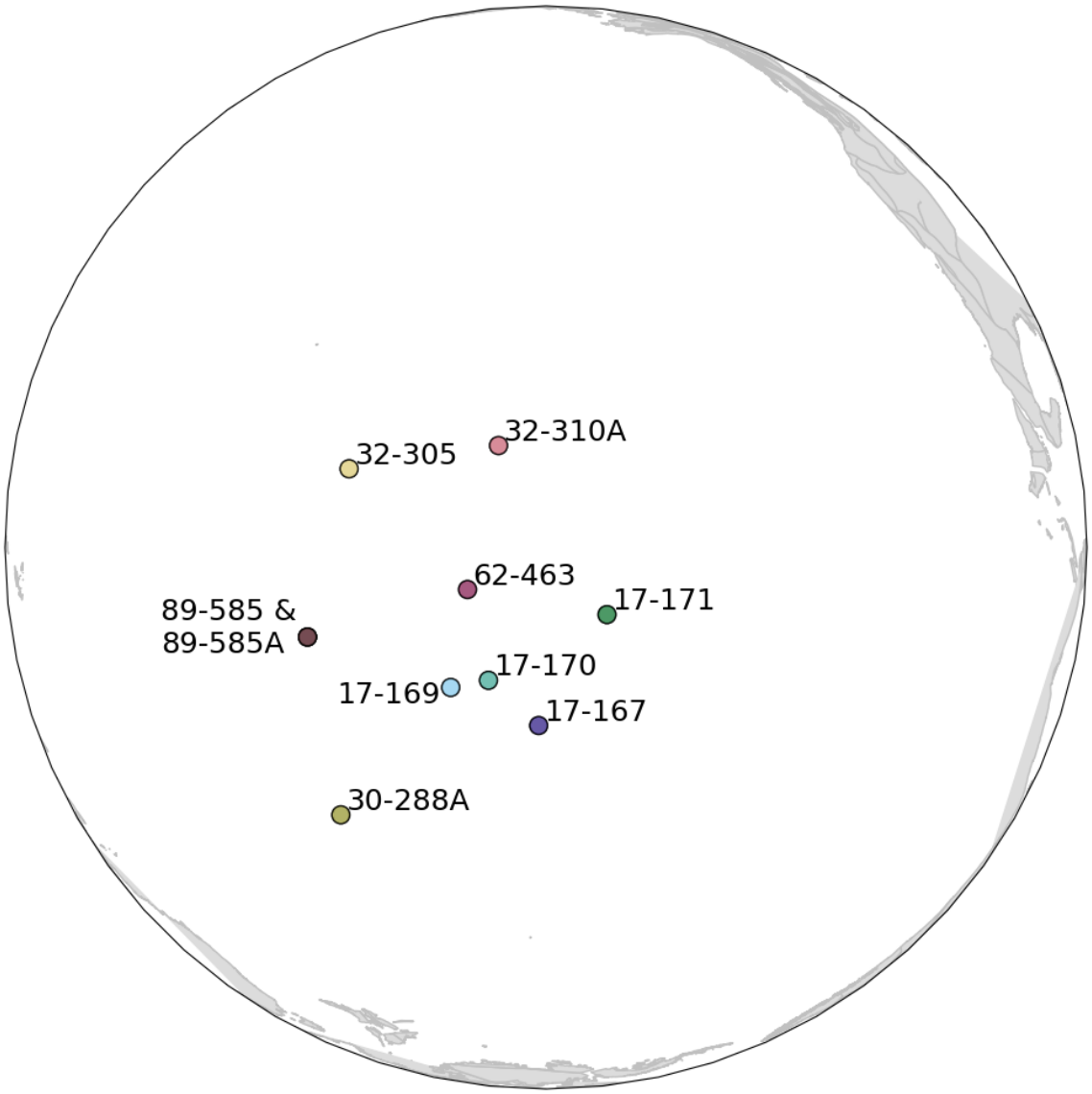

Figure 3.1: Paleomap of the Pacific Ocean at 93.9 Ma with central longitude of 140°W, showing the locations of the 10 DSDP holes that are the focus of this thesis. Paleogeography from Müller et al. (2019).

3.2 Paleodepth and depositional setting of Pacific sites in this thesis

I sort the Pacific sites in this thesis into three groups based on their paleodepth. The term "paleodepth" is used in the remainder of the text to mean "Cenomanian-Turonian estimated paleodepth." Paleodepths of sites were estimated as described in Section 2.4 (Appendix A.24; Table 3.1, Figure 3.2). It is important to consider whether a site was above or below the carbonate compensation depth (CCD; Section 1.1) around the time of OAE2, as the presence of carbonate at sites thought to be below the CCD requires explanation. Reconstruction of the global CCD during the Cretaceous period suggests it was about ∼3500 mbsl (Tyrrell and Zeebe, 2004; Zeebe and Tyrrell, 2019), while reconstruction specific to the equatorial Pacific region suggests it was shallower, about ∼3000 mbsl (Pälike et al., 2012; Zeebe and Tyrrell, 2019). I also consider the role of depositional setting of the sites (e.g. location on a structural high) when describing each paleodepth group. Seismic profiles and bathymetric maps (Appendix A.25) were used to determine the depositional setting of each site (Table 3.2, Figure 3.3).

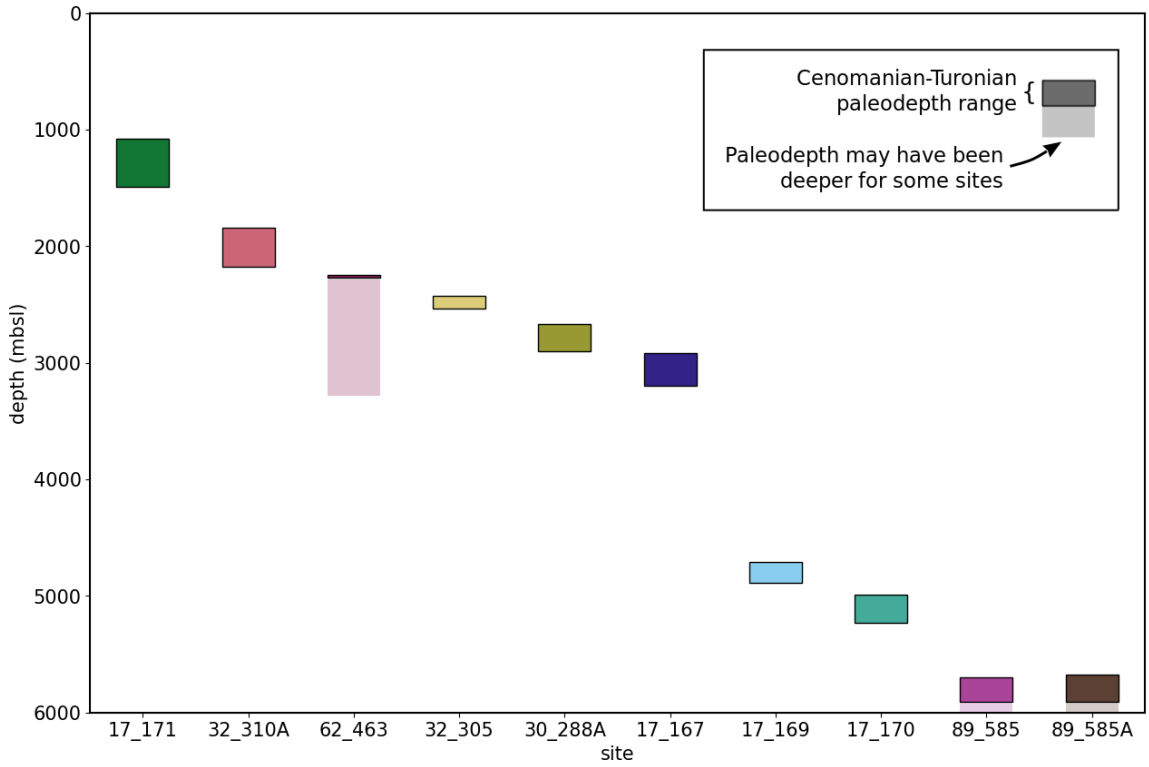

Figure 3.2: Estimated paleodepths for all Pacific sites in this thesis during the Cenomanian and Turonian. For each site the estimated Cenomanian-Turonian paleodepth range (colored block) is shown. At sites where the estimated paleodepth range is a minimum an extended colored block in a lighter color indicates that the site may have been deeper if the crustal depth is deeper (with results shown for crustal depth as deep as 2000 mbsf; see Section 2.4).

Group	Hole(s)	Present-day depth (mbsl)	Estimated paleodepth of Cenomanian-Turonian boundary (mbsl)	Estimated paleodepth during the Cenomanian-Turonian (mbsl)
shallow (<1500 mbsl)	17-171	2295	1380	1075 - 1489
intermediate (1500 - 3500 mbsl)	32-310A	3516	2093	1841 - 2179
	62-463	2525	2334*	2273 - 2334*
	32-305	2903	2540	2423 - 2540
	30-288A	3000	2850	2663 - 2904
	17-167	3176	3102	2920 - 3199
deep (> 4500 mbsl)	17-169	5415	4835	4712 - 4891
	17-170	5792	5145	4988 - 5232
	89-585	6109	5835*	5695 - 5906*
	89-585A	6109	5845*	5675 - 5905*

* Neither a measurement of crustal depth nor a model estimate consistent with penetration depth of drilling is available for this site. The paleodepth estimates are therefore a minimum and the actual Cenomanian-Turonian paleodepth range for this site may have been deeper (Section 2.4).

Table 3.1: The present-day depth, estimated depth of the Cenomanian-Turonian boundary, estimated paleodepth range during the Cenomanian, and estimated paleodepth for the Turonian for all Pacific sites included in this thesis.

Hole(s)	Present-day depositional setting
17-171	"Horizon Guyot, on a saddle between eastern and western summits"
32-310A	atop Hess Rise
62-463	"Mid-Pacific Mountains along the western arm"
32-305	south side of Shatsky Rise, "where the basement and sea floor begin to slope off the south side of the rise" ("just beyond the south edge" of "a channel-like feature about 150 meters deep and 15-20 km wide that is not apparent on other profiles")
30-288A	"on the southeastern flank of the Ontong-Java Plateau"
17-167	atop Magellan Rise
17-169	west area of Central Pacific basin, on the basin floor ("about 300 km east of Mejit Island in the Marshall Island Chain")
17-170	northwest area of Central Pacific basin, on the basin floor
89-585 and 89-585A	"in the East Mariana Basin surrounded on three sides by numerous seamounts," on the basin floor ("abyssal plain of the Mariana Basin")

Table 3.2: Summary of the depositional settings (i.e. locations on topographic highs or in basins) of Pacific sites in this thesis. Quotations are from the DSDP Initial Report corresponding to the site (Table 2.1).

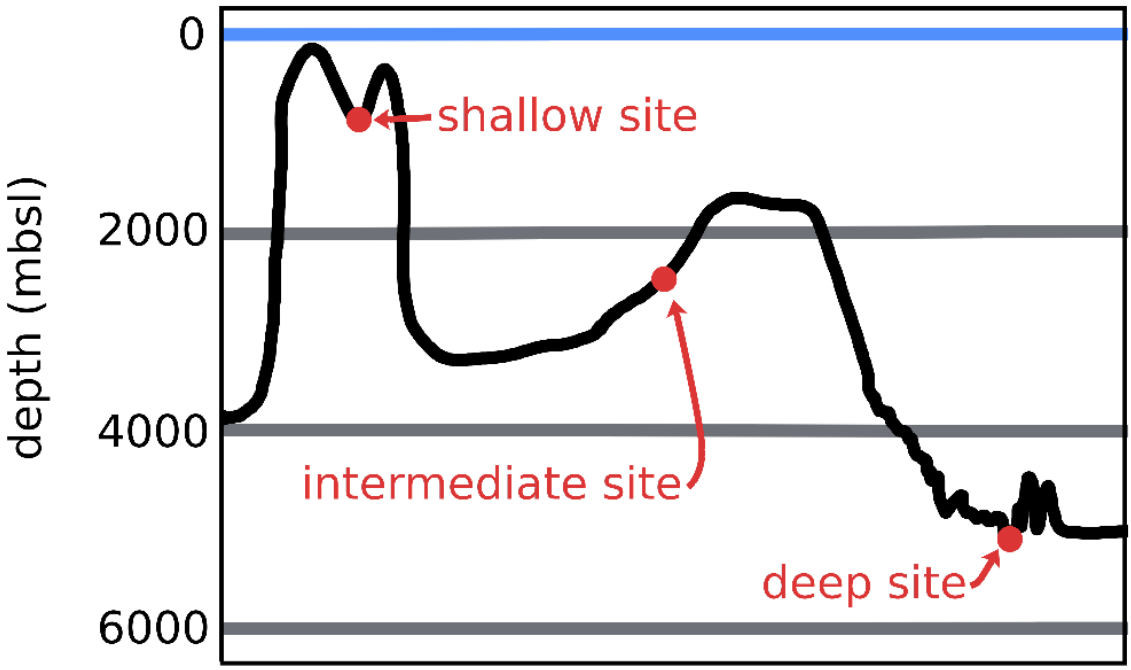

Figure 3.3: Cartoon giving examples of the paleodepths and depositional settings of the shallow, intermediate, and deep groups into which Pacific sites have been sorted. Sea surface (blue), seafloor (black), and example site locations (red) are shown.

The first group (the "shallow" group) has estimated Cenomanian-Turonian paleodepths of < 1500 mbsl and includes only 17-171. Aside from being the shallowest site, 17-171 is placed in its own group because it has shallow-water mollusc molds and/or algae fragments in cores indicated by biostratigraphy to be from the Cenomanian or Turonian (334 to 479 mbsl; Shipboard Scientific Party, 1973e). These materials are interpreted to indicate shallow-water carbonate formation in a lagoon on a nearby island, followed by transportation of the carbonate to the site in a debris flow downslope (Shipboard Scientific Party, 1973e). Therefore 17-171 sediment may originate from a very shallow, semi-restricted environment such as a carbonate platform. In support of this interpretation, 17-171 lies between two summits of the topographic high Horizon Guyot, and in the present-day these summits are $\sim$ 1100 m above the sediments at 17-171 that contain shallow-water material (Table 3.2; Shipboard Scientific Party, 1973e). The possibility that these summits may have been very shallow or above water in Cenomanian-Turonian time is consistent with the paleodepth range of 1075 - 1489 mbsl estimated for 17-171 (Table 3.1).

The second group (the "intermediate" group) has estimated Cenomanian-Turonian paleodepths of 1800 - 3200 mbsl (32-310A, 62-463, 32-305, 30-288A, 17-167; Table 3.1, Figure 3.2). The sites in this group lie on the tops and flanks of mid-basinal topographic highs (Hess Rise, Mid-Pacific Mountains, Shatsky Rise, Ontong-Java Plateau; Table 3.2). They were likely located above the CCD, thought to have been 3000 - 4000 mbsl during the Cretaceous (Tyrrell and Zeebe, 2004; Zeebe and Tyrrell, 2019), and carbonate sediments accumulated during the Cenomanian-Turonian at the sites are consistent with an intermediate paleodepth above the CCD. For example, carbonate sediments accumulated during the Cenomanian-Turonian at 62-463 include abundant calcareous nannoplankton and well-preserved foraminifera shells and no more than 5-10% clay content (Shipboard Scientific Party, 1981b; Timofeev et al., 1981). 32-310A, which has an estimated Cenomanian-Turonian paleodepth lying between the ranges of the other sites in the "intermediate group" and the "shallow" range of 17-171, is placed in the "intermediate" group because of its depositional setting on the flank of the Hess Rise (Shipboard Scientific Party, 1975e). Also, 32-310A sediments lack material apparently derived from very shallow areas like the material observed at 17-171.

The third group (the "deep" group) has estimated Cenomanian-Turonian paleodepths of > 4500 mbsl (17-169, 17-170, 89-585 and 89-585A; Table 3.1, Figure 3.2). The sites in this group lie on the abyssal plains of ocean basins (Table 3.2). Because

these sites are likely below the carbonate compensation depth (Tyrrell and Zeebe, 2004; Zeebe and Tyrrell, 2019), the presence of carbonate sediments at these sites requires explanation. In this thesis their carbonate sediments are assumed to be sourced from adjacent topographic highs and subsequently buried before the carbonate could completely dissolve. Relatively high mid-Cretaceous sediment accumulation rates of ∼4 m/Myr at 17-169 and 17-170 (Shipboard Scientific Party, 1973c,d) are consistent with this scenario. At 89-585 and 89-585A, a "pulse" of sedimentation with a rate of 5-10 m/Myr is thought to have occurred in the middle Cenomanian to Turonian, with an unconformity noted below and a period of reduced sedimentation above (Shipboard Scientific Party, 1986). Also at 89-585 and 89-585A, turbidites are noted in middle Albian to Campanian sediments, corroborating the expectation that the sediments are redeposited (Shipboard Scientific Party, 1986). 89-585 and 89-585A are adjacent to topographic highs on three sides (Table 3.2; Shipboard Scientific Party, 1986). These highs have flat tops ∼4000 m above 89-585 and 89-585A and are within 50-100 km of 89-585 and 89-585A (Ryan et al., 2009). Beginning in the Cenomanian, the sediments at 89-585 and 89-585A lack coarse-grained shallow-water debris that is present in older sediments, and contain foraminifera species thought to live at intermediate depths (1000-4000 mbsl), so intermediate-depth topographic highs 50-100 km away are the likely source of Cenomanian and Turonian sediments at 89-585 and 89-585A (Shipboard Scientific Party, 1986).

At 17-169 and 17-170, the source of carbonate must have been more distant. There is no area of seafloor more than 500 m above the present-day site depth within a 100 km radius around either 17-169 or 17-170, i.e. neither site is adjacent to any notable topographic highs (Ryan et al., 2009). The nearest topographic highs to 17-169 and 17-170 are ∼160 and ∼120 km away respectively (Ryan et al., 2009), as opposed to 50-100 km away at 89-585 and 89-585A. Carbonate sediment could have reached 17-169 and 17-170 from these highs via turbidites, which can travel hundreds of kilometers in the deep ocean (Leeder, 2011). In Campanian sediments at 17-170, some reworked older foraminifera are noted, corroborating the expectation that redeposited sediments reached the site in mid-late Cretaceous time (Shipboard Scientific Party, 1973d). Therefore intermediate-depth topographic highs (∼4000 m above 17-169 and 17-170) are the likely source of carbonate sediments at 17-169 and 17-170 during Cenomanian and Turonian time.

3.3 Paleogeography and paleoenvironment of selected sites outside the Pacific

Compared to Pacific sites, non-Pacific sites discussed in this thesis (Figure 1.7) were located in shallower and potentially more restricted areas of the world ocean. According to paleogeographic reconstructions, Eastbourne, Clot Chevalier, and Pont d'Issole (North Atlantic and Western Tethys sites) were located within ∼1000 km of each other in connected, relatively shallow epicontinental basins. Eastbourne was located in the epicontinental Anglo-Paris Basin, connected to a young, narrow North Atlantic via the present-day English Channel (Figure A.5; Roth, 1986; Leary and Peryt, 1991). Clot Chevalier and Pont d'Issole were in the epicontinental Vocontian Basin (Grosheny et al., 2006; Jarvis et al., 2011), adjacent to the channels connecting the Western Tethys to the North Atlantic (Figure A.5; Philip et al., 2000b; Falzoni et al., 2016). Eastbourne was ∼1000 km northwest of Clot Chevalier and Pont d'Issole, with a shallow marine seaway between (Figure A.5; Philip et al., 2000b; Jarvis et al., 2011). Accumulation of turbiditic marine sediments in this seaway from the late Cenomanian supports the interpretation that Eastbourne was well connected to the Western Tethys (Philip et al., 2000a), as it attests that a seaway deep enough to produce turbidites existed between Eastbourne and Western Tethys sites. Further to the south, paleogeographic reconstructions locate wadi Bahloul on a wide continental shelf (the Saharian Platform) on the margin of Africa (Caron et al., 2006; Gabtni et al., 2013), with a deep marine channel lying between this site and Eastbourne, Clot Chevalier, and Pont d'Issole (Philip et al., 2000b). Gongzha in the Neotethys was located in a different region of the world ocean altogether (Figure 1.7), on the margin of the Indian continent (Willems et al., 1996).

Paleogeographic reconstructions of the depositional settings of these non-Pacific sites are corroborated by observations of the sections. Sediments at these sites have pelagic biogenic components (e.g. foraminifera) as well as components derived from shallow and terrestrial environments (e.g. detrital quartz; Table A.4 and references therein). This combination is typical for marine sediments that accumulate near land, along the margins of continents. Also, some carbonaceous sediments at certain sites are interpreted to be sourced from shallow shelf or platform areas. For example, a shallow marine platform (∼50-70 m deep) to the east of Eastbourne (∼100 km away) is thought to have contributed sediment to the site in Turonian time (Gale, 1996; Philip et al., 2000b; Jarvis et al., 2011).

As they were deposited close to land or shallow shelf or platform areas, the non-Pacific sediments examined in this thesis were likely deposited at much shallower depths than the depositional depth of the Pacific sites estimated in Section 3.2. The same quantitative approach to paleodepth estimation (Section 2.4) cannot be used because it assumes that the only process changing the depth of the site since sediment deposition has been subsidence of ocean crust, and the non-Pacific sites are on continental crust. Because the non-Pacific sections were deposited in marine environments at ∼93.9 Ma but are today found as subaerial outcrops, they must have undergone tectonic uplift or sea level must have fallen. Paleodepth estimates made with other methods are not available for most of the sites. The basin where Clot Chevalier and Pont d'Issole are located (the Vocontian Basin) was likely no more than a few hundred meters deep during the early Cretaceous, based on dinoflagellate cyst distribution (Wilpshaar and Leereveld, 1994). At wadi Bahloul and Gongzha, sediments are interpreted by past authors to have been deposited in marine continental slope environments (Maamouri et al., 1994; Willems et al., 1996; Li et al., 2006; Bomou et al., 2013). In the modern ocean, the depth of continental slopes is between ∼100 and ∼3000 mbsl (Scarselli, 2020), and wadi Bahloul and Gongzha may have been in this depth range.

Results

4.1 Overview of beam area / mass ratios, $\delta^{13}C_{carbonate}$ values, and $\delta^{18}O_{carbonate}$ values

In this thesis I measured the $\delta^{13}C_{carbonate}$ and $\delta^{18}O_{carbonate}$ values of 274 samples successfully (i.e. analyses of these samples were not excluded for low beam area or another reason; Section 2.6.2). Samples with very low carbonate content (n = 16, 6% of successfully measured samples from this thesis) are not considered together with the majority of the data. Specifically, these samples required aliquots of 9.762 - 47.892 mg of powder to yield a beam area above the cutoff (Section 2.6.2; Figure A.4), much larger than the aliquot sizes for which the mass spectrometer was calibrated. The $\delta^{13}C_{carbonate}$ and $\delta^{18}O_{carbonate}$ distributions of these low-carbonate samples are broadly similar to the $\delta^{13}C_{carbonate}$ and $\delta^{18}O_{carbonate}$ distributions of the rest of the data, except that the low-carbonate samples account for 6 outlier $\delta^{13}C_{carbonate}$ values and 4 outlier $\delta^{18}O_{carbonate}$ (Figure 4.1). The following discussion concerns the remaining samples (n = 258), which were measured using aliquots of 0.767 - 1.888 mg.

Among the samples with aliquot sizes 0.767 - 1.888 mg, there are 3 samples with negative $\delta^{13}C_{carbonate}$ values, noticeably lower than the rest of the $\delta^{13}C_{carbonate}$ values (Figure 4.1). These samples appear in the same core within a 7-cm interval (89-585A-7-3 96-97cm, 97-98 cm, and 102-103 cm) and have $\delta^{13}C_{carbonate}$ values -2.70‰, -2.49‰, and -2.47‰ respectively. It is unlikely that these $\delta^{13}C_{carbonate}$ values are explained by the same processes controlling the $\delta^{13}C_{carbonate}$ values of the rest of the samples. Therefore, I do not consider these samples in the discussion that follows. (They are discussed in Appendix A.22).

Bulk $\delta^{13}C_{carbonate}$ and $\delta^{18}O_{carbonate}$ values from Pacific sites are similar to $\delta^{13}C_{DIC}$ and $\delta^{18}O_{seawater}$ values measured in the modern ocean. The bulk $\delta^{13}C_{carbonate}$ and $\delta^{18}O_{carbonate}$ values considered here include those measured in this thesis (n = 255) as well as some (n = 13) measured by previous authors from the same Pacific sites (Table A.5; Coplen and Schlanger, 1973; Douglas and Savin, 1973; Price et al., 1998).

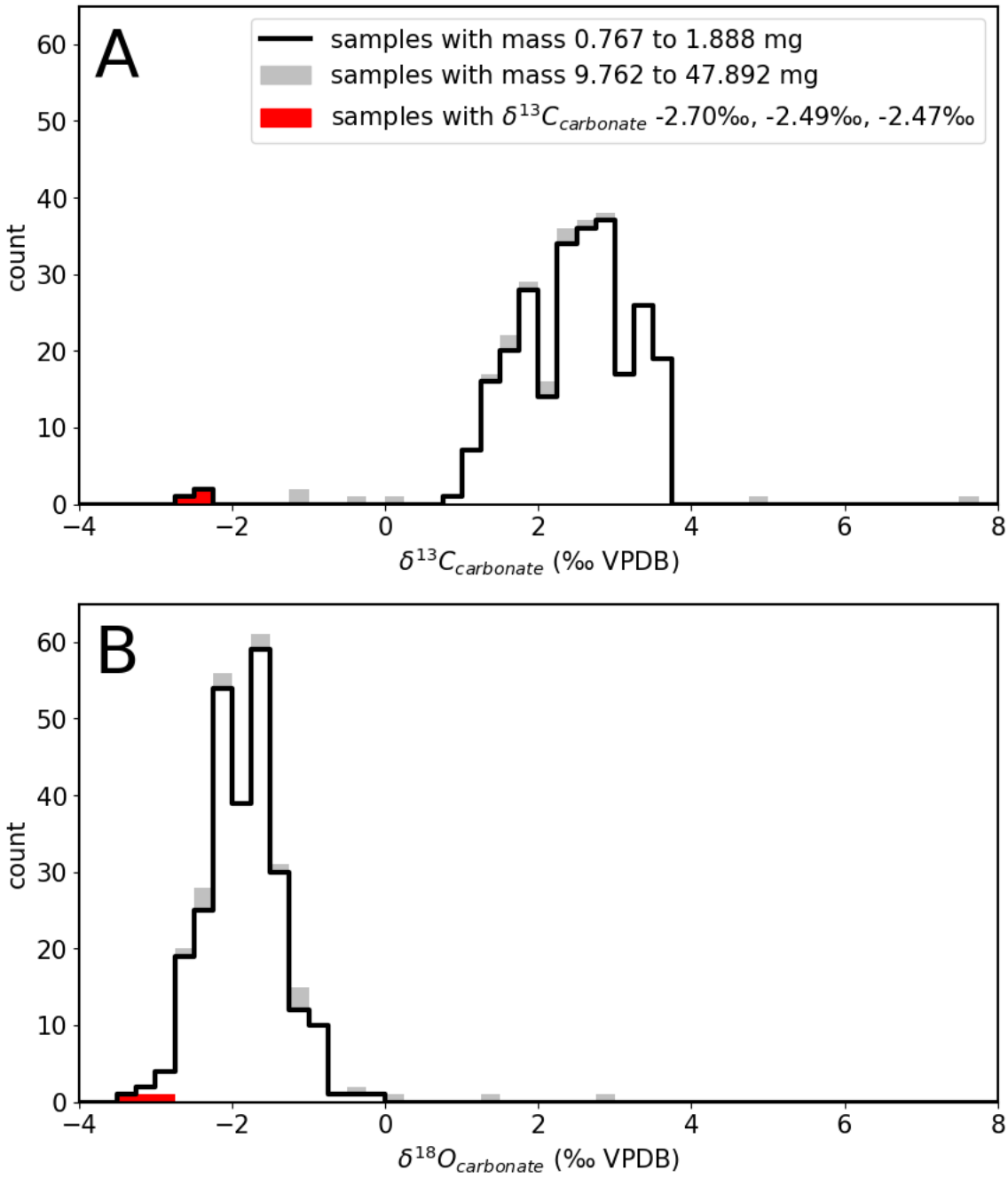

Figure 4.1: Histograms of the δ^{13}C and δ^{18}O values of Pacific bulk carbonate data collected in this thesis.

In this dataset, Pacific bulk $\delta^{13}C_{carbonate}$ values have a minimum value of 0.88‰ (this thesis) and a maximum value of 4.20‰ (Coplen and Schlanger, 1973) for a range of 3.32‰. Pacific bulk $\delta^{18}O_{carbonate}$ values have a minimum value of -3.08‰ and a

maximum value of -0.22‰ (both from this thesis) for a range of 2.86‰.

4.2 Sediments, $\delta^{13}C_{carbonate}$ values, and $\delta^{18}O_{carbonate}$ values of each Pacific site in this thesis

Table 4.1 summarizes the $\delta^{13}C_{carbonate}$ values at each Pacific site in this thesis.

Hole	$\delta^{13}C_{carbonate}$ minimum (‰VPDB)	$\delta^{13}C_{carbonate}$ maximum (‰VPDB)	$\delta^{13}C_{carbonate}$ range (‰VPDB)
17-171	0.88	3.66	2.78
32-310A	1.82	2.91	1.09
62-463	1.41	3.19	1.78
32-305	1.61	2.94	1.33
30-288A	2.28	3.54	1.26
17-167	2.53	4.20	1.67
17-169	3.07	3.55	0.48
17-170	1.97	3.16	1.19
89-585	1.31	2.61	1.30
89-585A	1.59	2.93	1.34

Table 4.1: The $\delta^{13}C_{carbonate}$ minimum, maximum, and range for all Pacific holes included in this thesis, excluding the 16 samples with oversize aliquots and the 3 samples with $\delta^{13}C_{carbonate}$ values between -2.5 and -2.7‰ at 89-585A (see text). Holes are in order of estimated paleodepth from shallowest to deepest.

In one sample (17-167-60-2-41/42), two visually distinct zones were micro-drilled and analyzed separately (Section 2.6.1). The zones of the sample have distinct shades (light vs. dark, Figure A.3) and very different beam area / mass ratios of 3.1 $\times$ 10^{-7} C·mg^{-1} vs. 0.6 $\times$ 10^{-7} C·mg^{-1}, suggesting that the carbonate content of the light zone is substantially higher than the carbonate content of the dark zone. The two zones also have slightly different $\delta^{13}C$ values of 3.26‰ (light) vs. 3.79‰ (dark).

Figure 4.2 is a legend for the stratigraphic columns showing the lithologies at all Pacific sites in this thesis (Figures 4.3 - 4.12). The calcareous lithologies carbonate ooze, chalk, and limestone are distinguished by their degree of induration when they

are brought shipboard. A carbonate ooze can be deformed by a finger or the flat of a spatula, a chalk is more indurated than an ooze but can be deformed by a fingernail or spatula edge, and a limestone is more indurated than an ooze or chalk (Winterer, 1973).

In Figure 4.3 through Figure 4.12, geologic stage names are noted on the left-most panels of the figures (determined as described in Section 2.4). Note that if I examine only sediments that could have Cenomanian and/or Turonian age based on biostratigraphy, some samples are excluded (2 samples at 32-310A, 9 samples at 32-305, 3 samples at 17-167, 1 sample at 17-169, 23 samples at 17-170, and 1 sample at 89-585A), but interpretations are not affected.

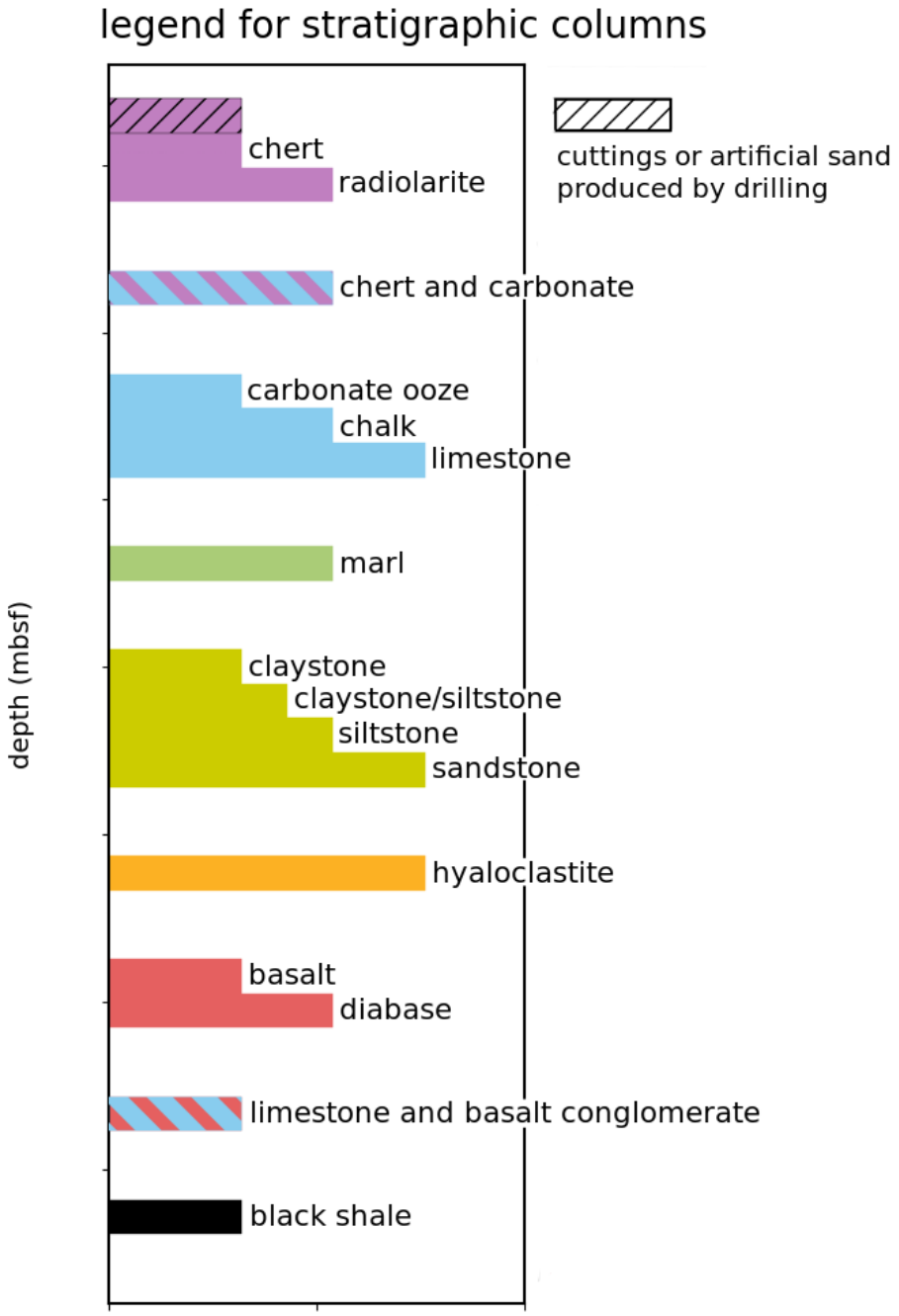

Figure 4.2: Stratigraphic column legend showing the lithologies depicted in stratigraphic columns of Figures 4.3 - 4.12. Generally, chert lithologies are purple; carbonate lithologies are blue; siliciclastic lithologies are yellow; volcanic lithologies are red.

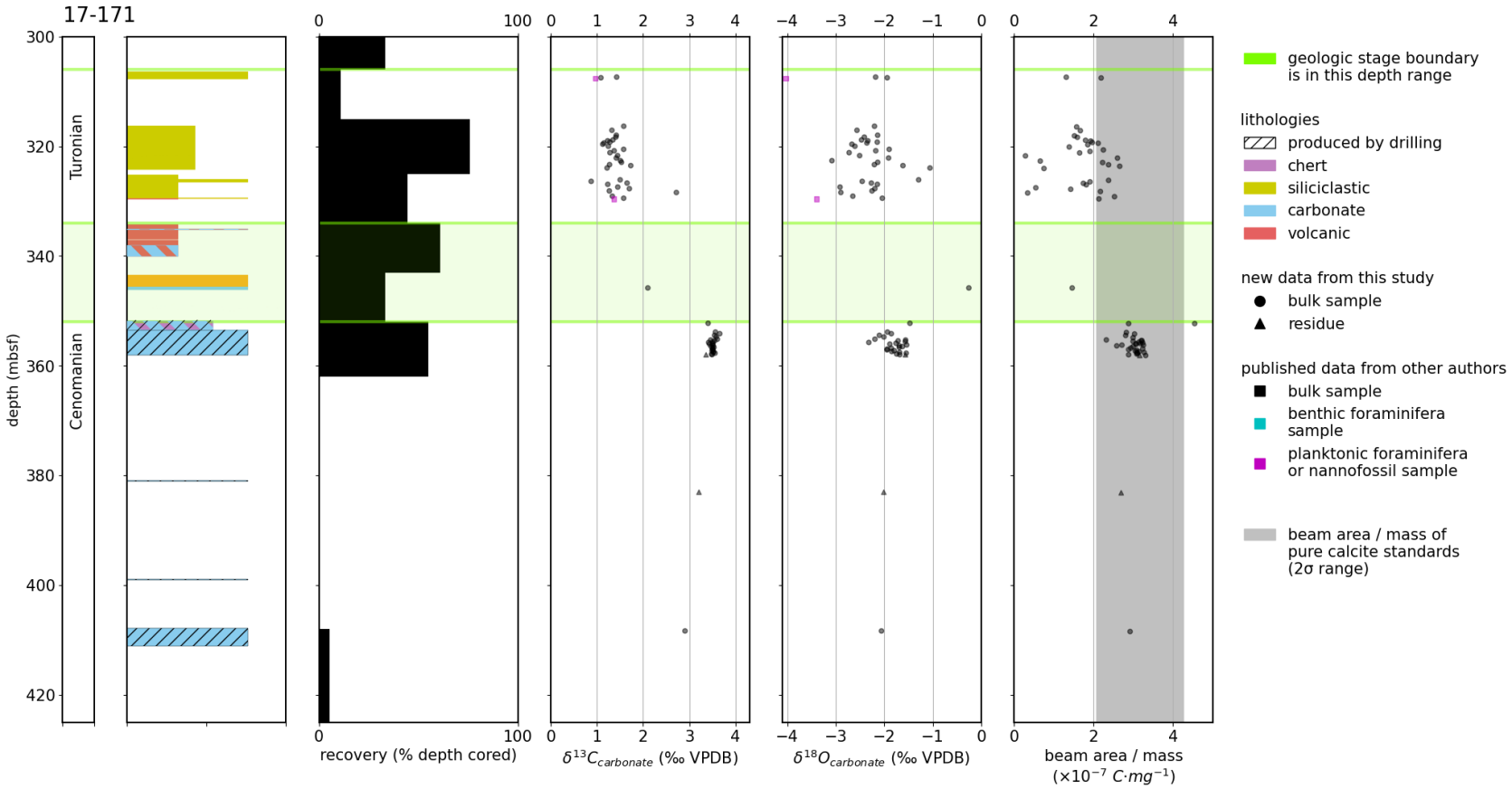

Figure 4.3: Stratigraphic column of 17-171, including geologic stage assignments based on biostratigraphy, lithologies of recovered sediments, proportion of sediment recovered relative to depth cored, $\delta^{13}C_{carbonate}$ and $\delta^{18}O_{carbonate}$ values of samples, and beam area / mass ratios of samples.

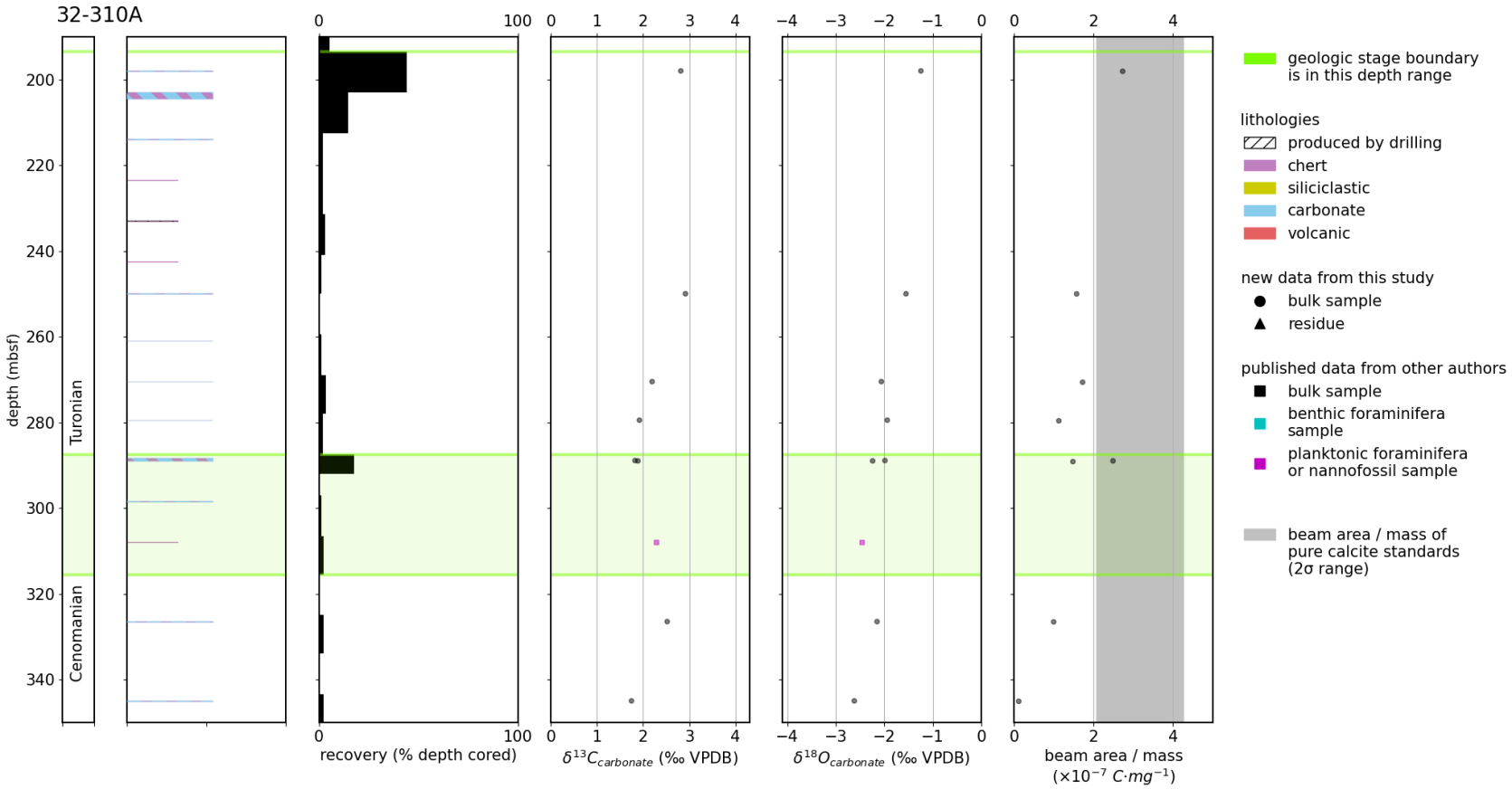

Figure 4.4: Stratigraphic column of 32-310A, including geologic stage assignments based on biostratigraphy, lithologies of recovered sediments, proportion of sediment recovered relative to depth cored, $\delta^{13}C_{carbonate}$ and $\delta^{18}O_{carbonate}$ values of samples, and beam area / mass ratios of samples.

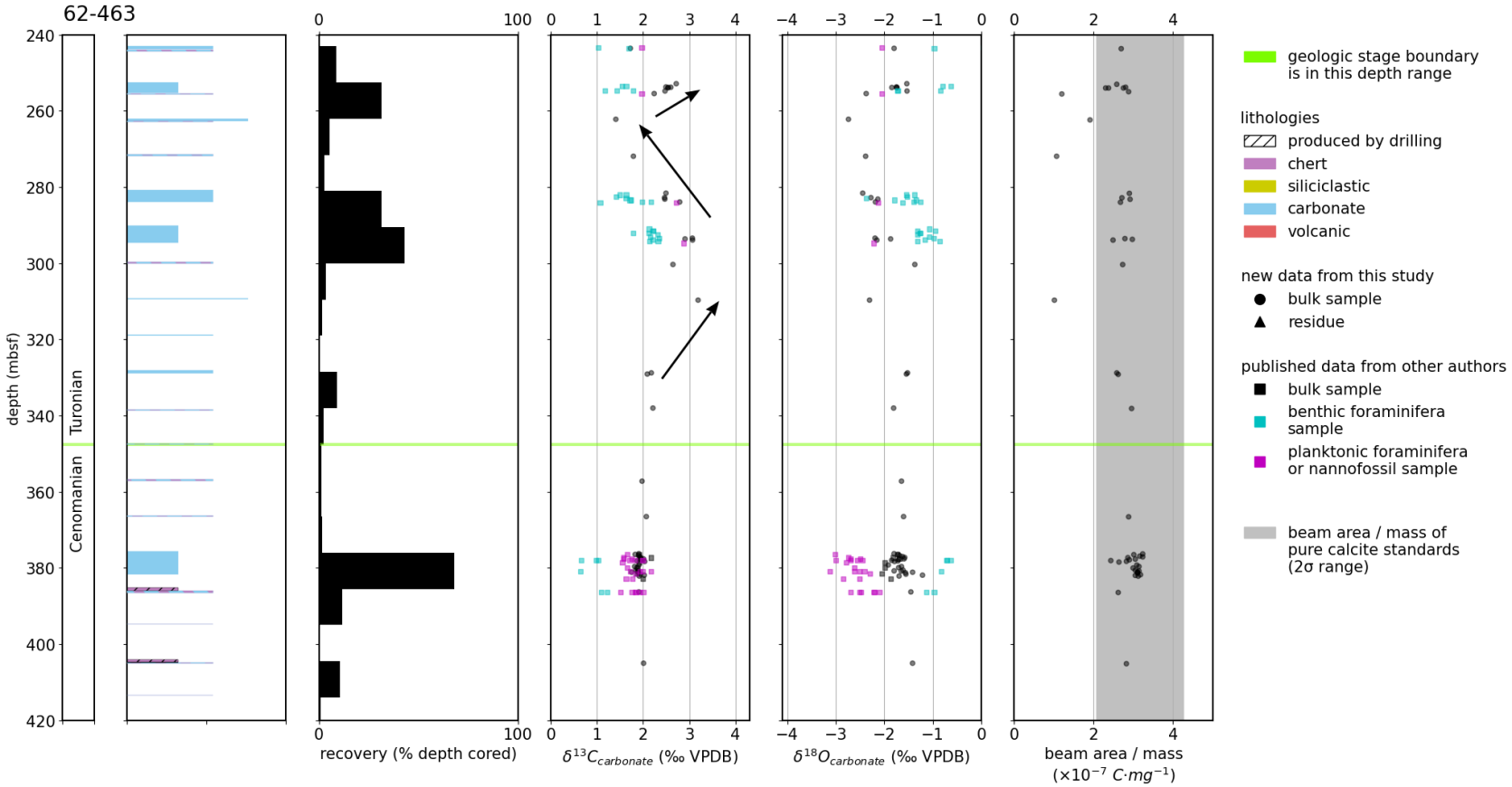

Figure 4.5: Stratigraphic column of 62-463, including geologic stage assignments based on biostratigraphy, lithologies of recovered sediments, proportion of sediment recovered relative to depth cored, $\delta^{13}C_{carbonate}$ and $\delta^{18}O_{carbonate}$ values of samples, and beam area / mass ratios of samples. Arrows show changes in $\delta^{13}C_{carbonate}$ values discussed in Section 5.1.2.2.

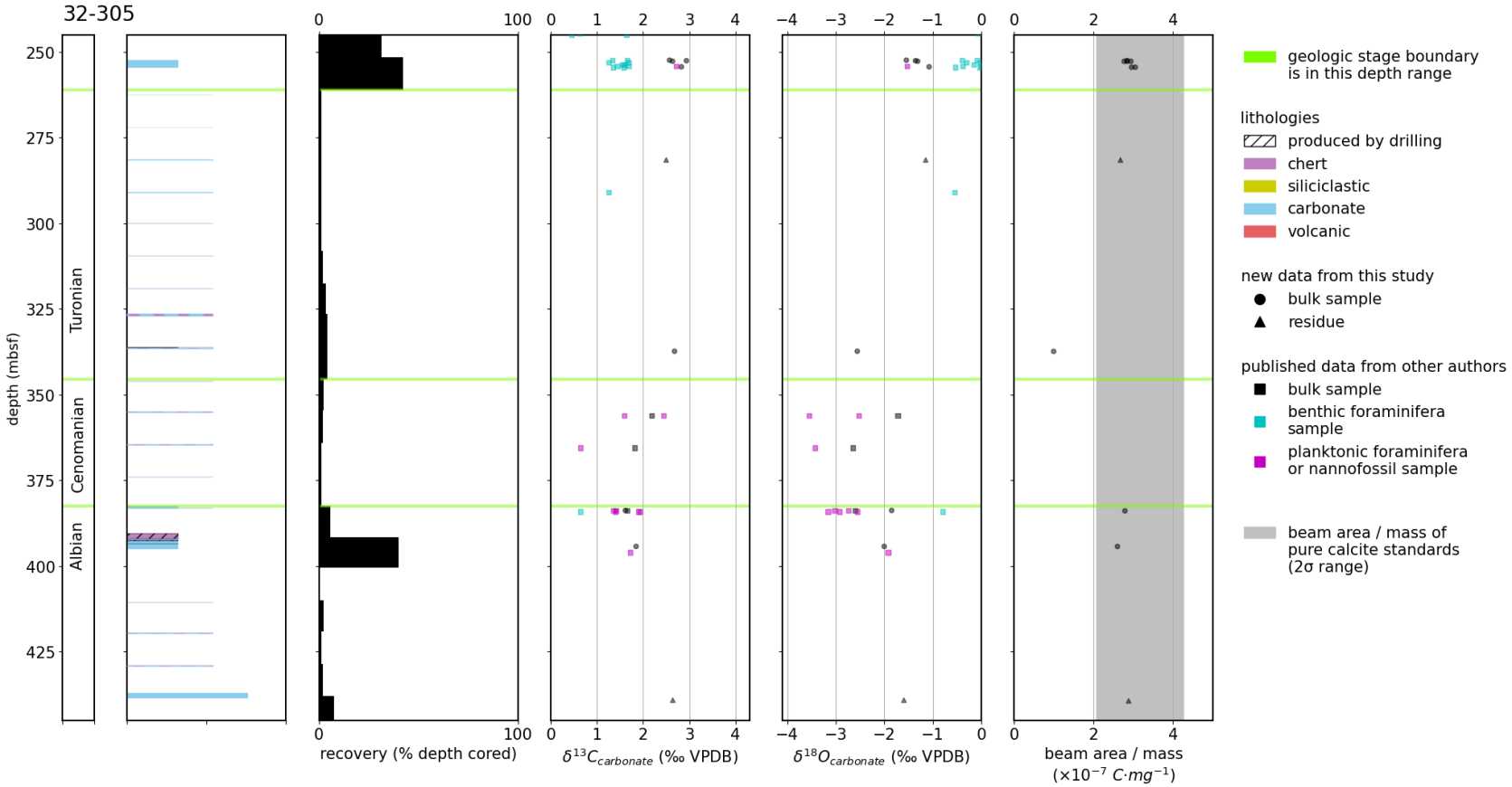

Figure 4.6: Stratigraphic column of 32-305, including geologic stage assignments based on biostratigraphy, lithologies of recovered sediments, proportion of sediment recovered relative to depth cored, $\delta^{13}C_{carbonate}$ and $\delta^{18}O_{carbonate}$ values of samples, and beam area / mass ratios of samples.

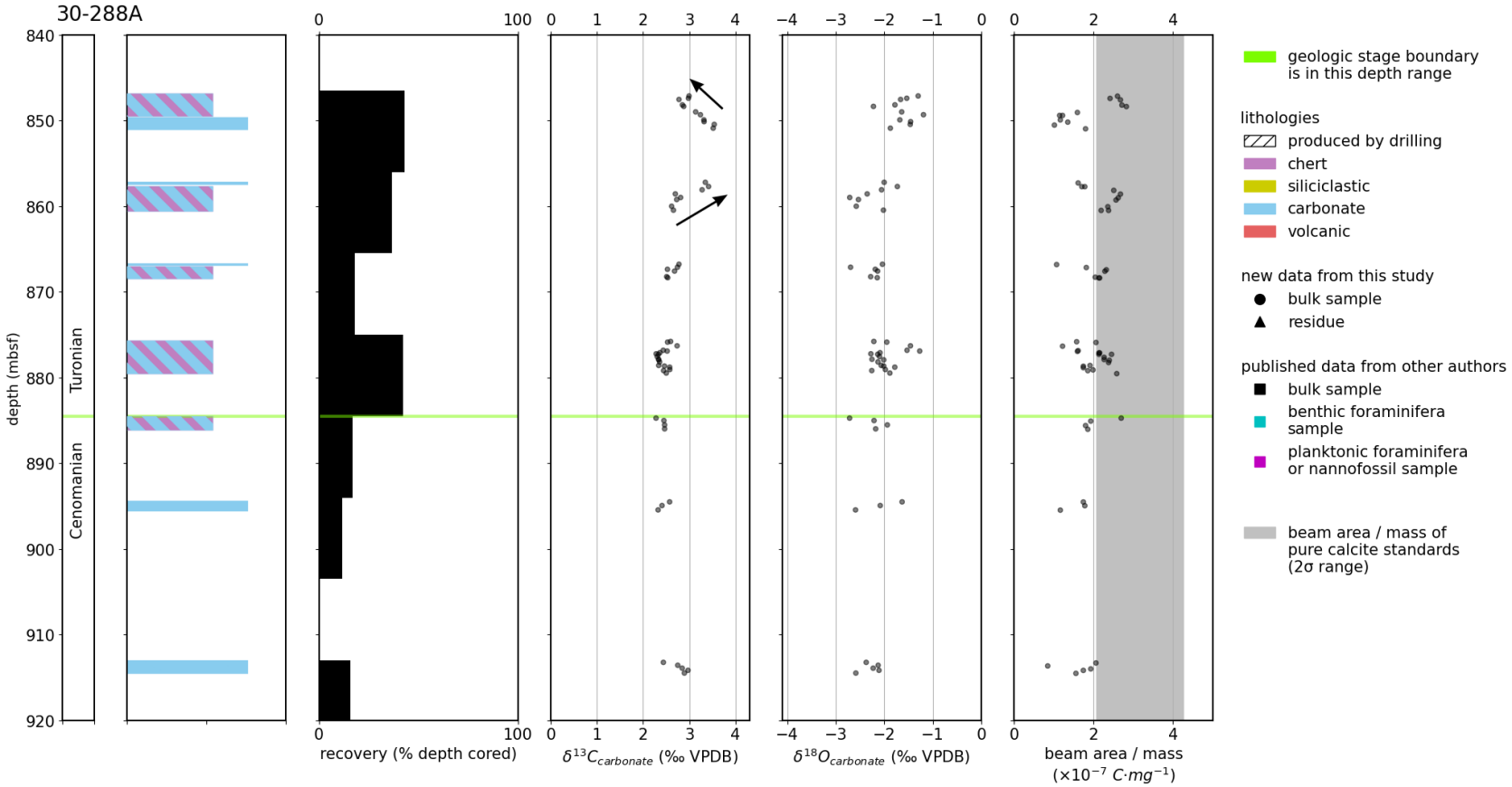

Figure 4.7: Stratigraphic column of 30-288A, including geologic stage assignments based on biostratigraphy, lithologies of recovered sediments, proportion of sediment recovered relative to depth cored, $\delta^{13}C_{carbonate}$ and $\delta^{18}O_{carbonate}$ values of samples, and beam area / mass ratios of samples. Arrows show changes in $\delta^{13}C_{carbonate}$ values discussed in Section 5.1.2.1.

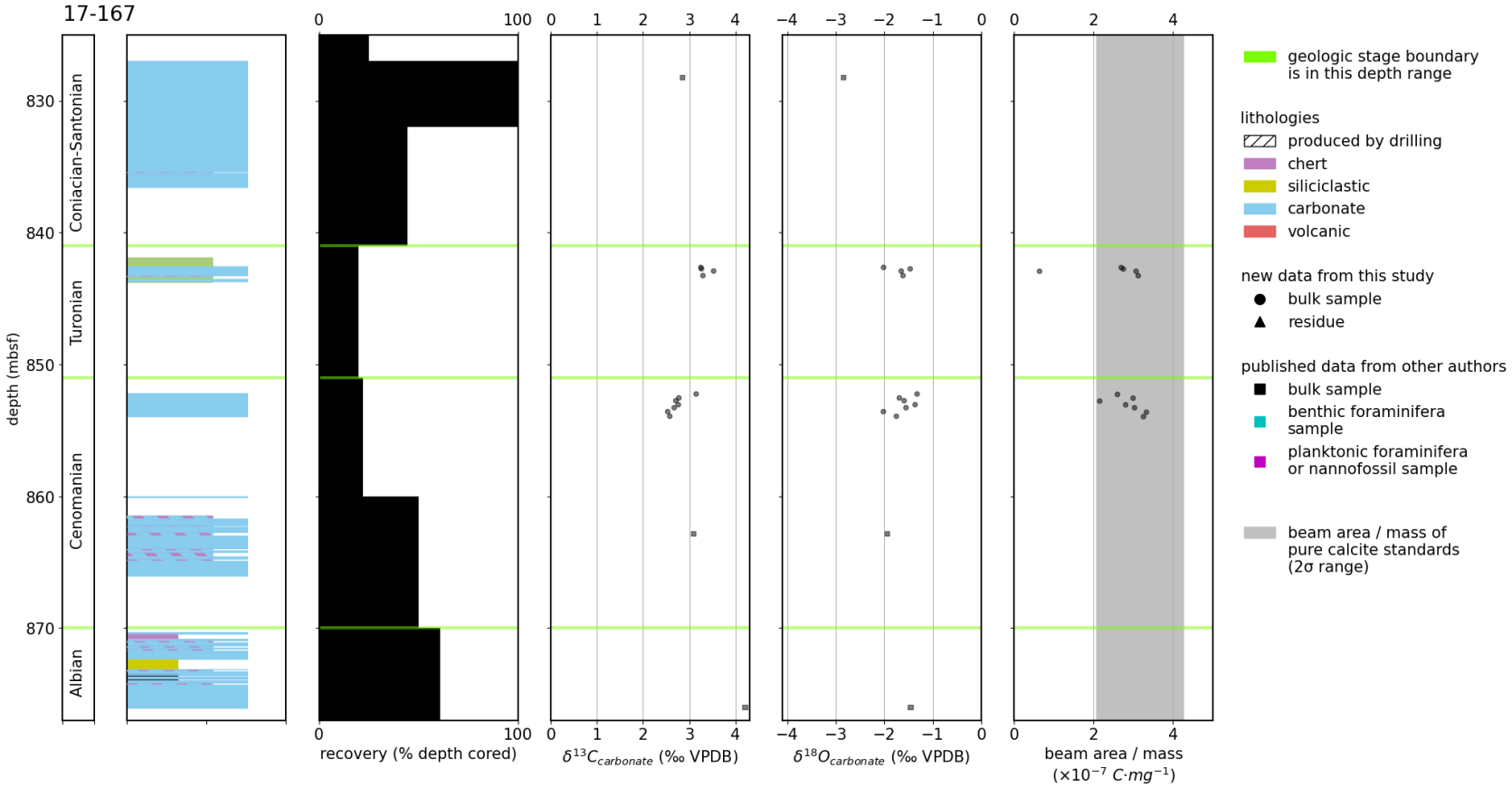

Figure 4.8: Stratigraphic column of 17-167, including geologic stage assignments based on biostratigraphy, lithologies of recovered sediments, proportion of sediment recovered relative to depth cored, $\delta^{13}C_{carbonate}$ and $\delta^{18}O_{carbonate}$ values of samples, and beam area / mass ratios of samples.

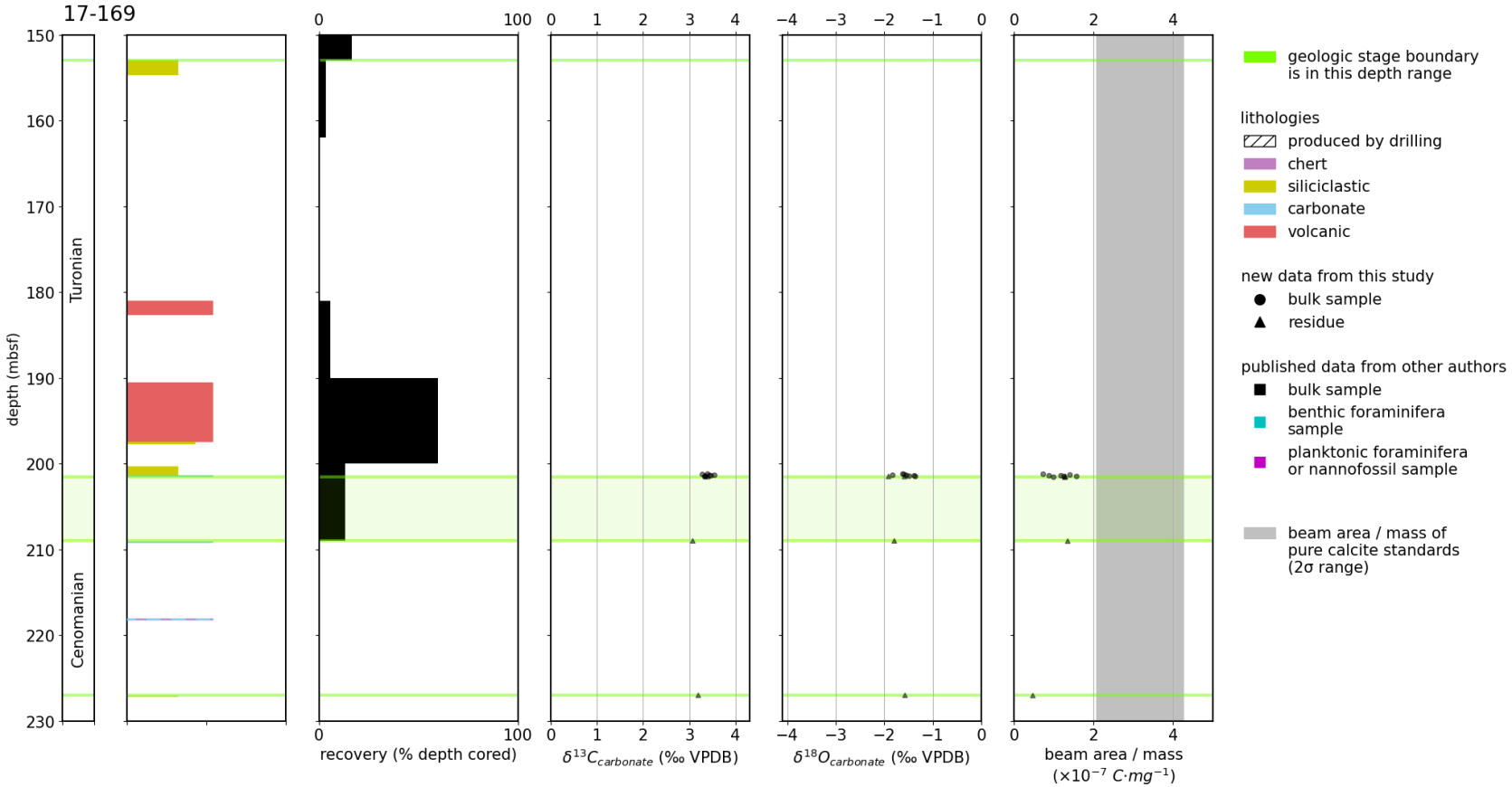

Figure 4.9: Stratigraphic column of 17-169, including geologic stage assignments based on biostratigraphy, lithologies of recovered sediments, proportion of sediment recovered relative to depth cored, $\delta^{13}C_{carbonate}$ and $\delta^{18}O_{carbonate}$ values of samples, and beam area / mass ratios of samples.

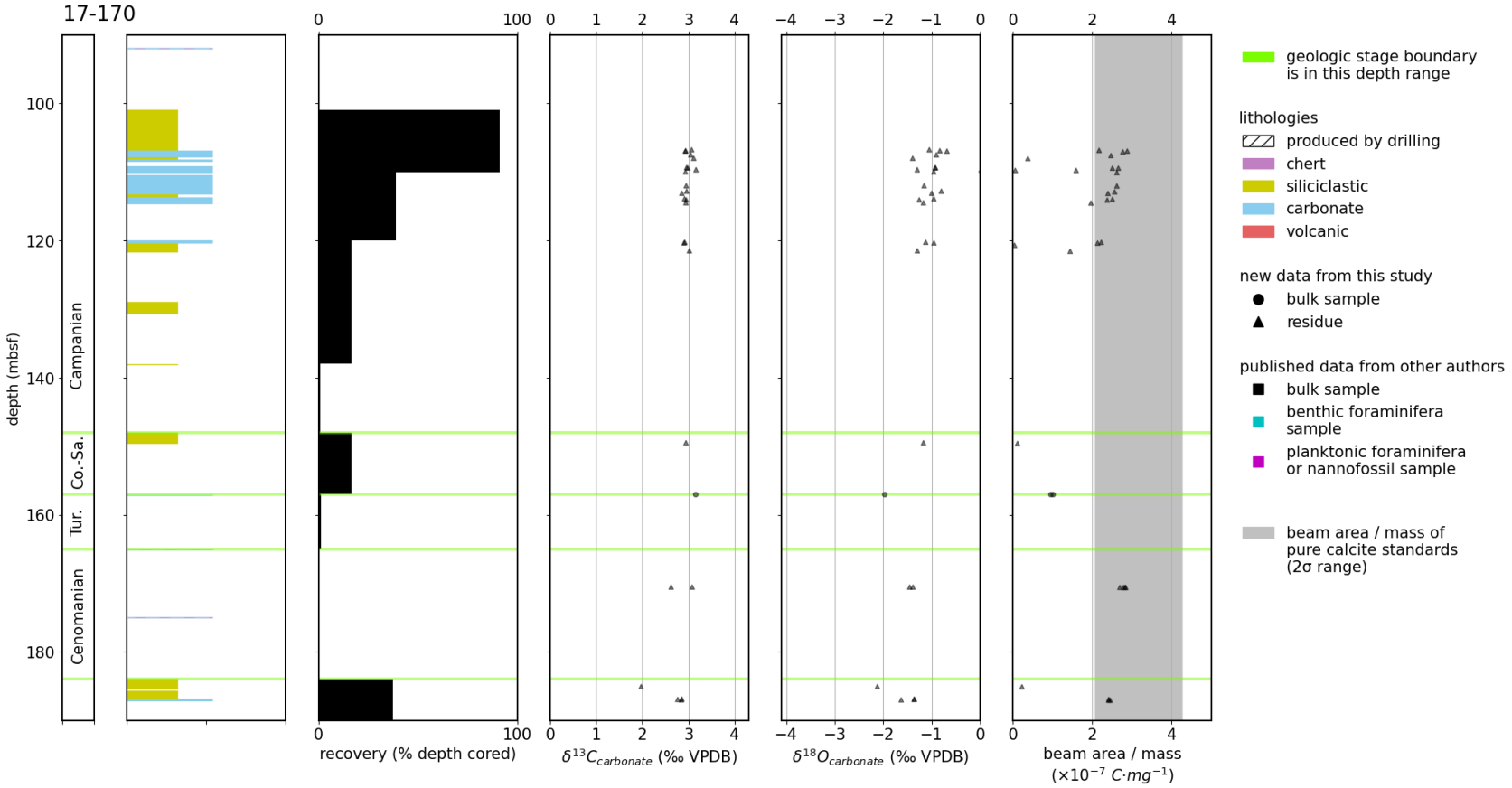

Figure 4.10: Stratigraphic column of 17-170, including geologic stage assignments based on biostratigraphy, lithologies of recovered sediments, proportion of sediment recovered relative to depth cored, $\delta^{13}C_{carbonate}$ and $\delta^{18}O_{carbonate}$ values of samples, and beam area / mass ratios of samples. Turonian is abbreviated to Tur. and Coniacian-Santonian is abbreviated to Co.-Sa.

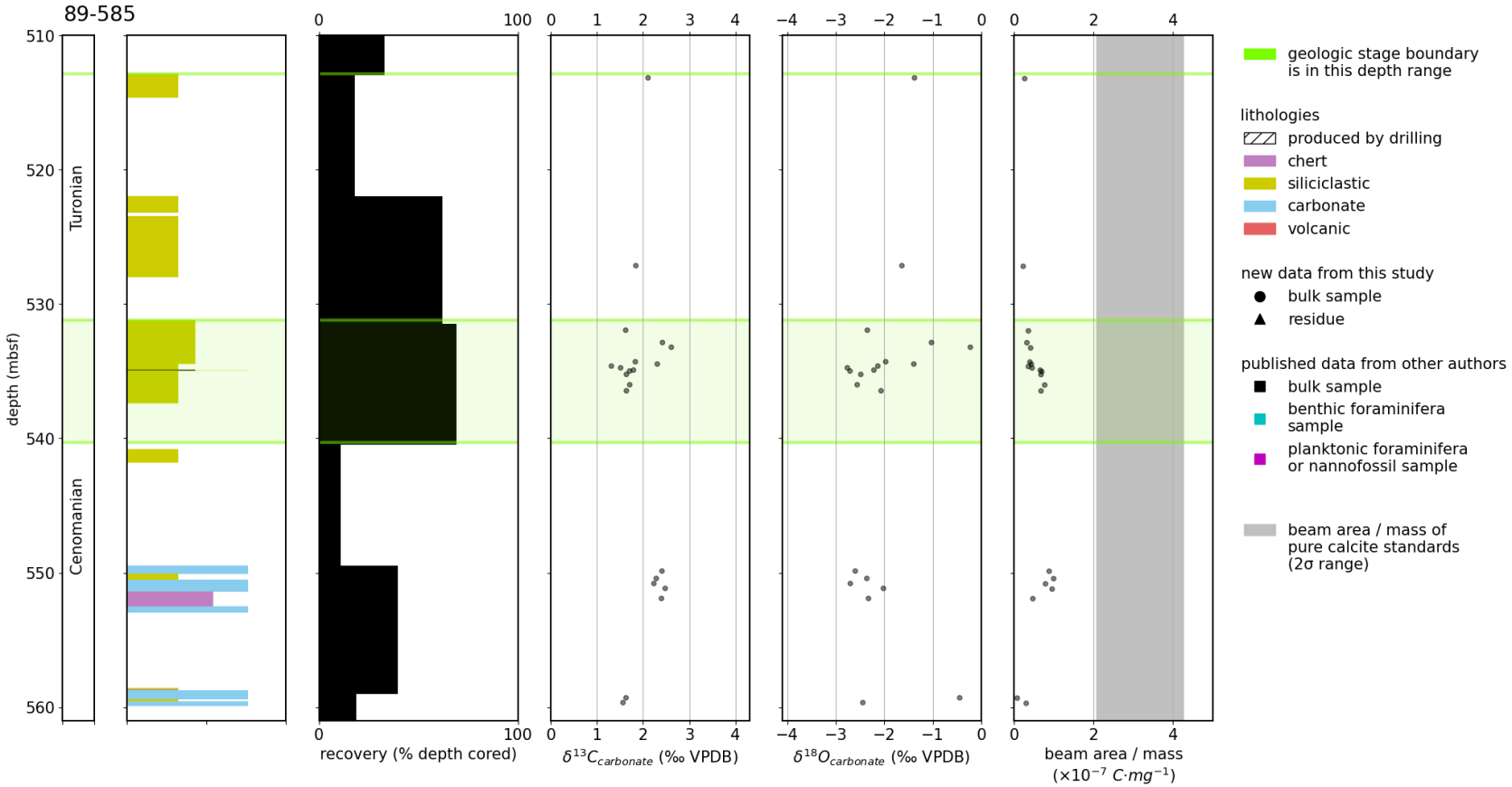

Figure 4.11: Stratigraphic column of 89-585, including geologic stage assignments based on biostratigraphy, lithologies of recovered sediments, proportion of sediment recovered relative to depth cored, $\delta^{13}C_{carbonate}$ and $\delta^{18}O_{carbonate}$ values of samples, and beam area / mass ratios of samples.

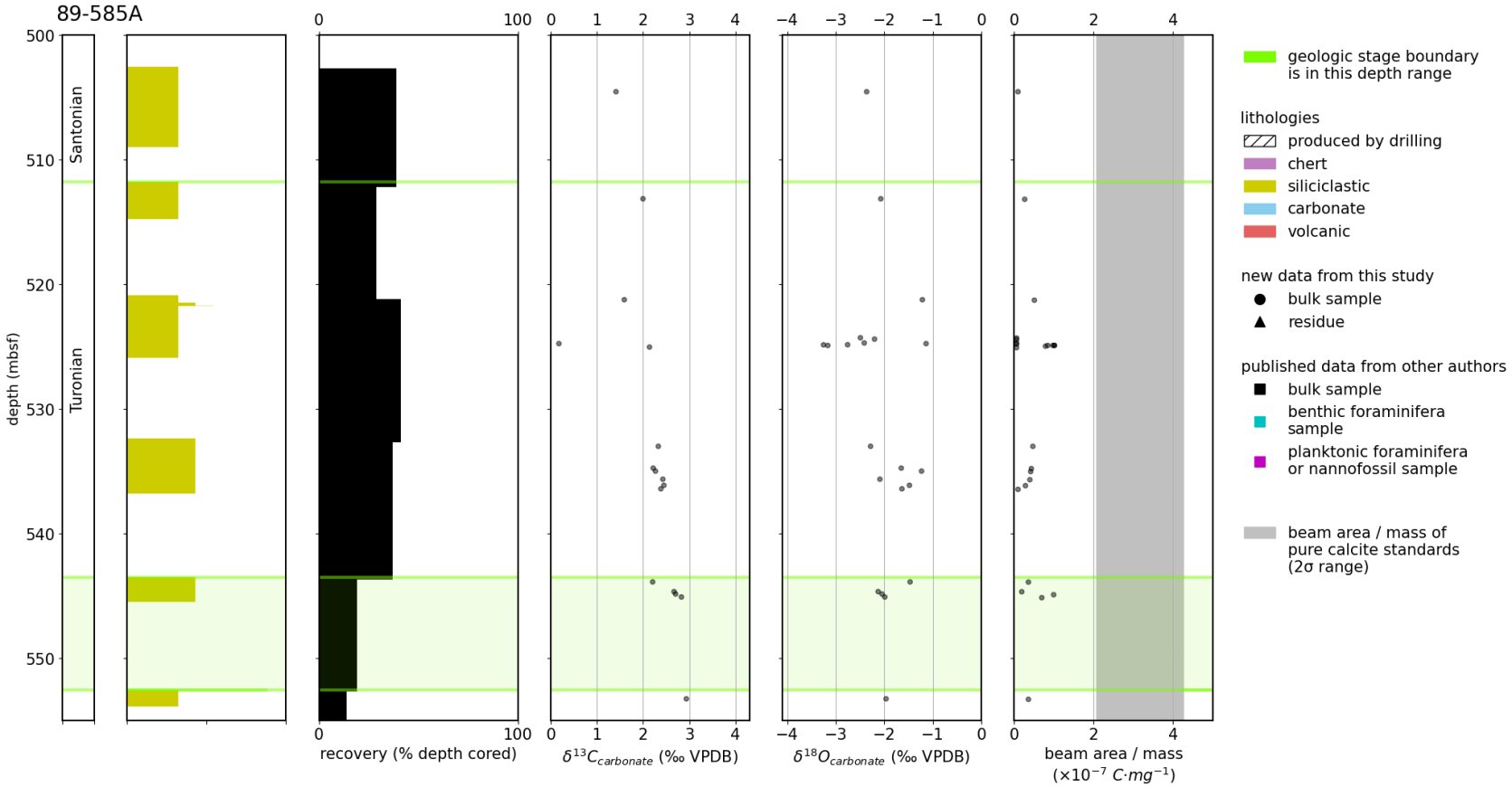

Figure 4.12: Stratigraphic column of 89-585A, including geologic stage assignments based on biostratigraphy, lithologies of recovered sediments, proportion of sediment recovered relative to depth cored, $\delta^{13}C_{carbonate}$ and $\delta^{18}O_{carbonate}$ values of samples, and beam area / mass ratios of samples.

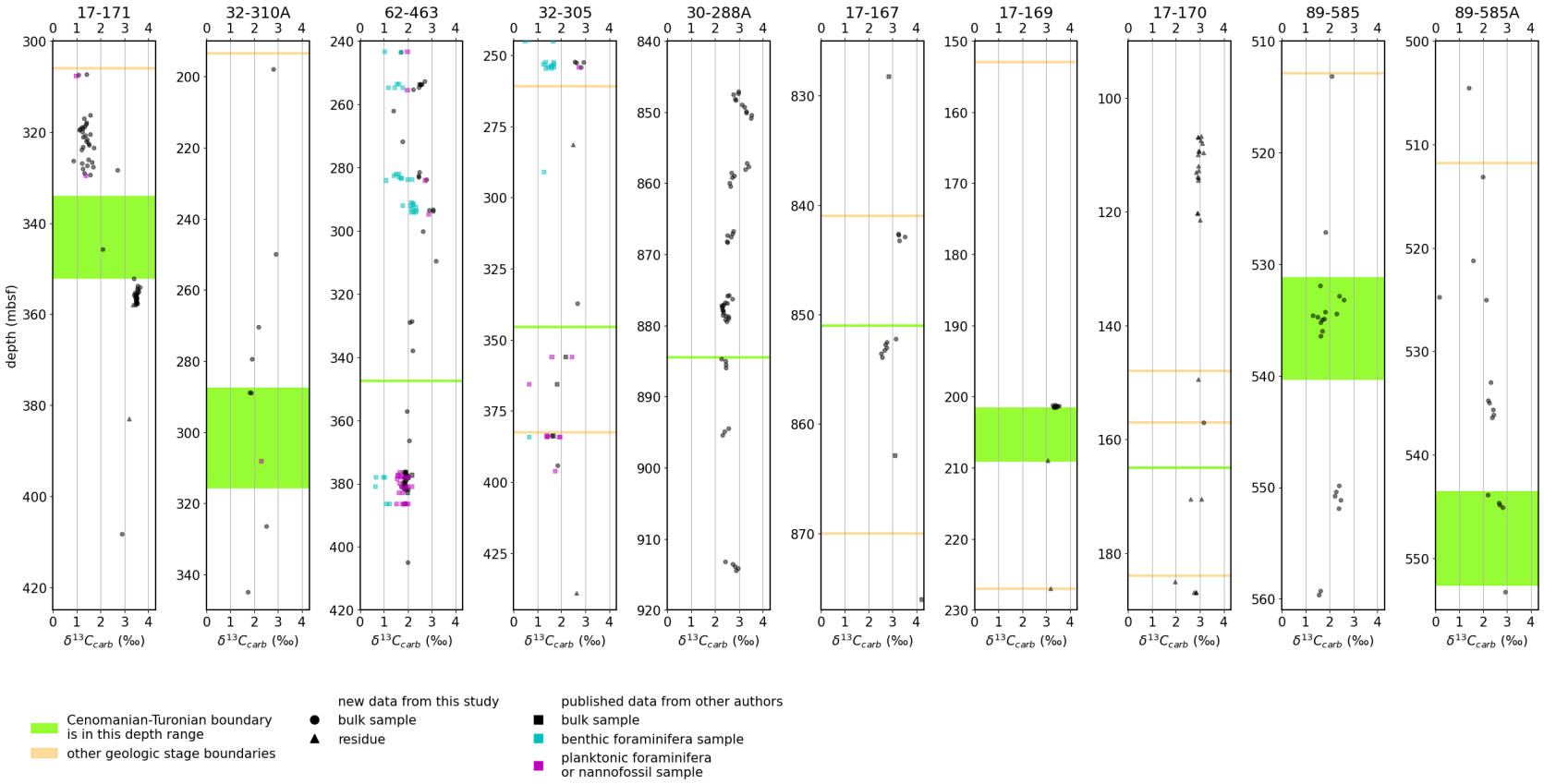

Figure 4.13: $\delta^{13}C_{carbonate}$ values at all sites (in ‰VPDB). See Figures 4.3 - 4.12 for stage names.

4.3 Paleodepth (and paleolatitude), $\delta^{13}C_{carbonate}$ values, and carbonate content

Generally sites with shallower Cenomanian-Turonian paleodepth ranges have larger variability in $\delta^{13}C_{carbonate}$ values (Figure 4.14). Notably, the "shallow" paleodepth site 17-171 has 61 samples falling into a bimodal $\delta^{13}C_{carbonate}$ distribution, with low $\delta^{13}C_{carbonate}$ values (including the overall minimum $\delta^{13}C_{carbonate}$ value 0.88‰) around 1-2‰ in the Turonian and high $\delta^{13}C_{carbonate}$ values (including the overall second-highest $\delta^{13}C_{carbonate}$ value 3.66‰) around 3-4‰ in the Cenomanian. In the "intermediate" paleodepth group, the sites have 7-55 samples each and similar standard deviations between 0.34‰ and 0.46‰. Of the sites in the "deep" paleodepth group, 17-169 and 17-170 have 11 and 26 samples, respectively, and both have small $\delta^{13}C_{carbonate}$ standard deviations of 0.12‰ and 0.23‰ respectively. The only exception to the overall trend of greater $\delta^{13}C_{carbonate}$ variability at shallower depositional depth are the "deep"-paleodepth holes 89-585 and 89-585A, which have $\delta^{13}C_{carbonate}$ standard deviations of 0.39‰ and 0.36‰ respectively, comparable to the $\delta^{13}C_{carbonate}$ standard deviation of sites in the "intermediate" depth group rather than the other sites in the "deep" group.

Among the "intermediate" paleodepth and "deep" paleodepth sites, it is also apparent that some sites have high (> 3‰) $\delta^{13}C_{carbonate}$ values and others do not. Most of the "intermediate" paleodepth and "deep" paleodepth sites with high (> 3‰) $\delta^{13}C_{carbonate}$ values, namely 30-288A, 17-167, 17-169, and 17-170, were located to the south and east of "intermediate" paleodepth and "deep" paleodepth sites that lack such values, namely 32-310A, 32-305, 89-585, and 89-585A (Figure 3.1).

Using beam area / mass ratio as a proxy for carbonate content (Section 2.6.1), carbonate content is generally higher in carbonate lithologies and lower in non-carbonate lithologies at Pacific sites in this thesis (Figures 4.3 - 4.12). For example, at the "shallow" paleodepth site 17-171, the beam area / mass ratios of samples from non-carbonate lithologies range from 2.7×10^{-8} C·mg^{-1} to 2.7×10^{-7} C·mg^{-1}, while the beam area / mass ratios of samples from carbonate lithologies range from 2.3×10^{-7} C·mg^{-1} to 4.5×10^{-7} C·mg^{-1}. Secondarily, "deep" paleodepth sites have a greater number of samples with beam area / mass ratios lower than 8×10^{-8} C·mg^{-1} than "intermediate" paleodepth sites. "Deep" paleodepth sites have 49 such samples, while "intermediate" paleodepth sites have only 3 such samples.

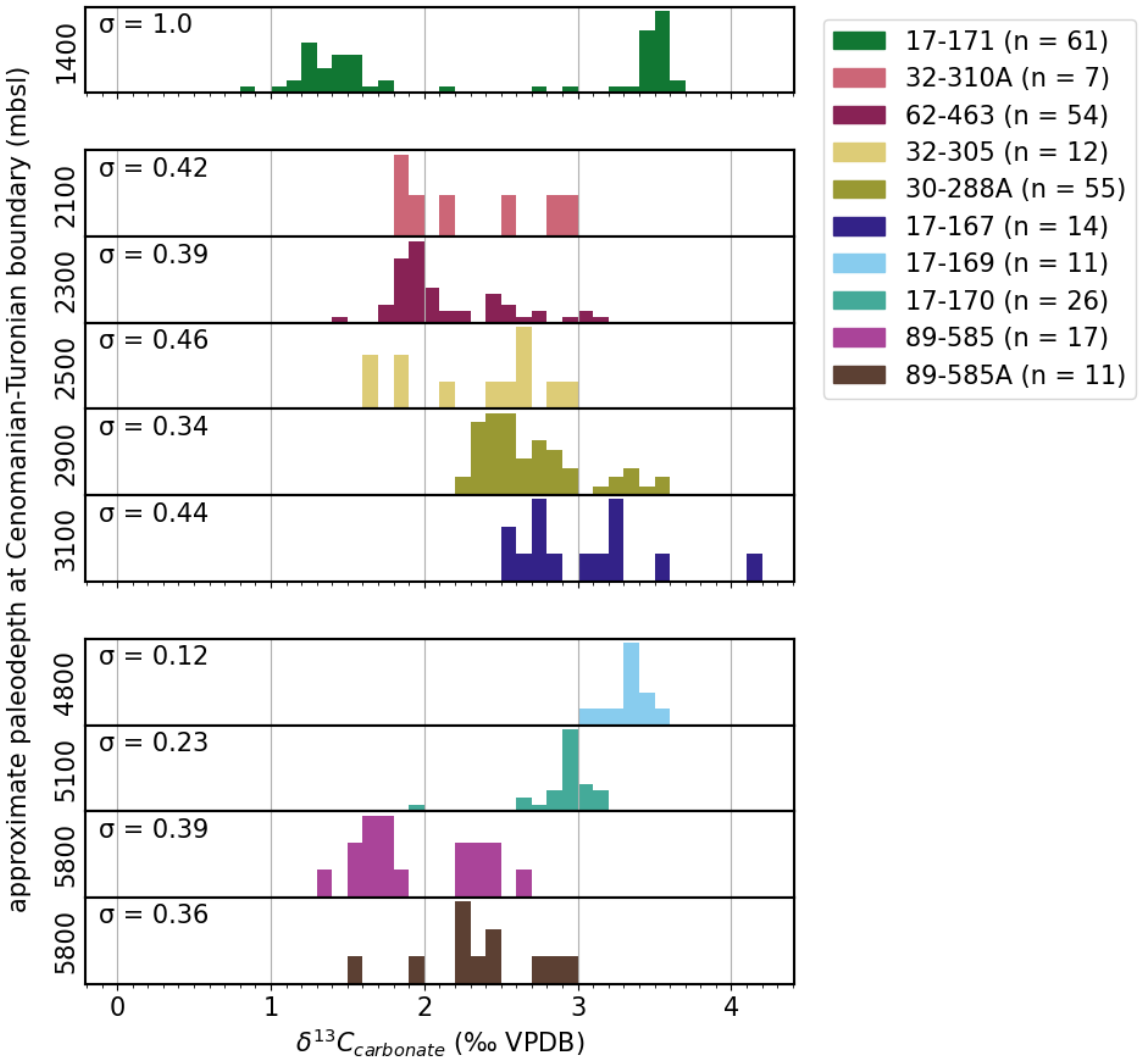

Figure 4.14: $\delta^{13}C_{carbonate}$ distributions at Pacific sites in this thesis, plotted in order of increasing estimated paleodepth of site at the Cenomanian-Turonian boundary. Sites are categorized as either "shallow" $<$ 1500 mbsl (17-171), "intermediate" 1500 - 3500 mbsl (32-310A, 62-463, 32-305, 30-288A, 17-167), or "deep" $>$ 4500 mbsl (17-169, 17-170, 89-585 and 89-585A) during the Cenomanian-Turonian. For each site the standard deviation (σ) is calculated (which assumes a Gaussian distribution). For a version of this figure including only sediments that could have Cenomanian and/or Turonian age based on biostratigraphy see Figure A.6.

4.4 Comparison of $\delta^{13}C_{carbonate}$ values between Pacific sites and selected sites outside the Pacific

In this thesis, planktonic foraminiferal biostratigraphy is used to compare sediments at selected sites in non-Pacific basins to the Pacific sediments studied, because abundant planktonic foraminifera occurrence data are available at all sites and planktonic foraminifera are generally good biostratigraphic tools (Section 2.3). 65 species of planktonic foraminifera occur across all Pacific sites examined in this thesis (Figure A.7). Each non-Pacific site examined in this thesis has planktonic foraminifera present in its sediments that are present at 5 or more of the Pacific sites examined in this thesis (Figure 4.15).[1] Herein I call the interval between the lowest and highest occurrence of a given species at a given site the "fossil occurrence interval" of that species at that site (Figure 4.16). When I compare $\delta^{13}C_{carbonate}$ and $\delta^{18}O_{carbonate}$ values between sites, I compare $\delta^{13}C_{carbonate}$ and $\delta^{18}O_{carbonate}$ values from the fossil occurrence interval for the same species. In other words, I associate a given species with a given $\delta^{13}C_{carbonate}$ or $\delta^{18}O_{carbonate}$ value if the species was logged both stratigraphically above and stratigraphically below the sample that yielded the $\delta^{13}C_{carbonate}$ or $\delta^{18}O_{carbonate}$ value.

[1] At some of the Pacific sites examined in this thesis (e.g. 62-463), many planktonic foraminifera species are present that are also present at the 5 non-Pacific sites examined in this thesis. At other Pacific sites few or no such species are present (e.g. 17-169, 17-170, and 89-585). It is possible that this variation records a difference in planktonic foraminiferal species between sites due e.g. to differences in local productivity. It is also possible that the sediments at some sites have yielded more planktonic foraminiferal identifications than others because they have better recovery or better preserved microfossils.

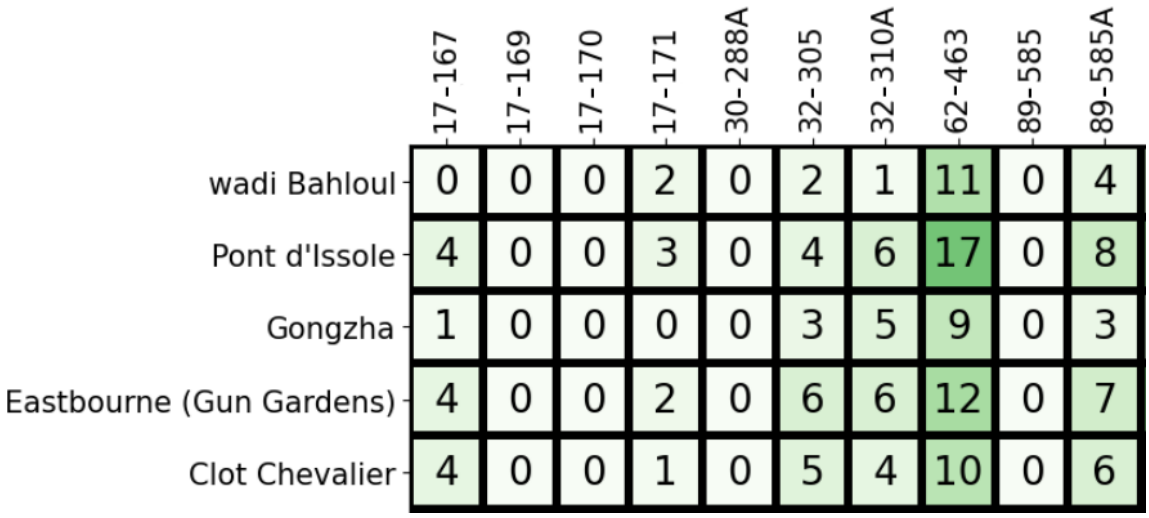

	17-167	17-169	17-170	17-171	30-288A	32-305	32-310A	62-463	89-585	89-585A
wadi Bahloul	0	0	0	2	0	2	1	11	0	4
Pont d'Issole	4	0	0	3	0	4	6	17	0	8
Gongzha	1	0	0	0	0	3	5	9	0	3
Eastbourne (Gun Gardens)	4	0	0	2	0	6	6	12	0	7
Clot Chevalier	4	0	0	1	0	5	4	10	0	6

Figure 4.15: For each possible pair of one Pacific site examined in this thesis and one non-Pacific site examined in this thesis, the number of planktonic foraminiferal species present in the sediments studied at both sites.

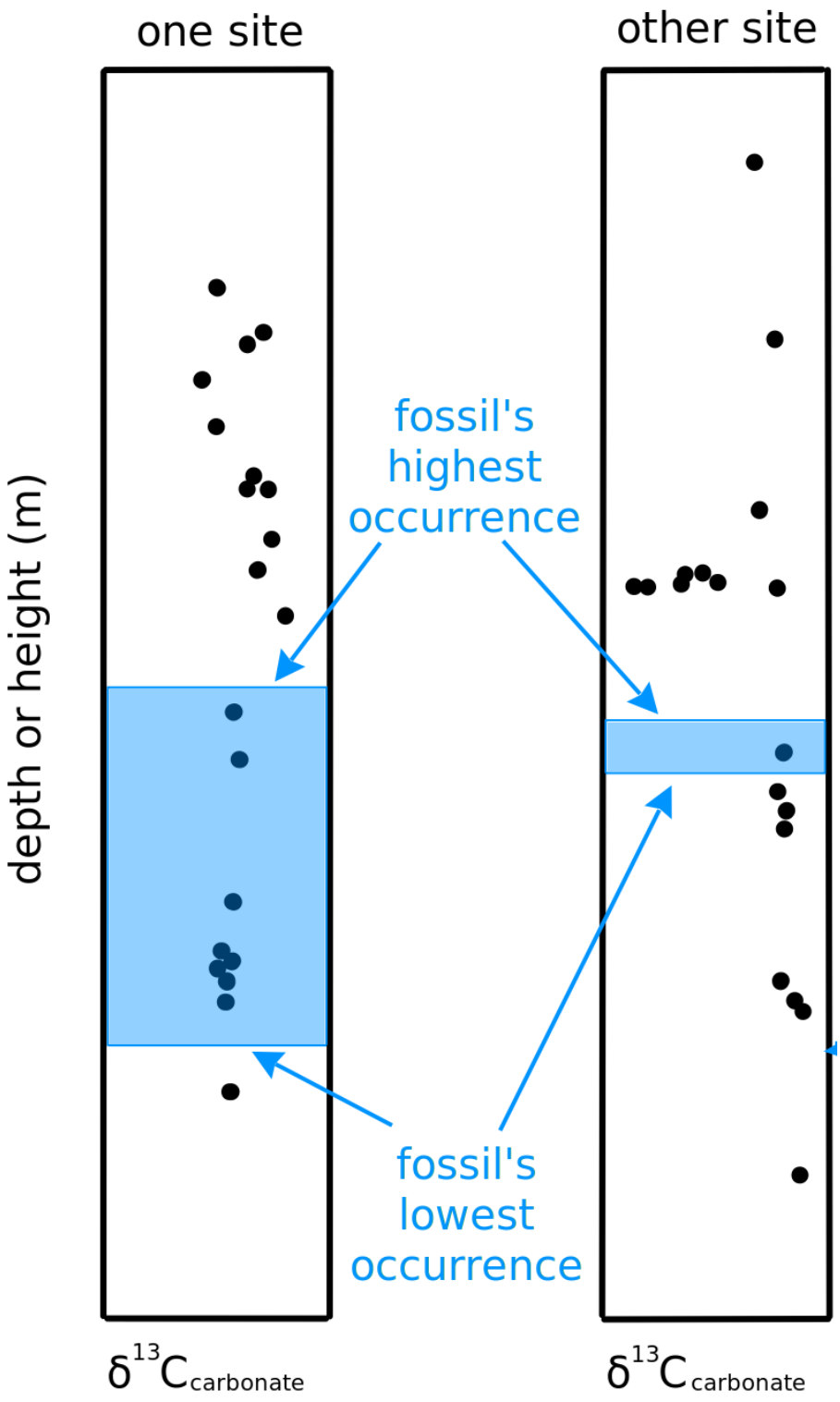

Figure 4.16: Conceptual diagram of a fossil occurrence interval for a fossil that is present in the sediments at two sites, pictured on plots of $\delta^{13}C_{carbonate}$ vs. depth for both sites.

In a given fossil occurrence interval, $\delta^{13}C_{carbonate}$ values from Eastbourne, Clot Chevalier, and Pont d'Issole are higher than $\delta^{13}C_{carbonate}$ values from Gongzha and the Pacific sites in this thesis. As for $\delta^{13}C_{carbonate}$ values from wadi Bahloul, depending on the fossil occurrence interval, they may be closer to $\delta^{13}C_{carbonate}$ values from Eastbourne, Clot Chevalier, and Pont d'Issole (e.g. *Dicarinella algeriana*, *Whiteinella inornata*) or to $\delta^{13}C_{carbonate}$ values from Gongzha and the Pacific (e.g. *Whiteinella archaeocretacea*, *Whiteinella praehelvetica*), or in between (e.g. *Rotalipora greenhornensis*, *Whiteinella brittonensis*; see Figure 4.17). The overall ranges and distributions of the $\delta^{13}C_{carbonate}$ values from Eastbourne, Clot Chevalier, Pont d'Issole, wadi Bahloul, Gongzha, and the Pacific basin (not broken down by fossil occurrence interval) are also consistent with these observations (Table 4.2; Figure 4.18). (See Appendix A.26 for histograms of $\delta^{13}C_{carbonate}$ values from the fossil occurrence interval of every species considered.)

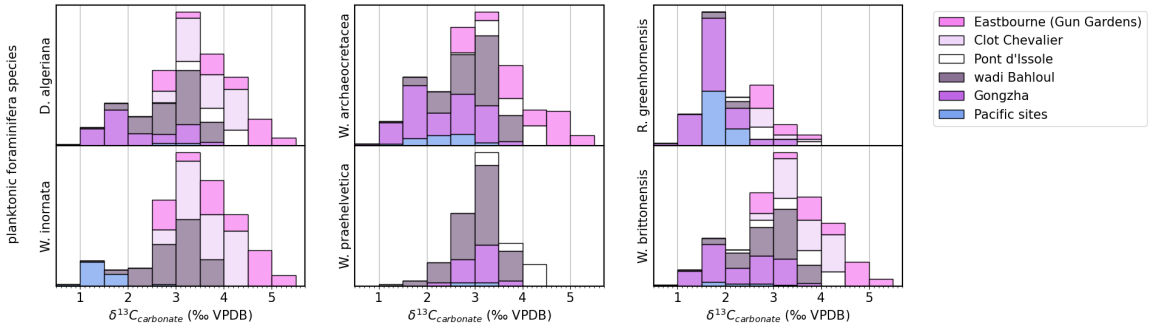

Figure 4.17: Histograms of $\delta^{13}C_{carbonate}$ values in the fossil occurrence intervals of selected species. In left panel, *Dicarinella algeriana* and *Whiteinella inornata* histograms show wadi Bahloul $\delta^{13}C_{carbonate}$ values are closer to those from Eastbourne, Clot Chevalier, and Pont d'Issole; in middle panel, *Whiteinella archaeocretacea* and *Whiteinella praehelvetica* histograms show wadi Bahloul $\delta^{13}C_{carbonate}$ values are closer to those from Gongzha and the Pacific; in right panel, *Rotalipora greenhornensis* and *Whiteinella brittonensis* histograms show wadi Bahloul $\delta^{13}C_{carbonate}$ values in between those from Eastbourne, Clot Chevalier, and Pont d'Issole vs. Gongzha and the Pacific. For histograms associated with all planktonic foraminifera species occurring at the examined sites, see Appendix A.26.

Site	Ocean region during the Cenomanian-Turonian	Shares planktonic foraminifera species with these Pacific sites:	$\delta^{13}C_{carbonate}$ range (‰VPDB)
Eastbourne (Gun Gardens), UK	North Atlantic	62-463, 89-585A, 32-305, 32-310A, 17-167, 17-171	2.61 - 5.41
Clot Chevalier, Vocontian Basin, France*	Western Tethys	62-463, 89-585A, 32-305, 32-310A, 17-167, 17-171	2.55 - 4.41
Pont d'Issole, Vocontian Basin, France*	Western Tethys	62-463, 89-585A, 32-305, 32-310A, 17-167, 17-171	2.28 - 4.40
wadi Bahloul, Tunisia	Western Tethys	62-463, 89-585A, 32-305, 17-171	1.08 - 3.74
Gongzha, Tibet	Neotethys	62-463, 89-585A, 32-305, 32-310A, 17-167	0.89 - 3.61
All Pacific sites in this thesis	Pacific	all	0.88 - 4.20

* In the present day Clot Chevalier and Pont d'Issole are about 15 km apart. Both are located in the Vocontian Basin, "a relatively deep subtropical basin (estimated mid-Cretaceous palaeolatitude of ∼30°N)" (Falzoni et al., 2016 and citations therein).

Table 4.2: The Cenomanian-Turonian ocean region, Pacific sections which have planktonic foraminiferal species that were also noted in this section by biostratigraphers, and $\delta^{13}C_{carbonate}$ range of shallow marine sections where Cenomanian-Turonian $\delta^{13}C_{carbonate}$ values have been measured by other authors (the Gun Gardens section at Eastbourne, UK; Clot Chevalier, Vocontian Basin, France; Pont d'Issole, Vocontian Basin, France; wadi Bahloul, Tunisia; Gongzha, Tibet). For detailed information about planktonic foraminifera species occurring at each site and their associated $\delta^{13}C_{carbonate}$ values, see Appendix A.26.

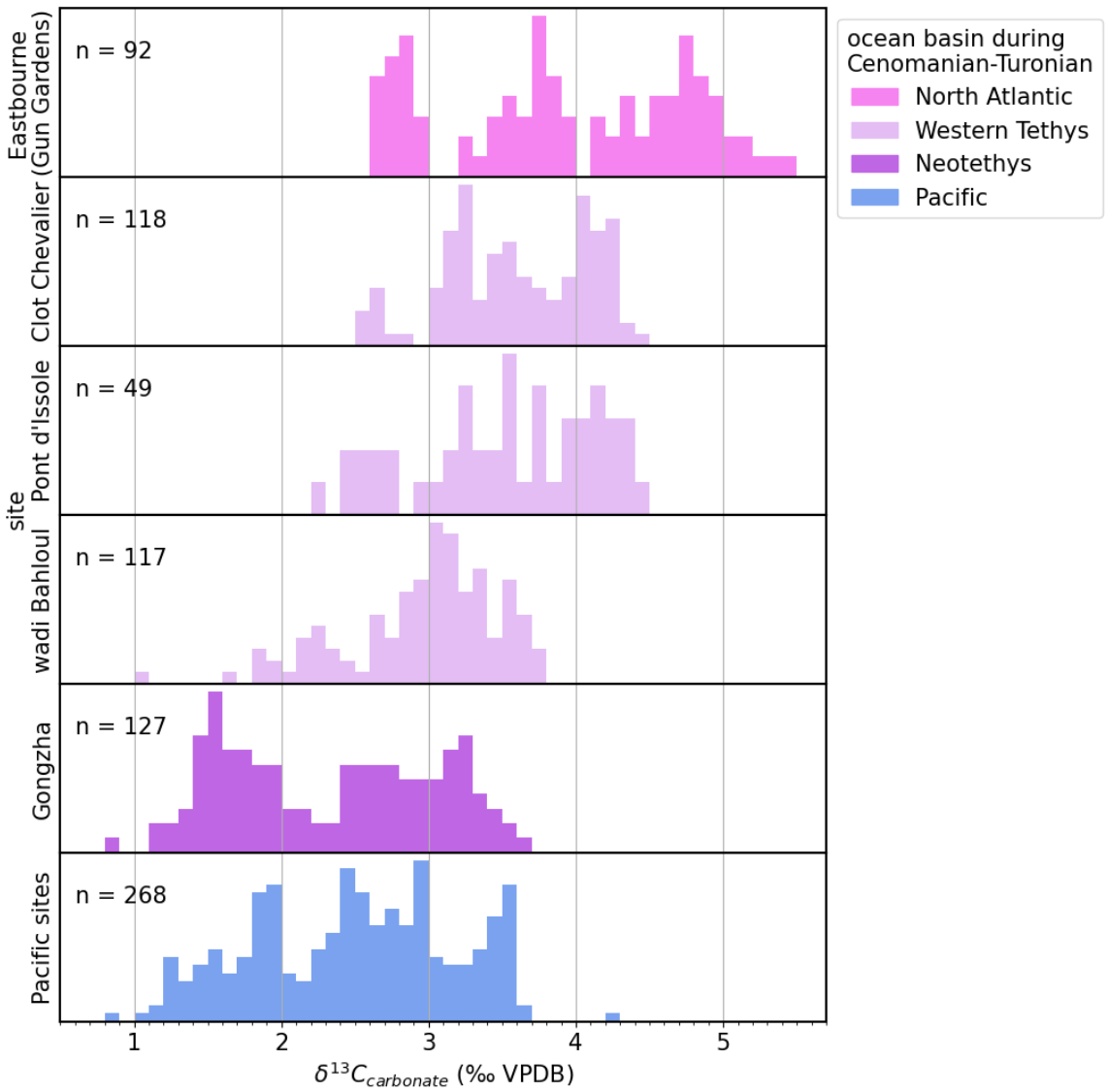

Figure 4.18: $\delta^{13}C_{carbonate}$ distributions at sites in different basins (North Atlantic, Western Tethys, Neotethys, Pacific) with combined $\delta^{13}C_{carbonate}$ distribution for Pacific sites from this thesis shown at bottom. For histograms associated with all planktonic foraminifera species occurring at the examined sites, see Appendix A.26.

Discussion

5.1 Explaining Pacific bulk $\delta^{13}C_{carbonate}$ values

In this section I argue that differences in bulk $\delta^{13}C_{carbonate}$ values between and within Pacific sites in this thesis are best explained by the following:

1. factors local to individual sites, such as variation in paleoenvironment of deposition and/or sediment source

2. change in global ocean $\delta^{13}C_{DIC}$ over time

I first consider $\delta^{13}C_{DIC}$ and $\delta^{13}C_{carbonate}$ in the modern ocean. I argue that $\delta^{13}C_{carbonate}$ values of the Pacific sites in this thesis at least partially record coeval water column $\delta^{13}C_{DIC}$, and then consider that $\delta^{13}C_{DIC}$ differences in depositional environments of different depth can help explain why the Pacific site with the shallowest Cenomanian-Turonian paleodepth range has a wider $\delta^{13}C_{carbonate}$ range than sites with deeper Cenomanian-Turonian paleodepths (Figure 4.14).

5.1.1 Factors local to individual sites

In the following, I examine modern analogues of "intermediate"-paleodepth and "shallow"-paleodepth Pacific sites in this thesis, to help establish expectations for $\delta^{13}C_{carbonate}$ values at these sites (Section 5.1.1.1). I then examine the $\delta^{13}C_{carbonate}$ and $\delta^{18}O_{carbonate}$ values of coincident samples of bulk carbonate, benthic foraminifera, and planktonic foraminifera at 62-463 and 32-305 (Section 5.1.1.2), and consider the origin of bulk $\delta^{13}C_{carbonate}$ values at all Pacific sites in this thesis (Section 5.1.1.3). Building on these sections, I present the argument that high $\delta^{13}C_{carbonate}$ variability, including high ($>$ 3‰) $\delta^{13}C_{carbonate}$ values, occurs in sediments derived from shallow semi-restricted settings (Section 5.1.1.4) and expound that argument for 17-171 (Section 5.1.1.5).

5.1.1.1 Modern analogues

Modern observations provide a starting point for considering the past. The Pacific sites in this thesis can be compared to modern ocean sites with similar paleodepth and depositional setting, including both open-ocean and shallow semi-restricted carbonate-platform sites. In the modern open ocean, the shallowest part of the water column has the highest $\delta^{13}C_{DIC}$ and the highest $\delta^{13}C_{DIC}$ variance (Gruber et al., 1999; Schmittner et al., 2013; Figure 5.1), driven by high surface productivity (Section 1.2.1). In the modern mid-Pacific open ocean, $\delta^{13}C_{DIC}$ has its maximum at the surface, decreases rapidly with depth between 0 and 300 m and reaches its minimum between 1000 and 2000 m (Schmittner et al., 2013; Figure 5.1). In the modern mid-Pacific open ocean, these features of the water column $\delta^{13}C_{DIC}$ profile are the same whether $\delta^{13}C_{DIC}$ is measured over a mid-basin topographic high like the Ontong-Java Plateau, where the seafloor is 2.2 - 3.2 km deep, or the abyssal plain, where the seafloor is 4.7 - 5.9 km deep (Figure 5.1). In this thesis, Pacific sites in the "intermediate" and "deep" paleodepth groups are both open-ocean sites, with the "intermediate" sites on mid-basinal topographic highs and the "deep" sites on the abyssal plain.

Compared to open-ocean $\delta^{13}C_{DIC}$ values, $\delta^{13}C_{DIC}$ values in shallow, more restricted parts of the modern ocean are more variable (Swart et al., 2009; Geyman and Maloof, 2019, 2021; Pederson et al., 2021). Over carbonate platforms, water does not exchange frequently with the open ocean, as illustrated by the residence time of 250 days for water on the Bahama Banks (Broecker and Takahashi, 1966). A restricted DIC pool allows local factors to drive $\delta^{13}C_{DIC}$ values higher or lower compared to the global open ocean. For example, also in the Bahamas, $\delta^{13}C_{DIC}$ values are elevated by up to ∼1‰ relative to the open ocean average of ∼1‰ (Swart et al., 2009; Geyman and Maloof, 2019; Figure 5.2), presumably driven by photosynthesis. Other $\delta^{13}C_{DIC}$ values measured in the Bahamas are as much as ∼7‰ lower than the open ocean average of ∼1‰ (Geyman and Maloof, 2021; Figure 5.2). The $\delta^{13}C_{DIC}$ values in shallow environments can be driven lower by the discharge of meteoric water in which terrestrial organic matter has been oxidized, as in Florida Bay (Patterson and Walter, 1994) and Hawai'i (Richardson et al., 2017), or by the *in situ* decomposition of organic carbon during early marine diagenesis, as in Abu Dhabi (Pederson et al., 2021; Figure 5.2). In this thesis, the "shallow" paleodepth site 17-171 may have been adjacent to a carbonate platform, where the processes described here may have been occurring (see Section 3.2).

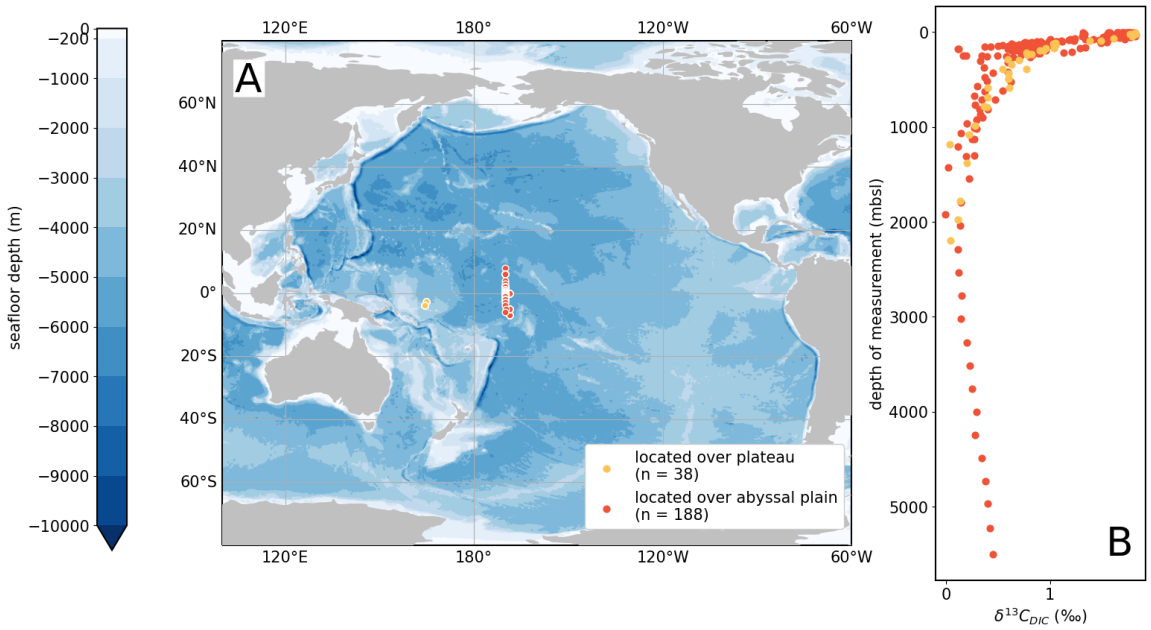

Figure 5.1: (A) Sampling locations and (B) $\delta^{13}C_{DIC}$ vs. depth of modern seawater samples taken by Schmittner et al. (2013). Samples shown were taken above the Ontong-Java plateau (2°S - 4°S, 164°E - 165°E in the depth range 7 to 2197 mbsl over seafloor of depth 2231- 3284 mbsl; shown in orange) and above the abyssal plain (7°S - 7°N, 171°W - 168°W in the depth range 2 - 5497 mbsl over seafloor of depth 4791 to 5873 mbsl; shown in red). Bathymetry from Natural Earth (vector and raster map data @ `naturalearthdata.com`).

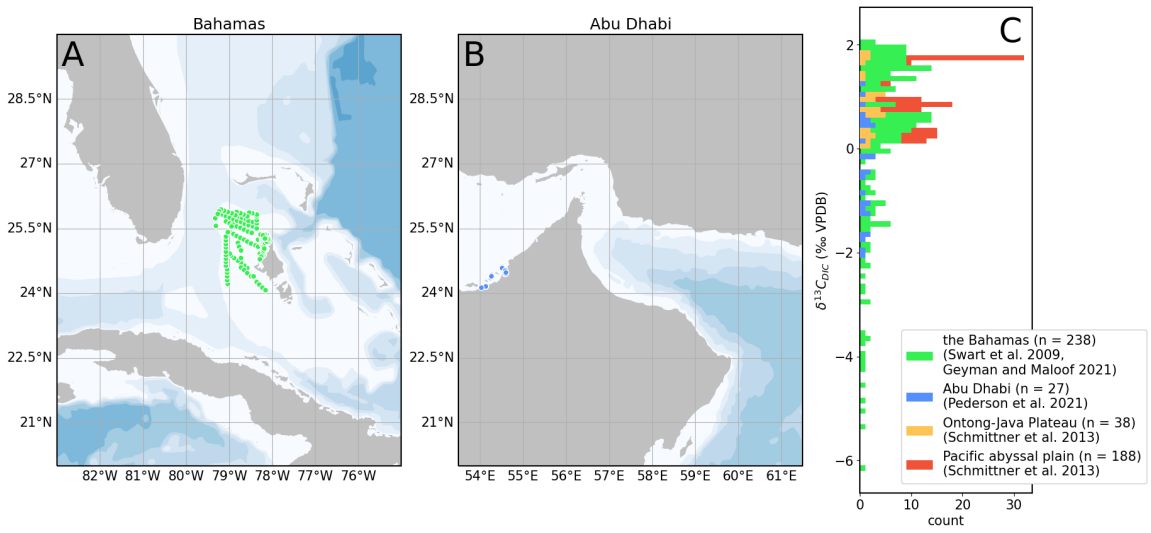

Figure 5.2: (A, B) Sampling locations and (C) histogram of $\delta^{13}C_{DIC}$ values of modern seawater samples taken by Swart et al. (2009) and Geyman and Maloof (2021) in the Bahamas (bottom depth < 15 m; shown in green) and Pederson et al. (2021) in Abu Dhabi (bottom depth < 10 m; shown in blue). Pacific $\delta^{13}C_{DIC}$ values from Figure 5.1 also appear on the histogram for comparison (shown in red and orange). Bathymetry from Natural Earth (vector and raster map data @ `naturalearthdata.com`), using same colorbar as Figure 5.1.

To understand Pacific sites in this thesis, $\delta^{13}C_{DIC}$ is important because the $\delta^{13}C_{DIC}$ of the water in which carbonate formed is one factor that sets the $\delta^{13}C_{carbonate}$ value of sediments. Variations in local processes affecting $\delta^{13}C_{DIC}$ may be responsible for variations in these $\delta^{13}C_{carbonate}$ values. At a given site, this thesis reports the $\delta^{13}C_{carbonate}$ values of sediments assumed to be deposited on top of each other over a period of time. At shallow sites, including the "shallow"-paleodepth Pacific site 17-171 in this thesis, $\delta^{13}C_{DIC}$ changes may be caused by changes in the processes described above, e.g. changes in the amount of meteoric discharge on a carbonate platform or changes in the degree of restriction of a shallow lagoonal area. At open-ocean sites, including the "intermediate"-paleodepth Pacific sites in this thesis, $\delta^{13}C_{DIC}$ changes may be caused by local changes in productivity. Finally, regarding "deep"-paleodepth sites below the CCD, carbonate at these sites must have been redeposited from "intermediate"-paleodepth and/or "shallow"-paleodepth locations above the CCD. Therefore understanding "intermediate"-paleodepth and "shallow"-paleodepth $\delta^{13}C_{carbonate}$ values is the starting point for understanding "deep"-paleodepth $\delta^{13}C_{carbonate}$ values.

In summary, $\delta^{13}C_{DIC}$ values in the modern ocean range from about 0‰ to about 1.8‰ in the open ocean (Figure 5.1) and from about -2.0‰ to about 2.3‰ in shallow settings (Figure 5.2). The $\delta^{13}C$ of carbonate sediments that form from these waters may record $\delta^{13}C_{DIC}$ or may be altered by other fluids after formation. To interpret the $\delta^{13}C_{carbonate}$ values in this thesis I consider the effects of various factors (carbonate source, vital effects, diagenesis) on $\delta^{13}C_{carbonate}$ at Pacific sites in this thesis, beginning by focusing on two sites (62-463 and 32-305) where some benthic foraminiferal, planktonic foraminiferal, and nannofossil $\delta^{13}C_{carbonate}$ values are also available.

5.1.1.2 Benthic vs. planktonic vs. bulk $\delta^{13}C_{carbonate}$ and $\delta^{18}O_{carbonate}$ values at 62-463 and 32-305

At 62-463 and 32-305, there are consistent $\delta^{13}C_{carbonate}$ offsets between samples of bulk carbonate, planktonic foraminifera or nannofossils, and benthic foraminifera from the same depths in the same cores (Figure 5.3). Planktonic foraminifera (n = 36) and nannofossils (n = 4) are grouped together because they both originate at the top of the water column, while benthic foraminifera grow in bottom water and pore water.[1] In the following, I argue that the observed differences in $\delta^{13}C_{carbonate}$ and $\delta^{18}O_{carbonate}$

[1]Although it is possible that planktonic foraminiferal and nannofossil vital effects differ (e.g. Anderson and Arthur, 1983; Ziveri et al., 2003), I do not analyze them separately here because there are many more planktonic foraminiferal samples than nannofossil samples.

values between these three types of carbonate sample suggest that bulk $\delta^{13}C_{carbonate}$ values record the $\delta^{13}C_{carbonate}$ of sediment at its initial deposition, not diagenetic processes.

Evaluated via moving average (unweighted boxcar size of 1 m), $\delta^{13}C_{carbonate}$ values from planktonic foraminifera and nannofossils and bulk carbonate $\delta^{13}C_{carbonate}$ values are similar, and both are consistently higher than benthic foraminiferal $\delta^{13}C_{carbonate}$ values by ∼1‰ (Figure 5.3). The difference between a bulk $\delta^{13}C_{carbonate}$ value and the nearest planktonic foraminiferal or nannofossil $\delta^{13}C_{carbonate}$ value within 1 m ranges from -0.42‰ to 0.59‰ with an average difference (i.e. $\Delta\delta^{13}C_{bulk\text{-}nearestplanktonic}$) of 0.12‰. As typically $\delta^{13}C_{DIC}$ is highest in the surface ocean and decreases with depth (Sections 1.2.1 and 5.1.1.1), planktonic foraminifera and nannofossils, which originate in the photic zone, would be expected to have $\delta^{13}C_{carbonate}$ values higher than bulk $\delta^{13}C_{carbonate}$ values, unless the bulk carbonate was 100% planktonic foraminifera and nannofossils. Therefore, the similarity between planktonic foraminifera and nannofossil and bulk $\delta^{13}C_{carbonate}$ values may indicate that bulk carbonate samples contain a very high proportion of planktonic foraminifera and/or nannofossil material.

By contrast, the average difference between each planktonic foraminiferal or nannofossil $\delta^{13}C_{carbonate}$ value and the nearest benthic foraminiferal $\delta^{13}C_{carbonate}$ value within 1 m (i.e. $\Delta\delta^{13}C_{planktonic\text{-}nearestbenthic}$) is 0.93‰, while $\Delta\delta^{13}C_{bulk\text{-}nearestbenthic}$ is 1.00‰. This observation is consistent with the expectation that benthic foraminiferal $\delta^{13}C_{carbonate}$ values recording the $\delta^{13}C_{DIC}$ of bottom water and pore water would be lower than bulk $\delta^{13}C_{carbonate}$ values (unless the bulk carbonate was 100% benthic foraminifera). The modern "intermediate"-depth water column shows an offset of ∼1‰ between the top and bottom (Figure 5.1), suggesting that $\delta^{13}C_{DIC}$ differences can entirely explain the offset between planktonic foraminiferal and nannofossil vs. benthic foraminiferal $\delta^{13}C_{carbonate}$ values, and can also explain the bulk vs. benthic foraminiferal $\delta^{13}C_{carbonate}$ values if the fraction of bulk carbonate consisting of benthic foraminifera is close to 0%. Also, the $\delta^{13}C_{carbonate}$ values of benthic foraminifera do not vary with the depth of their habitat in the sediment, so microhabitat vital effects are not evident (Appendix A.27).

Overall, it is likely that bulk $\delta^{13}C_{carbonate}$ values at 62-463 and 32-305 are at least in part controlled by the $\delta^{13}C_{DIC}$ of the water column, as the specific direction and magnitude of the $\delta^{13}C_{carbonate}$ offset between components originating from bottom water (benthic foraminifera) vs. the rest of the water column (planktonic foraminifera, nannofossils, and bulk carbonate sediment) is consistent with these components recording

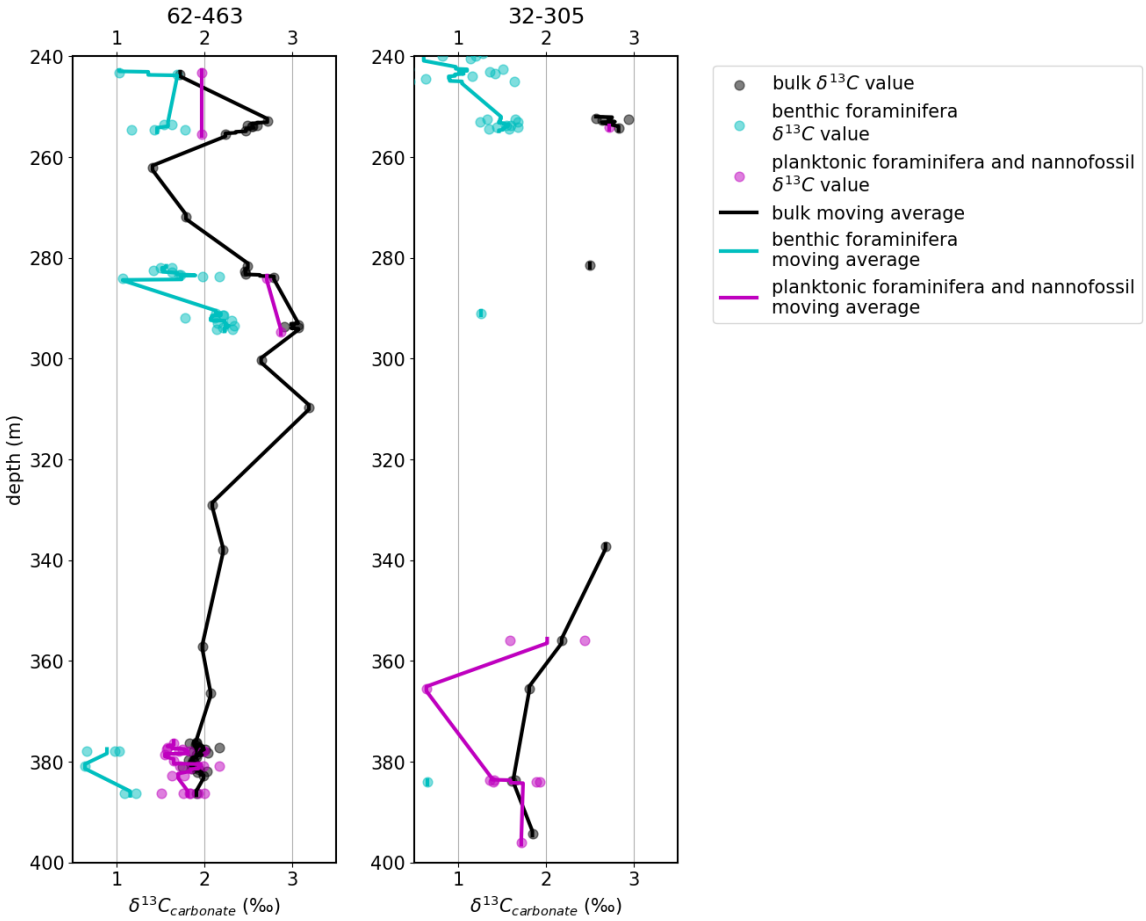

Figure 5.3: Bulk, benthic foraminifera, and planktonic foraminifera and nannofossil $\delta^{13}C_{carbonate}$ values plotted against depth for 62-463 and 32-305. Unweighted moving averages with a boxcar size of 1 m of the bulk, benthic foraminifera, and planktonic foraminifera and nannofossil $\delta^{13}C_{carbonate}$ values are shown. Where distance between samples is more than 25 m, moving average connecting line is not drawn.

the expected $\delta^{13}C_{DIC}$ of the water in which they formed. It is also unlikely that differing proportions of aragonite vs. calcite in samples or documented vital effects are responsible for the $\delta^{13}C_{carbonate}$ offsets between bulk and benthic foraminiferal samples (Appendix A.28). I next demonstrate that observations of $\delta^{18}O_{carbonate}$ values are consistent with the suggestion that these $\delta^{13}C_{carbonate}$ and $\delta^{18}O_{carbonate}$ values of these sediments are not altered by diagenesis.

The $\delta^{18}O_{carbonate}$ values of planktonic foraminifera and nannofossils are slightly lower than bulk $\delta^{18}O_{carbonate}$ values from the same depths in the same cores, which in turn are lower than benthic foraminiferal $\delta^{18}O_{carbonate}$ values from the same depths in the same cores (Figure 5.4). A bulk $\delta^{18}O_{carbonate}$ value is on average 0.79‰ higher than the nearest planktonic foraminiferal or nannofossil $\delta^{18}O_{carbonate}$ value and on average 0.73‰ lower than the nearest benthic foraminiferal $\delta^{18}O_{carbonate}$ value. (These averages are largely controlled by the $\delta^{18}O_{carbonate}$ values between 377 and 387 mbsl at 62-463, where sampling is notably dense.)[2] Assuming no ice sheets on Earth during the mid-Cretaceous Shackleton and Kennett (1975); MacLeod et al. (2013), and using the paleotemperature equation of Bemis et al. (1998) for planktonic foraminifera, the planktonic foraminiferal $\delta^{18}O_{carbonate}$ values reported here yield sea surface paleotemperatures of 20.6°C to 30.1°C with an average of 23.6°C, consistent with previous reconstructions of low- and mid-latitude sea surface temperature for the Cretaceous (O'Brien et al., 2017). Using the paleotemperature equation of Shackleton (1974) for benthic foraminifera (Figure A.1), the benthic foraminiferal $\delta^{18}O_{carbonate}$ values reported here yield bottom water temperatures of 7.7°C to 21.6°C with an average of 12.9°C, broadly consistent with previous reconstructions of bottom water temperature for the Cretaceous (Huber et al., 2002).

All else being equal, diagenetic processes would be expected to act to homogenize $\delta^{13}C_{carbonate}$ and $\delta^{18}O_{carbonate}$ values, erasing offsets between planktonic foraminiferal and nannofossil, bulk, and benthic foraminiferal samples. The expectation of homogenization is stronger for $\delta^{18}O_{carbonate}$ values because water contains much more oxygen than carbon, so $\delta^{18}O_{carbonate}$ values will be reset much more quickly than $\delta^{13}C_{carbonate}$ values when the same amount of solid material is exposed to the same

[2]There are a few exceptions. At 62-463 at 284 mbsl, a planktonic foraminiferal sample has the same $\delta^{18}O_{carbonate}$ value within uncertainty as two bulk carbonate samples within 1 meter (Figure 5.4). In 62-463 at two depths (255 and 283 mbsl), a benthic foraminiferal sample has $\delta^{18}O_{carbonate}$ at least 0.58‰ lower than other benthic foraminiferal $\delta^{18}O_{carbonate}$ values within 2 meters (Figure 5.4). Other than these anomalously low-$\delta^{18}O_{carbonate}$ benthic foraminiferal samples, every bulk $\delta^{18}O_{carbonate}$ value is lower than the nearest benthic foraminiferal $\delta^{18}O_{carbonate}$ value.

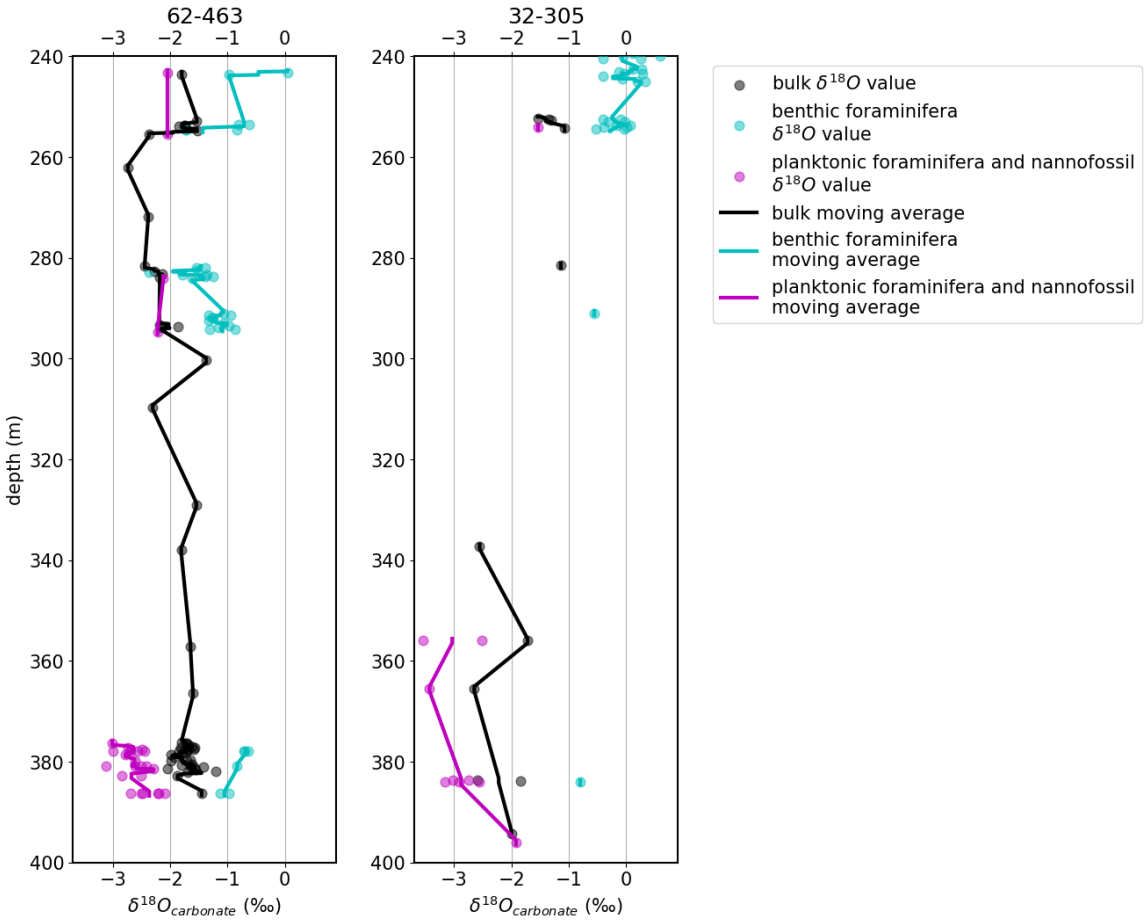

Figure 5.4: Bulk, benthic foraminifera, and planktonic foraminifera and nannofossil $\delta^{18}O_{carbonate}$ plotted against depth for 62-463 and 32-305. Unweighted moving averages with a boxcar size of 1 m of the bulk, benthic foraminifera, and planktonic foraminifera and nannofossil $\delta^{18}O_{carbonate}$ values are shown. Where distance between samples is more than 25 m, moving average connecting line is not drawn.

post-depositional fluid flow (e.g. Allan and Matthews, 1990). The consistent $\delta^{13}C_{carbonate}$ (Figure 5.3) and $\delta^{18}O_{carbonate}$ (Figure 5.4) offsets between coincident samples of the three types (bulk, planktonic foraminiferal or nannofossil, benthic foraminiferal) demonstrate that these samples are not wholly reset by post-depositional alteration. Instead, it is likely that $\delta^{18}O_{carbonate}$ values are at least in part controlled by water column temperatures, with higher $\delta^{18}O_{carbonate}$ values corresponding to colder paleotemperatures (Section 1.3). The observed high benthic foraminiferal $\delta^{18}O_{carbonate}$ values and low planktonic foraminiferal and nannofossil $\delta^{18}O_{carbonate}$ values are consistent with the reasonable expectation that bottom water temperatures will be colder than surface water temperatures.

In summary, based on observations of $\delta^{13}C_{carbonate}$ and $\delta^{18}O_{carbonate}$ values of planktonic foraminifera, nannofossils, benthic foraminifera, and bulk samples, it is likely the $\delta^{13}C_{carbonate}$ values at 62-463 and 32-305 record mainly the $\delta^{13}C_{carbonate}$ of sediment at its initial deposition, controlled mainly by the $\delta^{13}C_{DIC}$ of the seawater from which the carbonate sediment formed. Some benthic foraminiferal $\delta^{13}C_{carbonate}$ values may record pore water in upper sediments. If $\delta^{13}C_{carbonate}$ values from planktonic foraminifera and nannofossils are controlled by $\delta^{13}C_{DIC}$ values at the top of the water column and $\delta^{13}C_{carbonate}$ values from benthic foraminifera are controlled by $\delta^{13}C_{DIC}$ values at the bottom of the water column, material from the upper water column is likely the dominant component of bulk carbonate, so bulk $\delta^{13}C_{carbonate}$ values may largely record upper ocean $\delta^{13}C_{DIC}$ at 62-463 and 32-305.

Importantly, diagenesis would be expected to homogenize $\delta^{13}C_{carbonate}$ values and especially $\delta^{18}O_{carbonate}$ values, so the observed differences in $\delta^{13}C_{carbonate}$ and $\delta^{18}O_{carbonate}$ between different components (planktonic foraminifera, nannofossils, and benthic foraminifera) are evidence against extensive diagenetic alteration of the samples studied. Also, bulk $\delta^{18}O_{carbonate}$ values may record the temperatures in which the carbonate formed. Therefore it is unlikely that diagenesis systematically controls the observed $\delta^{13}C_{carbonate}$ and $\delta^{18}O_{carbonate}$ values at 62-463 and 32-305. In the next section, I consider bulk $\delta^{13}C_{carbonate}$ and $\delta^{18}O_{carbonate}$ values at other Pacific sites in this thesis, and compare them to compiled benthic foraminiferal $\delta^{13}C_{carbonate}$ and $\delta^{18}O_{carbonate}$ values of Cenomanian and Turonian age from the whole ocean.

5.1.1.3 Benthic vs. bulk $\delta^{13}C_{carbonate}$ and $\delta^{18}O_{carbonate}$ values at all Pacific sites

Bulk carbonate $\delta^{18}O$ values at other Pacific sites in this thesis are similar to those at 62-463 and 32-305 (Figure 5.5). Using the equation of Kim and O'Neil (1997) for inorganically precipitated calcite, the bulk $\delta^{18}O_{carbonate}$ values at all sites yield temperatures consistent with previous paleotemperature reconstructions for the Cretaceous ocean (Figure 5.5; O'Brien et al., 2017; Huber et al., 2002). If $\delta^{18}O_{carbonate}$ values at a given site had been extensively altered by diagenesis, they might be homogenized and have a narrower range than the range of $\delta^{18}O_{carbonate}$ values at sites where alteration had not taken place. If diagenesis had taken place at high temperatures, $\delta^{18}O_{carbonate}$-based paleotemperatures would be expected to record those temperatures (Section 1.3). That other Pacific sites in this thesis lack these diagenetic signatures indicates it is possible that $\delta^{18}O_{carbonate}$ values are unaltered, or at least in part controlled by $\delta^{18}O_{seawater}$ and water column temperatures at these sites. Generally, if $\delta^{18}O_{carbonate}$ values are diagenetically unaltered, then it is likely but not certain that $\delta^{13}C_{carbonate}$ values are as well. A possible exception is the 23.1-meter-thick unit at 17-171 in which the lowest $\delta^{13}C_{carbonate}$ values of any Pacific site in this thesis were measured (Section 5.1.1.5).

I also compare the bulk $\delta^{13}C_{carbonate}$ and $\delta^{18}O_{carbonate}$ values from Pacific sites in this thesis to benthic foraminiferal $\delta^{13}C_{carbonate}$ and $\delta^{18}O_{carbonate}$ values of Cenomanian and Turonian age from the whole ocean compiled by Cramer et al. (2009) and Friedrich et al. (2012). I omit from this comparison anomalous $\delta^{13}C_{carbonate}$ and $\delta^{18}O_{carbonate}$ values from Demerara Rise in the equatorial Atlantic (Section 5.2.2; Figure 5.7). Bulk carbonate samples from this thesis have $\delta^{13}C_{carbonate}$ on average 1.31‰ higher, and $\delta^{18}O_{carbonate}$ on average 0.95‰ lower, than compiled benthic foraminiferal samples of Cenomanian and Turonian age (omitting Cenomanian-Santonian Demerara Rise samples; Section 5.2.2), although the distributions have considerable overlap (Figure 5.6). In both direction and magnitude, these differences are very similar to the differences between bulk carbonate and benthic foraminiferal $\delta^{13}C_{carbonate}$ and $\delta^{18}O_{carbonate}$ values from the same depth in the same cores that were discussed for 62-463 and 32-305 (0.03‰ to 1.38‰ for $\delta^{13}C_{carbonate}$ and -1.21‰ to 0.24‰ for $\delta^{18}O_{carbonate}$; Section 5.1.1.2). Therefore, the differences in $\delta^{13}C_{carbonate}$ and $\delta^{18}O_{carbonate}$ values between bulk carbonate samples from this thesis and benthic foraminiferal samples are most simply explained as the expected differences between bulk carbonate and benthic

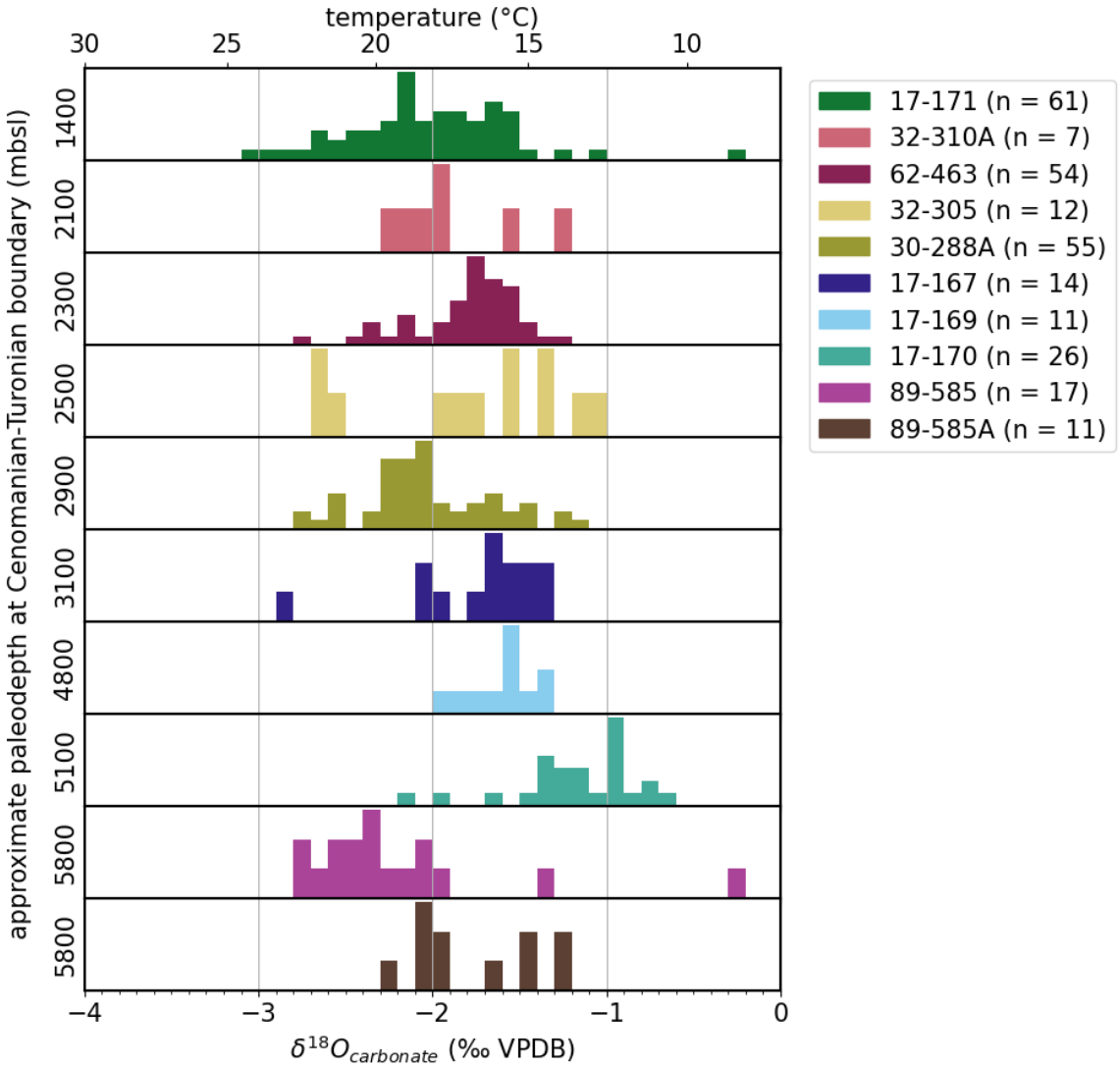

Figure 5.5: Bulk $\delta^{18}O_{carbonate}$ distributions at Pacific sites examined in this thesis, plotted in order of increasing estimated paleodepth of site at the Cenomanian-Turonian boundary. At the top are shown the temperatures corresponding to these $\delta^{18}O_{carbonate}$ values if temperature-controlled fractionation were the only control on $\delta^{18}O_{carbonate}$, using the equation of Kim and O'Neil (1997) for inorganically precipitated calcite (see Figure A.1). See Figure A.8 for a version of this figure in which only samples from sediments that could have Cenomanian and/or Turonian age, based on biostratigraphy, are included.

foraminiferal samples largely recording $\delta^{13}C_{DIC}$ and $\delta^{18}O_{seawater}$. This explanation is strongest if the global ocean is assumed to be largely homogeneous with respect to $\delta^{13}C_{DIC}$ and $\delta^{18}O_{seawater}$ during the Cenomanian-Turonian, and I later posit that it may not have been (Sections 5.2.1 and 5.3.1). In the benthic foraminiferal compilation differences in $\delta^{13}C_{carbonate}$ and $\delta^{18}O_{carbonate}$ between basins are not evident, but data are sparse (Appendix A.29). Site-specific benthic foraminiferal $\delta^{13}C_{carbonate}$ and $\delta^{18}O_{carbonate}$ values are needed to conclusively evaluate whether $\delta^{13}C_{carbonate}$ and $\delta^{18}O_{carbonate}$ are mainly controlled by $\delta^{13}C_{DIC}$ and $\delta^{18}O_{seawater}$ at Pacific sites in this thesis other than 62-463 and 32-305.

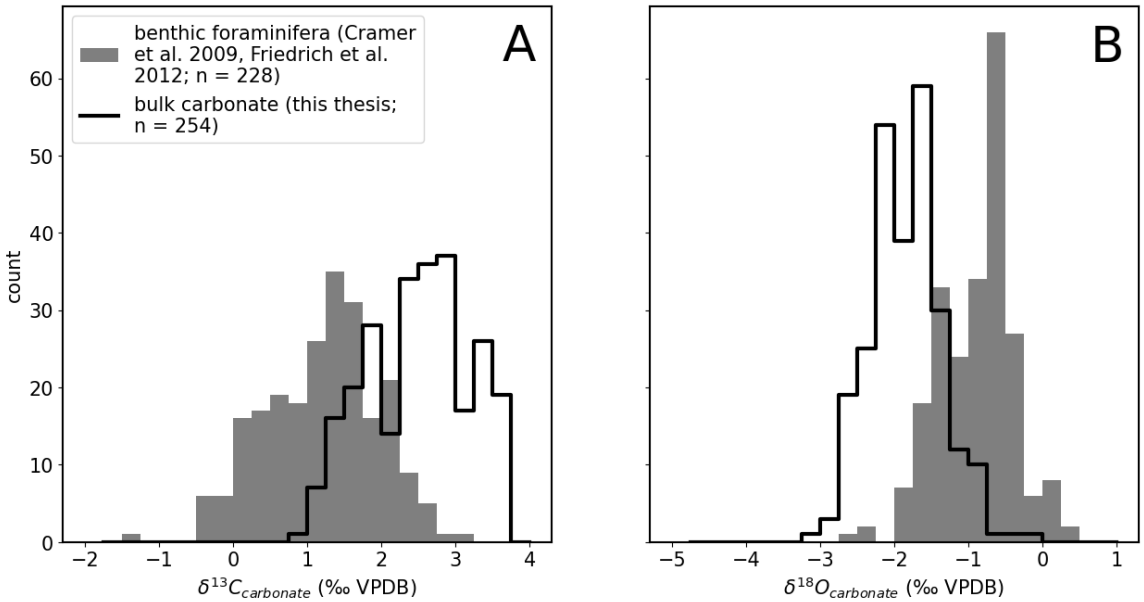

Figure 5.6: (A) Histogram of $\delta^{13}C_{carbonate}$ values of bulk carbonate samples from this thesis (outlined in black, n = 254) and of benthic foraminifera samples of Cenomanian and Turonian age, compiled by Cramer et al. (2009) and Friedrich et al. (2012) (in grey, n = 228, omitting Cenomanian-Santonian samples from Demerara Rise; Section 5.2.2). (B) Histogram of $\delta^{18}O_{carbonate}$ values of the same.

In summary, Pacific bulk $\delta^{18}O_{carbonate}$ values from this thesis are consistent with paleotemperature reconstructions for the Cretaceous ocean (Figure 5.5; O'Brien et al., 2017; Huber et al., 2002), and $\delta^{13}C_{carbonate}$ and $\delta^{18}O_{carbonate}$ values are apparently consistent with expected bulk $\delta^{13}C_{carbonate}$ and $\delta^{18}O_{carbonate}$ values for the Cenomanian-Turonian based on global benthic foraminiferal compilations (Cramer et al., 2009; Friedrich et al., 2012). These differences in $\delta^{13}C_{carbonate}$ and $\delta^{18}O_{carbonate}$ values between bulk carbonate samples from this thesis and benthic foraminiferal samples are

consistent with the explanation that Pacific sites in this thesis do not have $\delta^{13}C_{carbonate}$ and $\delta^{18}O_{carbonate}$ values systematically controlled by diagenesis. I largely focus on other possible explanations in my interpretation of $\delta^{13}C_{carbonate}$ values at Pacific sites in this thesis. I will next address the wide distribution of $\delta^{13}C_{carbonate}$ values at 17-171, which may be explained by the site's proximity to a shallow semi-restricted environment.

5.1.1.4 Possible explanation that high $\delta^{13}C_{carbonate}$ variability, including high $\delta^{13}C_{carbonate}$ values, occurs in sediments derived from shallow semi-restricted settings

The site with the shallowest paleodepth (17-171) has the highest bulk $\delta^{13}C_{carbonate}$ variability of all Pacific sites in this thesis, including high (> 3‰) bulk $\delta^{13}C_{carbonate}$ values (Figure 4.14). Sediment at 17-171 is possibly derived from a very shallow, semi-restricted environment where $\delta^{13}C_{carbonate}$ values might be expected to be significantly higher or lower than those in the open ocean (Section 3.2), consistent with the observation that modern bulk $\delta^{13}C_{carbonate}$ values in shallow semi-restricted settings are wide-ranging and have the potential to be especially elevated relative to $\delta^{13}C_{DIC}$ (Section 5.1.1.1).

The explanation that highly variable bulk $\delta^{13}C_{carbonate}$ values, including high (> 3‰) bulk $\delta^{13}C_{carbonate}$ values, are derived from shallow semi-restricted settings, can be extended to most bulk $\delta^{13}C_{carbonate}$ values at other Pacific sites in this thesis. By comparison to 17-171, sites in the "intermediate" paleodepth group have narrower bulk $\delta^{13}C_{carbonate}$ distributions, with similar $\delta^{13}C_{carbonate}$ standard deviations (between 0.34‰ and 0.46‰), consistent with an open-ocean source of the carbonate sediments at those sites (Section 3.2). Also consistent with the explanation that high $\delta^{13}C_{carbonate}$ values are derived from shallow semi-restricted settings, most $\delta^{13}C_{carbonate}$ values at "intermediate"-paleodepth sites are not high (> 3‰). The exceptions (high bulk $\delta^{13}C_{carbonate}$ values at observed at 30-288A and 17-167; Figure 4.14) will be addressed in Section 5.1.2.

For "deep"-paleodepth sites to have similar $\delta^{13}C_{carbonate}$ values to "intermediate"-paleodepth sites would also be consistent with this explanation that high $\delta^{13}C_{carbonate}$ values are derived from shallow semi-restricted settings. Observations of modern bathymetry imply that intermediate-depth topographic highs were the source of Cenomanian and Turonian sediments at all "deep"-paleodepth sites (17-169, 17-170, 89-585,

and 89-585A; Section 3.2). Accordingly, 89-585 and 89-585A have bulk $\delta^{13}C_{carbonate}$ distributions comparable to those of "intermediate"-paleodepth sites (Section 4.3), with standard deviations 0.39‰ and 0.36‰ respectively (Figure 4.14). Another "deep"-paleodepth site 17-170 has bulk $\delta^{13}C_{carbonate}$ values generally within the range observed at "intermediate"-paleodepth sites, and also below the high values at the "shallow"-paleodepth site 17-171 (Figure 4.14; Table 4.1), again consistent with an "intermediate"-depth carbonate source. However, the remaining "deep"-paleodepth site 17-169 has high bulk $\delta^{13}C_{carbonate}$ values (around 3-4‰) which are not consistent with an "intermediate"-depth carbonate source, and are instead comparable to the high values at the "shallow"-paleodepth site 17-171 (Figure 4.14). These high $\delta^{13}C_{carbonate}$ values at 17-169 are therefore not consistent with the explanation that high $\delta^{13}C_{carbonate}$ values are derived from shallow semi-restricted settings, and I will address them in Section 5.1.2.

The explanation that high $\delta^{13}C_{carbonate}$ variability, including high $\delta^{13}C_{carbonate}$ values, occurs in sediments derived from shallow semi-restricted settings is an explanation that concerns variations in depositional setting between sites. In other words, the setting in which carbonate sediments were initially deposited (not the depth in the water column from which they derive) is proposed to explain high $\delta^{13}C_{carbonate}$ values. If the bulk carbonate samples at all Pacific sites in this thesis are largely made up of material derived from the upper water column (Sections 5.1.1.2 and 5.1.1.3), the explanation still applies because open-ocean planktonic carbonate sediments are expected to have different $\delta^{13}C_{carbonate}$ values than shallow-platform-derived planktonic carbonate sediment. Importantly, however, the $\delta^{13}C_{carbonate}$ values at a site can be affected by changes in the source of carbonate to that site which are not related to the depositional setting. For example, a change in the source of carbonate to a site could occur due to shifts in local bathymetry and currents, or in productivity in the surface ocean above affecting the strength of the biologic pump. Such changes might not manifest as changes in the local depositional environment, and might not be recorded as changes in the lithology of the sediments. I do not elaborate on them in this thesis as they are incompletely constrained, but do note that they could help explain the $\delta^{13}C_{carbonate}$ values observed, or provide an alternative explanation to the one presented here. In the next section, I consider closely how the bulk $\delta^{13}C_{carbonate}$ values at 17-171 may be explained by local variations that do affect estimates of paleodepth and observations of depositional setting and lithology.

5.1.1.5 Explaining bulk $\delta^{13}C_{carbonate}$ values at 17-171 vs. other Pacific sites

The shallowest of the Pacific sites studied in this thesis (17-171) has sediment possibly derived from a very shallow, semi-restricted environment where $\delta^{13}C_{carbonate}$ values might be expected to be significantly higher or lower than those in the open ocean (Section 3.2). Changes in bulk $\delta^{13}C_{carbonate}$ values across 3 lithologic units of Cenomanian-Turonian stratigraphy at 17-171 (Figure 4.3; Table 5.1) can be attributed to local changes in the depositional setting of the sediment, interpreted from observations of the lithology.

# of samples	Depth (mbsf)	Lithology	Bulk $\delta^{13}C_{carbonate}$ range (‰)
32	$<$ 329.5	claystone, siltstone, and sandstone	0.88 - 1.73, except one sample with 2.72*
0	329.5 - 345.7	basalt, hyaloclastite, and limestone-basalt conglomerate	-
1	345.8	firmly cemented carbonate rich in volcanic components	2.10
28	$>$ 352.3	carbonate and chert cuttings from the drill bit	2.91 - 3.66

* There is one sample in this lithologic unit with a higher bulk $\delta^{13}C_{carbonate}$ value of 2.72‰ (17-171-26-3-41/42). The sample is second in a series of 7 samples taken from a layer of friable, mottled brown claystone about 2.8 m thick; all 6 other samples from the layer have bulk $\delta^{13}C_{carbonate}$ values of $\leq$ 1.70‰. No distinguishing features were noted in sample 17-171-26-3-41/42 when it was examined under a microscope.

Table 5.1: The number of samples, depth below seafloor, lithology, and bulk $\delta^{13}C_{carbonate}$ range for each of 4 lithologic units noted in sediments at 17-171.

The lowermost lithological unit studied at 17-171 consists of carbonate sediment

and chert cuttings from the drill bit and yields high bulk $\delta^{13}C_{carbonate}$ values (2.91 - 3.66‰ from 28 samples; Figure 4.3; Table 5.1). Moldic porosity (i.e. empty spaces from the dissolution of rock components) and dolomitization occur in this lithologic unit, suggesting that post-depositional alteration of the carbonate occurred (Shipboard Scientific Party, 1973e), but $\delta^{18}O_{carbonate}$ values at 17-171 are similar to those at other sites, suggesting that this alteration did not affect the bulk rock oxygen isotopic composition very much (Section 5.1.1.3). Although diagenesis may have affected $\delta^{13}C_{carbonate}$ values, it does not offer a likely explanation for these high $\delta^{13}C_{carbonate}$ values because it is generally expected to lower $\delta^{13}C_{carbonate}$ values (Section 1.2.5). The high bulk $\delta^{13}C_{carbonate}$ values in this unit could be explained if the carbonate was deposited in a shallow setting where $\delta^{13}C_{carbonate}$ values were elevated by the mechanisms discussed in Section 5.1.1.1, such as photosynthesis occurring in a semi-restricted DIC pool. 17-171 is adjacent to summits of the topographic high Horizon Guyot (Section 3.2) which may have been very shallow or above sea level and may have contributed carbonate to the site. Unless the Horizon Guyot summits were overcoming subsidence and building closer to the sea surface during the Cenomanian, the summits may no longer have been restricted when later sediments were deposited at 17-171.

Immediately above the lithologic unit described in the previous paragraph, there is a 38-cm-thick layer of zeolitic, volcanic-rich limestone (Shipboard Scientific Party, 1973e). Within this layer, black manganese dendrites and sparry calcite were observed (Figure A.9; Shipboard Scientific Party, 1973e) and one bulk $\delta^{13}C_{carbonate}$ value of 2.10‰, lower than the $\delta^{13}C_{carbonate}$ values from the underlying unit, was measured. One possible explanation for this bulk $\delta^{13}C_{carbonate}$ value is that the sediment was initially deposited in a shallow lagoonal or platform-top environment (like the underlying unit) before its transport to its final depositional environment at 17-171, and the $\delta^{13}C_{carbonate}$ value was initially higher but was lowered by diagenesis. This explanation is supported by the zeolites, which are the product of post-depositional alteration of volcanic material (Deffeyes, 1959); by the dendrites, which form when manganese-rich fluids mix with oxygen-rich pore water and indicate that the geochemistry of the sediment may have been significantly altered by fluid flow (Hou et al., 2023); and by the sparry calcite, which is another indication of post-depositional fluid flow and cementation (Folk, 1965, 1974).

Above the layer of volcanic-rich limestone is a 16.2-m-thick unit consisting largely of basalt and hyaloclastite (Figure 4.3; Table 5.1) in which no $\delta^{13}C_{carbonate}$ values

were measured. Within the basalt and hyaloclastite unit, a conglomerate of limestone and basalt pebbles is interpreted as the result of a debris flow from a nearby island that could have occurred during a volcanic episode (Shipboard Scientific Party, 1973e). If we accept the interpretation that the sediments in the oldest lithologic unit were initially deposited in a shallow lagoonal or platform-top environment and then transported to 17-171, the limestone and basalt conglomerate may indicate shallowly derived sediment continued to arrive at 17-171 through the episode of volcanism represented by this volcanic unit.

Above this volcanic unit lie 23.1 m of siliciclastic sediments including claystone, siltstone, and sandstone, with a low proportion of carbonate including foraminifera, nannofossils, and calcite cement (Shipboard Scientific Party, 1973e). Compared to stratigraphically lower units, these sediments have lower bulk $\delta^{13}C_{carbonate}$ values (0.88‰ - 1.73‰ from 31 samples, and one sample with 2.72‰). There are two possible explanations for these $\delta^{13}C_{carbonate}$ values:

1. Sediment derived from the Horizon Guyot semi-restricted shallow environment continued to be supplied to 17-171 during the deposition of this unit, including siliciclastic sediment such as sand and carbonate sediment with elevated $\delta^{13}C_{carbonate}$ values. The elevated $\delta^{13}C_{carbonate}$ values were later lowered by diagenesis. In this case, the volcanic unit below may have acted as a barrier to fluid flow, explaining why these $\delta^{13}C_{carbonate}$ values were diagenetically lowered but $\delta^{13}C_{carbonate}$ values from the lowermost lithologic unit were not.

2. Alternatively, the water depth of Horizon Guyot and 17-171 was deeper during the deposition of this unit. Paleodepth calculations that take into account the accumulation and subsidence between the lower units and this uppermost unit suggest that the deposition of this uppermost unit occurred in water about 200 m deeper (Section 3.2; Appendix A.24). In this case, as the site deepened, the adjacent topographic highs of Horizon Guyot may no longer have been a lagoonal or platform-top environment and therefore may have ceased to contribute sediments with elevated $\delta^{13}C_{carbonate}$ values to 17-171. This unit is dated to the Turonian (Shipboard Scientific Party, 1973e). Therefore, the lower bulk $\delta^{13}C_{carbonate}$ value of the youngest lithologic unit at 17-171 may record a shift towards open-ocean $\delta^{13}C_{DIC}$ values during the Turonian.

In summary, at 17-171, most samples fall into two groups with different bulk $\delta^{13}C_{carbonate}$ values, depths, and lithologies (Figure 4.3; Table 5.1). The ranges of

$\delta^{13}C_{carbonate}$ values in these two units do not overlap, and the standard deviation of $\delta^{13}C_{carbonate}$ values in each unit is small (0.14‰ and 0.30‰, respectively). High bulk $\delta^{13}C_{carbonate}$ values (2.91 - 3.66‰) are associated with the oldest lithologic unit and may record lagoonal or platform-top $\delta^{13}C_{carbonate}$ values elevated by the mechanisms discussed in Section 5.1.1.1. One bulk $\delta^{13}C_{carbonate}$ value of 2.10‰ in the unit immediately above the oldest lithologic unit may have originally been elevated but lowered by diagenesis. Low bulk $\delta^{13}C_{carbonate}$ values (0.88 - 1.73‰, except one sample with 2.72‰) are associated with the youngest lithologic unit and may record either diagenesis or a shift towards an open-ocean depositional setting. In Section 5.1.2 I will address the hypothesis that $\delta^{13}C_{carbonate}$ variation can be explained by changes in global ocean $\delta^{13}C_{DIC}$ value over time, considering specifically 30-288A, 17-167, 17-169, 17-171, and 62-463.

5.1.2 Changes in global ocean $\delta^{13}C_{DIC}$ over time

Changes in the global carbon cycle during the Cenomanian and Turonian could change the average global ocean $\delta^{13}C_{DIC}$ value over time. Such changes in global ocean $\delta^{13}C_{DIC}$ may help explain

1. elevated bulk $\delta^{13}C_{carbonate}$ values at some "intermediate"-paleodepth and "deep"-paleodepth sites (30-288A, 17-167, and 17-169), and

2. changes in bulk $\delta^{13}C_{carbonate}$ values over time at individual sites (the decrease between units already noted at 17-171, and monotonic increases and decreases at 30-288A and 62-463).

There is reason to believe that global $\delta^{13}C_{carbonate}$ values may have changed in the Cenomanian and Turonian. OAE2 is commonly understood as a global positive $\delta^{13}C_{carbonate}$ excursion occurring in the latest Cenomanian to Cenomanian-Turonian boundary, and the magnitude of the excursion is different at different geographic locations (Section 1.4). Some of the discussion below describes high $\delta^{13}C_{carbonate}$ values with biostratigraphic ages too young to be consistent with OAE2. It is therefore relevant that previous authors have described a second major positive $\delta^{13}C_{carbonate}$ excursion in Cenomanian-Turonian time: the "Late Turonian Event," also called the Hitch Wood event after the Hitch Wood fossil bed, which has a distinctive faunal assemblage and has been used for correlation of sections in southern England (Figure 1.2; Gale, 1996; Cramer and Jarvis, 2020; Gale et al., 2020). The Late Turonian event

has been observed in Europe, Japan, and the U.S. western interior (Gale et al., 2020; Wiese, 1999; Stoll and Schrag, 2000; Takashima et al., 2019; Joo and Sageman, 2014), with different magnitudes in these locations (most about 1‰, with the greatest being 6.5‰ at Demerara Rise; Jones, 2018). In this section, I consider sites with elevated (> 3‰) bulk $\delta^{13}C_{carbonate}$ values (30-288A, 17-167, 17-169, 17-171) that may be related to OAE2 or the Late Turonian Event. I then consider a site that does not have elevated bulk $\delta^{13}C_{carbonate}$ values but does have changes over time in bulk $\delta^{13}C_{carbonate}$ values (62-463).

5.1.2.1 Explaining elevated bulk $\delta^{13}C_{carbonate}$ values

While high (> 3‰) bulk $\delta^{13}C_{carbonate}$ values at the "shallow"-paleodepth site 17-171 may be elevated because they are derived from carbonates deposited in a semi-restricted shallow setting, similarly high values at "intermediate"- and "deep"-paleodepth sites cannot be explained in this way (Section 5.1.1.4). Such values are observed at 30-288A and 17-167, "intermediate"-paleodepth sites both about 2 km deeper than 17-171 (Table 3.1; Figure 3.2), and 17-169, a "deep"-paleodepth site whose sediments are taken to be sourced from an "intermediate"-paleodepth setting because there are no "shallow"-paleodepth topographic highs near enough to the site to have contributed sediments (Section 3.2). Here I consider the possibility that the high (> 3‰) bulk $\delta^{13}C_{carbonate}$ values record changes in the average global ocean $\delta^{13}C_{DIC}$ value over time.

At the "intermediate"-paleodepth site 30-288A, a monotonic increase in $\delta^{13}C_{carbonate}$ values (2.61‰ to 3.42‰) is followed by a decrease (3.53‰ to 2.78‰; Figure 4.7). These sediments are tentatively dated to the Turonian based on biostratigraphy (Shipboard Scientific Party, 1975a). This feature includes all the high (> 3‰) bulk $\delta^{13}C_{carbonate}$ values at 30-288A and I will refer to it as the 30-288A positive excursion. The 30-288A positive excursion may record a positive excursion in average global ocean $\delta^{13}C_{DIC}$. Its tentative biostratigraphic age is inconsistent with the timing of OAE2 but could correspond to the Late Turonian Event (Figure 1.2).

At another "intermediate"-paleodepth site 17-167, high bulk $\delta^{13}C_{carbonate}$ values are clustered in one 70-cm-thick layer dated to the Turonian, while lower $\delta^{13}C_{carbonate}$ values and one $\delta^{13}C_{carbonate}$ value > 3‰ are measured below in a 179-cm-thick layer dated to the Cenomanian (Shipboard Scientific Party, 1973b). In the Turonian sediments at 17-167, the high bulk $\delta^{13}C_{carbonate}$ values are between 3.25‰ and 3.52‰

(Figure 4.8), falling within the range of the $\delta^{13}C_{carbonate}$ values that are part of the 30-288A positive excursion (2.61‰ to 3.53‰). As the ages of these 17-167 high bulk $\delta^{13}C_{carbonate}$ values and the 30-288A positive excursion both fall in the Turonian based on biostratigraphy, they may both record the same global high-$\delta^{13}C_{carbonate}$ event, again potentially the Late Turonian Event. Consistent with this explanation, the "baseline" (lower) bulk $\delta^{13}C_{carbonate}$ values are comparable between 30-288A (2.28‰ to 2.97‰) and 17-167 (2.53‰ to 2.77‰; Figures 4.7 and 4.8). In the Cenomanian sediments at 17-167, the single high $\delta^{13}C_{carbonate}$ value of 3.15‰ may correspond to another positive excursion, such as OAE2.

Finally, the "deep"-paleodepth site 17-169 only has high (> 3‰) bulk $\delta^{13}C_{carbonate}$ values (3.07‰ to 3.55‰; Table 4.1), with 1 sample dated to the Cenomanian, 9 samples dated to the Turonian, and 1 sample dated to the Albian based on biostratigraphy (Shipboard Scientific Party, 1973c). The high $\delta^{13}C_{carbonate}$ values at this site could be from multiple positive $\delta^{13}C_{carbonate}$ excursions,[3] although it is unlikely that similar $\delta^{13}C_{carbonate}$ values within the narrow range of 0.48‰ would be recorded from different positive excursions. The explanation for elevated $\delta^{13}C_{carbonate}$ values at 17-169 is not evident. It may be due to an aspect of the local environment such as ongoing high productivity in the surface ocean above elevating the $\delta^{13}C$ of the source of carbonate at the site (Section 5.1.1.4).

In sum, change in global ocean $\delta^{13}C_{DIC}$ is a possible explanation for high (> 3‰) bulk $\delta^{13}C_{carbonate}$ values at Pacific sites in this thesis. At 17-171, 30-288A, and 17-167, high $\delta^{13}C_{carbonate}$ values are part of changes in bulk $\delta^{13}C_{carbonate}$ values over time at the individual sites. Changes in bulk $\delta^{13}C_{carbonate}$ values over time, although not including high (> 3‰) $\delta^{13}C_{carbonate}$ values, can also be observed at 62-463 (Figures 4.5 and 4.13).

5.1.2.2 Explaining changes in bulk $\delta^{13}C_{carbonate}$ values over time at 62-463

At the "intermediate"-paleodepth site 62-463, there is a largely monotonic increase, decrease, and increase in bulk $\delta^{13}C_{carbonate}$ values through time within a unit of uni-

[3]By biostratigraphic age, the Cenomanian and Turonian $\delta^{13}C_{carbonate}$ values could correspond to OAE2, and the Albian-dated $\delta^{13}C_{carbonate}$ value of 3.19‰ might correspond to another positive excursion. Positive $\delta^{13}C_{carbonate}$ excursions dated to the Albian include OAEs 1b, 1c, and 1d, although the geographic extent of these excursions may have been regional rather than global (Herrle et al., 2004, 2015; Gale et al., 2011; Jenkyns, 2010).

form carbonate (Figure 4.5).[4] Based on biostratigraphy, the first increase occurs across the Cenomanian-Turonian boundary (32 samples dated to the Cenomanian and 4 dated to the Turonian), and the rest of the changes are dated to the Turonian (Shipboard Scientific Party, 1981b). These bulk $\delta^{13}C_{carbonate}$ changes may record changes in global ocean $\delta^{13}C_{DIC}$ over time. By biostratigraphic age, the Cenomanian-Turonian bulk $\delta^{13}C_{carbonate}$ increase could correspond to OAE2, and the Turonian increase could correspond to the Late Turonian Event.

At 62-463, change in the average global ocean $\delta^{13}C_{DIC}$ value is more likely to explain observations of bulk $\delta^{13}C_{carbonate}$ values than change in the paleodepth of initial deposition of sediments. The unit of uniform carbonate containing $\delta^{13}C_{carbonate}$ changes at 62-463 has no indications of changes in depositional setting before, during, or after the Cenomanian and Turonian (Figure 4.5; Shipboard Scientific Party, 1981b) suggesting variation in $\delta^{13}C_{carbonate}$ is not due to changes in paleodepth of deposition (Section 5.1.1.4).

In summary, change in global ocean $\delta^{13}C_{DIC}$ is a possible explanation for high ($>$ 3‰) bulk $\delta^{13}C_{carbonate}$ values, as well as change in $\delta^{13}C_{carbonate}$ values over time, at Pacific sites in this thesis. Biostratigraphic age constraints put a positive $\delta^{13}C_{carbonate}$ excursion at 30-288A and high $\delta^{13}C_{carbonate}$ values at 17-167 in the Turonian, so these $\delta^{13}C_{carbonate}$ values may record the Late Turonian Event, but not OAE2. Meanwhile, age constraints on certain high ($>$ 3‰) bulk $\delta^{13}C_{carbonate}$ values at "intermediate"-paleodepth site 17-167 do not rule out the possibility that these $\delta^{13}C_{carbonate}$ values record a global OAE2 positive $\delta^{13}C_{carbonate}$ excursion of at least 1‰ magnitude, perhaps comparable to the magnitude of the 30-288A positive excursion. This possibility also applies at "shallow"-paleodepth site 17-171, where high ($>$ 3‰) bulk $\delta^{13}C_{carbonate}$ values are dated to the Cenomanian by biostratigraphy (Section 5.1.1.4) and may represent an excursion of magnitude $\sim$2‰ or greater. Finally, a monotonic increase in $\delta^{13}C_{carbonate}$ values over time at "intermediate"-paleodepth site 62-463 likewise could be attributed to OAE2. To further evaluate the possibility that OAE2 may be recorded at Pacific sites in this thesis, I next compare all Pacific bulk $\delta^{13}C_{carbonate}$ values from this thesis to the bulk carbonate $\delta^{13}C_{carbonate}$ values from samples of Cenomanian-Turonian age in other basins.

[4]The first increase includes 36 samples with bulk $\delta^{13}C_{carbonate}$ 1.75‰ to 3.19‰, 309.7 - 405 mbsf, then the decrease includes 11 samples (counting the one overlapping) with bulk $\delta^{13}C_{carbonate}$ 1.41‰ to 3.19‰, 262.2 - 309.7 mbsf, then the second increase includes 9 samples (counting the one overlapping) with bulk $\delta^{13}C_{carbonate}$ 1.41‰ to 2.72‰, 243.6 - 262.2 mbsf.

5.2 Pacific bulk carbonate $\delta^{13}C_{carbonate}$ values in the context of $\delta^{13}C_{carbonate}$ and $\delta^{18}O_{carbonate}$ values from the rest of the ocean

Pacific bulk $\delta^{13}C_{carbonate}$ values from this thesis are compared to shallow marine bulk carbonate samples from other basins dated to the Cenomanian-Turonian (i.e. containing a number of planktonic foraminifera species also found in the Pacific sediments sampled for this thesis; Section 4.4). Bulk $\delta^{13}C_{carbonate}$ values are generally lower from Cenomanian-Turonian sediments in the Pacific (this thesis) as well as the margin of the Neotethys which is connected to the Pacific (Bomou et al., 2013), relative to $\delta^{13}C_{carbonate}$ values from marginal North Atlantic and Western Tethys sites (Caron et al., 2006; Falzoni et al., 2016; Jarvis et al., 2011). These observations are consistent with the hypothesis that during the Cenomanian-Turonian the North Atlantic and Western Tethys were shallower and more restricted than the Neotethys and Pacific and maintained higher average $\delta^{13}C_{DIC}$.

Pacific bulk carbonate samples from this thesis also have higher $\delta^{13}C_{carbonate}$ values and lower $\delta^{18}O_{carbonate}$ values than late Cretaceous benthic foraminifera samples compiled by Cramer et al. (2009) and Friedrich et al. (2012). For the majority of the samples, the differences are as expected for bulk carbonate vs. benthic foraminifera. I first compare the Pacific bulk carbonate $\delta^{13}C_{carbonate}$ values from this thesis to the bulk carbonate $\delta^{13}C_{carbonate}$ values from samples of Cenomanian-Turonian age in other basins.

5.2.1 Bulk carbonate $\delta^{13}C_{carbonate}$ sections from the Cenomanian-Turonian outside the Pacific

Bulk samples from Cenomanian-Turonian sediments (compared within the same fossil occurrence intervals) have generally lower $\delta^{13}C_{carbonate}$ values at sites in the Neotethys and Pacific Oceans than the North Atlantic and Western Tethys (Figure 4.18; Section 4.4). One site in the Western Tethys, wadi Bahloul, has $\delta^{13}C_{carbonate}$ values that generally fall between these lower and higher groups of $\delta^{13}C_{carbonate}$ values (Figures 4.17 and 4.18). In this section I argue that these observations can be explained by differences in the degree of restriction of the water masses whence carbonate sediments are sourced. My argument has three parts:

1. At all non-Pacific sites examined in this thesis, semi-restricted shelf or platform areas were close by and may have provided high-$\delta^{13}C$ carbonate sediment, as $\delta^{13}C_{carbonate}$ values may be systematically elevated in such areas (Section 5.1.1.1).

2. It is possible that more restricted, shallower basins (North Atlantic and smaller basins within the Western Tethys) had overall higher $\delta^{13}C_{DIC}$ than better-connected, wider basins (Neotethys and Pacific) during the Cenomanian and Turonian.

3. Meteoric diagenesis may also play a role in setting $\delta^{13}C_{carbonate}$ values at wadi Bahloul, but cannot explain the overall differences between the North Atlantic and Western Tethys versus the Neotethys and Pacific.

Regarding (1), one possible shortcoming of this explanation is that it may not account for Pacific site 17-171, where sourcing of carbonate sediment from a shallow semi-restricted setting was proposed as a possible way to explain high $\delta^{13}C_{carbonate}$ values in the lowermost lithologic unit (Section 5.1.1.5). At non-Pacific sites, the highest $\delta^{13}C_{carbonate}$ values are part of the positive $\delta^{13}C_{carbonate}$ excursions noted there (Table 1.1; Figure 1.6). Therefore, I propose that a positive $\delta^{13}C_{DIC}$ excursion not recorded at 17-171 accounts for the $\delta^{13}C_{carbonate}$ values at non-Pacific sites that are higher than the highest $\delta^{13}C_{carbonate}$ values at 17-171. The highest $\delta^{13}C_{carbonate}$ values at 17-171 are comparable to "baseline" values from non-Pacific sites Eastbourne, Clot Chevalier, and Pont d'Issole, consistent with the explanation that all record elevated $\delta^{13}C_{carbonate}$ values from shallow semi-restricted settings and that no $\delta^{13}C_{carbonate}$ excursion is recorded at 17-171 (Section 5.1.1.5).

Regarding (2), paleogeographic reconstructions indicate both the North Atlantic and the Western Tethys were relatively shallow and restricted in Cenomanian-Turonian time (Figure 1.7; Section 1.5). Therefore, the water in the North Atlantic and the Western Tethys may not have been well mixed with the rest of the ocean and could have retained a different $\delta^{13}C_{DIC}$. Moreover, because Eastbourne and the Vocontian Basin (where Clot Chevalier and Pont d'Issole were located) were connected by a shallow seaway (Section 3.3; Figure A.5), similar $\delta^{13}C_{DIC}$ values at Eastbourne, Clot Chevalier, and Pont d'Issole would be expected. For the time of OAE2, past workers have remarked that $\delta^{13}C_{carbonate}$ curves and planktonic foraminiferal bioevents can be precisely correlated between Eastbourne and Pont d'Issole (Jarvis et al., 2011; Falzoni et al., 2016), consistent with these sites being in the same water mass. Also, in

the compilation of Owens et al. (2018), the estimated maximum OAE2 positive $\delta^{13}C$ excursion in this region of the North Atlantic and Western Tethys ranges from 1-3‰, in contrast to some higher estimated maximum excursion magnitudes occuring elsewhere, which could also be consistent with similar $\delta^{13}C_{DIC}$ between Eastbourne, Clot Chevalier, and Pont d'Issole. If $\delta^{13}C_{carbonate}$ values at Eastbourne, Clot Chevalier, and Pont d'Issole at least partially reflect $\delta^{13}C_{DIC}$ values from the same water mass, they might be high relative to Pacific $\delta^{13}C_{carbonate}$ values because basinal $\delta^{13}C_{DIC}$ was higher in the North Atlantic and the Western Tethys than the Pacific during the Cenomanian and Turonian. Also, the Neotethys was relatively well-connected to the Pacific during Cenomanian-Turonian time (Figure 1.7; Section 1.5). If $\delta^{13}C_{carbonate}$ values at Gongzha at least partially reflect $\delta^{13}C_{DIC}$ values, they would be expected to be similar to Pacific $\delta^{13}C_{carbonate}$ values as observed.

As wadi Bahloul was located in the Western Tethys, the observation that wadi Bahloul $\delta^{13}C_{carbonate}$ values are lower on average than the other Western Tethys sites (Clot Chevalier, Pont d'Issole) suggests that wadi Bahloul may have been better connected to the Neotethys. Paleogeographic maps (Figure 1.7) show wadi Bahloul was not as close to Eastbourne, Clot Chevalier, and Pont d'Issole as those sites were to each other, and that it was located in a different epicontinental basin of the Western Tethys which was closer to the Neotethys and therefore potentially better connected to it. It is therefore plausible that the $\delta^{13}C_{carbonate}$ values at wadi Bahloul record $\delta^{13}C_{DIC}$ of water better-mixed with Neotethys water than the water at Eastbourne, Clot Chevalier, and Pont d'Issole. It would be expected for such water to have a $\delta^{13}C_{DIC}$ in between the higher $\delta^{13}C_{DIC}$ of North Atlantic and the Western Tethys water and the lower $\delta^{13}C_{DIC}$ of Neotethys and Pacific water.

Finally, regarding (3), meteoric diagenesis likely does not explain why $\delta^{13}C_{carbonate}$ values at North Atlantic and Western Tethys sites (Eastbourne, Clot Chevalier, and Pont d'Issole) are generally higher than $\delta^{13}C_{carbonate}$ values at Neotethys and Pacific sites (Gongzha, sites in this thesis). Diagenesis is generally expected to lower $\delta^{13}C_{carbonate}$ values, including meteoric diagenesis (e.g. Allan and Matthews, 1990; Section 1.2.5), which might affect outcrop sections such as the non-Pacific sections examined here. Pacific bulk $\delta^{13}C_{carbonate}$ values (especially at 62-463 and 32-305) are likely not extensively reset by diagenesis (Sections 5.1.1.2 and 5.1.1.3). Eastbourne $\delta^{13}C_{carbonate}$ values are thought to be relatively unaffected by diagenesis across the 27-meter section, although sub-meter variations in $\delta^{13}C_{carbonate}$ are correlated with lithologic changes and attributed to diagenesis (Paul et al., 1999). If diagenesis has

systematically lowered $\delta^{13}C_{carbonate}$ values at Eastbourne, Clot Chevalier, and Pont d'Issole, then they would have been originally even higher than Pacific $\delta^{13}C_{carbonate}$ values. As for Gongzha, Bomou et al. (2013) invoke diagenetic alteration to explain $\delta^{18}O_{carbonate}$ values of -11.9‰ to -6.2‰ they observed in that section, and acknowledge that $\delta^{13}C_{carbonate}$ values there may be diagenetically altered as well. If diagenesis has systematically lowered $\delta^{13}C_{carbonate}$ values at Gongzha, the systematically lower Pacific $\delta^{18}O_{carbonate}$ values relative to sites from other basins would still have to be explained. Finally, regarding the wadi Bahloul section examined in this thesis, Caron et al. (2006) acknowledge diagenetic alteration could have affected its $\delta^{13}C_{carbonate}$ values, noting covariance in $\delta^{13}C_{carbonate}$ and $\delta^{18}O_{carbonate}$ values in the unit above. It is possible that mild meteoric diagenesis at wadi Bahloul does help explain the $\delta^{13}C_{carbonate}$ values there, if those $\delta^{13}C_{carbonate}$ values were originally similar to higher $\delta^{13}C_{carbonate}$ values at other Western Tethys sites but were diagenetically lowered.

In summary, it is possible that the North Atlantic and Western Tethys had higher $\delta^{13}C_{DIC}$ than the Neotethys and Pacific during Cenomanian-Turonian time. Although compiled benthic foraminiferal $\delta^{13}C_{carbonate}$ and $\delta^{18}O_{carbonate}$ values do not seem to support a large (e.g., > 1‰) interbasinal difference in $\delta^{13}C_{DIC}$ between the North Atlantic and the Pacific, these data are relatively sparse (Appendix A.29; Cramer et al., 2009; Friedrich et al., 2012). Differences in $\delta^{13}C_{carbonate}$ values between sections may be best explained by basin-scale differences in $\delta^{13}C_{DIC}$ between shallow, semi-restricted basins such as the North Atlantic and Western Tethys vs. deeper, better-circulated basins such as the Neotethys and Pacific (Section 1.5). A complementary possibility is that high-$\delta^{13}C_{carbonate}$ sediment from nearby semi-restricted shelf or platform areas arrived at individual sites in different proportions. Information about the paleoenvironments of non-Pacific sites examined in this thesis is insufficiently detailed to deconvolve this possibility and the possibility that interbasinal $\delta^{13}C_{DIC}$ differences explain $\delta^{13}C_{carbonate}$ differences. In the following section, I place $\delta^{13}C_{carbonate}$ and $\delta^{18}O_{carbonate}$ values from Pacific sites in this thesis in an even broader spatial and temporal context, comparing them to compiled benthic foraminiferal $\delta^{13}C_{carbonate}$ and $\delta^{18}O_{carbonate}$ values from across the globe of ages 115 Ma - present.

5.2.2 Benthic foraminifera $\delta^{13}C_{carbonate}$ and $\delta^{18}O_{carbonate}$ compilation from the late Cretaceous and Cenozoic

From the late Cretaceous through the present, benthic foraminiferal $\delta^{13}C_{carbonate}$ values generally become lower and benthic foraminiferal $\delta^{18}O_{carbonate}$ values generally become higher (Figure 5.7). The overall increase in benthic foraminiferal $\delta^{18}O_{carbonate}$ values over the Cenozoic is largely monotonic and is understood to reflect long-term cooling of global climate and growth of ice sheets (Zachos et al., 2001, 2008). The overall decrease in benthic foraminiferal $\delta^{13}C_{carbonate}$ values is not as monotonic. Compilers of $\delta^{13}C_{carbonate}$ data typically do not describe a decrease across the Cenozoic but instead note $\delta^{13}C_{carbonate}$ decreases from roughly the beginning of the Neogene through the present (e.g. Hayes et al., 1999; Zachos et al., 2001; Cramer et al., 2009). It is widely accepted that baseline global ocean $\delta^{13}C_{DIC}$, reflected by benthic foraminiferal $\delta^{13}C_{carbonate}$ values, changes in the long term (e.g. over millions of years). Explanations for the decreasing trend from the Neogene through the present either invoke a decrease in the proportion of carbon buried as organic matter vs. carbonate sediments (Lasaga et al., 1985; Shackleton, 1987), or an increase in the average $\delta^{13}C$ of buried organic matter (Arthur et al., 1985; Hayes et al., 1999).

Cenomanian and Santonian sediments from Demerara Rise, a submarine plateau off the coast of northeastern South America, do not have $\delta^{13}C_{carbonate}$ and $\delta^{18}O_{carbonate}$ values consistent with the trends described above. The benthic foraminiferal samples considered here include a subset from Demerara Rise (n = 914) measured by Friedrich et al. (2012) that have on average lower $\delta^{13}C_{carbonate}$ and $\delta^{18}O_{carbonate}$ values than all other compiled benthic foraminiferal samples as well as the bulk carbonate samples measured for this thesis (Figure 5.7). Because the Cenomanian and Santonian Demerara Rise data are anomalous, possibly derived from a unique water mass (MacLeod et al., 2008; Jiménez Berrocoso et al., 2010), I omit them from consideration. Cramer et al. (2009) and Friedrich et al. (2012) measured other benthic foraminiferal samples from the Cenomanian through the Santonian (n = 323), including samples collected from the Atlantic (n = 207), and these data do not share the especially low $\delta^{13}C$ and $\delta^{18}O$ of the Demerara Rise data. The anomalous values all came from a sedimentary sequence notable for its very high proportion of black shale (organic carbon content of 6-8wt.%) (Shipboard Scientific Party, 2004) and the exceptional preservation of glassy foraminiferal tests (Friedrich et al., 2012). Explaining the anomaly is beyond the scope of this thesis, but previous authors have suggested that a regional water

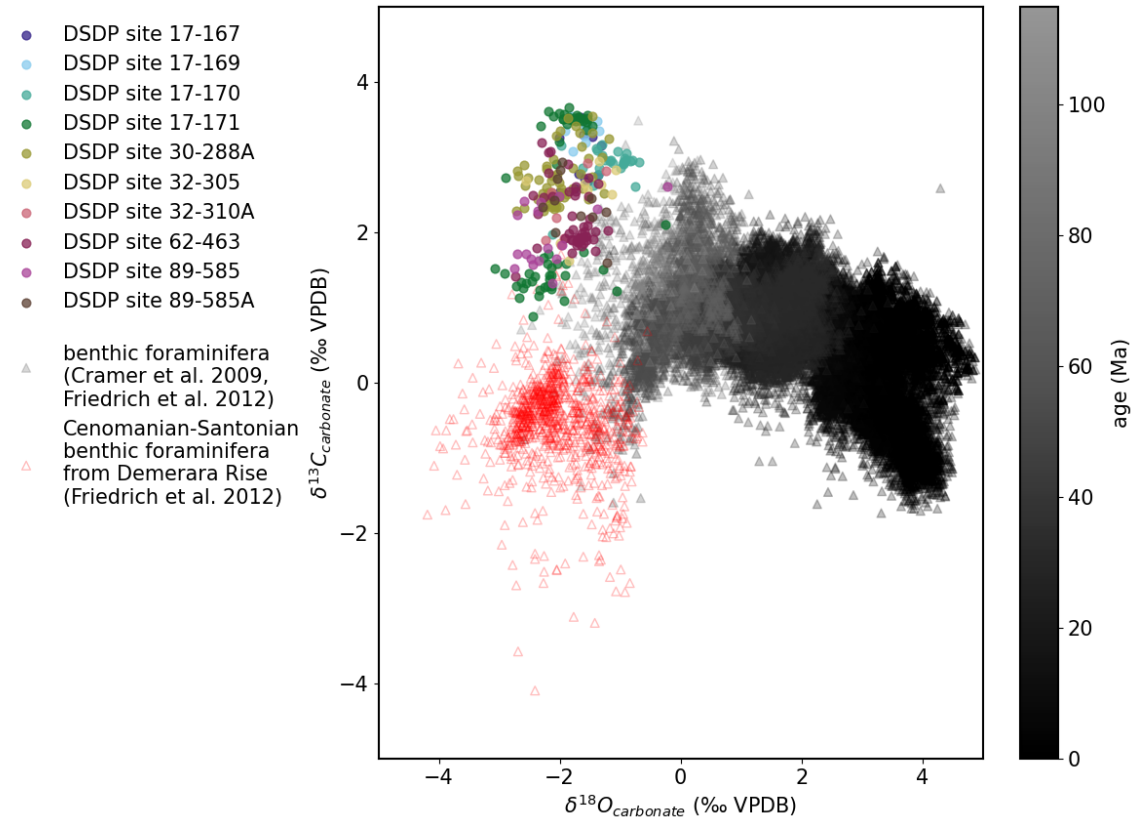

Figure 5.7: $\delta^{13}C_{carbonate}$ values plotted against $\delta^{18}O_{carbonate}$ values of benthic foraminifera samples compiled by Cramer et al. (2009) and Friedrich et al. (2012), indicated with triangle-shaped markers in red (for benthic foraminifera samples from Cenomanian-Santonian sediments on Demerara Rise, n = 914) or colored by age according to the greyscale colorbar (all other Cenomanian-Turonian benthic foraminifera samples, n = 31163). (Lighter grey samples are older, whereas darker grey samples are younger.) Also, $\delta^{13}C_{carbonate}$ values plotted against $\delta^{18}O_{carbonate}$ values of bulk carbonate samples from this thesis (n = 254), indicated with circle-shaped markers.

mass with high temperature and salinity ("Demerara Bottom Water") was trapped on Demerara Rise during the deposition of this sequence (MacLeod et al., 2008; Jiménez Berrocoso et al., 2010).

The $\delta^{13}C_{carbonate}$ and $\delta^{18}O_{carbonate}$ values of Pacific bulk carbonate samples from this thesis are consistent with the trends discussed here, in that they have higher $\delta^{13}C_{carbonate}$ values and lower $\delta^{18}O_{carbonate}$ values than benthic foraminifera samples of the same age (Figure 5.7) to the extent expected for bulk carbonate samples vs. benthic foraminiferal samples recording $\delta^{13}C_{DIC}$ and $\delta^{18}O_{seawater}$ (Sections 5.1.1.2 and 5.1.1.3). However, Pacific bulk $\delta^{13}C_{carbonate}$ values from this thesis do not consistently record a positive $\delta^{13}C_{carbonate}$ excursion around the time of OAE2 (Section 5.1.1). Therefore, in the final section, I consider whether the Pacific $\delta^{13}C_{carbonate}$ record is consistent with a global positive excursion in $\delta^{13}C_{DIC}$ at the time of OAE2.

5.3 Implications for OAE2

5.3.1 Possible explanations for Pacific vs. non-Pacific bulk $\delta^{13}C_{carbonate}$ values in this thesis

The $\delta^{13}C_{carbonate}$ values at Pacific sites examined in this thesis, alongside $\delta^{13}C_{carbonate}$ values at non-Pacific sites where a $\delta^{13}C_{carbonate}$ excursion is evident in OAE2 time (Eastbourne, Clot Chevalier, Pont d'Issole, Gongzha, and other sites as documented in e.g. Owens et al., 2018) can be explained by two possible explanations:

1. A global ocean OAE2 $\delta^{13}C$ excursion occurred alongside a process that largely prevented its deposition, preservation, or recovery in the mid-Pacific.

2. The OAE2 $\delta^{13}C$ excursion occurred only in shallow epicontinental basins and continental slope environments.

In explanation (1), the OAE2 positive $\delta^{13}C$ excursion may be incompletely observed in the Pacific at 17-167, 17-171 and 62-463 (Section 5.1.2), and is not observed at any other Pacific sites in the samples examined here, even though all Pacific sites in this thesis have $\delta^{13}C_{carbonate}$ values dated to the Cenomanian and Turonian by biostratigraphy. Random chance leading to poor scientific drilling recovery may be invoked to help explain this incomplete observation of the OAE2 positive $\delta^{13}C$ excursion in the Pacific. However, if incomplete observation is not wholly due to random chance, it is also necessary to invoke some aspect of the Pacific Ocean during

Cenomanian-Turonian time that could systematically lead to incomplete observation. One possibility is that carbonate sediments were not deposited at most intermediate and deep paleodepths in the Pacific during the global ocean positive $\delta^{13}C$ excursion due to significant shallowing of the CCD relative to its estimated depth of ∼3000 mbsl (Tyrrell and Zeebe, 2004; Zeebe and Tyrrell, 2019) during that time (a "carbonate crash"). Another possibility is that carbonate sediments of OAE2 age do exist in the Pacific but that scientific drilling systematically failed to recover them. When sediments contain both carbonate and chert it is difficult to recover the carbonate, so if relatively more chert is present in sediments from the time of OAE2, that could explain lack of recovery of OAE2 carbonate sediments. As chert forms from biosilica, an increase in chert could indicate increased deposition of biosilica, which could in turn result from increased weathering of silicate minerals (e.g. Penman, 2016). As Equation 1.1 shows, increased weathering of silicate minerals would drive the production of more $CaCO_3$ as well as more SiO_2, so if a greater proportion of chert to carbonate was deposited in the open ocean around the time of OAE2, a greater proportion of carbonate to chert would have to be deposited elsewhere on the globe.

In explanation (2), an OAE2 positive $\delta^{13}C_{carbonate}$ excursion did not occur in the mid-Pacific and is therefore not observed. Change in $\delta^{13}C_{carbonate}$ values across the Cenomanian-Turonian boundary at 17-171 is explained by local paleoenvironmental changes (Section 5.1.1.5). Elevated $\delta^{13}C_{carbonate}$ values and changes in $\delta^{13}C_{carbonate}$ values during the Cenomanian-Turonian at other sites (17-167 and 62-463) are likewise explained by factors local to the sites, such as shifts in productivity in the surface ocean above. This explanation requires a systematic reason for an OAE2 positive $\delta^{13}C_{carbonate}$ excursion to occur in basins outside the Pacific, including in the Neotethys, which is well connected to the Pacific. A slightly different version of this explanation is explanation that an OAE2 positive $\delta^{13}C_{carbonate}$ excursion occurred only in shallow epicontinental basins and continental slope environments (< about 1000 mbsl paleodepth), in which case 17-171 does record OAE2 as suggested in Section 5.1.2. This explanation requires a systematic reason why an OAE2 positive $\delta^{13}C_{carbonate}$ excursion occurred in some parts of the global ocean but not others. For example, increased burial of organic carbon in a restricted basin could have affected the $\delta^{13}C_{DIC}$ of a water mass but not the $\delta^{13}C_{DIC}$ of the global ocean, if that water mass was not well mixed with the global ocean.

5.3.2 Hypothetical OAE2 scenarios in a simple carbon cycle model

To consider whether the Pacific $\delta^{13}C_{carbonate}$ record is consistent with a global positive excursion in $\delta^{13}C_{DIC}$ in OAE2 time, I return to the mass balance model in which the carbon entering the ocean and atmosphere must have the same mass and isotopic composition as the carbon buried as carbonate sediment or organic sediment over long time scales (Section 1.2). In this model, the OAE2 positive $\delta^{13}C_{carbonate}$ excursion represents a period of increased global burial fraction of organic matter, but in this thesis it is shown that multiple Pacific sites do not record the OAE2 positive $\delta^{13}C_{carbonate}$ excursion (Section 5.1.1). To explain this discrepancy in the context of the mass balance model, I consider two very simplified hypothetical scenarios:

1. A "carbonate crash" occurred in the Pacific at the time of a global OAE2 positive $\delta^{13}C_{carbonate}$ excursion. In this scenario, the Pacific $\delta^{13}C_{carbonate}$ values in this thesis (mostly) do not come from the time of OAE2 because little to no carbonate sediment was deposited in the Pacific at this time. (This scenario is synonymous to the standard model in that all available carbonate sediments from the time of OAE2 have a positive $\delta^{13}C_{carbonate}$ excursion.)

2. A majority of the carbonate sediments deposited at the time OAE2 were deposited in the Pacific. Specifically, carbonate sediment deposition is assumed to be directly proportional to ocean area, so ∼65% of carbonate sediment was deposited in the Pacific, where no OAE2 positive $\delta^{13}C_{carbonate}$ excursion occurred. (In this scenario, the average global positive $\delta^{13}C_{carbonate}$ excursion has a magnitude 35% of its magnitude in scenario 1.)

These hypothetical scenarios are end-members with different implications for the $\delta^{13}C_{carbonate}$ term, the $\delta^{13}C$ of carbonate sediments in the model as presented in Section 1.2. In scenario (1), the $\delta^{13}C_{carbonate}$ term matches $\delta^{13}C_{carbonate}$ values measured outside the Pacific. In scenario (2), the $\delta^{13}C_{carbonate}$ term is a weighted average of $\delta^{13}C_{carbonate}$ values measured in the Pacific and outside the Pacific. Importantly, in the model as presented in Section 1.2, the $\delta^{13}C$ of carbonate sediments is set by the fraction of carbon buried as organic matter sediment globally and is therefore the same everywhere in the global ocean (Equations 1.3 and 1.4). In order to model the many hypothetical scenarios between the two end-members above, the $\delta^{13}C$ of carbonate sediments $\delta^{13}C_{carbonate}$ must instead be calculated as a weighted average:

$$\delta^{13}C_{carbonate} = \mathrm{f}_{carbonate}^{Pacific}\delta^{13}C_{carbonate}^{Pacific} + \left(1 - \mathrm{f}_{carbonate}^{Pacific}\right)\delta^{13}C_{carbonate}^{non-Pacific} \quad (5.1)$$

where the term $\delta^{13}\mathrm{C}_{\mathrm{carbonate}}^{\mathrm{Pacific}}$ is the δ^{13}C of carbonate sediments in the Pacific, the term $\delta^{13}\mathrm{C}_{\mathrm{carbonate}}^{\mathrm{non-Pacific}}$ is the δ^{13}C of carbonate sediments outside of the Pacific, and $\mathrm{f}_{carbonate}^{Pacific}$ is the fraction of global carbon deposited in the Pacific (0% in the first end-member and 65% in the second end-member). Following the carbon isotope model of Owens et al. (2018), I assume that before OAE2 the high-pCO2 world has a $\delta^{13}\mathrm{C}_{\mathrm{carbonate}}$ of 1.7‰ for carbonate sediments both in the Pacific and outside the Pacific ($\delta^{13}\mathrm{C}_{\mathrm{carbonate}}^{\mathrm{Pacific}}$ and $\delta^{13}\mathrm{C}_{\mathrm{carbonate}}^{\mathrm{non-Pacific}}$), that the δ^{13}C of the total outflux from the ocean and atmosphere reservoir ($\delta^{13}\mathrm{C}_{\mathrm{total}}$) is -4.0‰, and that the δ^{13}C of organic matter ($\delta^{13}\mathrm{C}_{\mathrm{organic}}$) is offset by ε from $\delta^{13}\mathrm{C}_{\mathrm{carbonate}}$ (Equation 1.5) where ε is -28‰. Owens et al. (2018) use a time-dependent model after Kump and Arthur (1999) to model a 3‰ global OAE2 positive $\delta^{13}\mathrm{C}_{\mathrm{carbonate}}$ excursion, similar to scenario 1 but not directly comparable as their model excursion is transient. Using my simple mass balance model that assumes steady state (Equations 1.3-1.5 and Equation 5.1), the global burial fraction of organic matter is 20.4% before OAE2. In end-member scenario (1), to produce a global 3‰ positive $\delta^{13}\mathrm{C}_{\mathrm{carbonate}}$ excursion while no carbonate sediments are being deposited in the Pacific, the global burial fraction of organic matter ($\mathrm{f}_{organic}$) must increase to 31.1%. In end-member scenario (2), to produce a 3‰ positive $\delta^{13}\mathrm{C}_{\mathrm{carbonate}}$ excursion outside the Pacific while 65% of carbonate sediments with unchanged δ^{13}C are being deposited in the Pacific, $\mathrm{f}_{organic}$ must be 24.1%. The estimated change in $\mathrm{f}_{organic}$ for OAE2 is sensitive to the OAE2 positive $\delta^{13}\mathrm{C}_{\mathrm{carbonate}}$ excursion size. An excursion of 7‰ requires $\mathrm{f}_{organic}$ be 45.4% in scenario (1) but only 29.1% in scenario (2). The estimated change in $\mathrm{f}_{organic}$ for OAE2 in scenario 2 is always 35% of the estimated change in $\mathrm{f}_{organic}$ for OAE2 in scenario 1.

In summary, if an OAE2 positive $\delta^{13}\mathrm{C}_{\mathrm{carbonate}}$ excursion did not occur in the Pacific, a smaller global burial fraction of organic matter during the OAE is implied. Owens et al. (2018) estimated organic carbon burial at the time of OAE2 based on mapping organic-rich sediments of the correct age and found it was much smaller than the organic carbon burial required by the model to produce a 3‰ positive $\delta^{13}\mathrm{C}_{\mathrm{carbonate}}$ global excursion. My scenario 2 demonstrates that if OAE2 did not occur in the Pacific, it could help account for this discrepancy on the model side by requiring less organic carbon burial.

Conclusions and future work

To explain $\delta^{13}C_{carbonate}$ values at Pacific sites in this thesis from around the time of OAE2, I invoke both factors local to the sites, such as proximity to a shallow semi-restricted carbonate platform in the case of 17-171, and changes in global ocean $\delta^{13}C_{DIC}$ over time. Explanations are focused on $\delta^{13}C_{DIC}$ change because the $\delta^{13}C$ values of carbonate sediments at Pacific sites in this thesis likely mostly record the $\delta^{13}C_{DIC}$ of the waters in which they formed (Sections 5.1.1.2 and 5.1.1.3). Therefore I can use this newly collected data to test the hypothesis that there was a global change in the $\delta^{13}C_{DIC}$ of seawater at the time of OAE2 (Section 1.6), as is predicted by a model of a substantial increase in organic carbon burial (Section 1.2).

An OAE2 positive $\delta^{13}C_{carbonate}$ excursion is not observed at most Pacific sites in this thesis (Section 5.1.2), which challenges our current understanding of OAE2 as a perturbation to the global carbon cycle (Section 1.6). One possible explanation is that a global ocean OAE2 $\delta^{13}C$ excursion did occur, but that some process largely prevented its deposition, preservation, or recovery in the mid-Pacific. I propose that significant shallowing of the Pacific CCD at the time of OAE2, and/or an abundance of chert in sediments from the time of OAE2, could prevent deposition and recovery respectively. Another possible explanation is that the OAE2 $\delta^{13}C$ excursion occurred only in the shallow epicontinental basins and continental slope environments where it is observed (including the Atlantic, Western Tethys, Neotethys, and Western Interior Seaway of North America; Section 1.4.2) because organic carbon burial within these relatively restricted water masses changed their $\delta^{13}C_{DIC}$s but did not affect $\delta^{13}C_{DIC}$ in the mid-Pacific (Section 5.3.1).

This thesis underlines a few well-known challenges in the study of paleoclimate events. One such challenge is the challenge of extrapolating past global climate from the geographically limited records that survive. The preponderance of previously published evidence for a global OAE2 positive $\delta^{13}C$ excursion (Section 1.4.2) was limited because it did not include the large, climatically significant Pacific basin, and the Pacific $\delta^{13}C_{carbonate}$ records in this thesis raise the possibility that OAE2 may not

have been a global event. Another such challenge is the challenge of accurate and precise age determination. In this thesis, given the generally poor recovery of Pacific sediments from the time of OAE2, it would have been useful to know which sediments were exactly contemporaneous with well-known OAE2 sediments from outside the Pacific (e.g. sediments at Eastbourne), or if any exactly contemporaneous sediments were recovered at all. Another challenge, specific to working with deep-sea sediments, is the loss of information associated with drilling sediments from the bottom of the ocean rather than viewing exposed cross-sections. For example, the deep-sea Pacific sediments examined in this thesis could not be examined *in situ* and the reasons for poor recovery of some sediments are accordingly ambiguous. Future work could help circumvent these challenges to more completely characterize OAE2 in the Pacific.

First, future work could further test the possibility that a global ocean OAE2 $\delta^{13}C$ excursion occurred alongside a process that largely prevented its deposition, preservation, or recovery in the mid-Pacific (Section 5.3.1). Assuming such an excursion occurred and its magnitude was comparable to the magnitude of the positive $\delta^{13}C_{carbonate}$ excursion as recorded at non-Pacific sites, I could formally estimate the likelihood that it would be recorded in Pacific sediments examined in this thesis. I would use published records from non-Pacific sites to constrain the assumed duration and magnitude of the excursion in the global ocean. Then, I would use existing biostratigraphy and core recovery data (Section 4.2), assuming a range of possible sediment accumulation rates, to calculate the expected duration and magnitude at Pacific sites in this thesis. The results of this calculation would be compared to the $\delta^{13}C_{carbonate}$ values actually observed at the Pacific sites in this thesis. This calculation could constrain the sediment accumulation rate that would be needed to explain why a global OAE2 positive $\delta^{13}C_{carbonate}$ excursion is not observed at most Pacific sites in this thesis.

Second, future work could generate more geologic records from the Pacific around the time of OAE2. In addition to the Pacific sites examined in this thesis, I identified 19 other DSDP and ODP sites at which sediments were dated to the Cenomanian and/or Turonian (Section 3.1; Table A.3) and it may be possible to measure $\delta^{13}C_{carbonate}$ and $\delta^{18}O_{carbonate}$ in sediments from these holes. Also, pelagic limestone deposited in the Pacific around the time of OAE2 is today exposed in California, including the Calera Limestone formation deposited in the eastern Pacific (Sliter and McGann, 1992; Sliter, 1999) and the Laytonville Limestone formation, which is thought to have been deposited farther south than the Calera (Tarduno et al., 1986;

Sliter and Silva, 1990; Sliter, 1999). Measuring $\delta^{13}C_{carbonate}$ values from the time of OAE2 in any of these sediments would make available more records of OAE2 in the Pacific.

This thesis also touches on a few research questions outside the Pacific. One question that is not fully resolved is why benthic foraminiferal $\delta^{13}C_{carbonate}$ values generally become lower from the Neogene through the present. Another question concerns benthic foraminiferal $\delta^{13}C_{carbonate}$ and $\delta^{18}O_{carbonate}$ values in Cenomanian and Santonian sediments at Demerara Rise, which are anomalous in the context of global trends during the late Cretaceous and Cenozoic (Section 5.2.2). Future work on these questions could adjust our understanding of the long-term global carbon cycle and the potential for spatial heterogeneity in the surficial carbon reservoir.

In summary, to better understand whether there was a global change in the $\delta^{13}C_{DIC}$ at the time of OAE2, it would be useful to have more Pacific geologic records from around this time as well as higher-resolution age models for such records. Future work on these and other questions could adjust our understanding of OAE2 and, more broadly, our understanding of perturbations to the carbon cycle.

Bibliography

Ahm, A. S. C., Bjerrum, C. J., Blättler, C. L., Swart, P. K., and Higgins, J. A. (2018). Quantifying early marine diagenesis in shallow-water carbonate sediments. *Geochimica et Cosmochimica Acta*, 236:140–159.

Al-Rawi, M. M. (2002). The contribution of Ibn Sina (Avicenna) to the development of Earth sciences. In *Publication 4039*. Foundation for Science, Technology, and Civilisation.

Allan, J. and Matthews, R. K. (1990). Isotope signatures associated with early meteoric diagenesis. *Carbonate diagenesis*, pages 197–217.

Anderson, T. F. and Arthur, M. A. (1983). Stable isotopes of oxygen and carbon and their application to sedimentologic and paleoenvironmental problems. In *Stable isotopes in sedimentary geology*, pages 1–151. SEPM Short Course No. 10.

Arrhenius, S. (1896). On the influence of carbonic acid in the air upon the temperature of the ground. *Philosophical Magazine and Journal of Science*, 5(41):237–276.

Arthur, M. A., Brumsack, H. J., Jenkyns, H. C., and Schlanger, S. O. (1990). Stratigraphy, geochemistry, and paleoceanography of organic carbon- rich Cretaceous sequences. *Cretaceous resources, events and rhythms*, pages 75–119.

Arthur, M. A., Dean, W. E., and Claypool, G. E. (1985). Anomalous ^{13}C enrichment in modern marine organic carbon. *Nature*, 295:19–21.

Arthur, M. A., Dean, W. E., and Pratt, L. M. (1988). Geochemical and climatic effects of increased marine organic carbon burial at the cenomanian/turonian boundary. *Nature*, 335(6192):714–717.

Arthur, M. A., Schlanger, S. O., and Jenkyns, H. C. (1987). The Cenomanian-Turonian Oceanic Anoxic Event, II. Palaeoceanographic controls on organic-matter

production and preservation. *Geological Society, London, Special Publications*, 26(1):401–420.

Baltuck, M., Moberly, R., and Schlanger, S. O. (1986). Introduction and Explanatory Notes, Leg 89. *In* Moberly, R., Schlanger, S. O., *et al.*, Initial Reports of the Deep Sea Drilling Project, Volume 89. Washington (U.S. Government Printing Office), pages 5–28.

Banner, J. L. and Hanson, G. N. (1990). Calculation of simultaneous isotopic and trace element variations during water-rock interaction with applications to carbonate diagenesis. *Geochimica et Cosmochimica Acta*, 54(11):3123–3137.

Barron, E. J. (1983). A warm, equable Cretaceous: the nature of the problem. *Earth-Science Reviews*, 19(4):305–338.

Bathurst, R. (1972). Cementation. In *Carbonate sediments and their diagenesis*, pages 415–457. Elsevier.

Bathurst, R. (1983). Early diagenesis of carbonate sediments. In *Sediment diagenesis*. NATO ASI Series C: Mathematical and Physical Sciences.

Bemis, B. E., Spero, H. J., and Lea, W. (1998). Reevaluation of the oxygen isotopic composition of planktonic foraminifera: Experimental results and revised paleotemperature equations for both species can be described by relationships accurate with photosynthetic. *Paleoceanography*, 13(2):150–160.

Berger, W. H. and Vincent, E. (1986). Deep-sea carbonates: Reading the carbon-isotope signal. *Geologische Rundschau*, 75(1):249–269.

Berner, R. A. (2004). The long-term carbon cycle. In *The Phanerozoic carbon cycle: CO2 and O2*, pages 5–9. Oxford University Press.

Berner, R. A. and Caldeira, K. (1997). The need for mass balance and feedback in the geochemical carbon cycle. *Geology*, 25(10):955–956.

Blackmon, P. and Todd, R. (1959). Mineralogy of some foraminifera as related to their classification and ecology. *Journal of Paleontology*, 33(1):1–15.

Boersma, A. (1981). Cretaceous and Early Tertiary Foraminifers from Deep Sea Drilling Project Leg 62 Sites in the Central Pacific. *In* Thiede, J., Vallier, T. L., *et*

al., Initial Reports of the Deep Sea Drilling Project, Volume 62. Washington (U.S. Government Printing Office), pages 377–396.

Boersma, A. and Shackleton, N. (1981). Oxygen-and carbon-isotope variations and planktonic foraminifer depth habitats, Late Cretaceous to Paleocene, central Pacific, Deep Sea Drilling Project Sites 463 and 465. *In* Thiede, J., Vallier, T. L., *et al.*, Initial Reports of the Deep Sea Drilling Project, Volume 62. Washington (U.S. Government Printing Office), pages 513–526.

Bomou, B., Adatte, T., Aziz, A., Mort, H., Fleitmann, D., Huang, Y., and Föllmi, K. B. (2013). The expression of the Cenomanian-Turonian oceanic anoxic event in Tibet. *Palaeogeography, Palaeoclimatology, Palaeoecology*, 369:466–481.

Bralower, T., Leckie, R., Sliter, W., and Thierstein, H. (1995). An integrated Cretaceous microfossil biostratigraphy. *Geochronology Time Scales and Global Stratigraphic Correlation, SEPM Special Publication*, 54:65–78.

Brand, U. and Veizer, J. (1981). Chemical diagenesis of a multicomponent carbonate system - 2: Stable isotopes. *Journal of Sedimentary Research*, 51(3):987–997.

Brand, W. A., Coplen, T. B., Vogl, J., Rosner, M., and Prohaska, T. (2014). Assessment of international reference materials for isotope-ratio analysis (IUPAC technical report). *Pure and Applied Chemistry*, 86(3):425–467.

Broecker, W. S. (1975). Climatic change: are we on the brink of a pronounced global warming? *Science*, 189(4201):460–463.

Broecker, W. S. (2003). The oceanic $CaCO_3$ cycle. In *Treatise on Geochemistry*, volume 6-9, pages 529–549. Elsevier Inc.

Broecker, W. S. and Takahashi, T. (1966). Calcium carbonate precipitation on the Bahama Banks. *Journal of Geophysical Research*, 71(6):1575–1602.

Caron, M. (1975). Late Cretaceous Planktonic Foraminifera from the Northwestern Pacific, Leg 32 of the Deep Sea Drilling Project. *In* Larson, R. L., Moberly, R., *et al.*, Initial Reports of the Deep Sea Drilling Project, Volume 32. Washington (U.S. Government Printing Office), pages 719–724.

Caron, M., Dall'Agnolo, S., Accarie, H., Barrera, E., Kauffman, E. G., Amédro, F., and Robaszynski, F. (2006). High-resolution stratigraphy of the Cenomanian-Turonian boundary interval at Pueblo (USA) and wadi Bahloul (Tunisia): stable isotope and bio-events correlation. *Geobios*, 39(2):171–200.

Caron, M., Robaszynski, F., Amedro, F., Baudin, F., Deconinck, J.-F., Hochuli, P. A., von Salis-Perch Nielsen, K., and Tribovillard, N. (1999). Estimation de la durée de l'événement anoxique global au passage Cénomanien/Turonien: approche cyclostratigraphique dans la formation Bahloul en Tunisie centrale. *Bulletin de la Société Géologique de France*, 170(2):145–160.

Carrannante, G., Pugliese, A., Ruberti, D., Simone, L., Vigliotti, M., and Vigorito, M. (2009). Evoluzione cretacica di un settore della piattaforma apula da dati di sottosuolo e di affioramento (Appennino campano-molisano). *Ital. J. Geosci.*, 128(1):3–31.

Chappell, J. and Shackleton, N. (1986). Oxygen isotopes and sea level. *Nature*, 324(6093):137–140.

Cohen, K. M., Harper, D. A. T., and Gibbard, P. L. (2024). ICS International Chronostratigraphic Chart 2024/09. International Commission on Stratigraphy, IUGS. `www.stratigraphy.org`. Accessed: 2024-09-06.

Conci, N., Vargas, S., and Wörheide, G. (2021). The biology and evolution of calcite and aragonite mineralization in Octocorallia. *Frontiers in Ecology and Evolution*, 9:623774.

Coplen, T. and Schlanger, S. (1973). Oxygen and carbon isotope studies of carbonate sediments from Site 167, Magellan Rise, Leg 17. *In* Winterer, E. L., Ewing, J. I., *et al.*, Initial Reports of the Deep Sea Drilling Project, Volume 17. Washington (U.S. Government Printing Office), pages 505–510.

Coplen, T. B., Brand, W. A., Gehre, M., Gröning, M., Meijer, H. A., Toman, B., and Verkouteren, R. M. (2006). New guidelines for δ^{13}C measurements. *Analytical chemistry*, 78(7):2439–2441.

Corliss, B. H. (1985). Microhabitats of benthic foraminifera within deep-sea sediments. *Nature*, 314(April):435–438.

Craig, H. (1957). Isotopic standards for carbon and oxygen and correction factors for mass-spectrometric analysis of carbon dioxide. *Geochimica et Cosmochimica Acta*, 12:133–149.

Cramer, B. S. and Jarvis, I. (2020). Carbon isotope stratigraphy. In *Geologic time scale*, pages 309–343. Elsevier.

Cramer, B. S., Toggweiler, J. R., Wright, J. D., Katz, M. E., and Miller, K. G. (2009). Ocean overturning since the Late Cretaceous: Inferences from a new benthic foraminiferal isotope compilation. *Paleoceanography*, 24(4).

Daëron, M., Drysdale, R. N., Peral, M., Huyghe, D., Blamart, D., Coplen, T. B., Lartaud, F., and Zanchetta, G. (2019). Most Earth-surface calcites precipitate out of isotopic equilibrium. *Nature communications*, 10(1):429.

Deffeyes, K. S. (1959). Zeolites in sedimentary rocks. *Journal of Sedimentary Research*, 29(4):602–609.

Dilek, Y. and Furnes, H. (2018). Tethyan ophiolites and Tethyan seaways. *Journal of the Geological Society*, 176(5):899–912.

Divins, D. (2003). Total sediment thickness of the world's oceans & marginal seas. *NOAA National Geophysical Data Center, Boulder, CO*.

Donnadieu, Y., Pucéat, E., Moiroud, M., Guillocheau, F., and Deconinck, J. F. (2016). A better-ventilated ocean triggered by Late Cretaceous changes in continental configuration. *Nature Communications*, 7.

Douglas, R. (1973). Planktonic foraminiferal biostratigraphy in the Central North Pacific Ocean. *In* Winterer, E. L., Ewing, J. I., *et al.*, Initial Reports of the Deep Sea Drilling Project, Volume 17. Washington (U.S. Government Printing Office), pages 673–674.

Douglas, R. and Savin, S. (1973). Oxygen and carbon isotope analyses of Cretaceous and Tertiary foraminifera from the central North Pacific. *In* Winterer, E. L., Ewing, J. I., *et al.*, Initial Reports of the Deep Sea Drilling Project, Volume 17. Washington (U.S. Government Printing Office), pages 591–606.

Douglas, R. and Savin, S. (1975). Oxygen and carbon isotope analyses of Tertiary and Cretaceous microfossils from Shatsky Rise and other sites in the North Pacific

Ocean. *In* Larson, R. L., Moberly, R., *et al.*, Initial Reports of the Deep Sea Drilling Project, Volume 32. Washington (U.S. Government Printing Office), pages 509–520.

Du Vivier, A. D., Selby, D., Sageman, B. B., Jarvis, I., Gröcke, D. R., and Voigt, S. (2014). Marine $^{187}Os/^{188}Os$ isotope stratigraphy reveals the interaction of volcanism and ocean circulation during Oceanic Anoxic Event 2. *Earth and Planetary Science Letters*, 389:23–33.

Dubicka, Z., Wierzbowski, H., and Wierny, W. (2018). Oxygen and carbon isotope records of Upper Cretaceous foraminifera from Poland: vital and microhabitat effects. *Palaeogeography, Palaeoclimatology, Palaeoecology*, 500(December 2017):33–51.

Eagles, G. (2007). New angles on South Atlantic opening. *Geophys. J. Int*, 168:353–361.

Eldrett, J. S., Ma, C., Bergman, S. C., Lutz, B., Gregory, F. J., Dodsworth, P., Phipps, M., Hardas, P., Minisini, D., Ozkan, A., Ramezani, J., Bowring, S. A., Kamo, S. L., Ferguson, K., Macaulay, C., and Kelly, A. E. (2015). An astronomically calibrated stratigraphy of the Cenomanian , Turonian and earliest Coniacian from the Cretaceous Western Interior Seaway , USA : Implications for global chronostratigraphy. *Cretaceous Research*, 56:316–344.

Erbacher, J., Gerth, W., Schmiedl, G., and Hemleben, C. (1998). Benthic foraminiferal assemblages of late Aptian-early Albian black shale intervals in the Vocontian Basin, SE France. *Cretaceous Research*, 19:805–826.

Erez, J. and Luz, B. (1983). Experimental paleotemperature equation for planktonic foraminifera. *Geochimica et Cosmochimica Acta*, 47(6):1025–1031.

Fajgelj, A. and Assonov, S. (2016). Reference Sheet: Certified Reference Material IAEA-603 (calcite), Stable Isotope Reference Material for $\delta^{13}C$ and $\delta^{18}O$. International Atomic Energy Agency Department of Nuclear Sciences and Applications IAEA Environment Laboratories.

Falzoni, F. and Petrizzo, M. R. (2020). Patterns of planktonic foraminiferal extinctions and eclipses during Oceanic Anoxic Event 2 at Eastbourne (SE England) and other mid-low latitude locations. *Cretaceous Research*, 116:104593.

Falzoni, F., Petrizzo, M. R., Caron, M., Leckie, R. M., and Elderbak, K. (2018). Age and synchronicity of planktonic foraminiferal bioevents across the Cenomanian-Turonian boundary interval (Late Cretaceous). *Newsletters on Stratigraphy*, 51(3):343–380.

Falzoni, F., Petrizzo, M. R., Jenkyns, H. C., Gale, A. S., and Tsikos, H. (2016). Planktonic foraminiferal biostratigraphy and assemblage composition across the Cenomanian-Turonian boundary interval at Clot Chevalier (Vocontian Basin, SE France). *Cretaceous Research*, 59:69–97.

Fanton, K. C. and Holmden, C. (2007). Sea-level forcing of carbon isotope excursions in epeiric seas: Implications for chemostratigraphy. *Canadian Journal of Earth Sciences*, 44(6):807–818.

Ferreri, V., Weissert, H., D'Argenio, B., and Buonocunto, F. P. (1997). Carbon isotope stratigraphy: A tool for basin to carbonate platform correlation. *Terra Nova*, 9(2):57–61.

Folk, R. L. (1965). Some aspects of recrystallization in ancient limestones. *Dolomitization and Limestone Diagenesis (SP13)*.

Folk, R. L. (1974). The natural history of crystalline calcium carbonate: effect of magnesium content and salinity. *Journal of Sedimentary Research*, 44(1):40–53.

Foote, E. (1856). Circumstances affecting the heat of the sun's rays. *Am. J. Sci. Arts*, 22(66):382–383.

Forster, A., Schouten, S., Moriya, K., Wilson, P. A., and Sinninghe Damsté, J. S. (2007). Tropical warming and intermittent cooling during the Cenomanian/Turonian oceanic anoxic event 2: Sea surface temperature records from the equatorial Atlantic. *Paleoceanography*, 22(1):1–14.

Friedrich, O., Norris, R. D., and Erbacher, J. (2012). Evolution of middle to late Cretaceous oceans - A 55 m.y. record of Earth's temperature and carbon cycle. *Geology*, 40:107–110.

Friedrich, O., Schmiedl, G., and Erlenkeuser, H. (2006). Stable isotope composition of Late Cretaceous benthic foraminifera from the southern South Atlantic: Biological and environmental effects. *Marine Micropaleontology*, 58:135–157.

Gabtni, H., Jallouli, C., and Mickus, K. L. (2013). Geodynamics of the Southern Tethyan Margin in Tunisia and Maghrebian domain: new constraints from integrated geophysical study. *Arabian Journal of Geosciences*, 6:271–286.

Gale, A., Bown, P., Caron, M., Crampton, J., Crowhurst, S., Kennedy, W., Petrizzo, M., and Wray, D. (2011). The uppermost middle and upper albian succession at the col de palluel, hautes-alpes, france: An integrated study (ammonites, inoceramid bivalves, planktonic foraminifera, nannofossils, geochemistry, stable oxygen and carbon isotopes, cyclostratigraphy). *Cretaceous Research*, 32(2):59–130.

Gale, A. S. (1996). Turonian correlation and sequence stratigraphy of the Chalk in southern England. *Geological Society, London, Special Publications*, 103:177–195.

Gale, A. S., Mutterlose, J., Batenburg, S., Gradstein, F. M., Agterberg, F. P., Ogg, J. G., and Petrizzo, M. R. (2020). The Cretaceous period. In *Geologic time scale*, pages 1023–1086. Elsevier.

Gautier, D. L. and Claypool, G. E. (1984). Interpretation of methanic diagenesis in ancient sediments by analogy with processes in modern diagenetic environments: Part 1. Concepts and principles. *AAPG Special Volumes*.

Geyman, E. C. and Maloof, A. C. (2019). A diurnal carbon engine explains ^{13}C-enriched carbonates without increasing the global production of oxygen. *Proceedings of the National Academy of Sciences*, 116(49).

Geyman, E. C. and Maloof, A. C. (2021). Facies control on carbonate δ^{13}c on the great bahama bank. *Geology*, 49(9):1049–1054.

Granot, R. and Dyment, J. (2015). The Cretaceous opening of the South Atlantic Ocean. *Earth and Planetary Science Letters*, 414:156–163.

Grasby, S. E., Crowley, J. L., Mohr, M. T., Percival, J. B., Ardakani, O. H., Galloway, J., Bringué, M., Smith, I. R., and Yuan, W. (2024). Oceanic anoxic event 3 in Arctic Canada—Arc volcanism and ocean fertilization drove anoxia. *Geological Society of America Bulletin*.

Grosheny, D., Beaudoin, B., Morel, L., and Desmares, D. (2006). High-resolution biotratigraphy and chemostratigraphy of the Cenomanian/Turonian boundary event in the Vocontian Basin, southeast France. *Cretaceous Research*, 27(5):629–640.

Gruber, N., Keeling, C. D., Bacastow, R. B., Guenther, P. R., Lueker, T. J., Wahlen, M., Meijer, H. A. J., Mook, W. G., and Stocker, T. F. (1999). Spatiotemporal patterns of carbon-13 in the global surface oceans and the oceanic Suess effect. *Global Biogeochemical Cycles*, 13(2):307–335.

Hague, A. M., Thomas, D. J., Huber, M., Korty, R., Woodard, S. C., and Jones, L. B. (2012). Convection of North Pacific deep water during the early Cenozoic. *Geology*, 40(6):527–530.

Hall, R. (2012). Late Jurassic – Cenozoic reconstructions of the Indonesian region and the Indian Ocean. *Tectonophysics*, 570-571:1–41.

Harvey, D. (2005). Mass spectrometry: Ionization methods overview. In Worsfold, P., Townshend, A., and Poole, C., editors, *Encyclopedia of Analytical Science (Second Edition)*, pages 350–359. Elsevier, second edition.

Hasegawa, T., Crampton, J. S., Schiøler, P., Field, B., Fukushi, K., and Kakizaki, Y. (2013). Carbon isotope stratigraphy and depositional oxia through Cenomanian/Turonian boundary sequences (Upper Cretaceous) in New Zealand. *Cretaceous Research*, 40:61–80.

Hashim, M. S. and Kaczmarek, S. E. (2021). The transformation of aragonite to calcite in the presence of magnesium: Implications for marine diagenesis. *Earth and Planetary Science Letters*, 574:117166.

Hayes, J. M., Strauss, H., and Kaufman, A. J. (1999). The abundance of ^{13}C in marine organic matter and isotopic fractionation in the global biogeochemical cycle of carbon during the past 800 Ma. *Chemical Geology*, 161:103–125.

Heine, C., Zoethout, J., and Muller, R. (2013). Kinematics of the South Atlantic rift. *Solid Earth*, 4:215–253.

Herrle, J. O., Kößler, P., Friedrich, O., Erlenkeuser, H., and Hemleben, C. (2004). High-resolution carbon isotope records of the Aptian to Lower Albian from SE France and the Mazagan Plateau (DSDP Site 545): a stratigraphic tool for paleoceanographic and paleobiologic reconstruction. *Earth and Planetary Science Letters*, 218(1-2):149–161.

Herrle, J. O., Schröder-Adams, C. J., Davis, W., Pugh, A. T., Galloway, J. M., and Fath, J. (2015). Mid-Cretaceous High Arctic stratigraphy, climate, and oceanic anoxic events. *Geology*, 43(5):403–406.

Heuer, V. B., Pohlman, J. W., Torres, M. E., Elvert, M., and Hinrichs, K.-U. (2009). The stable carbon isotope biogeochemistry of acetate and other dissolved carbon species in deep subseafloor sediments at the northern Cascadia Margin. *Geochimica et Cosmochimica Acta*, 73(11):3323–3336.

Higgins, J. A., Blättler, C. L., Lundstrom, E. A., Santiago-Ramos, D. P., Akhtar, A. A., Crüger Ahm, A. S., Bialik, O., Holmden, C., Bradbury, H., Murray, S. T., and Swart, P. K. (2018). Mineralogy, early marine diagenesis, and the chemistry of shallow-water carbonate sediments. *Geochimica et Cosmochimica Acta*, 220:512–534.

Hochuli, P. A., Menegatti, A. P., Weissert, H., Riva, A., Erba, E., and Silva, I. P. (1999). Episodes of high productivity and cooling in the early Aptian Alpine Tethys. *Geology*, 27(7):657–660.

Hoffman, D. W. and Rasmussen, C. (2022). Absolute carbon stable isotope ratio in the Vienna Peedee Belemnite isotope reference determined by 1H NMR spectroscopy. *Analytical Chemistry*, 94(13):5240–5247.

Hollis, C. J., Dunkley Jones, T., Anagnostou, E., Bijl, P. K., Cramwinckel, M. J., Cui, Y., Dickens, G. R., Edgar, K. M., Eley, Y., Evans, D., Foster, G. L., Frieling, J., Inglis, G. N., Kennedy, E. M., Kozdon, R., Lauretano, V., Lear, C. H., Littler, K., Lourens, L., Meckler, A. N., Naafs, B. D. A., Pälike, H., Pancost, R. D., Pearson, P. N., Röhl, U., Royer, D. L., Salzmann, U., Schubert, B. A., Seebeck, H., Sluijs, A., Speijer, R. P., Stassen, P., Tierney, J., Tripati, A., Wade, B., Westerhold, T., Witkowski, C., Zachos, J. C., Zhang, Y. G., Huber, M., and Lunt, D. J. (2019). The DeepMIP contribution to PMIP4: methodologies for selection, compilation and analysis of latest Paleocene and early Eocene climate proxy data, incorporating version 0.1 of the DeepMIP database. *Geoscientific Model Development*, 12(7):3149–3206.

Hoogakker, B., Ishimura, T., de Nooijer, L., Rathburn, A., and Schmiedl, G. (2024). A review of benthic foraminiferal oxygen and carbon isotopes. *Quaternary Science Reviews*, 342:108896.

Hou, Z., Wo, D., Tschegg, C., Rogowitz, A., Rice, A. H. N., Nasdala, L., Fusseis, F., Szymczak, P., and Grasemann, B. (2023). Three-dimensional mineral dendrites reveal a nonclassical crystallization pathway. *Geology*, 51(7):626–630.

Huber, B. T., Norris, R. D., Hole, W., Hole, W., and Macleod, K. G. (2002). Deep-sea paleotemperature record of extreme warmth during the Cretaceous. *Geology*, 30(2):123–126.

Huber, B. T., Petrizzo, M. R., Young, J. R., Falzoni, F., Gilardoni, S. E., Bown, P. R., Wade, B. S., Huber, B. T., Petrizzo, M. R., Young, J. R., Falzoni, F., Gilardoni, S. E., Bown, P. R., and Wade, B. S. (2016). Pforams @ microtax: A new online taxonomic database for planktonic foraminifera. *Micropaleontology*, 62(6):429–438.

Iglesias-Rodriguez, M. D., Armstrong, R., Feely, R., Hood, R., Kleypas, J., Milliman, J. D., Sabine, C., and Sarmiento, J. (2002). Progress made in study of ocean's calcium carbonate budget. *Eos*, 83(34):2000–2002.

Immenhauser, A., Holmden, C., and Patterson, W. (2008). Interpreting the carbon-isotope record of ancient shallow epeiric seas: lessons from the recent. In *Dynamics of Epeiric Seas*, pages 137–174. Geological Association of Canada Special Paper 48.

IODP-MI (2011). IODP Depth Scales Terminology version 2.0. Retrieved November 15, 2024, from `https://www.iodp.org/policies-and-guidelines/142-iodp-depth-scales-terminology-april-2011/file`.

Ishimura, T., Tsunogai, U., Hasegawa, S., Nakagawa, F., Oi, T., Kitazato, H., Suga, H., and Toyofuku, T. (2012). Variation in stable carbon and oxygen isotopes of individual benthic foraminifera: Tracers for quantifying the magnitude of isotopic disequilibrium. *Biogeosciences*, 9(11):4353–4367.

Jackson, E. and Schlanger, S. (1976). Regional synthesis, Line Islands Chain, Tuamotu Island Chain, and Manihiki Plateau, Central Pacific Ocean. *Initial Reports of the Deep Sea Drilling Project*, 33:915–927.

Jarvis, I., Gale, A. S., Jenkyns, H. C., and Pearce, M. A. (2006). Secular variation in Late Cretaceous carbon isotopes: A new δ^{13}C carbonate reference curve for the Cenomanian-Campanian (99.6-70.6 Ma). *Geological Magazine*, 143(5):561–608.

Jarvis, I., Lignum, J. S., Gröcke, D. R., Jenkyns, H. C., and Pearce, M. A. (2011). Black shale deposition, atmospheric CO_2 drawdown, and cooling during the Cenomanian-Turonian Oceanic Anoxic Event. *Paleoceanography*, 26(3):1–17.

Jefferies, R. P. S. (1961). The palaeoecology of the Actinocamax plenus subzone (lowest Turonian) in the Anglo-Paris Basin. *Palaeontology*, 4(Jefferies):609–647.

Jenkyns, H. C. (2003). Evidence for rapid climate change in the Mesozoic-Palaeogene greenhouse world. *Philosophical Transactions of the Royal Society of London Series A: Mathematical, Physical and Engineering Sciences*, 361(1810):1885–1916.

Jenkyns, H. C. (2010). Geochemistry of oceanic anoxic events. *Geochemistry, Geophysics, Geosystems*, 11(3).

Jenkyns, H. C., Dickson, A. J., Ruhl, M., and van den Boorn, S. H. (2017). Basalt-seawater interaction, the Plenus Cold Event, enhanced weathering and geochemical change: deconstructing Oceanic Anoxic Event 2 (Cenomanian–Turonian, Late Cretaceous). *Sedimentology*, 64(1):16–43.

Jenkyns, H. C., Gale, A. S., and Corfield, R. M. (1994). Carbon- and oxygen-isotope stratigraphy of the English Chalk and Italian Scaglia and its palaeoclimatic significance. *Geological Magazine*, 131(1):1–34.

Jiménez Berrocoso, Á., MacLeod, K. G., Martin, E. E., Bourbon, E., Londoño, C. I., and Basak, C. (2010). Nutrient trap for Late Cretaceous organic-rich black shales in the tropical North Atlantic. *Geology*, 38(12):1111–1114.

Jones, M. M. (2018). Turonian sea level and paleoclimatic events in astronomically tuned records from the tropical North Atlantic and Western Interior Seaway. *Paleoceanography and Paleoclimatology*, 33(5):470–492.

Jones, M. M., Sageman, B. B., Selby, D., Jicha, B. R., Singer, B. S., and Titus, A. L. (2021). Regional chronostratigraphic synthesis of the Cenomanian-Turonian Oceanic Anoxic Event 2 (OAE2) interval, Western Interior Basin (USA): New Re-Os chemostratigraphy and $^{40}Ar/^{39}Ar$ geochronology. *Bulletin of the Geological Society of America*, 133(5):1090–1104.

Joo, Y. J. and Sageman, B. B. (2014). Cenomanian to Campanian carbon isotope chemostratigraphy from the Western Interior Basin, USA. *Journal of Sedimentary Research*, 84(7):529–542.

Kaneps, A. (1976). Deep Sea Drilling Project. *Geotimes*, pages 16–17.

Katz, M. E., Katz, D. R., Wright, J. D., Miller, K. G., Pak, D. K., Shackleton, N. J., and Thomas, E. (2003). Early Cenozoic benthic foraminiferal isotopes: Species reliability and interspecies correction factors. *Paleoceanography*, 18(2):1–12.

Keller, G., Mateo, P., Punekar, J., Khozyem, H., Gertsch, B., Spangenberg, J., Bitchong, A. M., and Adatte, T. (2018). Environmental changes during the Cretaceous-Paleogene mass extinction and Paleocene-Eocene thermal maximum: implications for the Anthropocene. *Gondwana Research*, 56:69–89.

Kerr, A. (1998). Oceanic plateau formation: a cause of mass extinction and black shale deposition around the Cenomanian – Turonian boundary? *Journal of the Geological Society, London*, 155:619–626.

Kim, J. H., van der Meer, J., Schouten, S., Helmke, P., Willmott, V., Sangiorgi, F., Koç, N., Hopmans, E. C., and Damsté, J. S. (2010). New indices and calibrations derived from the distribution of crenarchaeal isoprenoid tetraether lipids: Implications for past sea surface temperature reconstructions. *Geochimica et Cosmochimica Acta*, 74(16):4639–4654.

Kim, S.-T. and O'Neil, J. R. (1997). Equilibrium and nonequilibrium oxygen isotope effects in synthetic carbonates. *Geochimica et Cosmochimica Acta*, 61(16):3461–3475.

Kimoto, K. (2015). Planktic foraminifera. In Ohtsuka, S., Suzaki, T., Horiguchi, T., Suzuki, N., and Not, F., editors, *Marine protists*. Springer, Tokyo.

Kump, L. R. and Arthur, M. A. (1999). Interpreting carbon-isotope excursions: carbonates and organic matter. *Chemical Geology*, 161(1-3):181–198.

Kump, L. R., Brantley, S. L., and Arthur, M. A. (2000). Chemical weathering, atmospheric CO_2, and climate. *Annual Review of Earth and Planetary Sciences*, 28(January 2014):611–667.

Kuroda, J., Ogawa, N. O., Tanimizu, M., Coffin, M. F., Tokuyama, H., Kitazato, H., and Ohkouchi, N. (2007). Contemporaneous massive subaerial volcanism and late cretaceous Oceanic Anoxic Event 2. *Earth and Planetary Science Letters*, 256(1-2):211–223.

Lamolda, M. A., Peryt, D., and Ion, J. (2007). Planktonic foraminiferal bioevents in the Coniacian/Santonian boundary interval at Olazagutia, Navarra province, Spain. *Cretaceous Research*, 28(1):18–29.

Lancelot, Y., Hathaway, J., and Hollister, C. (1972). Lithology of Sediments from the Western North Atlantic, Leg 11, Deep Sea Drilling Project. *Initial Reports of the Deep Sea Drilling Project*, 11:901–949.

Larson, R. L. and Erba, E. (1999). Onset of the mid-Cretaceous greenhouse in the Barremian-Aptian: Igneous events and the biological, sedimentary, and geochemical responses. *Paleoceanography*, 14(6):663–678.

Larson, R. L., Moberly, R., Bukry, D., Foreman, H. P., Gardner, J., Keene, J., Lancelot, Y., Luterbacher, H., Marshall, M., and Matter, A. (1975). Site 303: Japanese Magnetic Lineations. *In* Larson, R. L., Moberly, R., *et al.*, Initial Reports of the Deep Sea Drilling Project, Volume 32. Washington (U.S. Government Printing Office), pages 17–44.

Lasaga, A. C., Berner, R. A., and Garrels, R. M. (1985). The Carbon Cycle and Atmospheric CO2: Natural Variations Archean to Present, Volume 32. In *An improved geochemical model of atmospheric CO_2 fluctuations over the past 100 million years*, pages 397—411. Geophysical Monograph Series.

Laske, G., Masters, G., Ma, Z., and Pasyanos, M. (2013). Update on CRUST1.0 - A 1-degree global model of Earth's crust. *EGU General Assembly 2013*, 15:2658.

Lawrence, J., Gieskes, J., and Broecker, W. (1975). Oxygen isotope and cation composition of DSDP pore waters and the alteration of Layer II basalts. *Earth and Planetary Science Letters*, 27:1–10.

Lazarus, D. (1994). Neptune: A marine micropaleontology database. *Mathematical Geology*, 26:817–832.

Leary, P. N. and Peryt, D. (1991). The late Cenomanian oceanic anoxic event in the western Anglo-Paris basin and southeast Danish-Polish trough: Survival strategies of and recolonisation by benthonic foraminifera. *Historical Biology*, 5:321–338.

Leeder, M. (2011). Deep ocean. In *Sedimentology and sedimentary basins: from turbulence to tectonics*, pages 514–560. John Wiley & Sons.

Li, X., Jenkyns, H. C., Wang, C., Hu, X., Chen, X., Wei, Y., Huang, Y., and Cui, J. (2006). Upper Cretaceous carbon- and oxygen-isotope stratigraphy of hemipelagic carbonate facies from southern Tibet, China. *Journal of the Geological Society*, 163(2):375–382.

Lowenstam, H. A. and Epstein, S. (1954). Paleotemperatures of the post-Aptian Cretaceous as determined by the oxygen isotope method. *The Journal of Geology*, 62(3):207–248.

Lowery, C. M., Cunningham, R., Barrie, C. D., Bralower, T., and Snedden, J. W. (2017). The Northern Gulf of Mexico during OAE2 and the relationship between water depth and black shale development. *Paleoceanography*, 32(12):1316–1335.

Lucchi, R., St. John, K., Ronge, T., and the Expedition 403 Scientists (2024). Expedition 403 Preliminary Report: Eastern Fram Strait Paleo-Archive. *International Ocean Discovery Program*.

Maamouri, A., Zaghbib-Turki, D., Matmati, M., Chikhaoui, M., and Salaj, J. (1994). La formation Bahloul en Tunisie centro-septentrionale: variations latérales, nouvelle datation et nouvelle interprétation en terme de stratigraphie séquentielle. *Journal of African Earth Sciences*, 18(1):37–50.

Mackensen, A. and Licari, L. (2003). Carbon isotopes of live benthic foraminifera from the South Atlantic: Sensitivity to bottom water carbonate saturation state and organic matter rain rates. In *The South Atlantic in the Late Quaternary: Reconstruction of Material Budgets and Current Systems*, pages 623–624. Springer-Verlag.

MacLeod, K. G., Huber, B. T., Jiménez Berrocoso, Á., and Wendler, I. (2013). A stable and hot Turonian without glacial δ^{18}O excursions is indicated by exquisitely preserved Tanzanian foraminifera. *Geology*, 41(10):1083–1086.

MacLeod, K. G., Londoño, C. I., Martin, E. E., Jiménez Berrocoso, Á., and Basak, C. (2011). Changes in North Atlantic circulation at the end of the Cretaceous greenhouse interval. *Nature Geoscience*, 4(October):779–782.

MacLeod, K. G., Martin, E. E., and Blair, S. W. (2008). Nd isotopic excursion across Cretaceous ocean anoxic event 2 (Cenomanian-Turonian) in the tropical North Atlantic. *Geology*, 2(10):811–814.

Malone, M. J., Slowey, N. C., and Henderson, G. M. (2001). Early diagenesis of shallow-water periplatform carbonate sediments, leeward margin, Great Bahama Bank (Ocean Drilling Program Leg 166). *Geological Society of America Bulletin*, 113(7):881–894.

McClymont, E. L., Ford, H. L., Ho, S. L., Tindall, J. C., Haywood, A. M., Alonso-Garcia, M., Bailey, I., Berke, M. A., Littler, K., Patterson, M. O., Petrick, B., Peterse, F., Ravelo, A. C., Risebrobakken, B., De Schepper, S., Swann, G. E. A., Thirumalai, K., Tierney, J. E., van der Weijst, C., White, S., Abe-Ouchi, A., Baatsen, M. L. J., Brady, E. C., Chan, W.-L., Chandan, D., Feng, R., Guo, C., von der Heydt, A. S., Hunter, S., Li, X., Lohmann, G., Nisancioglu, K. H., Otto-Bliesner, B. L., Peltier, W. R., Stepanek, C., and Zhang, Z. (2020). Lessons from a high-CO_2 world: an ocean view from ∼3 million years ago. *Climate of the Past*, 16(4):1599–1615.

McCorkle, D., Emerson, S., and Quay, P. (1985). Stable carbon isotopes in marine porewaters. *Earth and Planetary Science Letters*, 74(1):13–26.

McCorkle, D. C. and Emerson, S. R. (1988). The relationship between pore water carbon isotopic composition and bottom water oxygen concentration. *Geochimica et Cosmochimica Acta*, 52:1169–1178.

Meister, P. and Reyes, C. (2019). The carbon-isotope record of the sub-seafloor biosphere. *Geosciences*, 9(12):507.

Michael, F. Y. (1975). Mesozoic foraminifera, Leg 30, Hole 288A and Site 289. *In* Andrews, J.E., Packham, G., *et al.*, Initial Reports of the Deep Sea Drilling Project, Volume 30. Washington (U.S. Government Printing Office), pages 599–602.

Miller, K. G., Barrera, E., Olsson, R. K., Sugarman, P. J., and Savin, S. M. (1999). Does ice drive early Maastrichtian eustasy? *Geology*, 27(9):783–786.

Milliman, J. D. (1993). Production and accumulation of calcium carbonate in the ocean: Budget of a nonsteady state. *Global Biogeochemical Cycles*, 7(4):927–957.

Milliman, J. D. and Droxler, A. W. (1996). Neritic and pelagic carbonate sedimentation in the marine environment: Ignorance is not bliss. *Geologische Rundschau*, 85(3):496–504.

Mithal, R. and Becker, D. G. (2006). The Janus database: providing worldwide access to ODP and IODP data. In Rothwell, R., editor, *New Techniques in Sediment Core Analysis*, pages 253–259. The Geological Society of London.

Moberly, R., Gardner, J. V., and Larson, R. L. (1975). Introduction. *In* Larson, R. L., Moberly, R., *et al.*, Initial Reports of the Deep Sea Drilling Project, Volume 32. Washington (U.S. Government Printing Office), pages 5–14.

Moulin, M., Aslanian, D., and Unternehr, P. (2010). A new starting point for the South and Equatorial Atlantic Ocean. *Earth Science Reviews*, 98(1-2):1–37.

Müller, R. D., Zahirovic, S., Williams, S. E., Cannon, J., Seton, M., Bower, D. J., Tetley, M. G., Heine, C., Le Breton, E., Liu, S., et al. (2019). A global plate model including lithospheric deformation along major rifts and orogens since the Triassic. *Tectonics*, 38(6):1884–1907.

Mullins, H. T., Wise, S. W., Gardulski, A., Hinchey, E., Masters, P., and Siegel, D. (1985). Shallow subsurface diagenesis of Pleistocene periplatform ooze: northern Bahamas. *Sedimentology*, 32:473–494.

Murphy, D. P. and Thomas, D. J. (2012). Cretaceous deep-water formation in the Indian sector of the southern Ocean. *Paleoceanography*, 27(1):1–12.

National Research Council (2011). *Scientific ocean drilling: accomplishments and challenges*. National Academies Press.

Nederbragt, A. J. (2023). The effect of seawater carbonate chemistry on the stable isotope composition of Cibicidoides wuellerstorfi and other Cibicidoides species. *Paleoceanography and Paleoclimatology*, 38:1–17.

O'Brien, C. L., Robinson, S. A., Pancost, R. D., Sinninghe, J. S., Schouten, S., Lunt, D. J., Alsenz, H., Bornemann, A., Bottini, C., Brassell, S. C., Farnsworth, A., Forster, A., Huber, B. T., Inglis, G. N., Jenkyns, H. C., Linnert, C., Littler, K., Markwick, P., Mcanena, A., Mutterlose, J., Naafs, B. D. A., Püttmann, W., Sluijs, A., Helmond, N. A. G. M. V., Vellekoop, J., Wagner, T., and Wrobel, N. E. (2017). Cretaceous sea-surface temperature evolution: Constraints from TEX_{86} and planktonic foraminiferal oxygen isotopes. *Earth-Science Reviews*, 172(March 2016):224–247.

O'Connor, L. K., Jenkyns, H. C., Robinson, S. A., Remmelzwaal, S. R., Batenburg, S. J., Parkinson, I. J., and Gale, A. S. (2020). A re-evaluation of the Plenus Cold Event, and the links between CO_2, temperature, and seawater chemistry during OAE 2. *Paleoceanography and Paleoclimatology*, 35(4):1–23.

Okhouchi, N., Kuroda, J., and Taira, A. (2015). The origin of Cretaceous black shales: a change in the surface ocean ecosystem and its triggers. *Proc. Jpn. Acad.*, 91(7):273–291.

O'Neil, J. R., Clayton, R. N., and Mayeda, T. K. (1969). Oxygen isotope fractionation in divalent metal carbonates. *Journal of chemical physics*, 51(12):5547–5558.

Owens, J. D., Lyons, T. W., and Lowery, C. M. (2018). Quantifying the missing sink for global organic carbon burial during a Cretaceous oceanic anoxic event. *Earth and Planetary Science Letters*, 499:83–94.

Pälike, H., Lyle, M. W., Nishi, H., Raffi, I., Ridgwell, A., Gamage, K., Klaus, A., Acton, G., Anderson, L., Backman, J., et al. (2012). A cenozoic record of the equatorial pacific carbonate compensation depth. *Nature*, 488(7413):609–614.

Panchuk, K. M., Holmden, C., and Kump, L. R. (2005). Sensitivity of the epeiric sea carbon isotope record to local-scale carbon cycle processes: Tales from the Mohawkian Sea. *Palaeogeography, Palaeoclimatology, Palaeoecology*, 228:320–337.

Patterson, W. and Walter, L. (1994). Depletion of ^{13}C in seawater $\Sigma C02$ on modern carbonate platforms: Significance for the carbon isotopic record of carbonates. *Geology*, 22:885–888.

Paul, C. R., Lamolda, M. A., Mitchell, S. F., Vaziri, M. R., Gorostidi, A., and Marshall, J. D. (1999). The Cenomanian-Turonian boundary at Eastbourne (Sussex, UK): A proposed European reference section. *Palaeogeography, Palaeoclimatology, Palaeoecology*, 150(1-2):83–121.

Paul, D. and Skrzypek, G. (2007). Assessment of carbonate-phosphoric acid analytical technique performed using GasBench II in continuous flow isotope ratio mass spectrometry. *International Journal of Mass Spectrometry*, 262:180–186.

Paul, D., Skrzypek, G., and Fórizs, I. (2007). Normalization of measured stable isotopic compositions to isotope reference scales – a review. *Rapid Communications in Mass Spectrometry*, 21:3006–3014.

Pearce, M. A., Jarvis, I., and Tocher, B. A. (2009). The Cenomanian – Turonian boundary event, OAE2 and palaeoenvironmental change in epicontinental seas: New insights from the dinocyst and geochemical records. *Palaeogeography, Palaeoclimatology, Palaeoecology*, 280(1-2):207–234.

Pederson, C. L., Ge, Y., Lokier, S. W., Swart, P. K., Vonhof, H., Strauss, H., Schurr, S., Fiorini, F., Riechelmann, S., Licha, T., and Immenhauser, A. (2021). Seawater chemistry of a modern subtropical 'epeiric' sea: Spatial variability and effects of organic decomposition. *Geochimica et Cosmochimica Acta*, 314:159–177.

Penman, D. E. (2016). Silicate weathering and North Atlantic silica burial during the Paleocene-Eocene Thermal Maximum. *Geology*, 44(9):731–734.

Percival, L. M., van Helmond, N. A., Selby, D., Goderis, S., and Claeys, P. (2020). Complex interactions between Large Igneous Province emplacement and global-temperature changes during the Cenomanian-Turonian Oceanic Anoxic Event (OAE 2). *Paleoceanography and Paleoclimatology*, 35(10).

Philip et al. (2000a). Late Cenomanian. In Crasquin, S., editor, *Atlas Peri-Tethys, Palaeogeographical maps - Explanatory notes*, pages 16–18. Comm. de la Carte Geol. du Monde, Paris.

Philip et al. (2000b). Map 14: Late Cenomanian. In Dercourt, J., et al., editor, *Atlas Peri-Tethys Palaeogeographical Maps*. Comm. de la Carte Geol. du Monde, Paris.

Powell, J. H. and Moh'd, B. K. (2011). Evolution of Cretaceous to Eocene alluvial and carbonate platform sequences in central and south Jordan. *GeoArabia*, 16(4):29–82.

Pratt, L. and Threlkeld, C. (1984). Stratigraphic significance of $^{13}C/^{12}C$ ratios in mid-Cretaceous rocks of the Western Interior, USA. *Memoir of the Canadian Society of Petroleum Geologists*, 9.

Premoli Silva, I. and Bolli, H. M. (1973). Late Cretaceous to Eocene Planktonic Foraminifera and Stratigraphy of the Leg 15 Sites in the Caribbean Sea. *In* Edgar, N. T., Saunders, J. B., *et al.*, Initial Reports of the Deep Sea Drilling Project, Volume 15. Washington (U.S. Government Printing Office), pages 499–547.

Premoli Silva, I. and Sliter, W. (1986). Late Aptian and Cenomanian–Turonian Planktonic Foraminifers from Deep Sea Drilling Project Site 585, Leg 89, East

Mariana Basin. *In* Moberly, R., Schlanger, S. O., *et al.*, Initial Reports of the Deep Sea Drilling Project, Volume 89. Washington (U.S. Government Printing Office), pages 297–310.

Price, G. D. and Hart, M. B. (2002). Isotopic evidence for Early to mid-Cretaceous ocean temperature variability. *Marine Micropaleontology*, 46(1-2):45–58.

Price, G. D., Sellwood, B. W., Corfield, R. M., Clarke, L., and Cartlidge, J. E. (1998). Isotopic evidence for palaeotemperatures and depth stratification of Middle Cretaceous planktonic foraminifera from the Pacific Ocean. *Geological Magazine*, 135(2):183–191.

Rathburn, A. E., Corliss, B. H., Tappa, K. D., and Lohmann, K. C. (1996). Comparisons of the ecology and stable isotopic compositions of living (stained) benthic foraminifera from the Sulu and South China Seas. *Deep-Sea Research I*, 43(10):1617–1646.

Renaudie, J., Lazarus, D. B., and Diver, P. (2020). NSB (Neptune Sandbox Berlin): An expanded and improved database of marine planktonic microfossil data and deep-sea stratigraphy. *Palaeontologia Electronica*, 23(1):1–28.

Reolid, M., Mattioli, E., Duarte, L. V., and Ruebsam, W. (2021). The Toarcian oceanic anoxic event: Where do we stand? *Geological Society Special Publication*, 514(1):1–11.

Richardson, C. M., Dulai, H., Popp, B. N., Ruttenberg, K., and Fackrell, J. K. (2017). Submarine groundwater discharge drives biogeochemistry in two Hawaiian reefs. *Limnology and Oceanography*, 62:S348–S363.

Robinson, S. A., Dickson, A. J., Pain, A., Jenkyns, H. C., O'Brien, C. L., Farnsworth, A., and Lunt, D. J. (2019). Southern Hemisphere sea-surface temperatures during the Cenomanian-Turonian: Implications for the termination of Oceanic Anoxic Event 2. *Geology*, 47(2):131–134.

Romanek, C., Grossman, E., and Morse, J. (1992). Carbon isotopic fractionation in synthetic aragonite and calcite: effects of temperature and precipitation rate. *Geochimica et cosmochimica acta*, 56(1):419–430.

Roth, P. H. (1986). Mesozoic palaeoceanography of the North Atlantic and Tethys Oceans. *Geological Society, London, Special Publications*, 21:299–320.

Rubinson, M. and Clayton, R. N. (1969). Carbon-13 fractionation between aragonite and calcite. *Geochimica et Cosmochimica Acta*, 33(8):997–1002.

Ryan, W. B. and Cita, M. B. (1977). Ignorance concerning episodes of ocean-wide stagnation. *Marine Geology*, 23(1-2):197–215.

Ryan, W. B. F., Carbotte, S., Coplan, J., O'Hara, S., Melkonian, A., Arko, R., Weissel, R., Ferrini, V., Goodwillie, A., Nitsche, F., Bonczkowski, J., and Zemsky, R. (2009). Global Multi-Resolution Topography (GMRT) synthesis data set. *Geochem. Geophys. Geosyst.*, 10(Q03014).

Scarselli, N. (2020). Submarine landslides – architecture, controlling factors and environments. A summary. In *Regional geology and tectonics*, pages 417–439. Elsevier.

Schettino, A. and Turco, E. (2011). Tectonic history of the western Tethys since the Late Triassic. *GSA Bulletin*, 123(1):89–105.

Schlager, W. (2003). Benthic carbonate factories of the Phanerozoic. *International Journal of Earth Sciences*, 92(4):445–464.

Schlanger, S. and Jenkyns, H. (1976). Cretaceous Oceanic Anoxic Events: Causes and consequences. *Geologie en Mijnbouw*, 55(3-4).

Schlanger, S. O., Arthur, M. A., Jenkyns, H. C., and Scholle, P. A. (1987). The Cenomanian-Turonian Oceanic Anoxic Event, I. Stratigraphy and distribution of organic carbon-rich beds and the marine δ^{13}C excursion. *Geological Society Special Publication*, (26):371–399.

Schmittner, A., Bostock, H. C., Cartapanis, O., Curry, W. B., Filipsson, H. L., Galbraith, E. D., Gottschalk, J., Herguera, J. C., Hoogakker, B., Jaccard, S. L., Lisiecki, L. E., Lund, D. C., Martínez-Méndez, G., Lynch-Stieglitz, J., Mackensen, A., Michel, E., Mix, A. C., Oppo, D. W., Peterson, C. D., Repschläger, J., Sikes, E. L., Spero, H. J., and Waelbroeck, C. (2017). Calibration of the carbon isotope composition (δ^{13}C) of benthic foraminifera. *Paleoceanography and Paleoclimatology*, 32(6):512–530.

Schmittner, A., Gruber, N., Mix, A. C., Key, R. M., Tagliabue, A., and Westberry, T. K. (2013). Biology and air-sea gas exchange controls on the distribution of carbon isotope ratios (δ^{13}C) in the ocean. *Biogeosciences*, 10(9):5793–5816.

Scholle, P. A. and Arthur, M. A. (1980). Carbon isotope fluctuations in Cretaceous pelagic limestones: potential stratigraphic and petroleum exploration tool. *American Association of Petroleum Geologists Bulletin*, 64(1):67–87.

Scholle, P. A. and Halley, R. B. (1985). Burial diagenesis: out of sight, out of mind! *Carbonate Cements*, 4:309–334.

Shackleton, N. (1974). Attainment of isotopic equilibrium between ocean water and the benthonic foraminifera genus Uvigerina: isotopic changes in the ocean during the last glacial. *Colloque international du CNRS*, 219:203–210.

Shackleton, N. (1987). The carbon isotope record of the Cenozoic: History of organic carbon burial and of oxygen in the ocean and atmosphere. *Geological Society, London, Special Publications*, 26(1):423–434.

Shackleton, N. J. and Kennett, J. (1975). Paleotemperature history of the Cenozoic and the initiation of Antarctic glaciation: oxygen and carbon isotope analyses in DSDP Sites 277, 279, and 281. *Initial Reports Deep Sea Drilling Project*, 29:743–755.

Sharp, Z. (2017). Carbon in the low temperature environment. In *Principles of stable isotope geochemistry*, pages 7–1–7–29. Open Educational Resources.

Shipboard Scientific Party (1973a). Site 166. *In* Winterer, E. L., Ewing, J. I., *et al.*, Initial Reports of the Deep Sea Drilling Project, Volume 17. Washington (U.S. Government Printing Office), pages 103–144.

Shipboard Scientific Party (1973b). Site 167. *In* Winterer, E. L., Ewing, J. I., *et al.*, Initial Reports of the Deep Sea Drilling Project, Volume 17. Washington (U.S. Government Printing Office), pages 145–234.

Shipboard Scientific Party (1973c). Site 169. *In* Winterer, E. L., Ewing, J. I., *et al.*, Initial Reports of the Deep Sea Drilling Project, Volume 17. Washington (U.S. Government Printing Office), pages 247–262.

Shipboard Scientific Party (1973d). Site 170. *In* Winterer, E. L., Ewing, J. I., *et al.*, Initial Reports of the Deep Sea Drilling Project, Volume 17. Washington (U.S. Government Printing Office), pages 263–281.

Shipboard Scientific Party (1973e). Site 171. *In* Winterer, E. L., Ewing, J. I., *et al.*, Initial Reports of the Deep Sea Drilling Project, Volume 17. Washington (U.S. Government Printing Office), pages 283–334.

Shipboard Scientific Party (1975a). Site 288. *In* Andrews, J.E., Packham, G., *et al.*, Initial Reports of the Deep Sea Drilling Project, Volume 30. Washington (U.S. Government Printing Office), pages 175–230.

Shipboard Scientific Party (1975b). Site 304: Japanese Magnetic Lineations. *In* Larson, R. L., Moberly, R., *et al.*, Initial Reports of the Deep Sea Drilling Project, Volume 32. Washington (U.S. Government Printing Office), pages 45–74.

Shipboard Scientific Party (1975c). Site 305: Shatsky Rise. *In* Larson, R. L., Moberly, R., *et al.*, Initial Reports of the Deep Sea Drilling Project, Volume 32. Washington (U.S. Government Printing Office), pages 75–158.

Shipboard Scientific Party (1975d). Site 306: Shatsky Rise. *In* Larson, R. L., Moberly, R., *et al.*, Initial Reports of the Deep Sea Drilling Project, Volume 32. Washington (U.S. Government Printing Office), pages 159–192.

Shipboard Scientific Party (1975e). Site 310: Hess Rise. *In* Larson, R. L., Moberly, R., *et al.*, Initial Reports of the Deep Sea Drilling Project, Volume 32. Washington (U.S. Government Printing Office), pages 233–294.

Shipboard Scientific Party (1981a). Site 462: Nauru Basin, Western Pacific Ocean, Deep Sea Drilling Project Leg 61. *In* Larson, R. L., Schlanger, S. O., *et al.*, Initial Reports of the Deep Sea Drilling Project, Volume 61. Washington (U.S. Government Printing Office), pages 19–394.

Shipboard Scientific Party (1981b). Site 463: Western Mid-Pacific Mountains. *In* Thiede, J., Vallier, T. L., *et al.*, Initial Reports of the Deep Sea Drilling Project, Volume 62. Washington (U.S. Government Printing Office), pages 33–156.

Shipboard Scientific Party (1981c). Site 464: Northern Hess Rise. *In* Thiede, J., Vallier, T. L., *et al.*, Initial Reports of the Deep Sea Drilling Project, Volume 62. Washington (U.S. Government Printing Office), pages 157–198.

Shipboard Scientific Party (1981d). Site 465: Southern Hess Rise. *In* Thiede, J., Vallier, T. L., *et al.*, Initial Reports of the Deep Sea Drilling Project, Volume 62. Washington (U.S. Government Printing Office), pages 199–282.

Shipboard Scientific Party (1981e). Site 466: Southern Hess Rise. *In* Thiede, J., Vallier, T. L., *et al.*, Initial Reports of the Deep Sea Drilling Project, Volume 62. Washington (U.S. Government Printing Office), pages 283–326.

Shipboard Scientific Party (1986). Site 585. *In* Moberly, R., Schlanger, S. O., *et al.*, Initial Reports of the Deep Sea Drilling Project, Volume 89. Washington (U.S. Government Printing Office), pages 29–156.

Shipboard Scientific Party (1990a). Site 801. *In* Lancelot, Y., Larson, R., *et al.*, Proceedings of the Ocean Drilling Program Initial Reports, Volume 129. College Station, TX (Ocean Drilling Program), pages 91–170.

Shipboard Scientific Party (1990b). Site 802. *In* Lancelot, Y., Larson, R., *et al.*, Proceedings of the Ocean Drilling Program Initial Reports, Volume 129. College Station, TX (Ocean Drilling Program), pages 171–246.

Shipboard Scientific Party (1991). Site 807. *In* Kroenke, L. W., Berger, W. H., Janecek, T. R., *et al.*, Proceedings of the Ocean Drilling Program Initial Reports, Volume 130. College Station, TX (Ocean Drilling Program), pages 369–496.

Shipboard Scientific Party (1993a). Site 801. *In* Premoli Silva, I., Haggerty, J., Rack, F., *et al.*, Proceedings of the Ocean Drilling Program Initial Reports, Volume 144. College Station, TX (Ocean Drilling Program), pages 313–330.

Shipboard Scientific Party (1993b). Site 865. *In* Sager, W.W., Winterer, E.L., Firth, J.V., *et al.*, Proceedings of the Ocean Drilling Program Initial Reports, Volume 143. College Station, TX (Ocean Drilling Program), pages 111–180.

Shipboard Scientific Party (1993c). Site 869. *In* Sager, W.W., Winterer, E.L., Firth, J.V., *et al.*, Proceedings of the Ocean Drilling Program Initial Reports, Volume 143. College Station, TX (Ocean Drilling Program), pages 297–374.

Shipboard Scientific Party (2002). Site 1207. *In* Bralower, T.J., Premoli Silva, I., Malone, M.J., *et al.*, Proceedings of the Ocean Drilling Program Initial Reports, Volume 198. College Station, TX (Ocean Drilling Program).

Shipboard Scientific Party (2004). Leg 207 Summary. *In* Erbacher, J. Mosher, D.C., Malone, M.J., *et al.*, Proc. ODP, Init. Repts., 207. College Station TX (Ocean Drilling Program), pages 1–89.

Simo, J. A., Emerson, N. R., Byers, C. W., and Ludvigson, G. A. (2003). Anatomy of an embayment in an Ordovician epeiric sea , Upper Mississippi Valley, USA. *Geology*, 31:545–548.

Sinninghe Damsté, J. S., van Bentum, E. C., Reichart, G. J., Pross, J., and Schouten, S. (2010). A CO_2 decrease-driven cooling and increased latitudinal temperature gradient during the mid-Cretaceous Oceanic Anoxic Event 2. *Earth and Planetary Science Letters*, 293(1-2):97–103.

Skrzypek, G. and Dunn, P. J. H. (2020). Absolute isotope ratios defining isotope scales used in isotope ratio mass spectrometers and optical isotope instruments. *Rapid Communications in Mass Spectrometry*, 34(20):e8890.

Sliter, W. V. (1989). Biostratigraphic zonation for Cretaceous planktonic foraminifers examined in thin section. *Journal of Foraminiferal Research*, 19(1):1–19.

Sliter, W. V. (1992). Cretaceous planktonic foraminiferal biostratigraphy and paleoceanographic events in the Pacific Ocean with emphasis on indurated sediment. In Ishizaki, K. and Saito, T., editors, *Centenary of Japanese Micropaleontology*, pages 281–299. Terra Scientific Publishing Company, Tokyo.

Sliter, W. V. (1999). Cretaceous planktic foraminiferal biostratigraphy of the Calera Limestone, northern California, USA. *The Journal of Foraminiferal Research*, 29(4):318–339.

Sliter, W. V. and McGann, M. (1992). Age and correlation of the Calera Limestone in the Permanente Terrane of northern California. Technical report, US Department of the Interior, US Geological Survey.

Sliter, W. V. and Silva, I. P. (1990). Age and origin of Cretaceous planktonic foraminifers from limestone of the Franciscan Complex near Laytonville, California. *Paleoceanography*, 5(5):639–667.

Spencer-Cervato, C. (1999). The Cenozoic deep sea microfossil record: Explorations of the DSDP/ODP sample set using the Neptune database. *Palaeontologia electronica*, 22(1):1–268.

Stanley, S. M. and Hardie, L. A. (1998). Secular oscillations in the carbonate mineralogy of reef-building and sediment-producing organisms driven by tectonically

forced shifts in seawater chemistry. *Palaeogeography, Palaeoclimatology, Palaeoecology*, 144(1-2):3–19.

Stein, C. and Stein, S. (1992). A model for the global variation in oceanic depth and heat flow with lithospheric age. *Nature*, 359(10):123–129.

Stichler, W. (2008). Interlaboratory comparison of new materials for carbon and oxygen isotope ratio measurements.

Stoll, H. M. and Schrag, D. P. (1996). Evidence for glacial control of rapid sea level changes in the Early Cretaceous. *Science*, 272(5269):1771–1774.

Stoll, H. M. and Schrag, D. P. (2000). High-resolution stable isotope records from the Upper Cretaceous rocks of Italy and Spain: Glacial episodes in a greenhouse planet? *Geological Society of America Bulletin*, 112(2):308–319.

Straume, E. O., Gaina, C., Medvedev, S., Hochmuth, K., Gohl, K., Whittaker, J. M., Abdul Fattah, R., Doornenbal, J. C., and Hopper, J. R. (2019). GlobSed: Updated total sediment thickness in the world's oceans. *Geochemistry, Geophysics, Geosystems*, 20(4):1756–1772.

Suan, G., Pittet, B., Bour, I., Mattioli, E., Duarte, L. V., and Mailliot, S. (2008). Duration of the Early Toarcian carbon isotope excursion deduced from spectral analysis: Consequence for its possible causes. *Earth and Planetary Science Letters*, 267(3-4):666–679.

Swart, P. K. (2015). The geochemistry of carbonate diagenesis: The past, present and future. *Sedimentology*, 62(5):1233–1304.

Swart, P. R. K., Reijmer, J. J. G., and Otto, R. (2009). A re-evaluation of facies on Great Bahama Bank II: variations in the δ^{13}C, δ^{18}O and mineralogy of surface sediments. *Int. Assoc. Sedimentol. Spec. Publ.*, 41:47–59.

Systems Engineer (2018). HS20-22 User's Manual V2.0. Sercon Ltd.

Taft, W. H. (1967). Modern carbonate sediments. *Developments in Sedimentology*, 9:29–50.

Takashima, R., Nishi, H., Yamanaka, T., Orihasi, Y., Tsujino, Y., Quidelleur, X., Hayashi, K., Sawada, K., Nakamura, H., and Ando, T. (2019). Establishment of

Upper Cretaceous bio- and carbon isotope stratigraphy in the northwest Pacific Ocean and radiometric ages around the Albian/Cenomanian, Coniacian/Santonian and Santonian/Campanian boundaries. *Newsletters on Stratigraphy*, 52(3):341–376.

Takashima, R., Nishi, H., Yamanaka, T., Tomosugi, T., Fernando, A. G., Tanabe, K., Moriya, K., Kawabe, F., and Hayashi, K. (2011). Prevailing oxic environments in the Pacific Ocean during the mid-Cretaceous Oceanic Anoxic Event 2. *Nature Communications*, 2(1).

Tarduno, J. A., McWilliams, M., Sliter, W. V., Cook, H. E., Blake, M. C., and Premoli-Silva, I. (1986). Southern hemisphere origin of the Cretaceous Laytonville Limestone of California. *Science*, 231(4744):1425–1428.

Theodor, M., Schmiedl, G., Jorissen, F., and Mackensen, A. (2016). Stable carbon isotope gradients in benthic foraminifera as proxy for organic carbon fluxes in the Mediterranean Sea. *Biogeosciences*, 13(23):6385–6404.

Thiede, J., Dean, W. E., and Claypool, G. E. (1982). Oxygen-deficient depositional paleoenvironments in the mid-Cretaceous tropical and subtropical Pacific Ocean. In *Nature and Origin of Cretaceous Carbon-rich Facies*, pages 79–100. Academic Press.

Thiede, J., Vallier, T. L., and Adelseck, C. G. (1981). Deep Sea Drilling Project Leg 62, North Central Pacific Ocean: Introduction, Cruise Narrative, Principal Results, and Explanatory Notes. *In* Thiede, J., Vallier, T. L., *et al.*, Initial Reports of the Deep Sea Drilling Project, Volume 62. Washington (U.S. Government Printing Office), pages 5–32.

Thiede, J. and Van Andel, T. H. (1977). The paleoenvironment of anaerobic sediments in the Late Mesozoic South Atlantic Ocean. *Earth and Planetary Science Letters*, 33(3):301–309.

Timofeev, P., Renngarten, N., and Eremeev, V. V. (1981). Lithologic-genetic characteristics of sediments in a section at Site 463. *In* Thiede, J., Vallier, T. L., *et al.*, Initial Reports of the Deep Sea Drilling Project, Volume 62. Washington (U.S. Government Printing Office), pages 607–616.

Tsikos, H., Jenkyns, H. C., Walsworth-Bell, B., Petrizzo, M. R., Forster, A., Kolonic, S., Erba, E., Premoli Silva, I., Baas, M., Wagner, T., and Sinninghe Damsté,

J. S. (2004). Carbon-isotope stratigraphy recorded by the Cenomanian-Turonian Oceanic Anoxic Event: Correlation and implications based on three key localities. *Journal of the Geological Society*, 161(4):711–719.

Turgeon, S. C. and Creaser, R. A. (2008). Cretaceous oceanic anoxic event 2 triggered by a massive magmatic episode. *Nature*, 454(July):323–327.

Tyrrell, T. and Zeebe, R. E. (2004). History of carbonate ion concentration over the last 100 million years. *Geochimica et Cosmochimica Acta*, 68(17):3521–3530.

Urey, H. (1952). Chemical processes during the formation of the planets: Chemical processes on the accumulating planets. In *The planets: their origin and development*, pages 142–149. Yale University Press.

Urey, H. C., Lowenstam, H. A., Epstein, S., and McKinney, C. R. (1951). Measurement of paleotemperatures and temperatures of the Upper Cretaceous of England, Denmark, and the southeastern United States. *Geological Society of America Bulletin*, 62(4):399–416.

Voigt, S., Aurag, A., Leis, F., and Kaplan, U. (2007). Late Cenomanian to Middle Turonian high-resolution carbon isotope stratigraphy: New data from the Münsterland Cretaceous Basin, Germany. *Earth and Planetary Science Letters*, 253:196–210.

Voigt, S., Erbacher, J., Mutterlose, J., Weiss, W., Westerhold, T., Wiese, F., Wilmsen, M., and Wonik, T. (2008). The Cenomanian – Turonian of the Wunstorf section (North Germany): global stratigraphic reference section and new orbital time scale for Oceanic Anoxic Event 2. *Newsletters in Stratigraphy*, 43(June):65–89.

Voigt, S., Jung, C., Friedrich, O., Frank, M., Teschner, C., and Hoffmann, J. (2013). Tectonically restricted deep-ocean circulation at the end of the Cretaceous greenhouse. *Earth and Planetary Science Letters*, 369-370:169–177.

Waelbroeck, C., Labeyrie, L., Michel, E., Duplessy, J.-C., Mcmanus, J. F., Lambeck, K., Balbon, E., and Labracherie, M. (2002). Sea-level and deep water temperature changes derived from benthic foraminifera isotopic records. *Quaternary science reviews*, 21(1-3):295–305.

Weiner, S. and Dove, P. M. (2003). An overview of biomineralization processes and the problem of the vital effect. *Reviews in mineralogy and geochemistry*, 54(1):1–29.

Westerhold, T., Marwan, N., Drury, A. J., Liebrand, D., Agnini, C., Anagnostou, E., Barnet, J. S., Bohaty, S. M., De Vleeschouwer, D., Florindo, F., et al. (2020). An astronomically dated record of earth's climate and its predictability over the last 66 million years. *Science*, 369(6509):1383–1387.

Westermann, S., Föllmi, K. B., Adatte, T., Matera, V., Schnyder, J., Fleitmann, D., Fiet, N., Ploch, I., and Duchamp-Alphonse, S. (2010). The Valanginian δ^{13}C excursion may not be an expression of a global oceanic anoxic event. *Earth and Planetary Science Letters*, 290(1-2):118–131.

Widmark, J. G. V. and Speijer, R. P. (1997). Benthic foraminiferal faunas and trophic regimes at the terminal Cretaceous Tethyan seafloor. *PALAIOS*, 12(4):354–371.

Wiese, F. (1999). Stable isotope data (δ^{13}C, δ^{18}O) from the Middle and Upper Turonian (Upper Cretaceous) of Liencres (Cantabria, northern Spain) with a comparison to northern Germany (Sölde & Salzgitter-Salder). *Newsletters on Stratigraphy*, 37(1/2):37–62.

Willems, H., Zhou, Z., Zhang, B., and Gräfe, K.-U. (1996). Stratigraphy of the Upper Cretaceous and Lower Tertiary strata in the Tethyan Himalayas of Tibet (Tingri area, China). *Geologische Rundschau*, 85:723–754.

Wilpshaar, M. and Leereveld, H. (1994). Palaeoenvironmental change in the Early Cretaceous Vocontian Basin (SE France) reflected by dinoflagellate cysts. *Review of Palaeobotany and Palynology*, 84(1-2):121–128.

Winterer, E. L. (1973). Introduction. *In* Winterer, E. L., Ewing, J. I., *et al.*, Initial Reports of the Deep Sea Drilling Project, Volume 17. Washington (U.S. Government Printing Office), pages 5–15.

Winterer, E. L., Ewing, J. I., Douglas, R., Jarrard, R., Lancelot, Y., Moberly, R., Moore, T., Roth, P., and Schlanger, S. O. (1973). Site 164. *In* Winterer, E. L., Ewing, J. I., *et al.*, Initial Reports of the Deep Sea Drilling Project, Volume 17. Washington (U.S. Government Printing Office), pages 17–46.

Winterer, E. L., Riedel, W. R., Moberly, R. M., Resig, J. M., Kroenke, L. W., Gealy, E. L., Heath, G. R., Bronnimann, P., Martini, E., and Worsley, T. R. (1971). Site 66. *In* Winterer, E. L. *et al.*, Initial Reports of the Deep Sea Drilling Project, Volume 7. Washington (U.S. Government Printing Office), pages 725–820.

Wolfgring, E., Petrizzo, M. R., MacLeod, K. G., Huber, B. T., and Watkins, D. K. (2022). Santonian deep sea benthic foraminifera from IODP Site U1513, Mentelle Basin (SW Australia): Reactions of benthic foraminiferal assemblages to surface water cooling at southern high latitudes. *Marine Micropaleontology*, 175:102152.

Working Group 1 of the Joint Committee for Guides in Metrology (2008). Evaluation of measurement data — guide to the expression of uncertainty in measurement. Joint Committee for Guides in Metrology.

WoRMS Editorial Board (2024). World Register of Marine Species (WoRMS). =https://www.marinespecies.org. Accessed: 2024-11-15.

Young, J. R., Bown, P. R., Wade, B. S., Pedder, B. E., Huber, B. T., Lazarus, D. B., Museum, N., and Washington, D. C. (2019). Mikrotax: Developing a genuinely effective platform for palaeontological geoinformatics. *Acta Geologica Sinica*, 93(supp. 1):70–72.

Zachos, J., Pagani, H., Sloan, L., Thomas, E., and Billups, K. (2001). Trends, rhythms, and aberrations in global climate 65 Ma to present. *Science*, 292(5517):686–693.

Zachos, J. C., Dickens, G. R., and Zeebe, R. E. (2008). An early Cenozoic perspective on greenhouse warming and carbon-cycle dynamics. *Nature*, 451(7176):279–283.

Zeebe, R. E. and Tyrrell, T. (2019). History of carbonate ion concentration over the last 100 million years II: Revised calculations and new data. *Geochimica et Cosmochimica Acta*, 257:373–392.

Zhang, L., Deng, J., Sun, S., Sui, Q., Wang, K., and Sun, W. (2023). Subduction of the Neo-Tethys ridge beneath the Eurasian continent during the Cretaceous. *Ore Geology Reviews*, 154(December 2022):105302.

Ziveri, P., Stoll, H., Probert, I., Klaas, C., Geisen, M., Ganssen, G., and Young, J. (2003). Stable isotope 'vital effects' in coccolith calcite. *Earth and Planetary Science Letters*, 210(1-2):137–149.

Appendices

Appendix A1: Additional figures and tables

A.1 Additional tables

Table A.1: "Unresolved" and "resolved" names of planktonic foraminiferal species used for biostratigraphy at the sites in this thesis, as well as the taxonomic organization database or other reference used to confirm each pair of "unresolved" and "resolved" names. (The purpose of "resolving" taxon names is to ensure the same taxon names are used to refer to the same species.) NSB = Neptune Sandbox Berlin; "within cores I sampled" = NSB matched these unresolved and resolved names for a sample within the Pacific cores that I sampled.

Unresolved name	Resolved name	Source of confirmation
Globotruncana primitiva	*Dicarinella primitiva*	NSB (within cores I sampled)
Globotruncana pseudolinneiana	*Marginotruncana pseudolinneiana*	NSB (within cores I sampled)
Globotruncana schneegansi	*Marginotruncana schneegansi*	NSB (within cores I sampled)
Globotruncana fornicata	*Contusotruncana fornicata*	NSB (within cores I sampled)
Globotruncana concavata concavata	*Dicarinella concavata*	NSB (within cores I sampled)

Unresolved name	Resolved name	Source of confirmation
Praeglobotruncana helvetica	*Helvetoglobotruncana helvetica*	NSB (within cores I sampled)
Globotruncana stuartiformis	*Globotruncanita stuartiformis*	NSB (within cores I sampled)
Globotruncana imbricata	*Dicarinella imbricata*	NSB (within cores I sampled)
Hedbergella brittonensis	*Whiteinella brittonensis*	NSB (within cores I sampled)
Heterohelix washitensis	*Heterohelix moremani*	NSB (within cores I sampled)
Hedbergella amabilis	*Clavihedbergella subcretacea*	NSB (within cores I sampled)
Heterohelix reussi	*Heterohelix globulosa*	NSB (within cores I sampled)
Globigerinelloides asper	*Globigerinelloides asperus*	NSB (within cores I sampled)
Praeglobotruncana praehelvetica	*Whiteinella praehelvetica*	NSB (within cores I sampled)
Globigerinelloides caseyi	*Globigerinelloides bentonensis*	NSB (within cores I sampled)
Hedbergella reussi	*Heterohelix globulosa*	NSB (within cores I sampled)
Marginotruncana difformis	*Abathomphalus intermedius*	NSB (within cores I sampled)
Marginotruncana inornata	*Whiteinella inornata*	NSB (within cores I sampled)
Marginotruncana helvetica	*Helvetoglobotruncana helvetica*	NSB (within cores I sampled)

Unresolved name	Resolved name	Source of confirmation
Marginotruncana roddai	*Dicarinella hagni*	NSB (within cores I sampled)
Globotruncana angustacarinata	*Marginotruncana angusticarenata*	pforams@mikrotax
Globotruncana concavata carinata	*Dicarinella asymetrica*	Lamolda et al. (2007)
Globotruncana sigali	*Marginotruncana sigali*	NSB
Globotruncana subspinosa	*Radotruncana subspinosa*	NSB
Globotruncana tricarinata	*Globotruncana linneiana*	NSB

Resolved name	Source of confirmation
Globotruncana bulloides	NSB
Globotruncana concavata primitiva	no confirmation
Globotruncanita elevata	NSB
Globotruncana linneiana	NSB
Hedbergella simplicissima	NSB
Praeglobotruncana aumalensis	no confirmation
Praeglobotruncana delrioensis	NSB
Praeglobotruncana paradubia	no confirmation
Rotalipora gandolfi	no confirmation
Planomalina buxtorfi	NSB
Praeglobotruncana delrioensis	NSB
Praeglobotruncana turbinata	WoRMS World Foraminifera Database
Globigerinelloides ultramicrus	NSB
Schackoina cenomana	NSB
Hedbergella simplex	NSB
Whiteinella baltica	NSB

Table A.2: Certain "resolved" names of planktonic foraminiferal species used for biostratigraphy at the sites in this thesis that were not already in the NSB database within the cores that I sampled (17-170, 17-171, 32-305, and 62-463), and the taxonomic organization database used to confirm that the name could be treated as a "resolved" name, i.e. did not correspond to a different "resolved" name. (The purpose of "resolving" taxon names is to ensure the same taxon names are used to refer to the same species.) NSB = Neptune Sandbox Berlin. WoRMS = World Register of Marine Species.

Table A.3: 29 holes in the Pacific, drilled during Deep Sea Drilling Project and the Ocean Drilling Program, that have sediments dated to the Cenomanian and/or Turonian stage. Notes on microfossil biostratigraphy and recovery and/or proportion of carbonate content are included in this table. The reference for the Deep Sea Drilling Project or Ocean Drilling Program Initial Report corresponding to each hole is also noted.

Site and hole	Notes on microfossil biostratigraphy	Notes on recovery and/or proportion of carbonate content	Reference
7-66	"Poorly preserved Cretaceous radiolarians of probable Turonian or Cenomanian age occur at 190 meters, just 2 meters above the base of the clay...Lying unconformably beneath the clay is altered vesicular basalt"	"Except for one brief time during the late Miocene, the sea floor at this site has been below the calcite compensation depth since the beginning of the sedimentary record."	Winterer et al. (1971)
17-164	Biostratigraphy is not direct, instead determined "by comparing the radiolarian assemblage found at this site with those found at subsequent sites, where control by calcareous microfossils is more substantial;" three cores of "Cenomanian to Turonian" age	"Aside from a few coccoliths in cores at 76 meters (Upper Cretaceous) and at 236 meters (Lower Cretaceous), no calcium carbonate was detected"	Winterer et al. (1973)

Site and hole	Notes on microfossil biostratigraphy	Notes on recovery and/or proportion of carbonate content	Reference
17-166	In core 20 "several broken specimens of foraminifera suggest a Cenomanian or Albian age" for core 20 and the cores below it; a "Middle Eocene" core overlies 8 cores (18 to 25) labeled "Late Albian to Cenomanian."	-	Shipboard Scientific Party (1973a)
17-167	"Core 60 and the upper part of Core 61 is Turonian, and the lower part of the same core is Cenomanian. Silicified foraminifera and nannofossils in Core 61 indicate it is early Cenomanian, and the late Cenomanian is missing."	-	Shipboard Scientific Party (1973b)
17-169	Cores of Cenomanian, Cenomanian-Turonian, and Turonian age recorded	Cenomanian-Turonian boundary crossed in cores 8-10; core recovery is very poor in cores 8-9 including core catchers only	Shipboard Scientific Party (1973c)

Site and hole	Notes on microfossil biostratigraphy	Notes on recovery and/or proportion of carbonate content	Reference
17-170	Early Cenomanian and late Turonian both recorded	Recovery is overall poor and Cenomanian and Turonian cores are only core catchers	Shipboard Scientific Party (1973d)
17-171	Turonian core recorded overlying "?Cenomanian" core	-	Shipboard Scientific Party (1973e)
30-288A	"Reworked sediments suggest... current scour and minor slumping from Aptian to Miocene;" "Middle and Lower Cenomanian" recorded underlying "Lower Turonian"	-	Shipboard Scientific Party (1975a)
32-303	"Greatly compressed section or unconformity between the Cenomanian and the Miocene" recorded	-	Larson et al. (1975)
32-303A	"Greatly compressed section or unconformity between the Cenomanian and the Miocene" recorded	-	Larson et al. (1975)

Site and hole	Notes on microfossil biostratigraphy	Notes on recovery and/or proportion of carbonate content	Reference
32-304	"Cenomanian to Valanginian cherty section" and unconformity between late Albian and late Miocene recorded	-	Shipboard Scientific Party (1975b)
32-305	Core 36 dated to "Early Turonian to Cenomanian"	"Below Campanian Core 28, sediment recoveries are mainly limited to small core-catcher samples of chert and firm chalks"	Shipboard Scientific Party (1975c)
32-306	Core 1 dated to Quaternary, cores 2-3 dated to late Albian/early Cenomanian	"The principal result of drilling at Site 306 was the penetration of nearly a half kilometer of cherts and carbonate rocks, mainly of Early Cretaceous age."	Shipboard Scientific Party (1975d)
32-310A	Cores of Cenomanian and Turonian age recorded	"We began continuous coring at 184 meters in the Campanian cherts and chalks. Hole 310A has very poor recoveries because it is in the Cretaceous cherty sequence..."	Shipboard Scientific Party (1975e)

Site and hole	Notes on microfossil biostratigraphy	Notes on recovery and/or proportion of carbonate content	Reference
61-462	Sediments noted "dated at about the C-T boundary"	-	Shipboard Scientific Party (1981a)
61-462A / 89-462A	Sediments noted "dated at about the C-T boundary;" one unit recorded as containing Santonian, Turonian, Cenomanian, and Albian sediments	-	Shipboard Scientific Party (1981a)
62-463	"Sub-unit is 405 meters thick and ranges in age from late Albian to early Maastrichtian"	-	Shipboard Scientific Party (1981b)
62-464	Unconformity recorded between late Cenomanian (98 Ma) and upper Cretaceous (75 Ma)	-	Shipboard Scientific Party (1981c)
62-465A	Unconformity recorded between late Cenomanian (98 Ma) and upper Cretaceous (75 Ma)	-	Shipboard Scientific Party (1981d)

Site and hole	Notes on microfossil biostratigraphy	Notes on recovery and/or proportion of carbonate content	Reference
62-466	Unconformity recorded between "Upper Albian" and "Coniacian to Turonian"	-	Shipboard Scientific Party (1981e)
89-585	Turonian recorded overlying late Cenomanian in core 32	-	Shipboard Scientific Party (1986)
89-585A	Turonian in core 8 recorded overlying late Cenomanian in core 9	-	Shipboard Scientific Party (1986)
129-801A	Cores 10 through 13 are all recorded as "Coniacian-Cenomanian"	Low carbonate content (<10%) measured in sediments of Coniacian-Cenomanian age	Shipboard Scientific Party (1990a)
129-802A	A thin unit of "claystone and radiolarite" coincides with a question-marked transition between Cenomanian and Coniacian	-	Shipboard Scientific Party (1990b)
130-807C	"Upper Albian - Lower Cenomanian" unit recorded underlying an "Upper Campanian - Lower Maastrichtian" unit	-	Shipboard Scientific Party (1991)

Site and hole	Notes on microfossil biostratigraphy	Notes on recovery and/or proportion of carbonate content	Reference
143-865B	One subunit is identified as "early to mid-Turonian and late Coniacian to late Campanian;" "cavings from above" are recorded in this unit	"... near the end of the Albian, the carbonate bank drowned... after the bank drowned,... later Cretaceous sediments were simply not deposited, or... they were removed by subaerial erosion."	Shipboard Scientific Party (1993b)
143-869B	Core 35 has "late Turonian-Coniacian" sediment, core 36 has "late Cenomanian" sediment	-	Shipboard Scientific Party (1993c)
144-801C	A unit is identified as Cenomanian – Coniacian	Lithology of the Cenomanian - Coniacian unit is "volcaniclastic turbidites and minor pelagic intervals" and "brown chert and porcellanite"	Shipboard Scientific Party (1993a)
198-1207B	"Major unconformity between the middle Miocene and upper Campanian" recorded	-	Shipboard Scientific Party (2002)

Table A.4: Lithologies, biogenous marine components noted in sediments, terrigenous or shallow-water-derived components noted in sediments, and interpretation of depositional environment by previous authors of shallow marine sections where Cenomanian-Turonian $\delta^{13}C_{carbonate}$ values have been measured (the Gun Gardens section at Eastbourne, UK; Clot Chevalier, Vocontian Basin, France; Pont d'Issole, Vocontian Basin, France; wadi Bahloul, Tunisia; Gongzha, Tibet). References consulted for each site are noted.

Site	Lithologies	Biogenous marine components in sediment	Terrigenous or shallow-water-derived components in sediment	Interpretation of depositional environment	References consulted
Eastbourne (Gun Gardens), UK	marls, marly chalks	planktonic and benthic foraminifera, calcareous nannofossils, belemnites, inoceramid bivalves, serpulid worms, ammonites	silt and sand in some beds accompanied by maxima in Si/Al and Ti/Al	"open-ocean epicontinental sea environment" (Pearce et al., 2009)	Jefferies (1961); Jenkyns et al. (1994); Gale (1996); Paul et al. (1999); Pearce et al. (2009)

Site	Lithologies	Biogenous marine components in sediment	Terrigenous or shallow-water-derived components in sediment	Interpretation of depositional environment	References consulted
Clot Chevalier, Vocontian Basin, France	marl, limestones; some marls are laminated and organic-rich	planktonic foraminifera, calcareous nannofossils, radiolaria	not noted for Clot Chevalier specifically, but assumed to be similar to Pont d'Issole	"a hemipelagic domain [at] a palaeodepth of few hundred metres deepening to the NE;" Pont d'Issole is NE of Clot Chevalier (Falzoni et al., 2016)	Falzoni et al. (2016)
Pont d'Issole, Vocontian Basin, France	marl, limestone, and black shale	abundant planktonic foraminifera, benthic foraminifera, radiolaria, sponge spicules, calcareous nannofossils, dinoflagel-late cysts	large amount of silt in shale beds, spores and pollen (terrestrial paly-nomorphs)	"hemipelagic . . . Paleowater depths were likely in the order of a few hundred meters in the central basin" (Jarvis et al., 2011)	Grosheny et al. (2006); Jarvis et al. (2011)

Site	Lithologies	Biogenous marine components in sediment	Terrigenous or shallow-water-derived components in sediment	Interpretation of depositional environment	References consulted
wadi Bahloul, Tunisia	calcareous marl and laminated organic-rich limestones; some detrital limestone (calcarenite)	ammonites, abundant planktonic and rare benthic foraminifera, radiolaria, filaments*, and rare calcispheres	abundant quartz grains in sandy limestone unit	"outer shelf of the Tunisian platform" (Caron et al., 2006);"located at the level of a gently sloping slope"** (Maamouri et al., 1994)	Maamouri et al. (1994); Caron et al. (1999, 2006)
Gongzha, Tibet	marl, limestone and marly limestone; some silty marl and shale	planktonic and benthic foraminifera, radiolaria, filaments*, and rare calcispheres	turbiditic layers containing silt-size clasts of quartz	"hemipelagic slope environment" (Bomou et al., 2013)	Willems et al. (1996); Li et al. (2006); Bomou et al. (2013)

* Bomou et al. (2013) identify the filaments as planktonic bivalve larvae shells

** translated from the French "situé au niveau de talus faiblement penté"

Site	Source for bulk $\delta^{13}C_{carbonate}$ and $\delta^{18}O_{carbonate}$ values	Source for planktonic foraminiferal and nannofossil $\delta^{13}C_{carbonate}$ and $\delta^{18}O_{carbonate}$ values	Source for benthic foraminiferal $\delta^{13}C_{carbonate}$ and $\delta^{18}O_{carbonate}$ values
17-167	this thesis; Douglas (1973); Coplen and Schlanger (1973)	-	-
17-169	this thesis	-	-
17-170	this thesis	-	-
17-171	this thesis	Douglas and Savin (1973)	-
30-288A	this thesis	-	-
32-305	this thesis; Price et al. (1998)	Douglas and Savin (1975); Price et al. (1998)	Friedrich et al. (2012); Douglas and Savin (1975)
32-310A	this thesis	Douglas and Savin (1975)	
62-463	this thesis; Price et al. (1998)	Boersma and Shackleton (1981); Price et al. (1998); Price and Hart (2002)	Boersma and Shackleton (1981); Friedrich et al. (2012); Price and Hart (2002)
89-585	this thesis	-	-
89-585A	this thesis	-	-

Table A.5: Sources of the bulk, planktonic foraminiferal and nannofossil, and benthic foraminiferal $\delta^{13}C_{carbonate}$ and $\delta^{18}O_{carbonate}$ values at Pacific sites examined in this thesis.

A.2 Additional figures

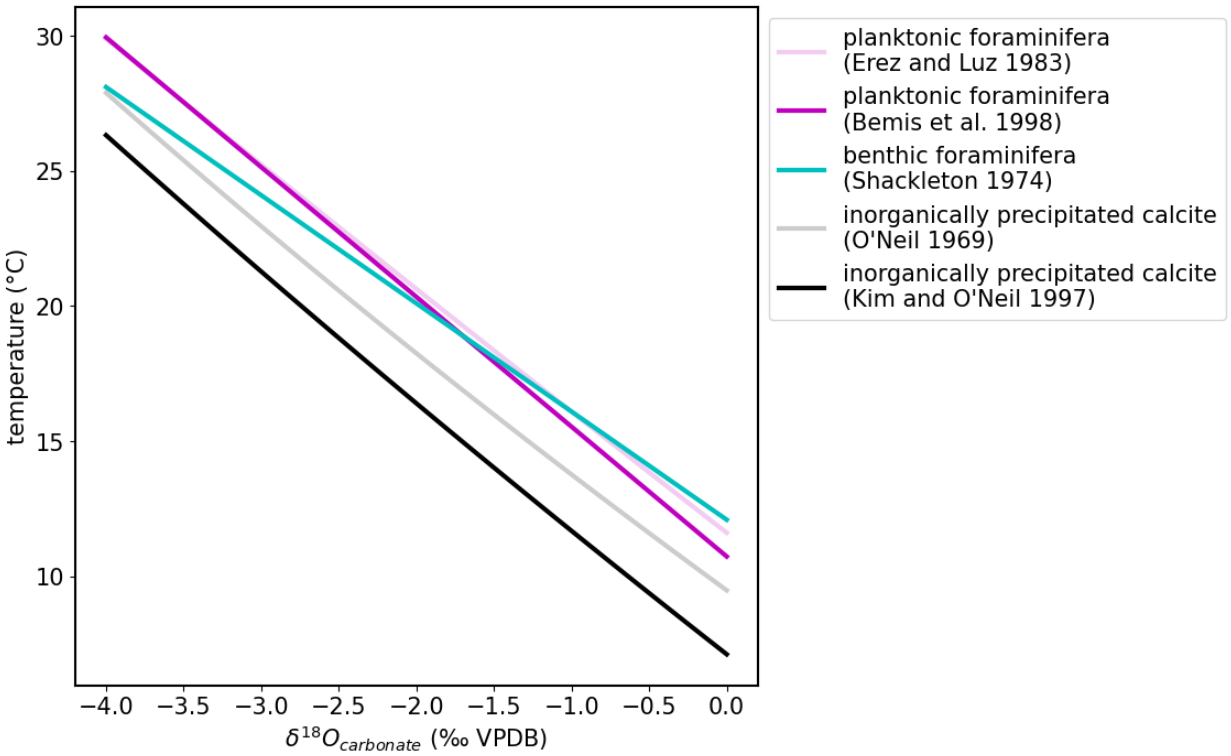

Figure A.1: Temperatures corresponding to $\delta^{18}O_{carbonate}$ values for the range of bulk $\delta^{18}O_{carbonate}$ values measured in this thesis, per the experimentally calibrated equations of Erez and Luz (1983) for planktonic foraminifera, Bemis et al. (1998) for planktonic foraminifera, Shackleton (1974) for benthic foraminifera, O'Neil et al. (1969) for inorganically precipitated calcite, and Kim and O'Neil (1997) for inorganically precipitated calcite. The Cretaceous ocean is assumed to have a $\delta^{18}O$ of -1.2‰ (Shackleton and Kennett, 1975).

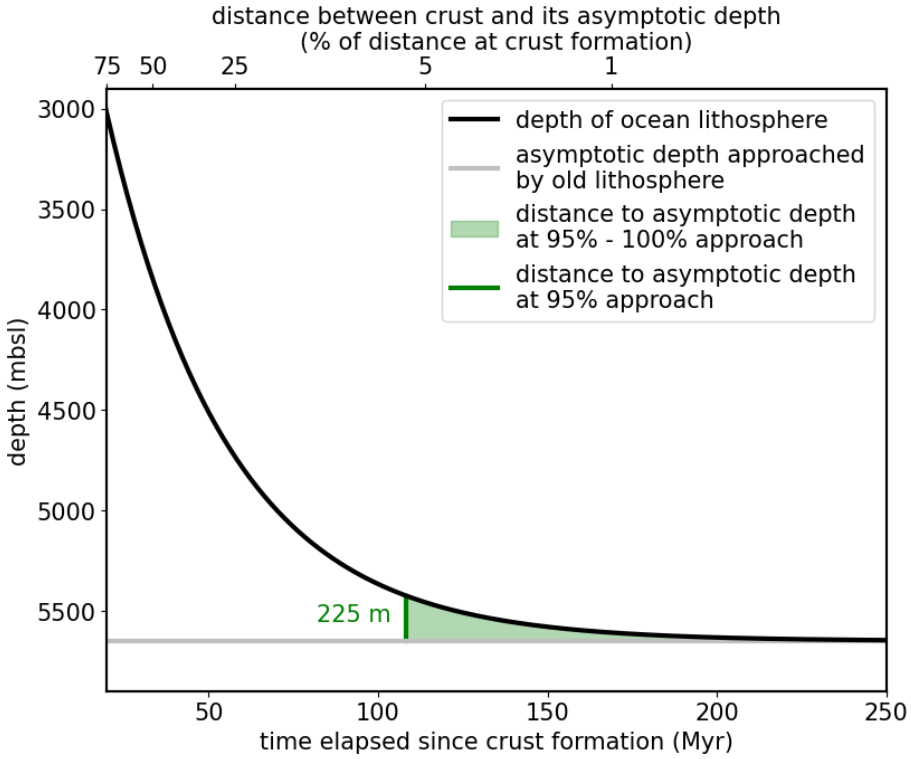

Figure A.2: Depth of old ($\geq$20 Myr) lithosphere as it approaches an asymptotic igneous basement depth of 5651 m, following the approximation of Stein and Stein (1992) (Equation 2.2). When the distance between the crust and its asymptotic depth is 5% of the distance at crustal formation (in other words, 95% of the approach to the asymptote is complete), the distance between the crust and the asymptotic depth is 225 m.

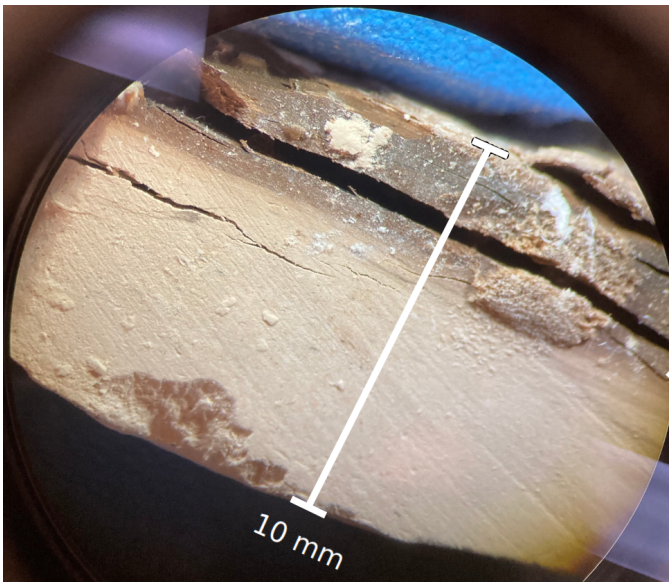

Figure A.3: The distinctly colored zones of sample 17-167-60-2-41/42 viewed under a microscope.

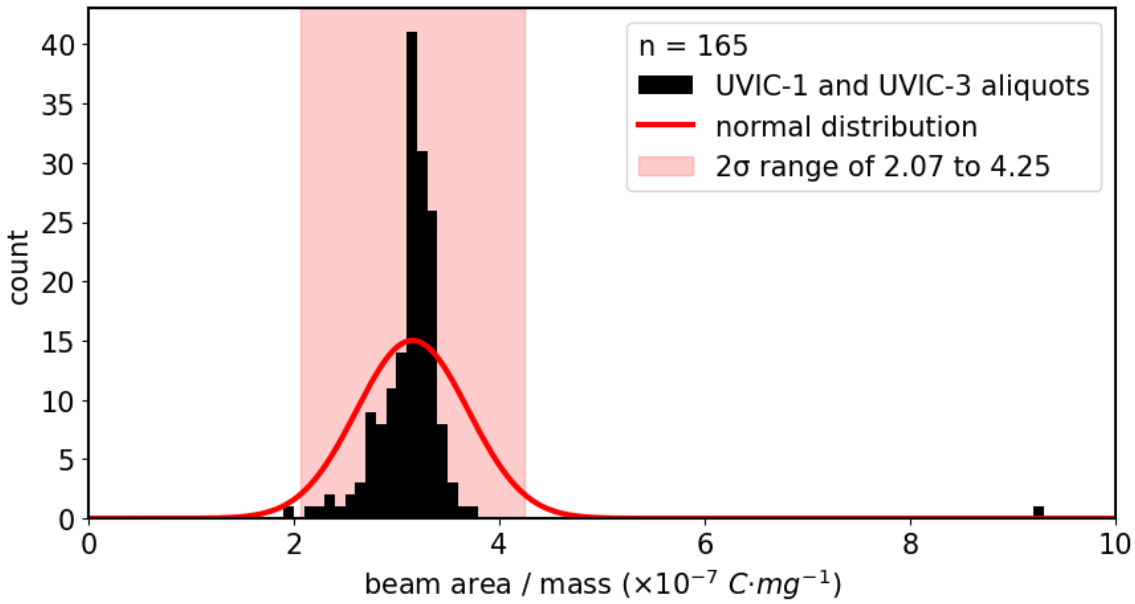

Figure A.4: Histogram of the beam area / mass ratios of aliquots of UVIC-1 and UVIC-3 (n = 189), which are pure calcite standards. Also shown are the normal distribution function with the same mean μ and standard deviation σ as this distribution (μ = 3.16 × 10^{-7} C·mg^{-1}, σ = 0.54 × 10^{-7} C·mg^{-1}), and the 2σ range (2.07 × 10^{-7} C·mg^{-1} to 4.25 × 10^{-7} C·mg^{-1}) associated with this normal distribution.

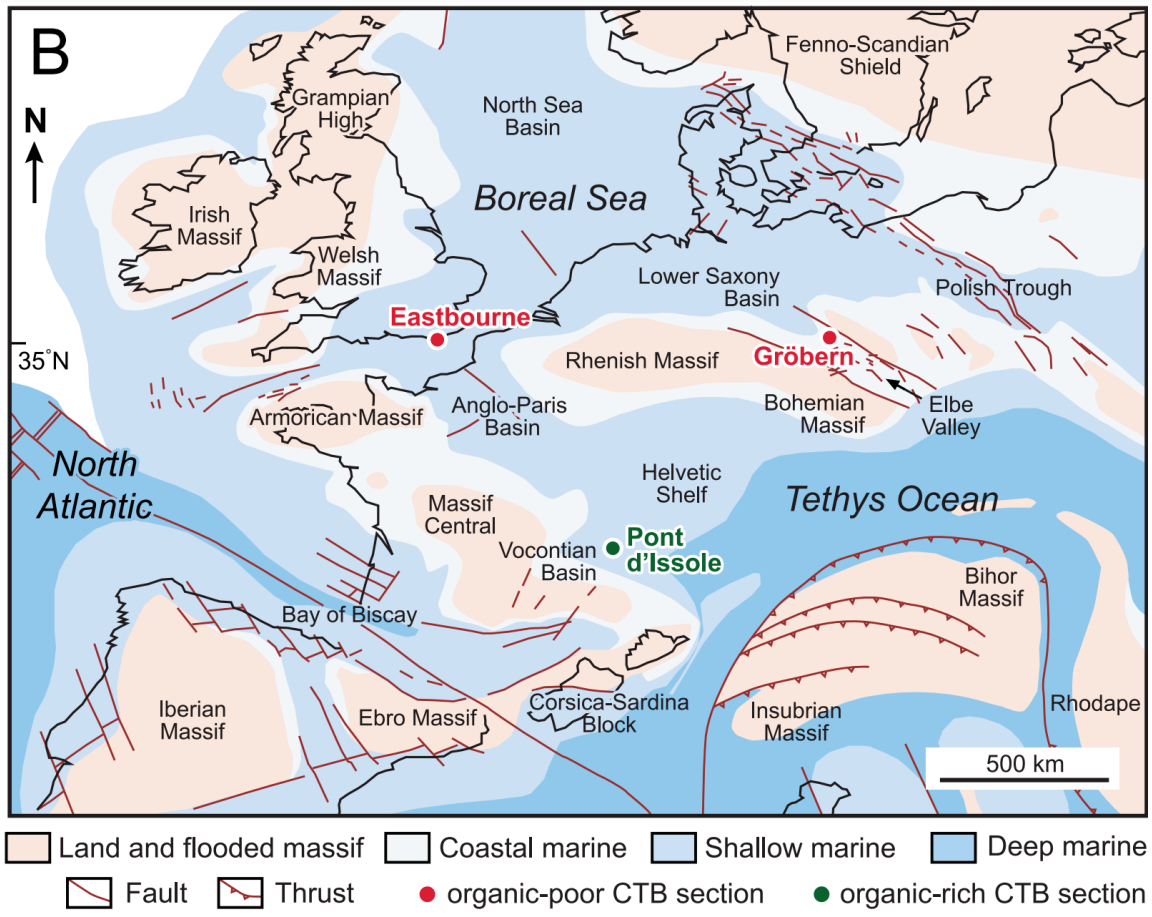

Figure A.5: From Jarvis et al. (2011), captioned "(b) Cenomanian paleogeography of Europe showing location of the main study sites. CTB is Cenomanian-Turonian boundary. Modified from Philip et al. [2000]."

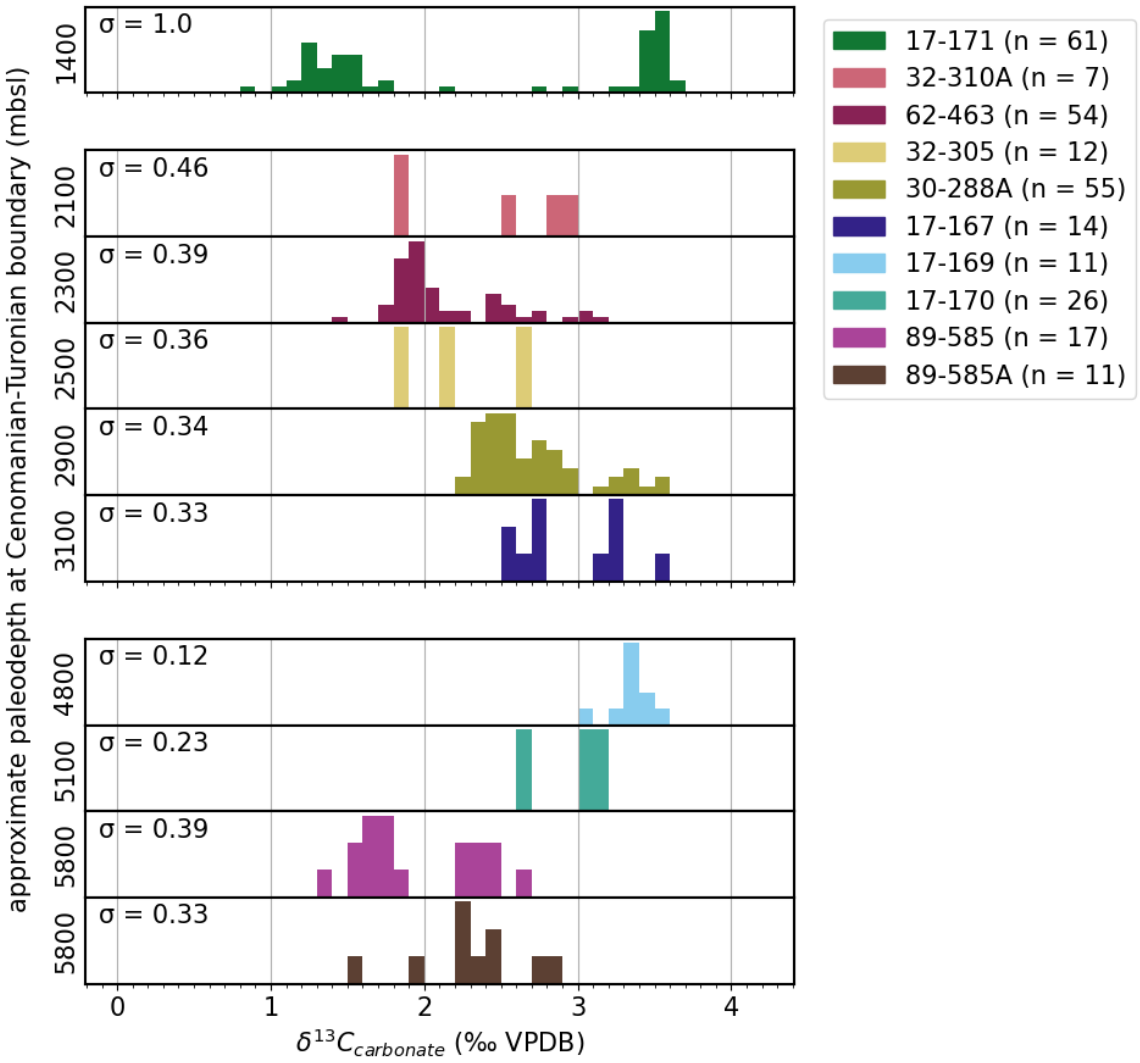

Figure A.6: $\delta^{13}C_{carbonate}$ distributions at Pacific sites in this thesis, plotted in order of increasing estimated paleodepth of site at the Cenomanian-Turonian boundary. Sites are categorized as either "shallow" $<$ 1500 mbsl (17-171), "intermediate" 1500 - 3500 mbsl (32-310A, 62-463, 32-305, 30-288A, 17-167), or "deep" $>$ 4500 mbsl (17-169, 17-170, 89-585 and 89-585A) during the Cenomanian-Turonian. For each site the standard deviation (σ) is calculated (which assumes a Gaussian distribution). Only samples from sediments that could have Cenomanian and/or Turonian age, based on biostratigraphy, are included.

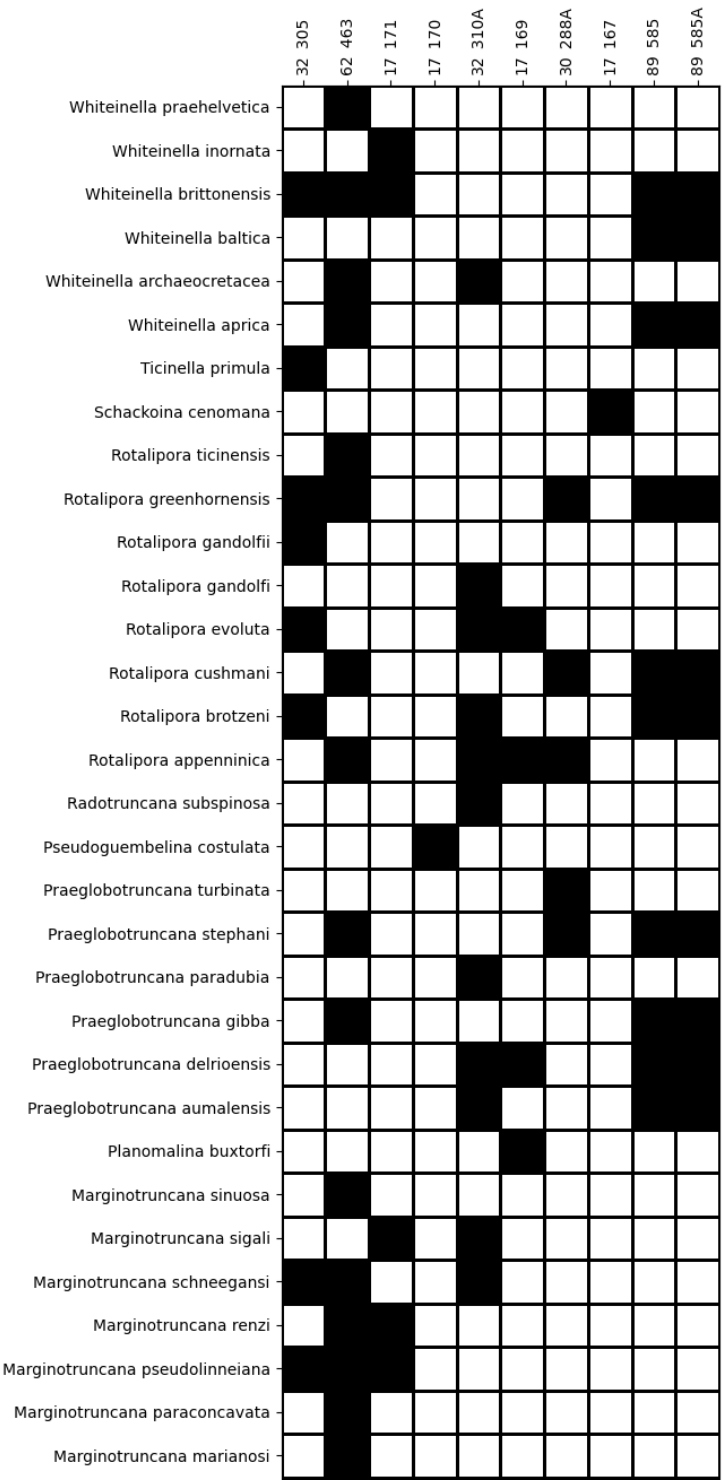
32 305
62 463
17 171
17 170
32 310A
17 169
30 288A
17 167
89 585
89 585A
Whiteinella praehelvetica
Whiteinella inornata
Whiteinella brittonensis
Whiteinella baltica
Whiteinella archaeocretacea
Whiteinella aprica
Ticinella primula
Schackoina cenomana
Rotalipora ticinensis
Rotalipora greenhornensis
Rotalipora gandolfii
Rotalipora gandolfi
Rotalipora evoluta
Rotalipora cushmani
Rotalipora brotzeni
Rotalipora appenninica
Radotruncana subspinosa
Pseudoguembelina costulata
Praeglobotruncana turbinata
Praeglobotruncana stephani
Praeglobotruncana paradubia
Praeglobotruncana gibba
Praeglobotruncana delrioensis
Praeglobotruncana aumalensis
Planomalina buxtorfi
Marginotruncana sinuosa
Marginotruncana sigali
Marginotruncana schneegansi
Marginotruncana renzi
Marginotruncana pseudolinneiana
Marginotruncana paraconcavata
Marginotruncana marianosi

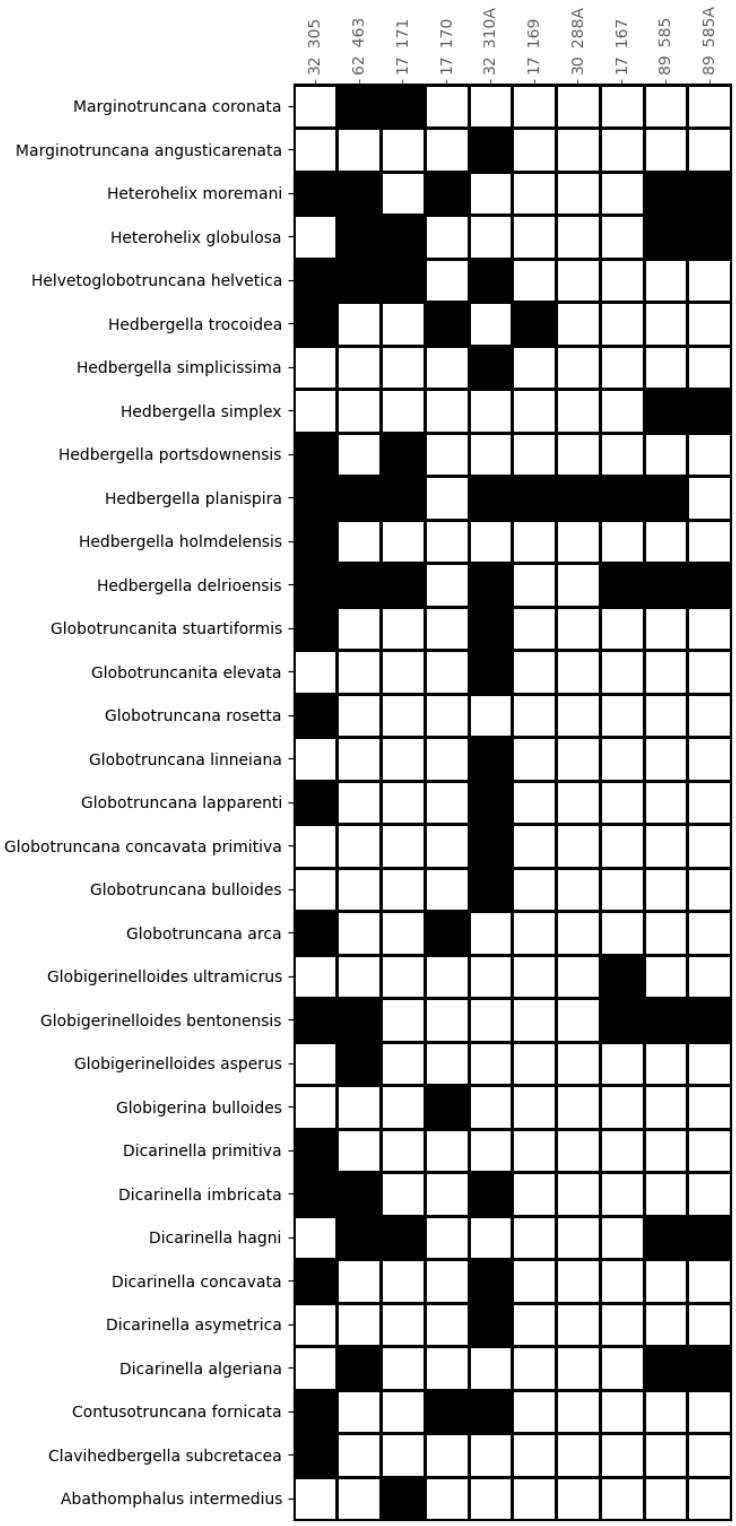

Figure A.7: Presence or absence of each of 65 species of planktonic foraminifera at each of 10 Pacific sites examined in this thesis.

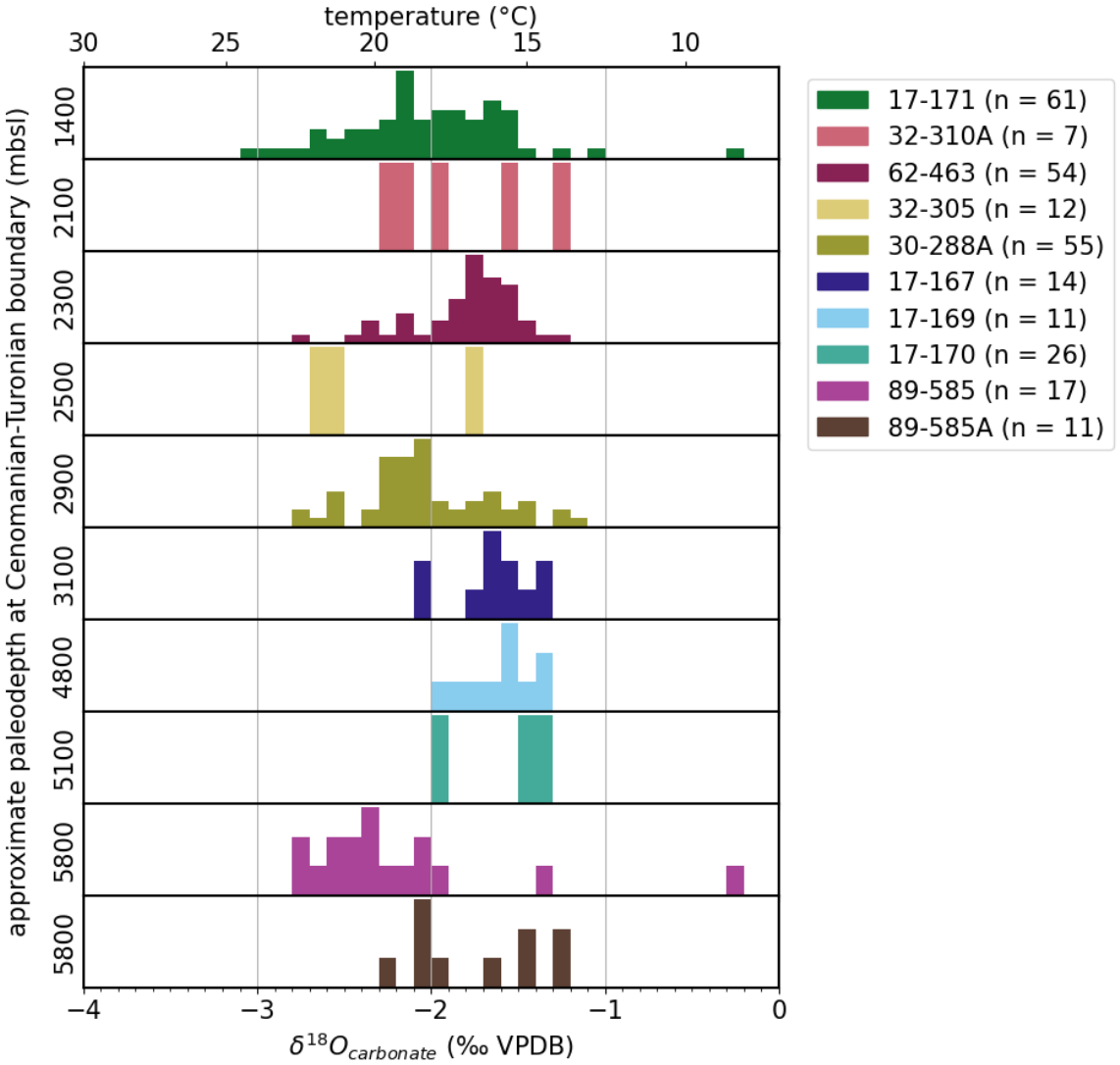

Figure A.8: Bulk $\delta^{18}O_{carbonate}$ distributions at Pacific sites examined in this thesis, plotted in order of increasing estimated paleodepth of site at the Cenomanian-Turonian boundary. Only samples from sediments that could have Cenomanian and/or Turonian age, based on biostratigraphy, are included. At the top are shown the temperatures corresponding to these $\delta^{18}O_{carbonate}$ values if temperature-controlled fractionation were the only control on $\delta^{18}O_{carbonate}$, per the equation of Kim and O'Neil (1997) for inorganically precipitated calcite (see Figure A.1).

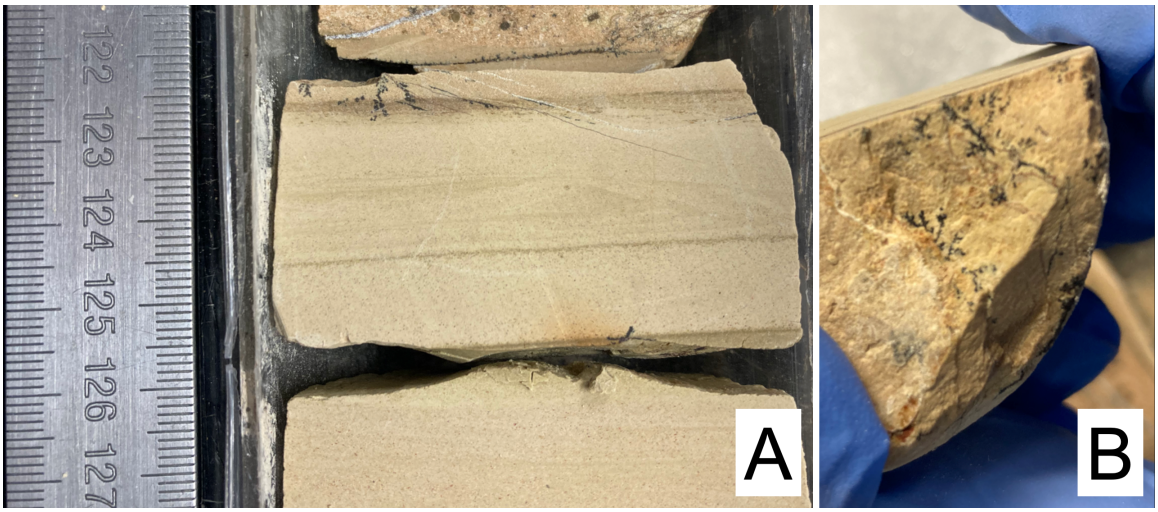

Figure A.9: (A) Black manganese dendrites observed at 122-123 cm in the layer of well cemented carbonate (122 - 150 cm) underlying hyaloclastite (base of hyaloclastite visible at 122 cm in photo) at 17-171. (B) Dendrites observed at 122 cm in cross-sectional view of core.

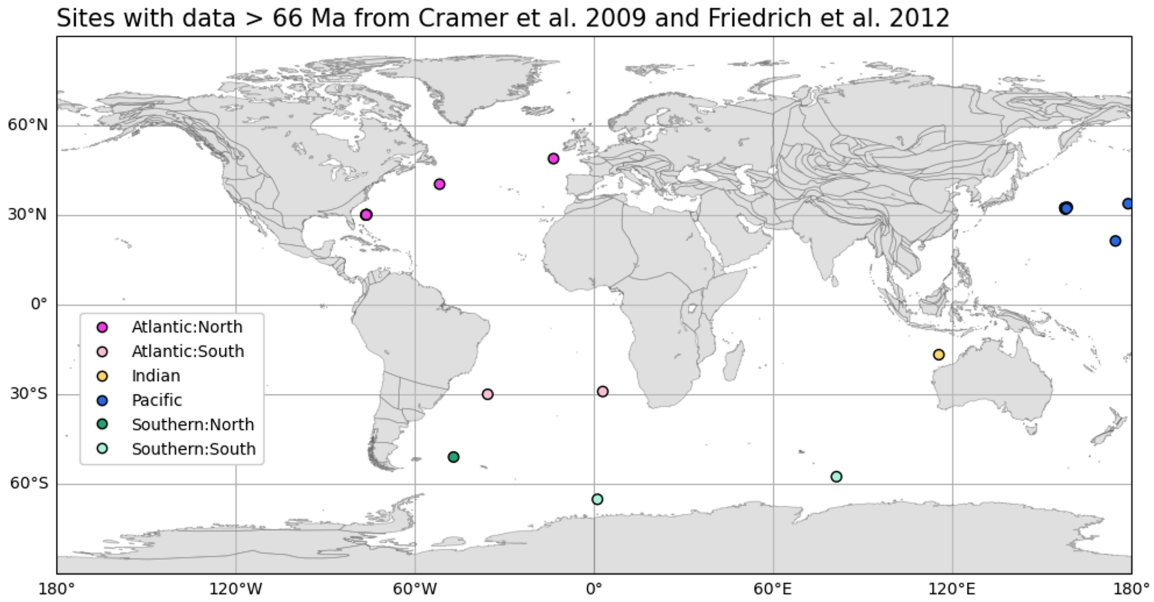

Figure A.10: Sites from the benthic foraminiferal $\delta^{13}C_{carbonate}$ and $\delta^{18}O_{carbonate}$ compilations of Cramer et al. (2009) and Friedrich et al. (2012) with $\delta^{13}C_{carbonate}$ data from samples of Cretaceous age (i.e. > 66 Ma). The map uses present-day geography (i.e. arrangement of continents).

Appendix A2: List of features noted in samples

Samples from DSDP expeditions were examined under a microscope and described. In samples that were not powder residues from previous workers I observed all sides of each sample, and noted features such as the grain size of the matrix and the presence or absence of chert. Here is a non-exhaustive list of features I noted in more than one sample, with examples shown in Figure A.11.

- Angular chert pieces more than 1 mm long at their longest dimension
- Dark flecks which may be organic matter
- Different-colored zones of the sample, e.g. in Figure A.3
- Fine layers
- Manganese dendrites
- Round white components which may be calcispheres
- Veins

I also noted certain features which likely developed after the samples were retrieved from the seafloor, including:

- Glutinous lumps on the surface of the sample only
- White filamentous crystals identified as gypsum on the surface of the sample only

Examples of these are also shown in Figure A.11.

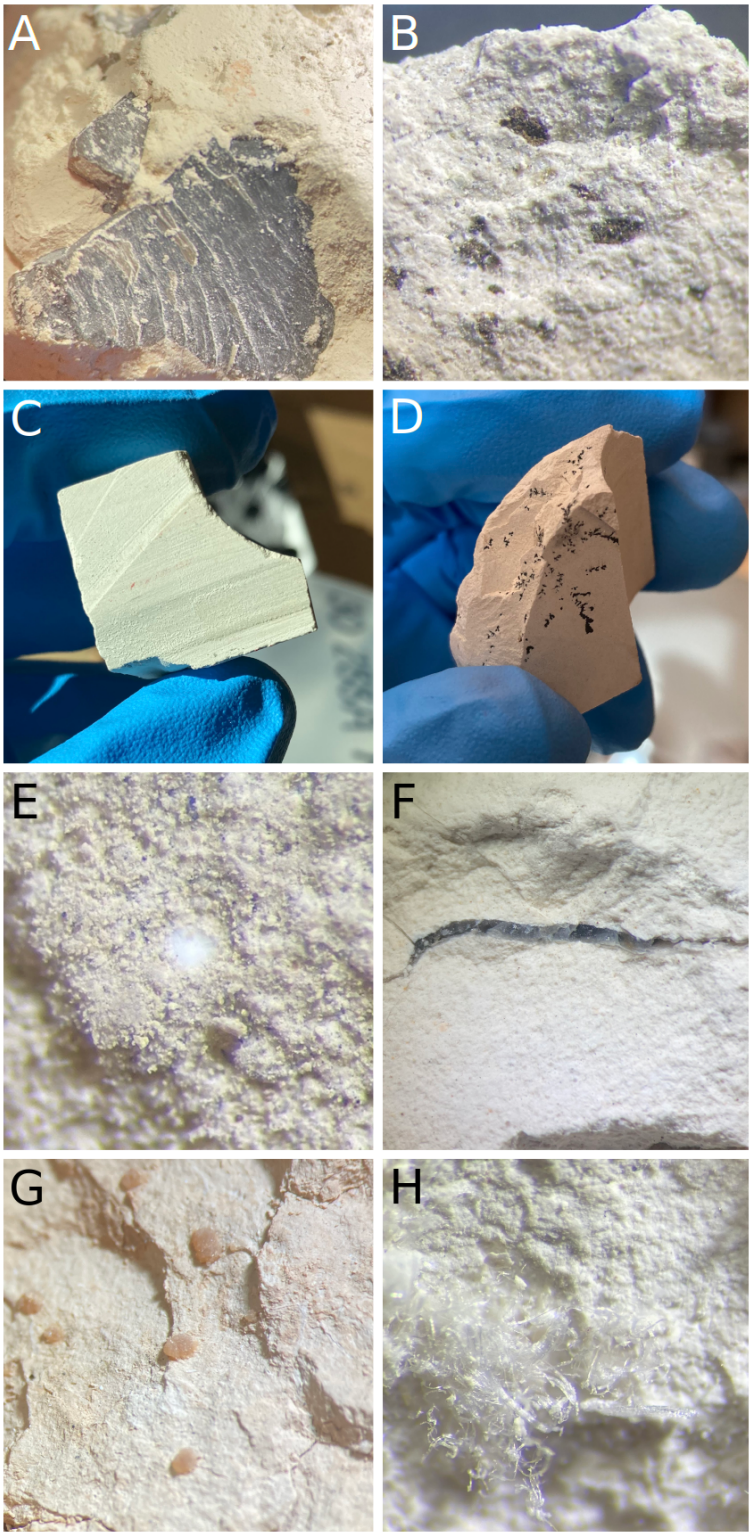

Figure A.11: (A) Piece of chert in the carbonate matrix of the sample 32-305-28-2-133/134, under a microscope. (B) Dark flecks in the sample 89-585-32-2-17/18, under a microscope. (C) Fine layers in the sample 30-288A-23-2-105/106. Note that the marks from cutting (on the top part of the sample) are oriented differently from the layers (identifiable because they vary in darkness of color). (D) Manganese dendrites in the sample 30-288A-25-1-93/94. (E) Round white component in the sample 89-585-32-2-52-53, under a microscope. (F) A vein in the sample 30-288A-26-1-57/58, under a microscope. (G) Glutinous lumps on the sample 17-169-4-CC, under a microscope. (H) Filamentous crystals on the sample 30-288A-20-2-17/18, under a microscope.

Appendix A3: Detail on three analyses excluded for reasons other than beam area

Two analyses were excluded because of concern about instrument stability immediately following analysis of a sample very rich in labile organic carbon. During one mass spectrometer run (12 June 2023), analyses of natural aliquots were conducted after powders of dried kelp were analyzed. I noted that the VTS standards run after the kelp were slightly lower than expected (after correction their δ^{13}C values were -1.62‰ to -1.74‰ compared to an expected value of -1.48‰). Due to concern that this unusual material might have temporarily affected the mass spectrometer, I excluded the analyses conducted in the block immediately following the kelp analysis, which accounts for 2 of the 3 analyses excluded for reasons other than beam area.

One analysis was excluded because the δ^{13}C and δ^{18}O values of the monitoring standard (VTS) at the end of the run diverged noticeably from the accepted values. During another mass spectrometer run (14 July 2023), the δ^{13}C and δ^{18}O values of the monitoring standard (VTS) at the end of the run (final block of standards) diverged noticeably from the accepted values (i.e. two subsequent measurements of VTS yielded δ^{13}Cs of 10.96‰ and 11.02‰ compared to an accepted value of -1.48‰, and δ^{18}Os of 30.73‰ and 30.58‰ compared to an accepted value of -8.54‰). I excluded all analyses conducted in the block immediately prior to this block of standards. This block had only two samples in it, and one was already excluded because its beam area was below the cutoff. The other sample accounts for the final analysis that was excluded for reasons other than beam area.

Appendix A4: Samples measured on 12 June 2023

Core	Section	Top offset (cm)	Bottom offset (cm)	Top depth (mbsf)	Bottom depth (mbsf)	Beam area ($\times 10^{-8}$ C $\cdot mg^{-1}$)	Mass (mg)	δ^{13}C (‰ VPDB)	δ^{18}O (‰ VPDB)
32	1	75	76	531.95	531.96	3.02	0.84	1.62	-2.35
32	3	10	11	534.3	534.31	3.64	0.933	1.83	-1.97
32	3	42	43	534.62	534.63	3.24	0.906	1.31	-2.13
32	3	55	56	534.75	534.76	3.83	0.856	1.51	-2.76
32	3	72	73	534.92	534.93	5.44	0.833	1.79	-2.21
32	3	79	80	534.99	535	6.31	0.927	1.71	-2.71
32	3	104	105	535.24	535.25	5.06	0.767	1.64	-2.48
32	4	31	32	536.01	536.02	6.91	0.91	1.71	-2.56
32	4	76	77	536.46	536.47	5.40	0.813	1.64	-2.06
34	1	37	38	549.87	549.88	6.82	0.782	2.41	-2.60
34	1	92	93	550.42	550.43	7.82	0.793	2.28	-2.36
34	1	130	131	550.8	550.81	7.03	0.905	2.23	-2.70
34	2	16	17	551.16	551.17	8.38	0.878	2.48	-2.02
34	2	91	92	551.91	551.92	3.67	0.803	2.40	-2.33
35	1	106	107	559.66	559.67	2.64	0.893	1.56	-2.44

Appendix A5: Subsidence curves for Pacific sites

Here I present, for each Pacific site in this thesis, a plot of depth (in mbsl) vs. age (in Myr), showing crust since the time of formation (in blue), sediments since the time of deposition (for the beginning of the Cenomanian, the Cenomanian-Turonian boundary, and the end of the Turonian, in red, orange, and yellow respectively), and present-day seafloor depth (in turquoise). Squares indicate that the depth shown is the depth of the seafloor at that time. Plots are in order of increasing estimated paleodepth of deposition at the Cenomanian-Turonian boundary. The inflection point that occurs 20 Myr after crustal formation in many of these plots is a consequence of using Equation 2.1 for ocean crust of age <20 Myr and Equation 2.4 for ocean crust of age ≥20 Myr (Section 2.4), not a realistic feature of crustal subsidence.

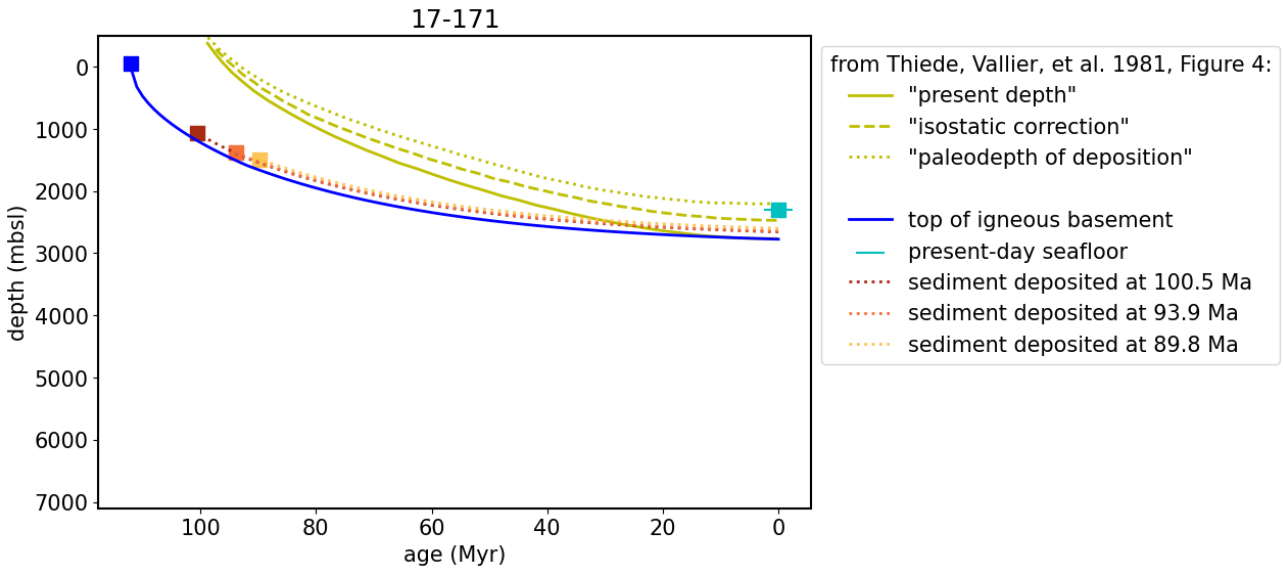

Shipboard Scientific Party (1981b) estimated the paleodepth of deposition at 17-171,

and their estimate is shown on this figure.

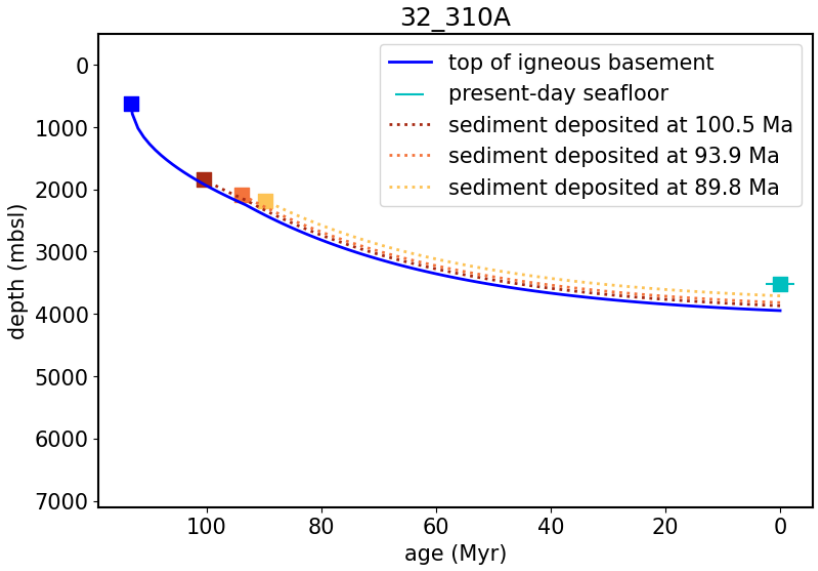

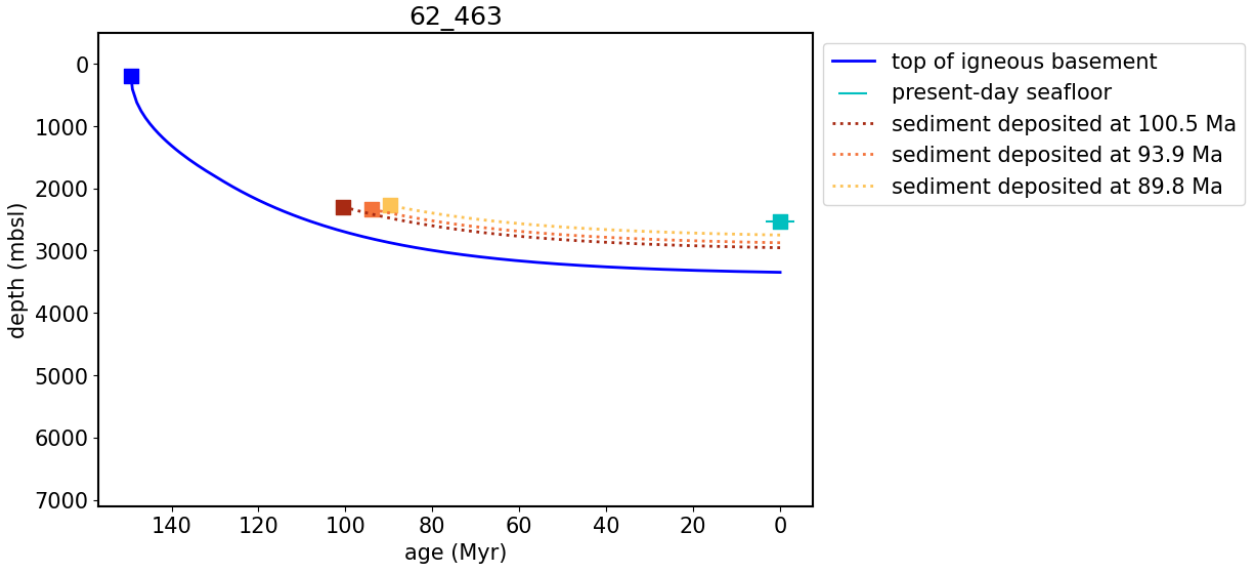

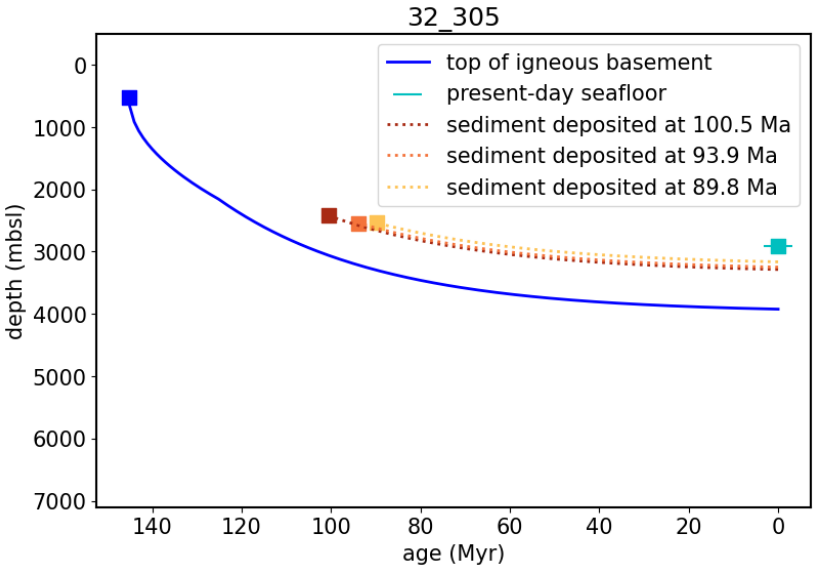
32_305
top of igneous basement
present-day seafloor
sediment deposited at 100.5 Ma
sediment deposited at 93.9 Ma
sediment deposited at 89.8 Ma
depth (mbsl)
0
1000
2000
3000
4000
5000
6000
7000
140
120
100
80
60
40
20
0
age (Myr)

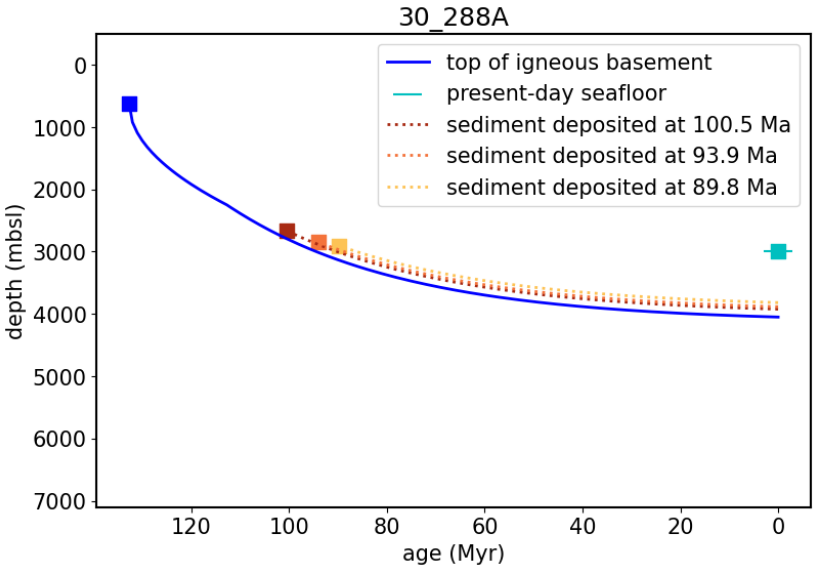
30_288A
top of igneous basement
present-day seafloor
sediment deposited at 100.5 Ma
sediment deposited at 93.9 Ma
sediment deposited at 89.8 Ma
depth (mbsl)
0
1000
2000
3000
4000
5000
6000
7000
120
100
80
60
40
20
0
age (Myr)

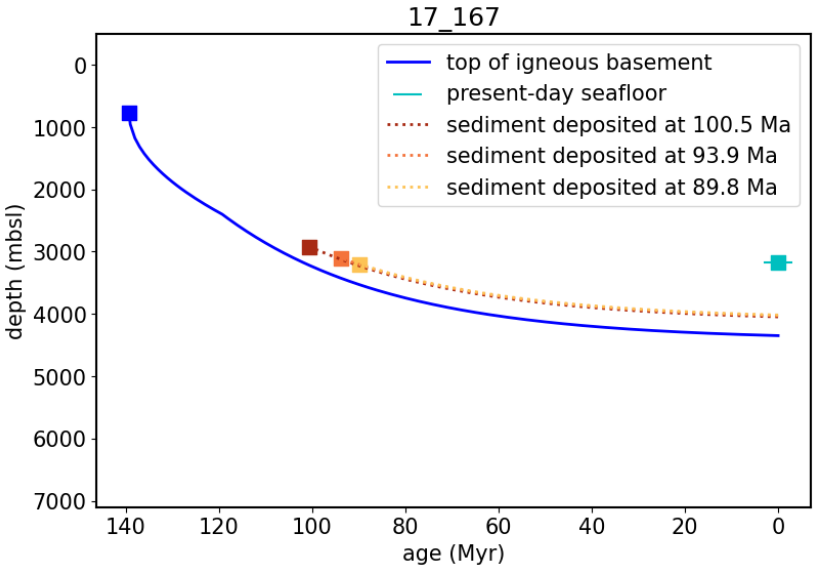
17_167
top of igneous basement
present-day seafloor
sediment deposited at 100.5 Ma
sediment deposited at 93.9 Ma
sediment deposited at 89.8 Ma
depth (mbsl)
0
1000
2000
3000
4000
5000
6000
7000
140
120
100
80
60
40
20
0
age (Myr)

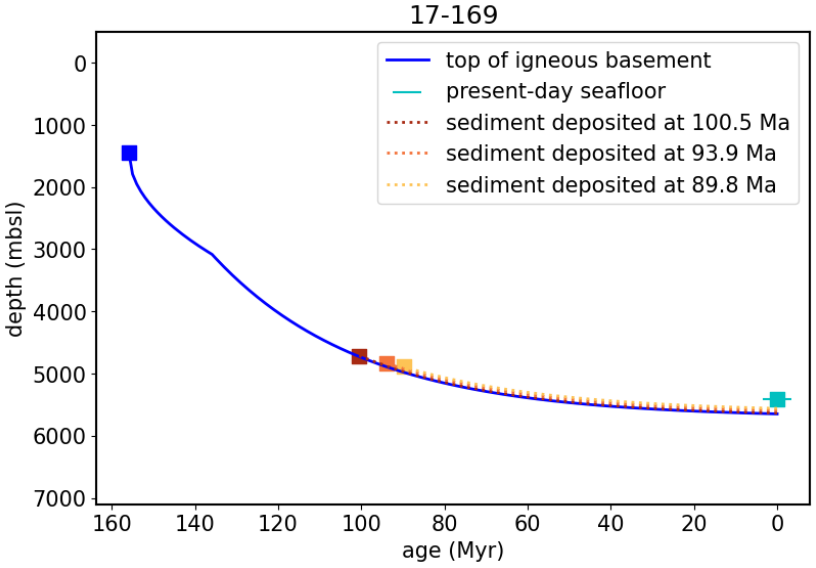
17-169
top of igneous basement
present-day seafloor
sediment deposited at 100.5 Ma
sediment deposited at 93.9 Ma
sediment deposited at 89.8 Ma
depth (mbsl)
0
1000
2000
3000
4000
5000
6000
7000
160
140
120
100
80
60
40
20
0
age (Myr)

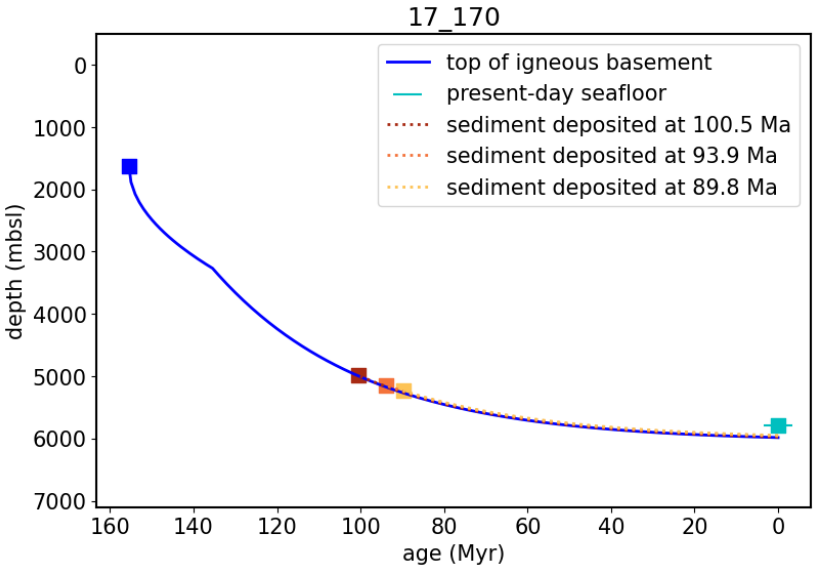
17_170
top of igneous basement
present-day seafloor
sediment deposited at 100.5 Ma
sediment deposited at 93.9 Ma
sediment deposited at 89.8 Ma
depth (mbsl)
0
1000
2000
3000
4000
5000
6000
7000
160
140
120
100
80
60
40
20
0
age (Myr)

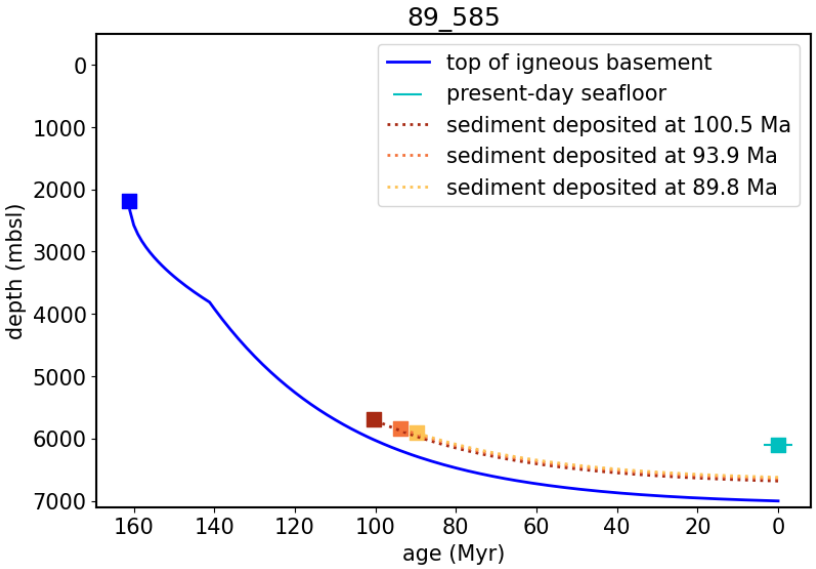
89_585
top of igneous basement
present-day seafloor
sediment deposited at 100.5 Ma
sediment deposited at 93.9 Ma
sediment deposited at 89.8 Ma
depth (mbsl)
0
1000
2000
3000
4000
5000
6000
7000
160
140
120
100
80
60
40
20
0
age (Myr)

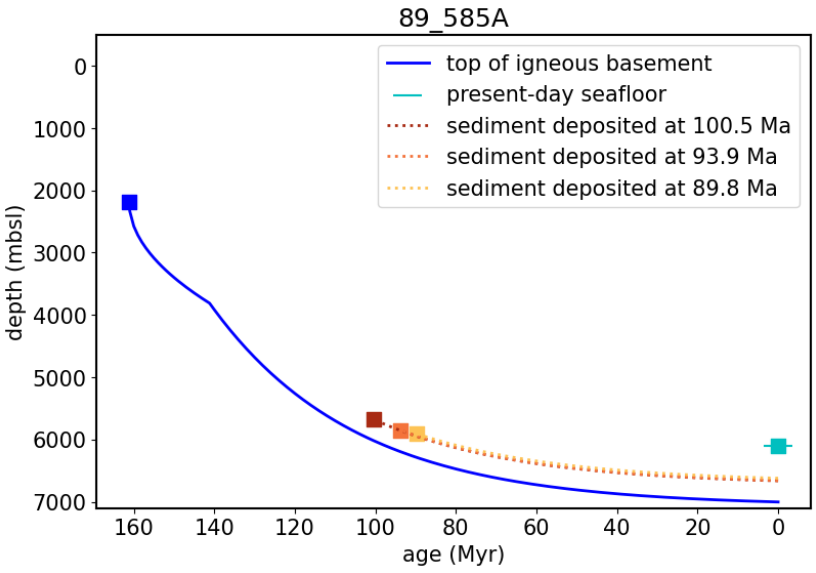
89_585A
top of igneous basement
present-day seafloor
sediment deposited at 100.5 Ma
sediment deposited at 93.9 Ma
sediment deposited at 89.8 Ma
depth (mbsl)
0
1000
2000
3000
4000
5000
6000
7000
160
140
120
100
80
60
40
20
0
age (Myr)

Appendix A6: Seismic profiles and bathymetric maps of Pacific sites

Seismic profiles and bathymetric maps are reproduced from the DSDP Initial Report for the Pacific sites studied in this thesis. Sites are presented in order of increasing estimated paleodepth of deposition at the Cenomanian-Turonian boundary.

17-171

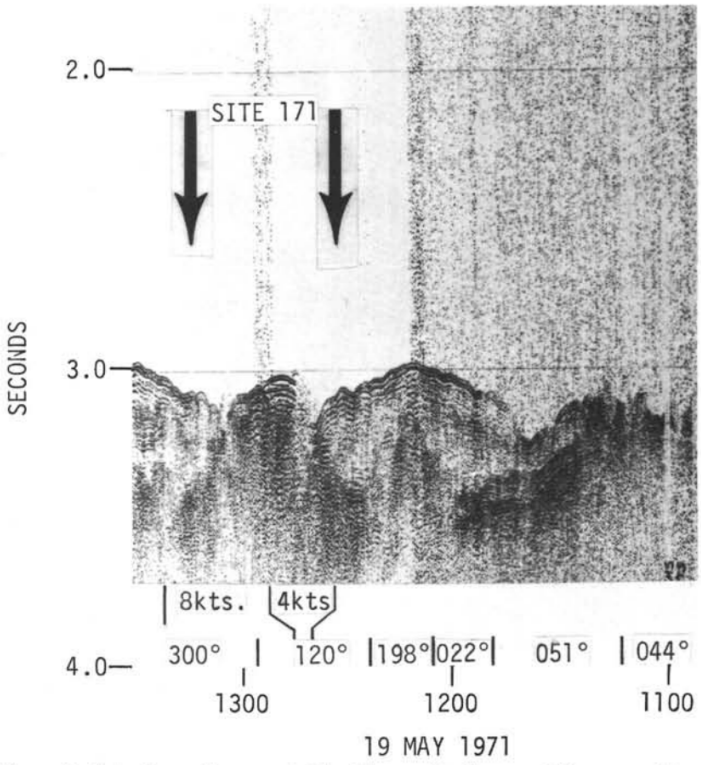

Figure 11 from Shipboard Scientific Party (1973e). Captioned, "Seismic profile recorded by *Glomar Challenger* in the vicinity of Site 171, showing south edge of guyot."

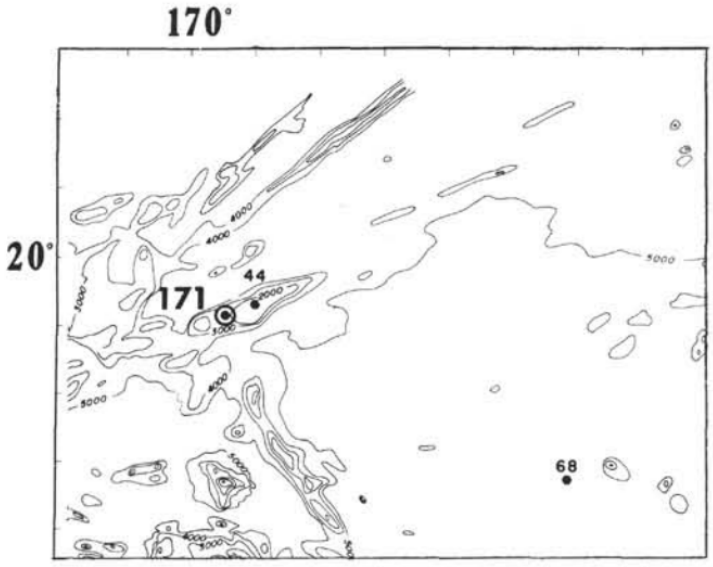

From the first page of Shipboard Scientific Party (1973e). No caption.

32-310A

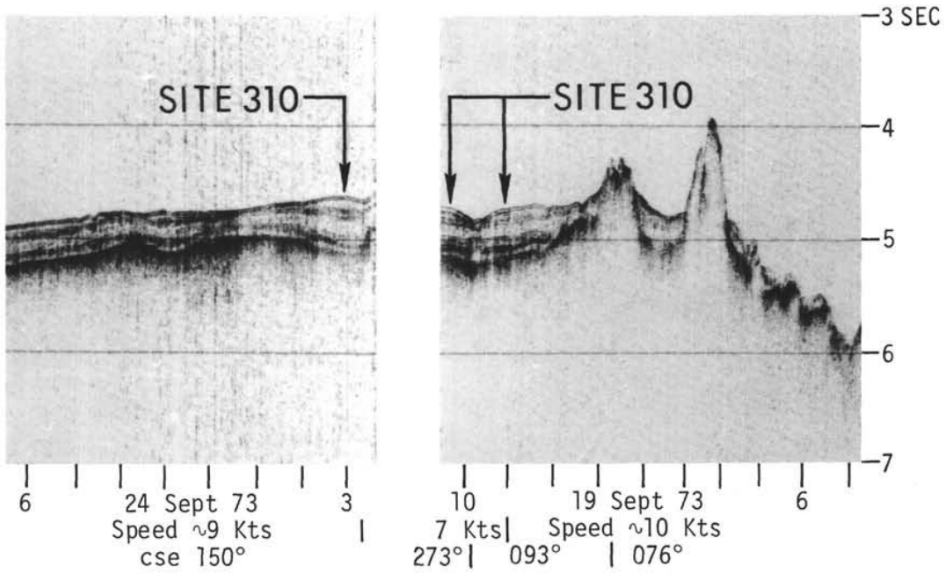

Figure 3 from Shipboard Scientific Party (1975e). Captioned "Seismic profiler section approaching and leaving Site 310."

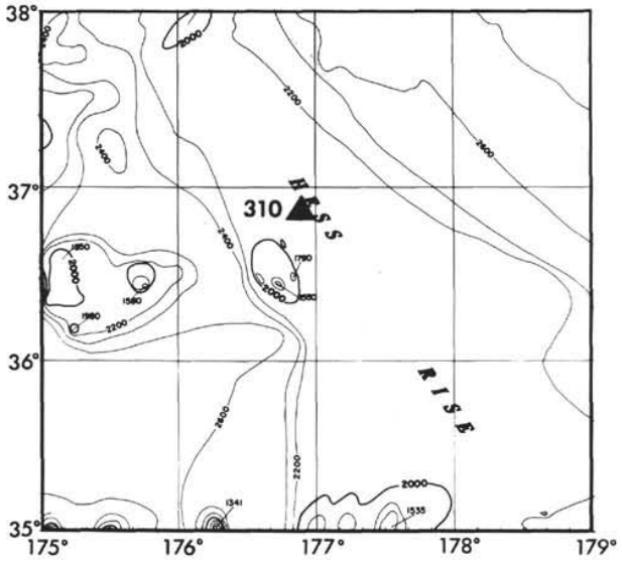

Figure 1 from Shipboard Scientific Party (1975e). Captioned "Bathymetry in the region of Site 310 (after Chase et al. 1971). Contour interval 200 fm uncorrected."

62-463

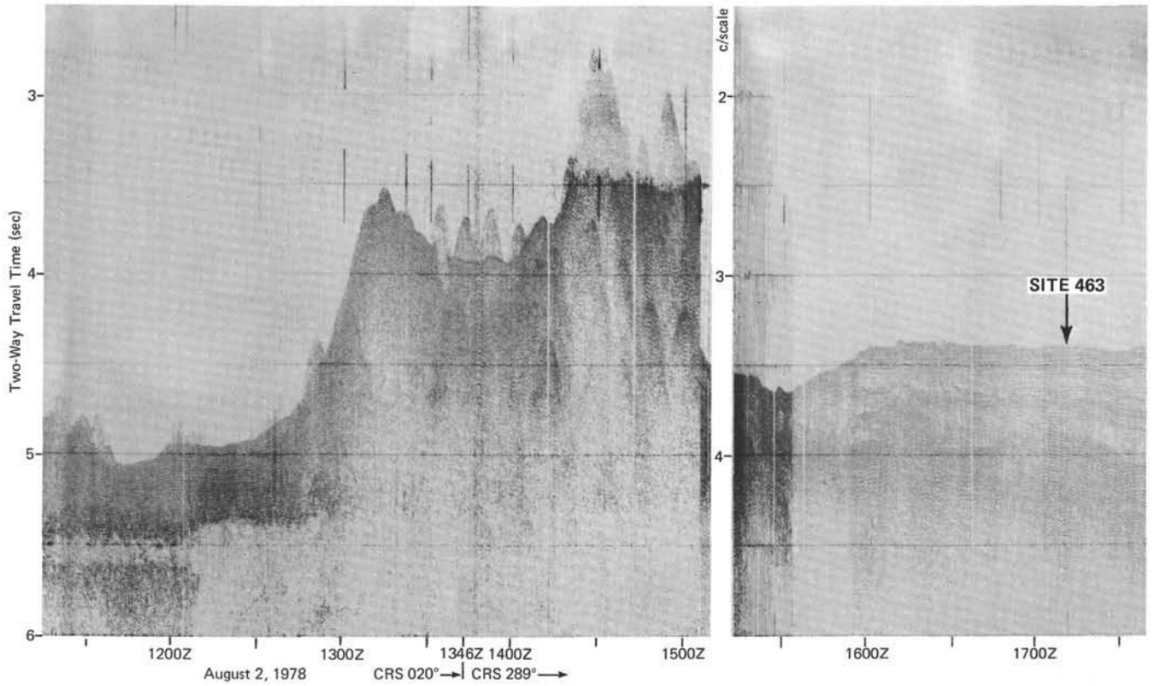

Figure 7 from Shipboard Scientific Party (1981b). Captioned "*Glomar Challenger* Leg 62 seismic-reflection profile made during the approach to Site 463."

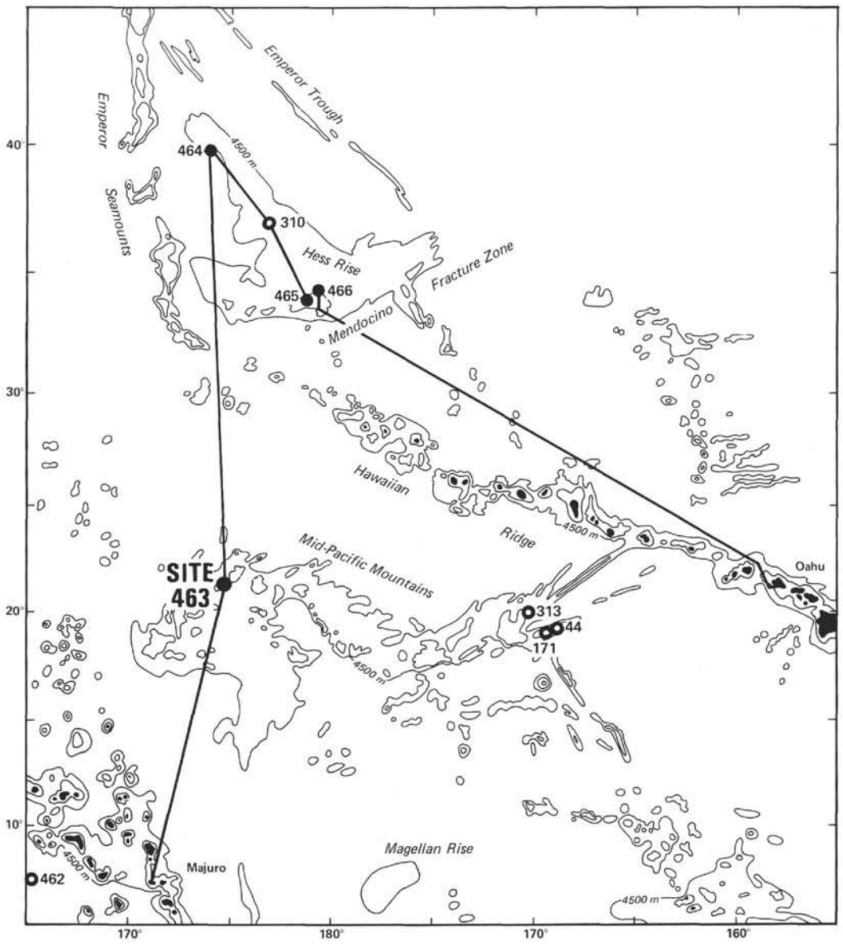

Figure 1 from Shipboard Scientific Party (1981b). Captioned "Location of DSDP sites in the central North Pacific."

32-305

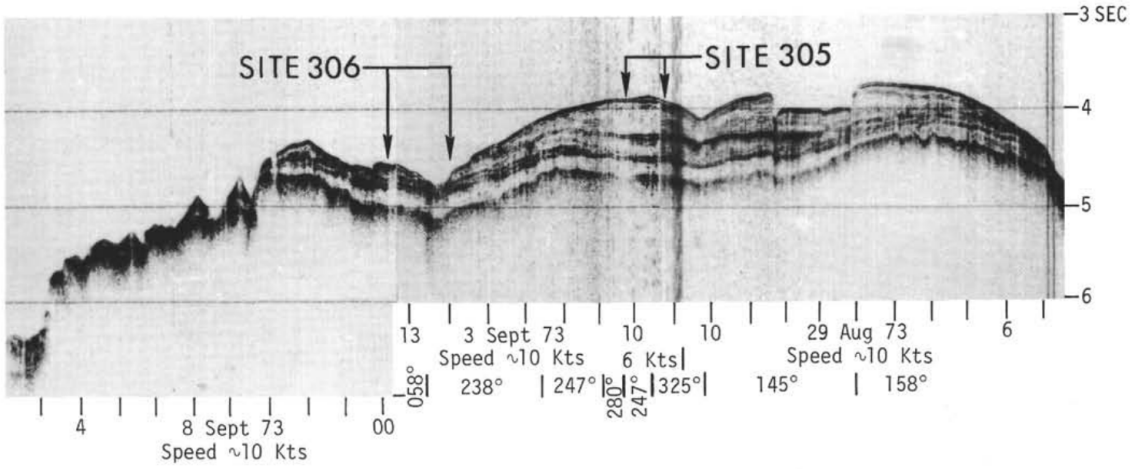

Figure 4 from Shipboard Scientific Party (1975c). Captioned "Seismic profiler section approaching and leaving Sites 305 and 306."

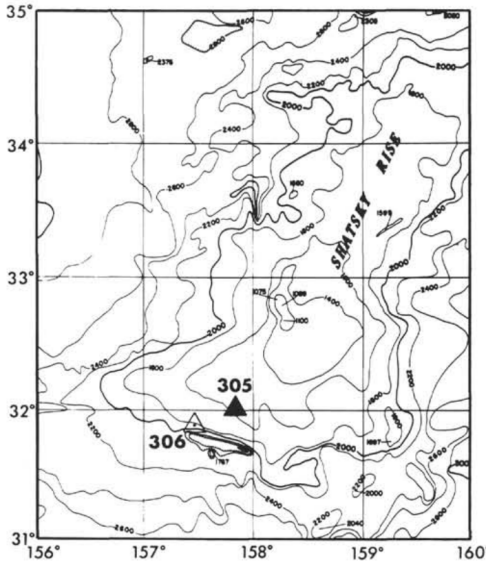

Figure 1 from Shipboard Scientific Party (1975c). Captioned "Bathymetry in the region of Sites 305 and 306 (after Chase et al. 1971). Contour interval 200 fm uncorrected."

30-288A

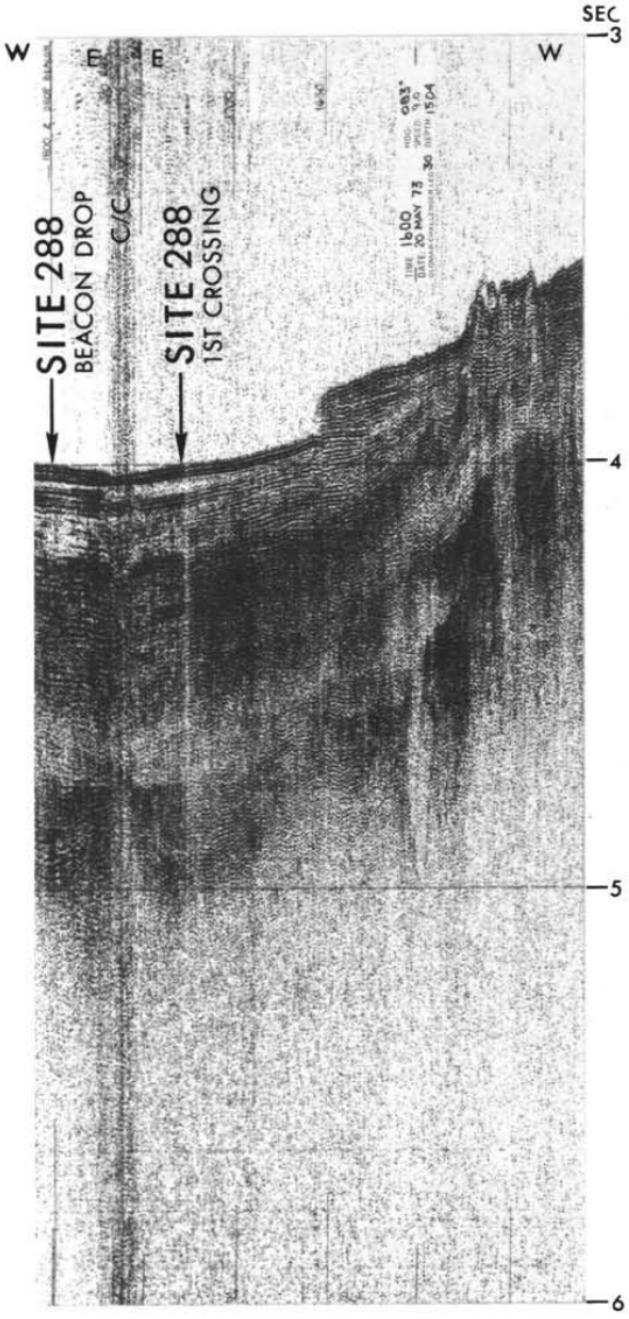

Figure 3 from Shipboard Scientific Party (1975a). Captioned "Seismic profile taken on D/V *Glomar Challenger* on approach to Site 288."

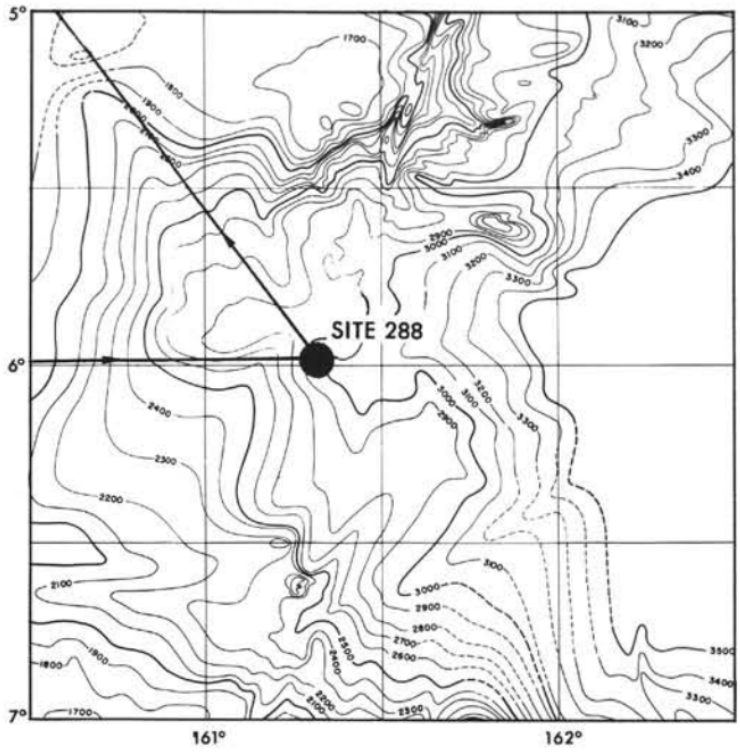

Figure 2 from Shipboard Scientific Party (1975a). Captioned "Location of Site 288 on the Steward Basin and the adjacent part of the Ontong Java Plateau. Contours in hundreds of meters. (Bathymetric map from Kroenke, 1972)."

17-167

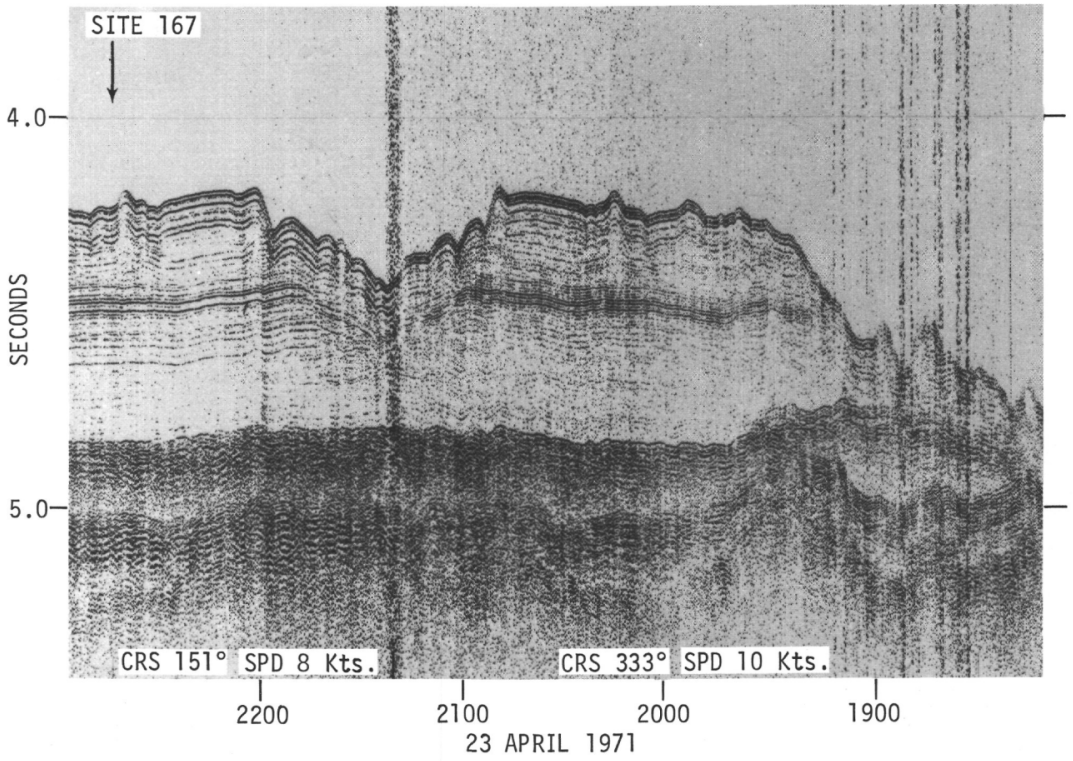

Figure 2a from Shipboard Scientific Party (1973b). Captioned, "Seismic profile recorded by *Glomar Challenger* while approaching Site 167."

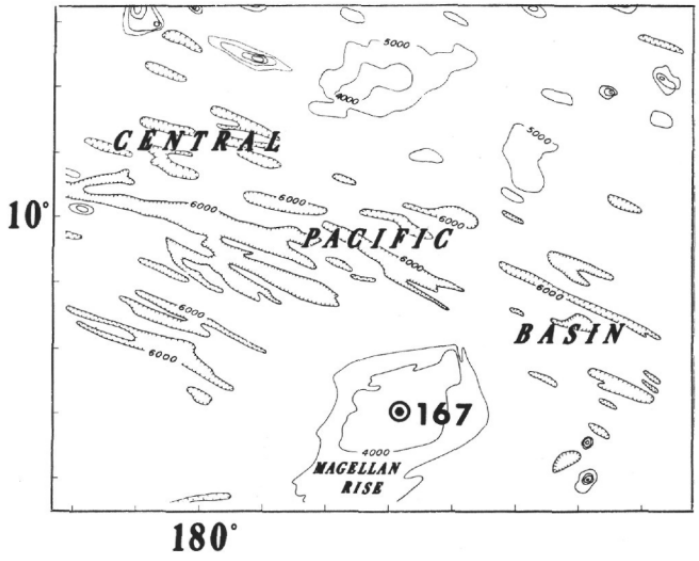

From the first page of Shipboard Scientific Party (1973b). No caption.

17-169

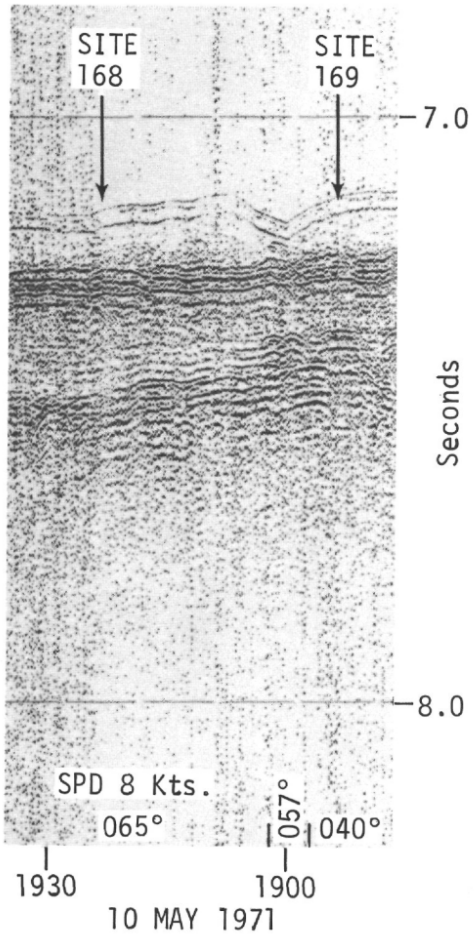

Figure 2 from Shipboard Scientific Party (1973c). Captioned, "Seismic profile recorded by *Glomar Challenger* along a course between Sites 168 and 169. See Figure 3 for track."

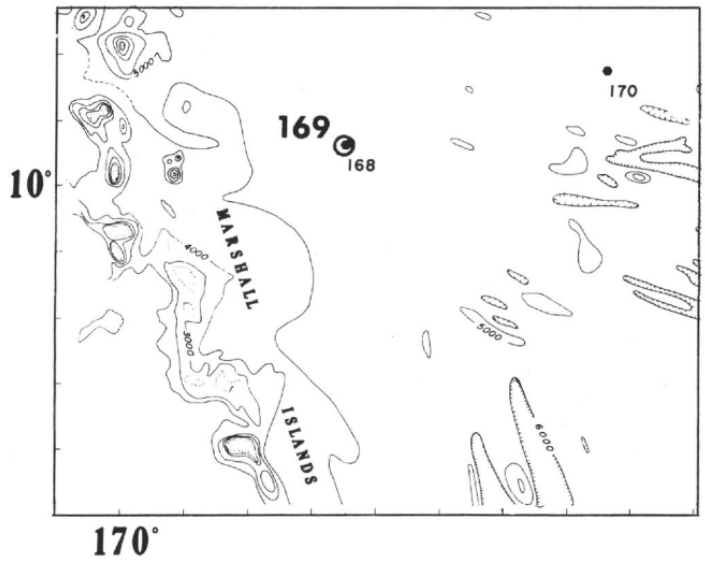

From the first page of Shipboard Scientific Party (1973c). No caption.

17-170

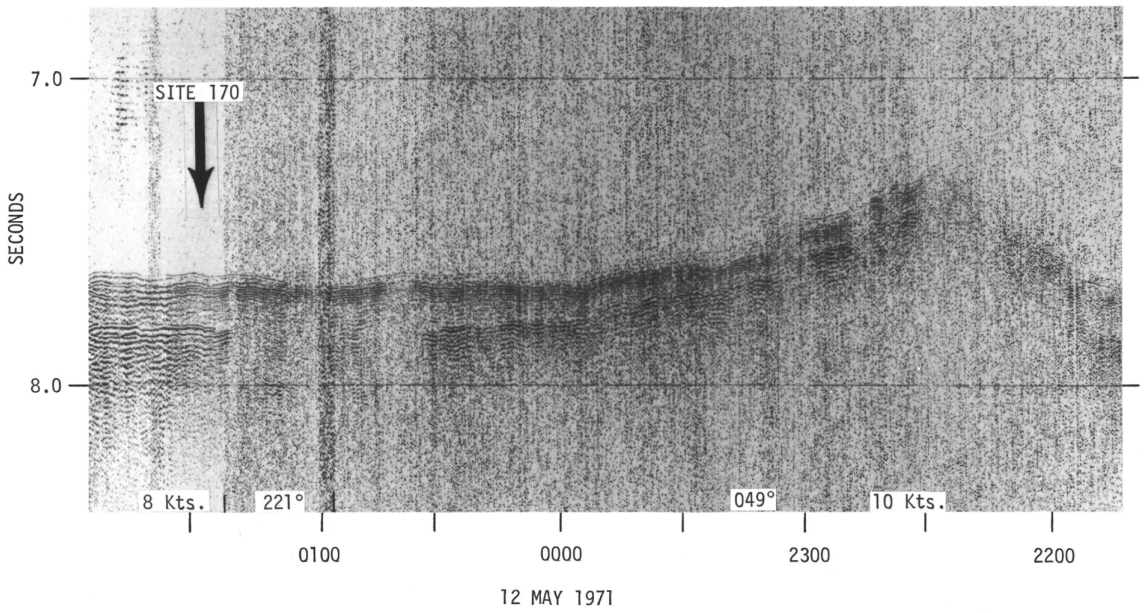

Figure 2 from Shipboard Scientific Party (1973d). Captioned, "Seismic profile recorded by *Glomar Challenger* while approaching Site 170."

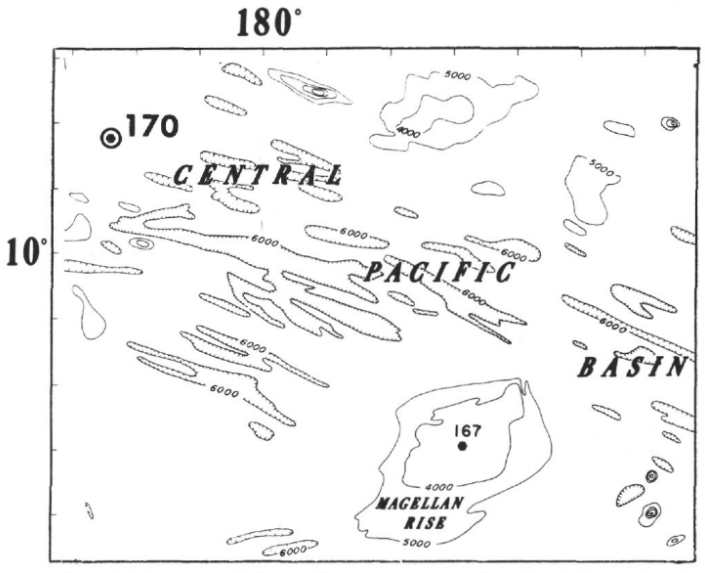

From the first page of Shipboard Scientific Party (1973d). No caption.

89-585 and 89-585A

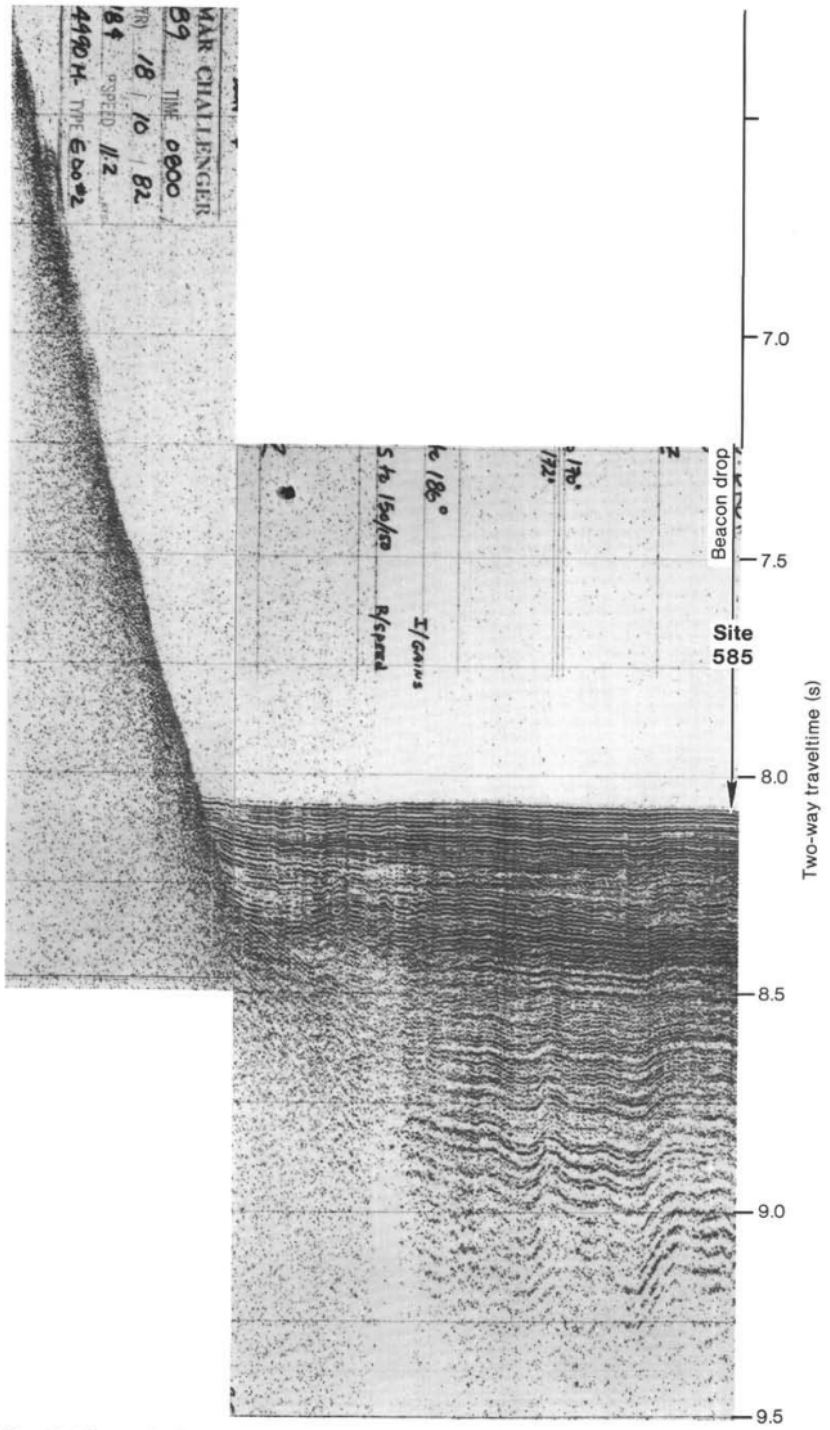

Figure 7 from Shipboard Scientific Party (1986). Captioned "Air gun seismic profile approaching MZP-6, which is Site 585, Mariana Basin."

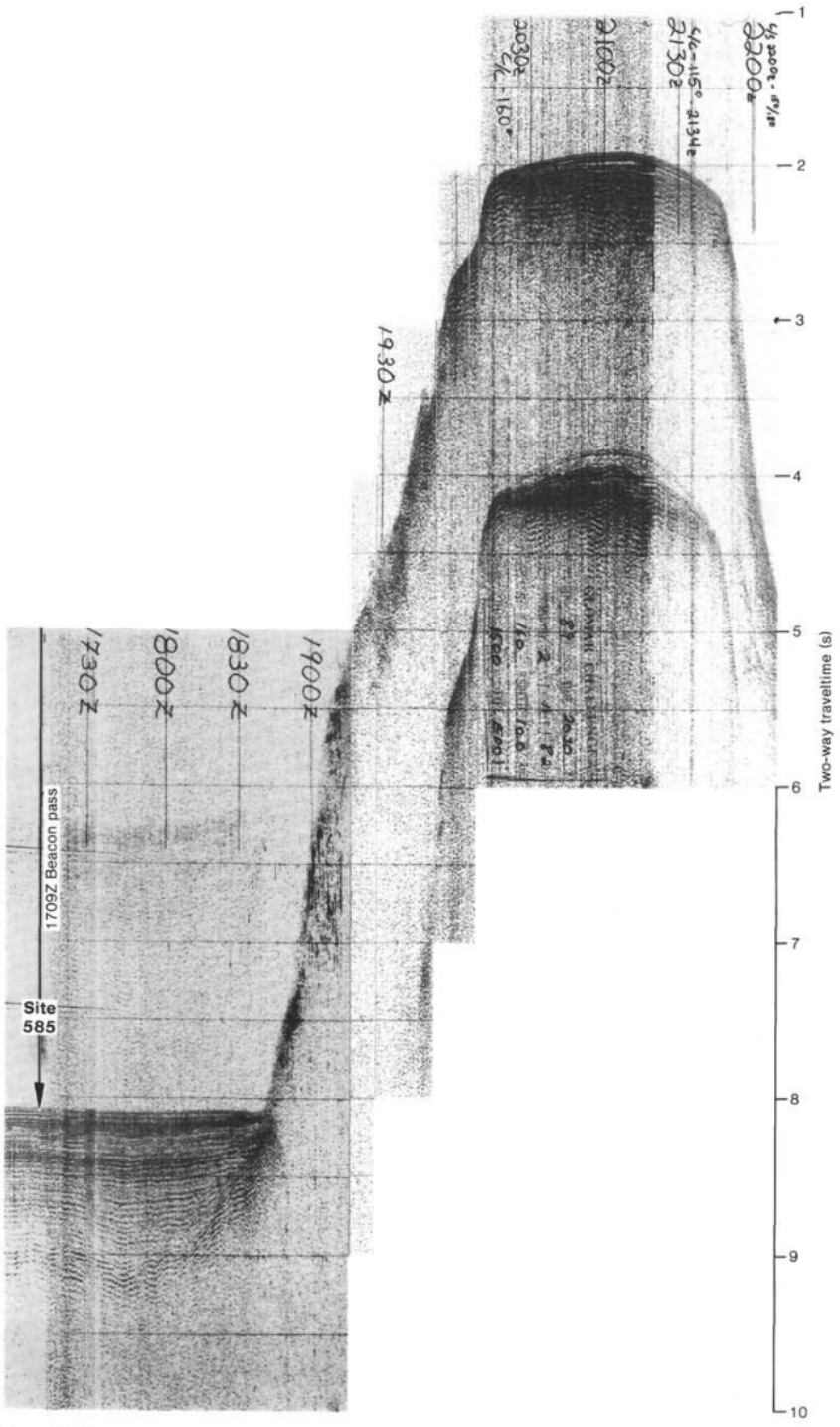

Figure 9 from Shipboard Scientific Party (1986). Captioned "Air-gun record upon leaving Site 585, showing Mariana Basin at left and the northern slope of Ita Maitai Guyot at right (south); c/s = change of scale; c/c = change of course."

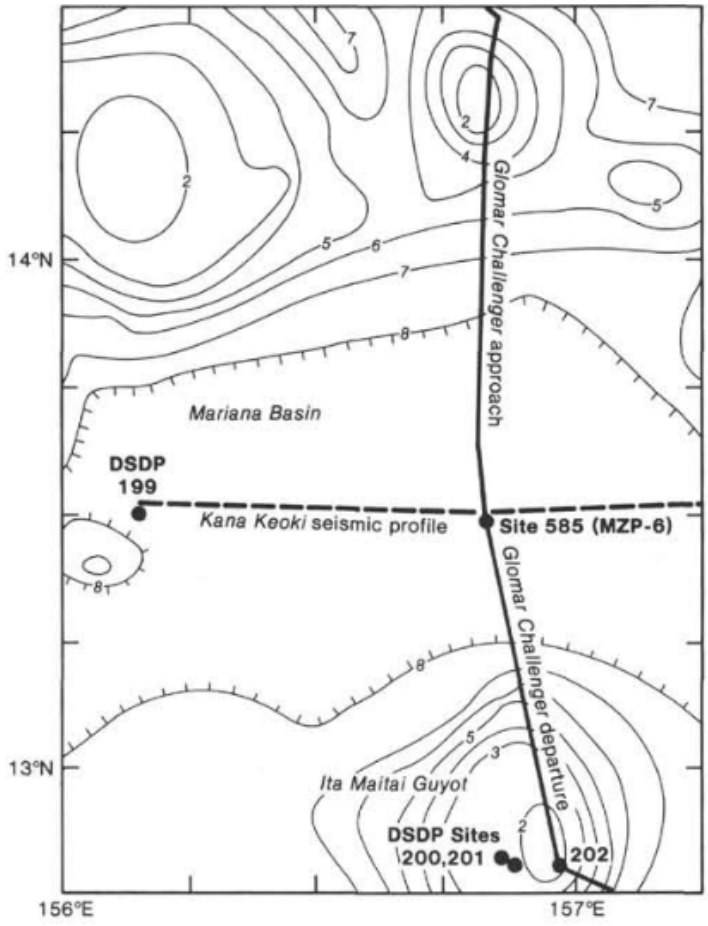

Figure 6 from Shipboard Scientific Party (1986). Captioned "*Glomar Challenger* track near Site 585. Bathymetry, contoured in seconds of two-way traveltime, from Duennebier and Petersen (1982), Chase et al., (1970), Heezen, MacGregor, et al., (1973a), and Figure 3 (this chapter). One second is about 750 m depth; therefore the abyssal plain of the Mariana Basin is slightly deeper than 6000 m."

Appendix A7: Histograms of fossil occurrence intervals

Histograms of $\delta^{13}C_{carbonate}$ values in the fossil occurrence intervals (see Section 4.4) of every species considered in this thesis (65 planktonic foraminifera species). Histograms are presented in order of lowest occurrence (sometimes called first occurrence) of the species according to pforams@mikrotax (`www.mikrotax.org/pforams/`, Huber et al., 2016; Young et al., 2019). When a range was given as the lowest occurrence, the early end of the range was taken as the lowest occurrence. *Globotruncana concavata primitiva* was not found in pforams@mikrotax, but Premoli Silva and Bolli (1973) write that "*G. concavata primitiva* has its first occurrence in the upper part of the latest Turonian-Early Coniacian *Globotruncana schneegansi* Zone," so its lowest occurrence was set to the base of the *Globotruncana schneegansi* zone according to pforams@mikrotax (89.75 Ma). If no $\delta^{13}C_{carbonate}$ values were reported within the fossil occurrence interval for a species at any of the sites in this thesis, no histogram for the species is presented.

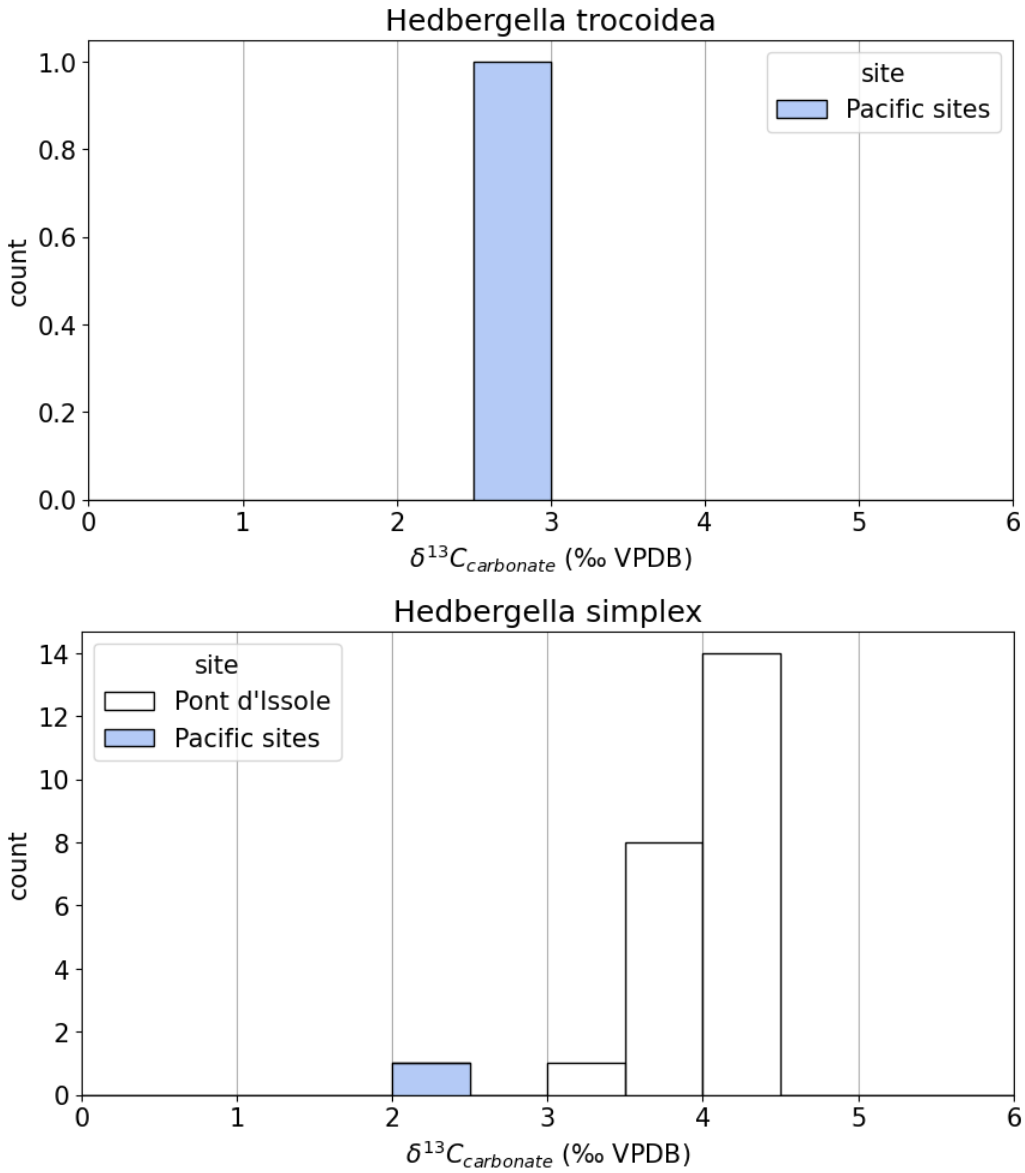
Hedbergella trocoidea
site
Pacific sites
count
1.0
0.8
0.6
0.4
0.2
0.0
0
1
2
3
4
5
6
$\delta^{13}C_{carbonate}$ (‰ VPDB)
Hedbergella simplex
site
Pont d'Issole
Pacific sites
count
14
12
10
8
6
4
2
0
0
1
2
3
4
5
6
$\delta^{13}C_{carbonate}$ (‰ VPDB)

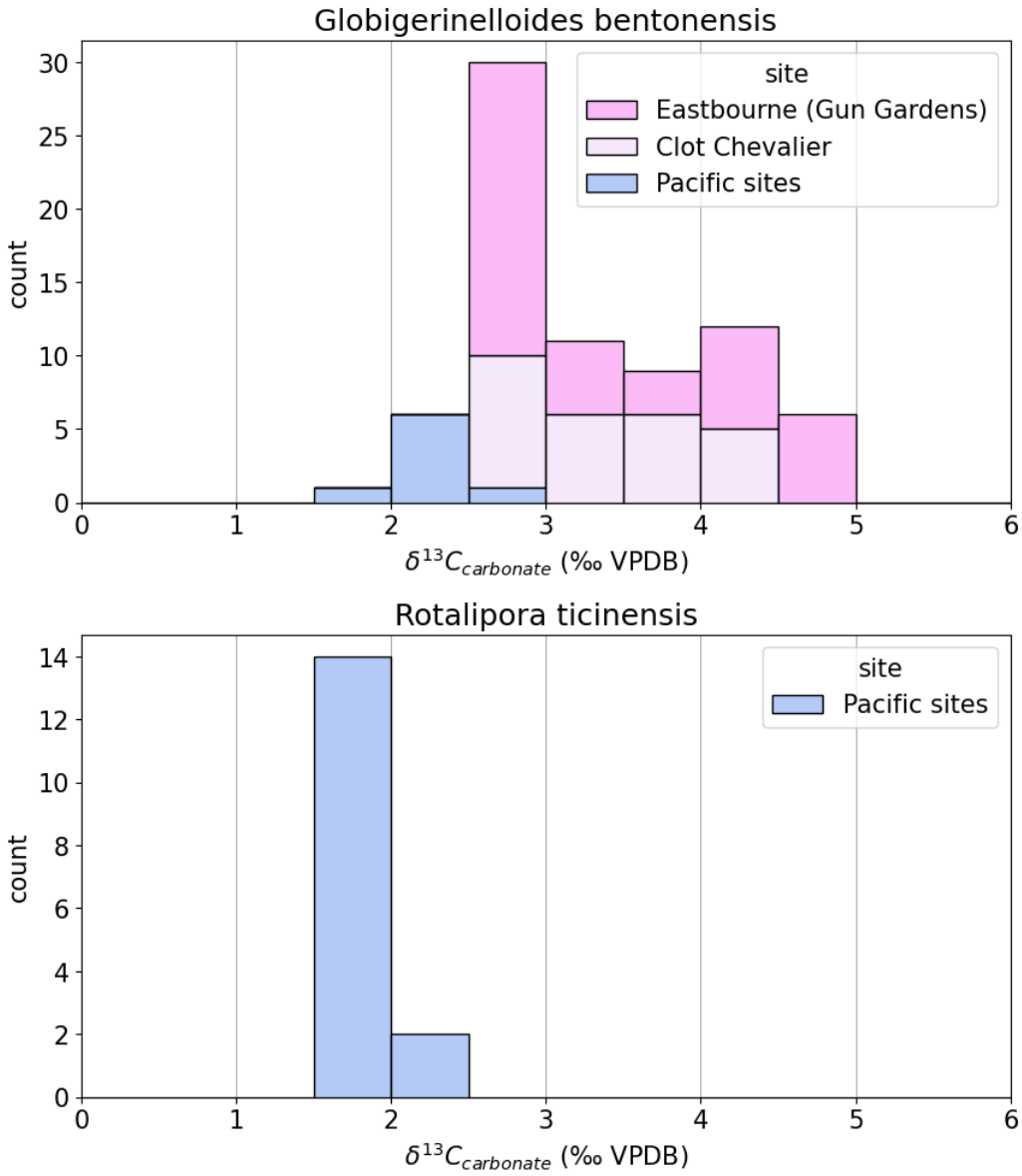
Globigerinelloides bentonensis
site
Eastbourne (Gun Gardens)
Clot Chevalier
Pacific sites
count
$\delta^{13}C_{carbonate}$ (‰ VPDB)
Rotalipora ticinensis
site
Pacific sites
count
$\delta^{13}C_{carbonate}$ (‰ VPDB)

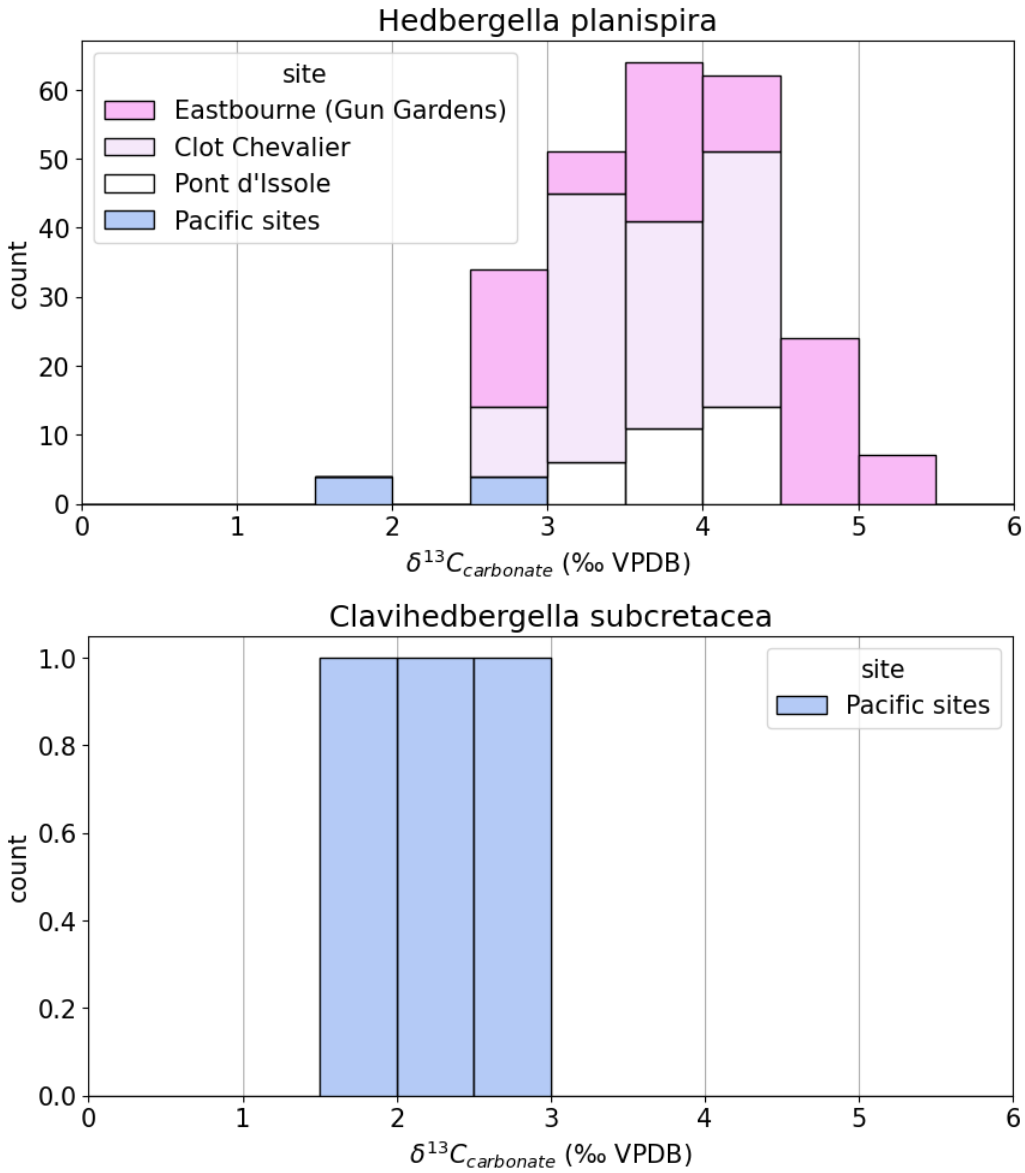
Hedbergella planispira
site
Eastbourne (Gun Gardens)
Clot Chevalier
Pont d'Issole
Pacific sites
count
$\delta^{13}C_{carbonate}$ (‰ VPDB)
Clavihedbergella subcretacea
site
Pacific sites
count
$\delta^{13}C_{carbonate}$ (‰ VPDB)

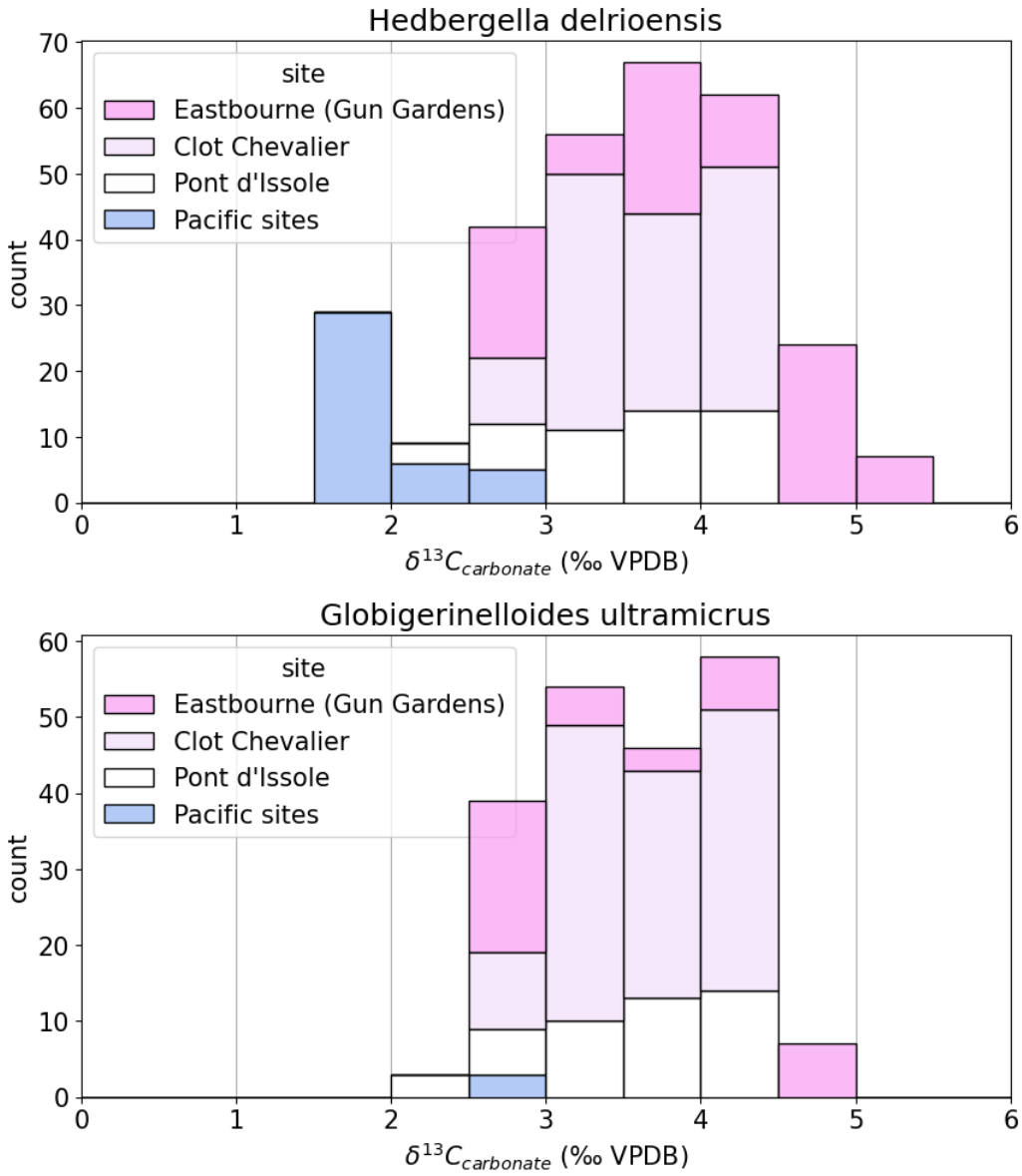
Hedbergella delrioensis
site
Eastbourne (Gun Gardens)
Clot Chevalier
Pont d'Issole
Pacific sites
count
$\delta^{13}C_{carbonate}$ (‰ VPDB)
Globigerinelloides ultramicrus
site
Eastbourne (Gun Gardens)
Clot Chevalier
Pont d'Issole
Pacific sites
count
$\delta^{13}C_{carbonate}$ (‰ VPDB)

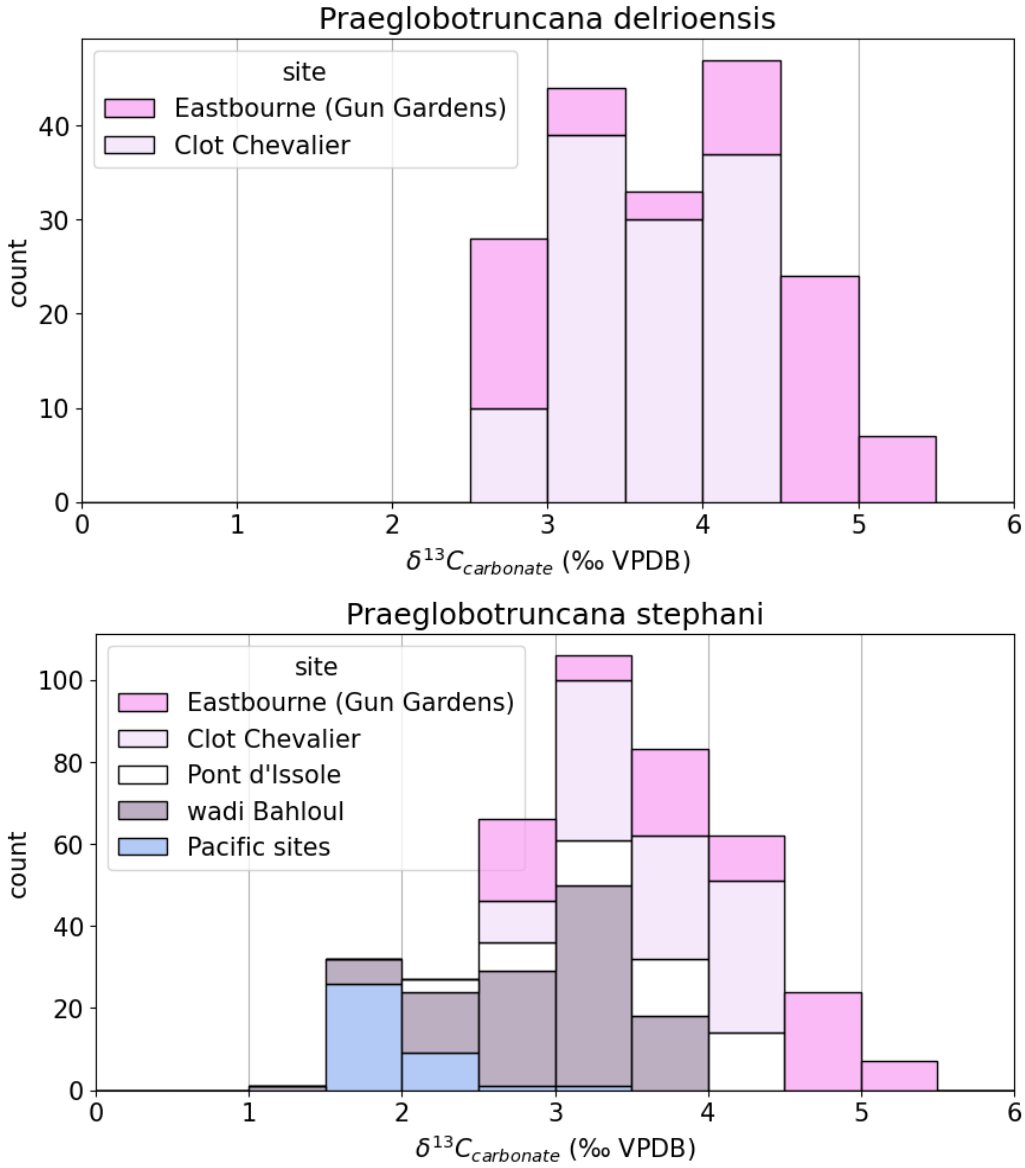
Praeglobotruncana delrioensis
site
Eastbourne (Gun Gardens)
Clot Chevalier
count
$\delta^{13}C_{carbonate}$ (‰ VPDB)
Praeglobotruncana stephani
site
Eastbourne (Gun Gardens)
Clot Chevalier
Pont d'Issole
wadi Bahloul
Pacific sites
count
$\delta^{13}C_{carbonate}$ (‰ VPDB)

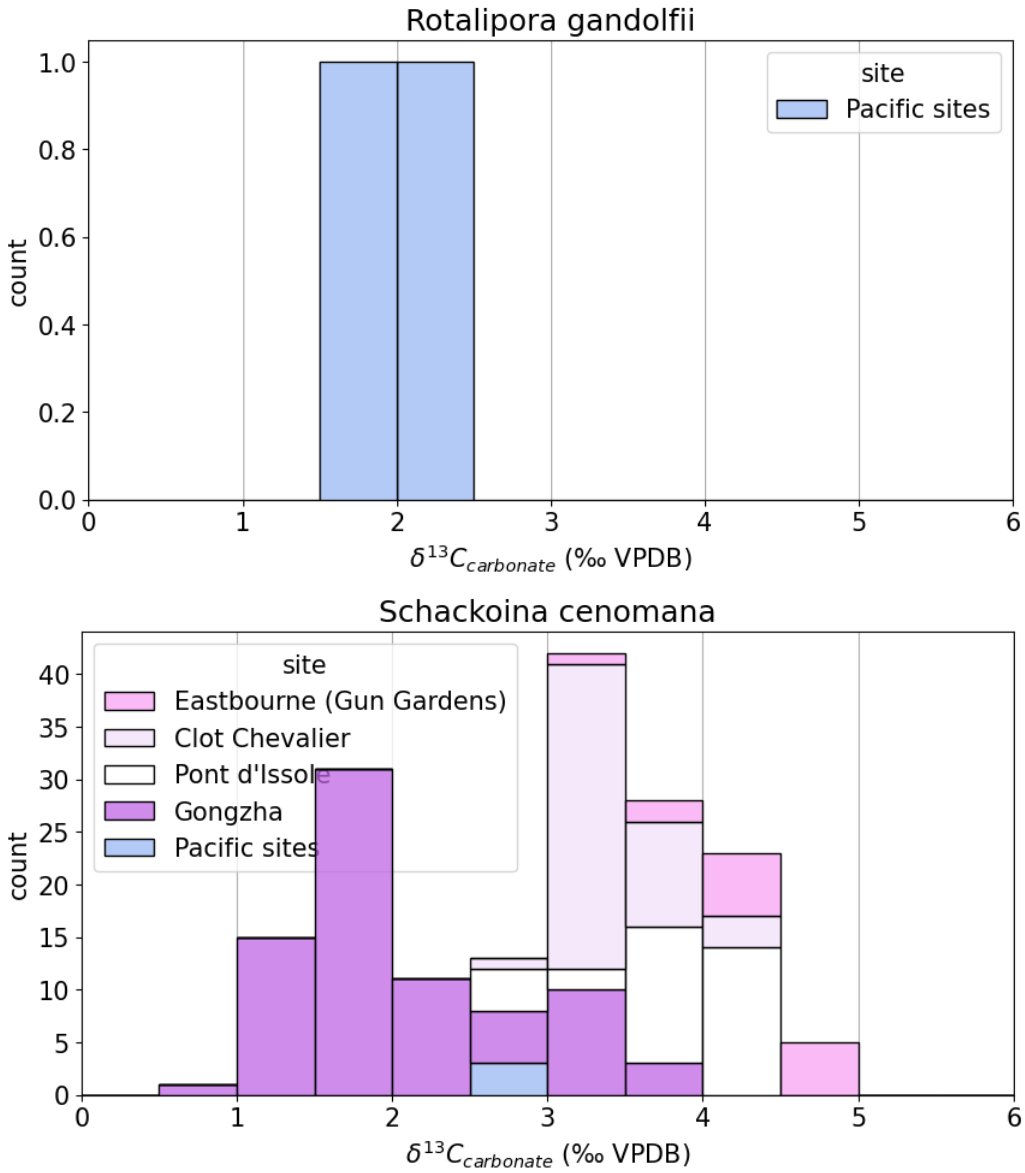
Rotalipora gandolfii
site
Pacific sites
count
$\delta^{13}C_{carbonate}$ (‰ VPDB)
Schackoina cenomana
site
Eastbourne (Gun Gardens)
Clot Chevalier
Pont d'Issole
Gongzha
Pacific sites
count
$\delta^{13}C_{carbonate}$ (‰ VPDB)

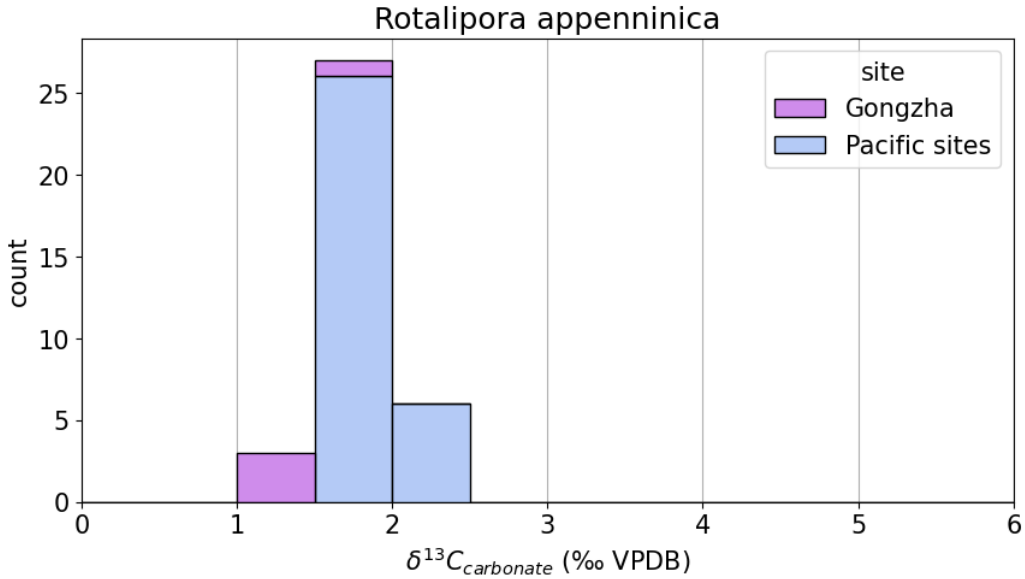
Rotalipora appenninica
site
Gongzha
Pacific sites
count
0
5
10
15
20
25
0
1
2
3
4
5
6
$\delta^{13}C_{carbonate}$ (‰ VPDB)

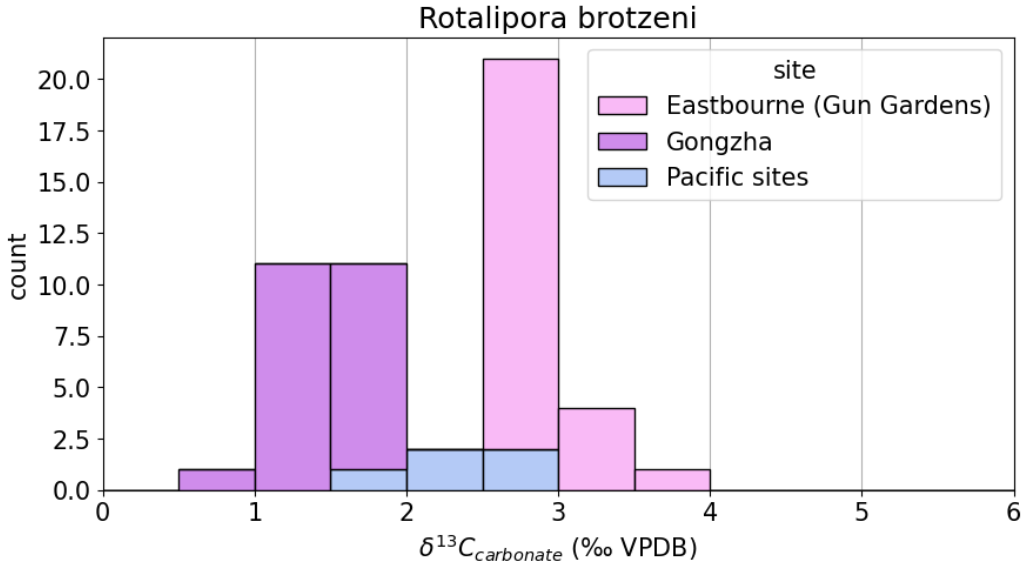
Rotalipora brotzeni
site
Eastbourne (Gun Gardens)
Gongzha
Pacific sites
count
0.0
2.5
5.0
7.5
10.0
12.5
15.0
17.5
20.0
0
1
2
3
4
5
6
$\delta^{13}C_{carbonate}$ (‰ VPDB)

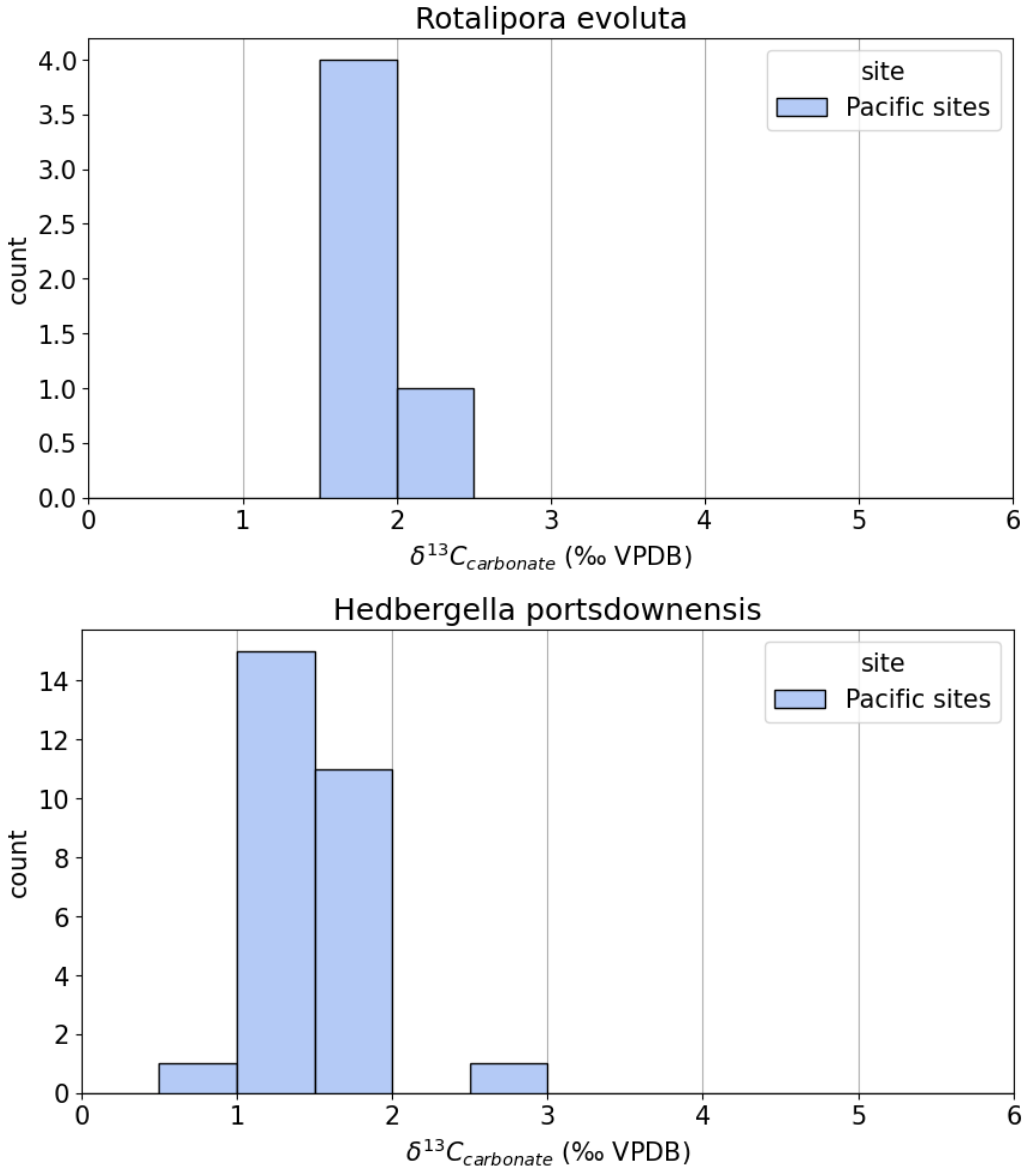
Rotalipora evoluta
site
Pacific sites
count
$\delta^{13}C_{carbonate}$ (‰ VPDB)
Hedbergella portsdownensis
site
Pacific sites
count
$\delta^{13}C_{carbonate}$ (‰ VPDB)

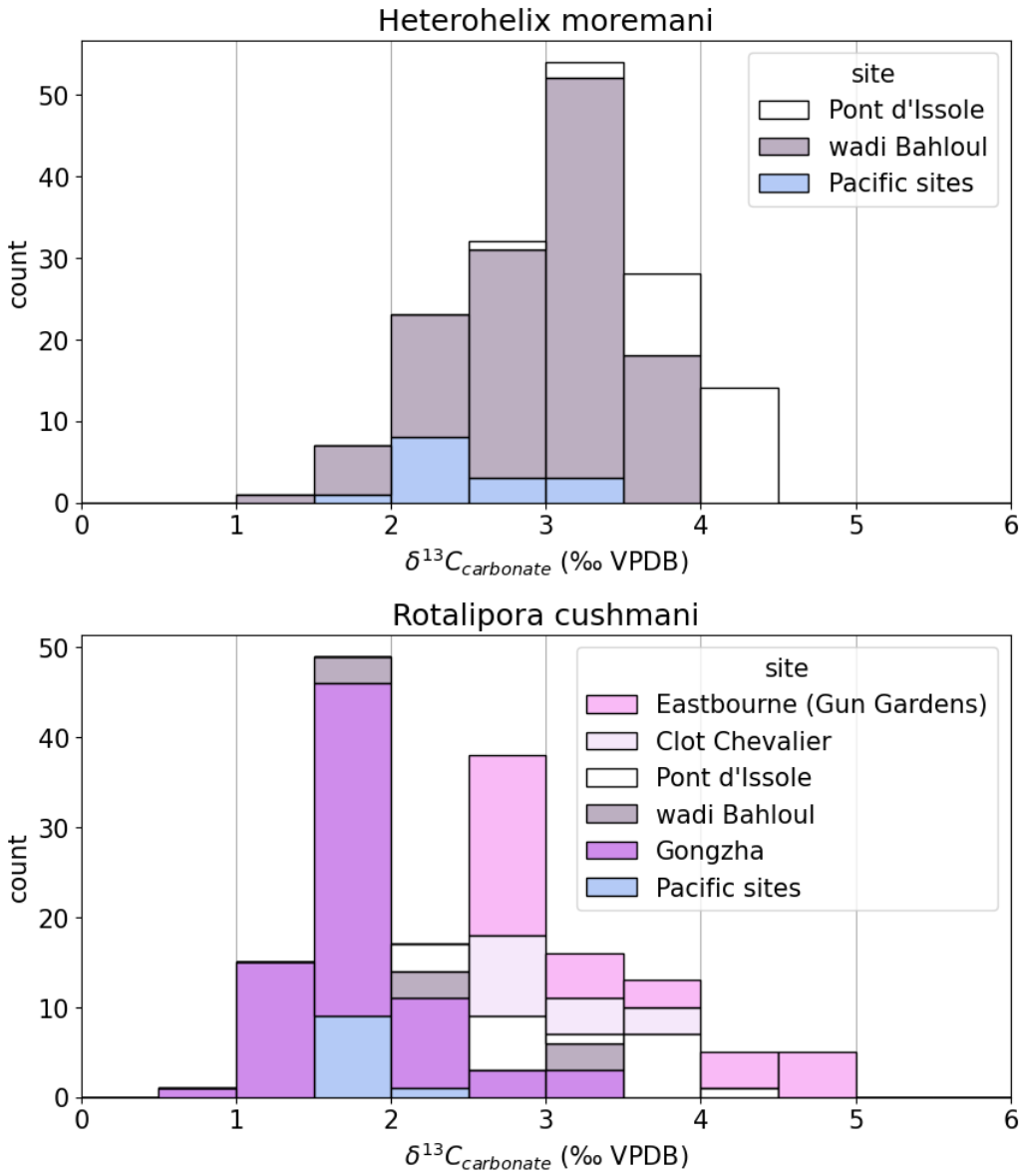
Heterohelix moremani
site
Pont d'Issole
wadi Bahloul
Pacific sites
count
$\delta^{13}C_{carbonate}$ (‰ VPDB)
Rotalipora cushmani
site
Eastbourne (Gun Gardens)
Clot Chevalier
Pont d'Issole
wadi Bahloul
Gongzha
Pacific sites
count
$\delta^{13}C_{carbonate}$ (‰ VPDB)

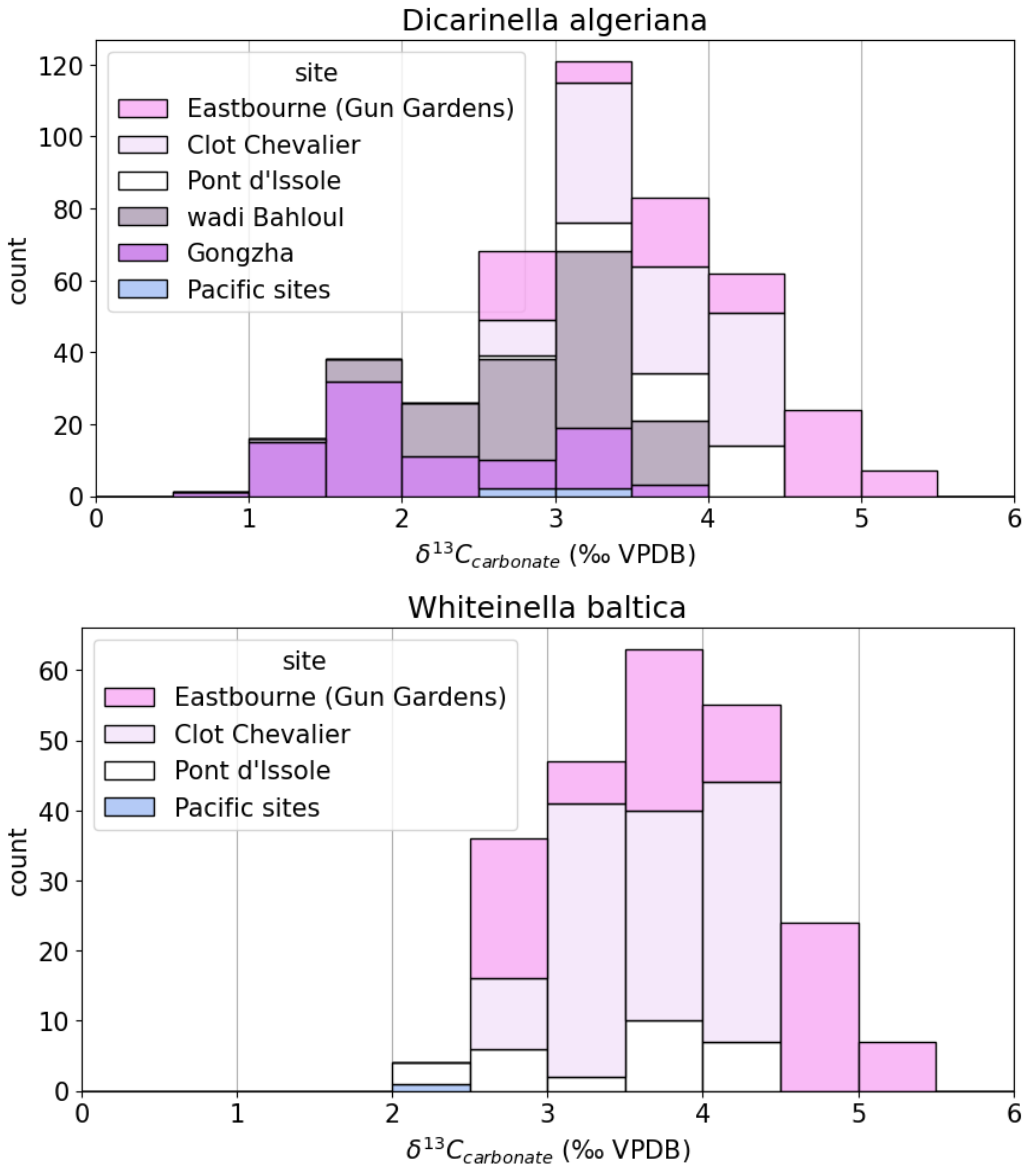
Dicarinella algeriana
site
Eastbourne (Gun Gardens)
Clot Chevalier
Pont d'Issole
wadi Bahloul
Gongzha
Pacific sites
count
$\delta^{13}C_{carbonate}$ (‰ VPDB)
Whiteinella baltica
site
Eastbourne (Gun Gardens)
Clot Chevalier
Pont d'Issole
Pacific sites
count
$\delta^{13}C_{carbonate}$ (‰ VPDB)

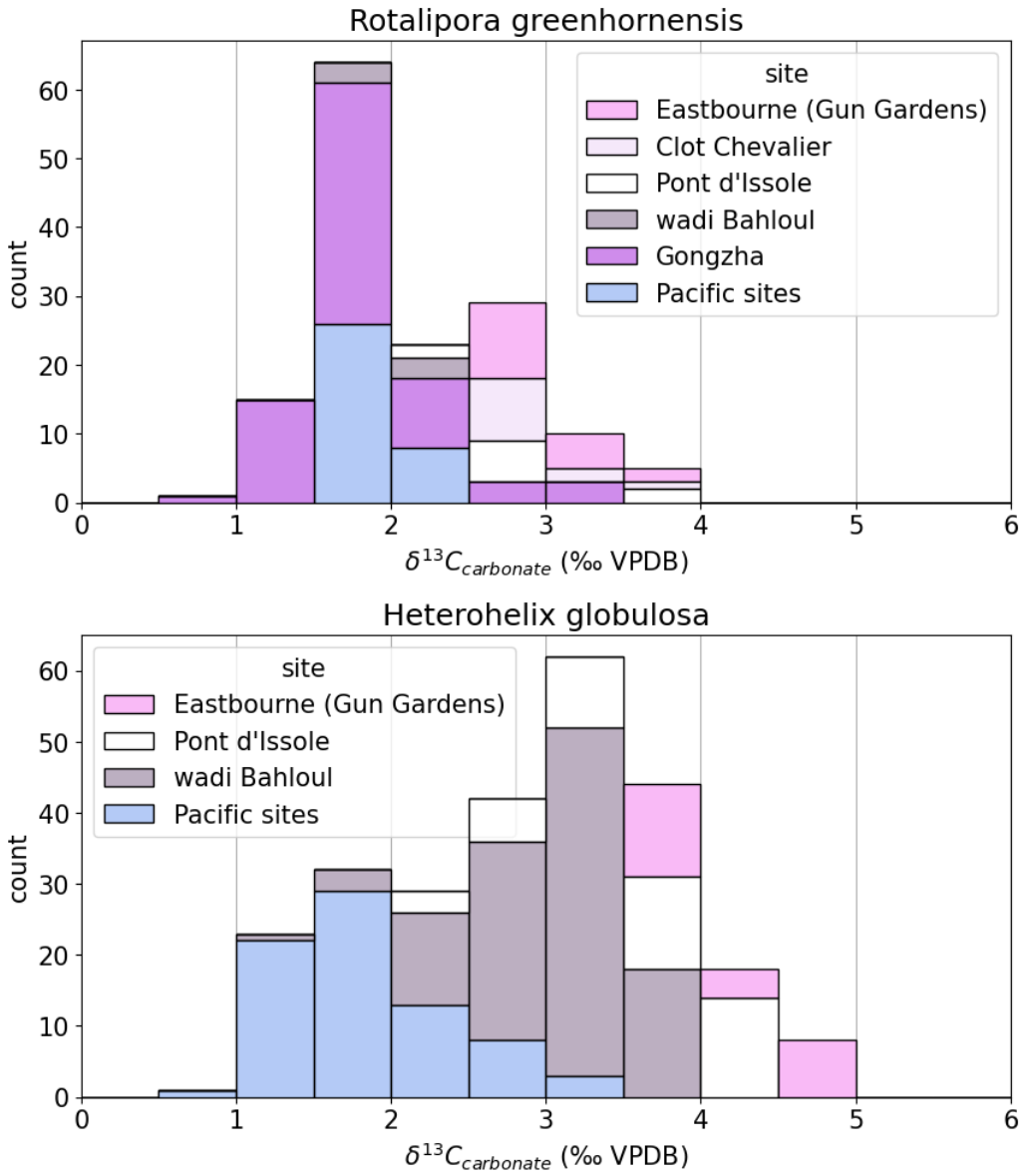
Rotalipora greenhornensis
site
Eastbourne (Gun Gardens)
Clot Chevalier
Pont d'Issole
wadi Bahloul
Gongzha
Pacific sites
count
$\delta^{13}C_{carbonate}$ (‰ VPDB)
Heterohelix globulosa
site
Eastbourne (Gun Gardens)
Pont d'Issole
wadi Bahloul
Pacific sites
count
$\delta^{13}C_{carbonate}$ (‰ VPDB)

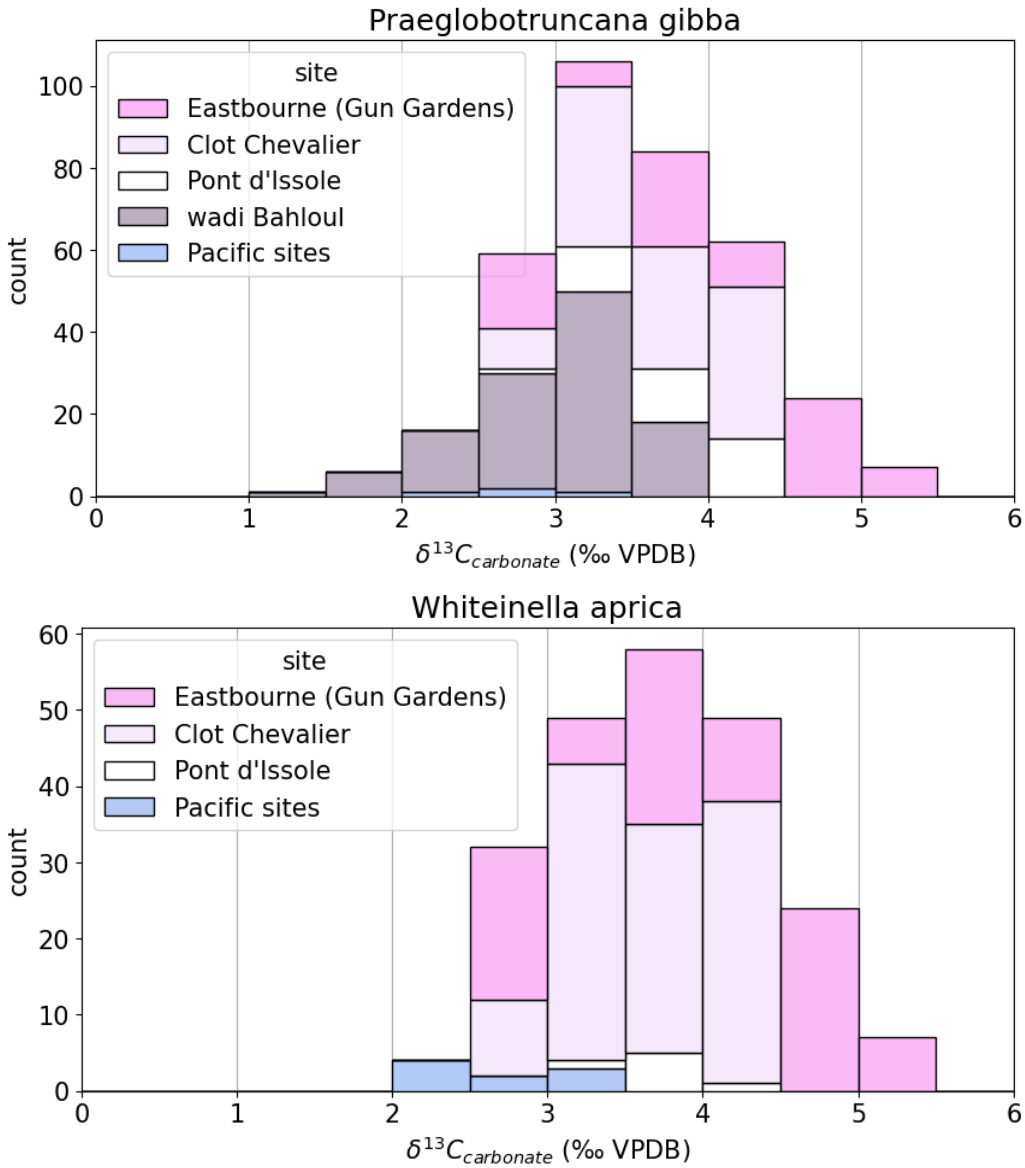
Praeglobotruncana gibba
site
Eastbourne (Gun Gardens)
Clot Chevalier
Pont d'Issole
wadi Bahloul
Pacific sites
count
$\delta^{13}C_{carbonate}$ (‰ VPDB)
Whiteinella aprica
site
Eastbourne (Gun Gardens)
Clot Chevalier
Pont d'Issole
Pacific sites
count
$\delta^{13}C_{carbonate}$ (‰ VPDB)

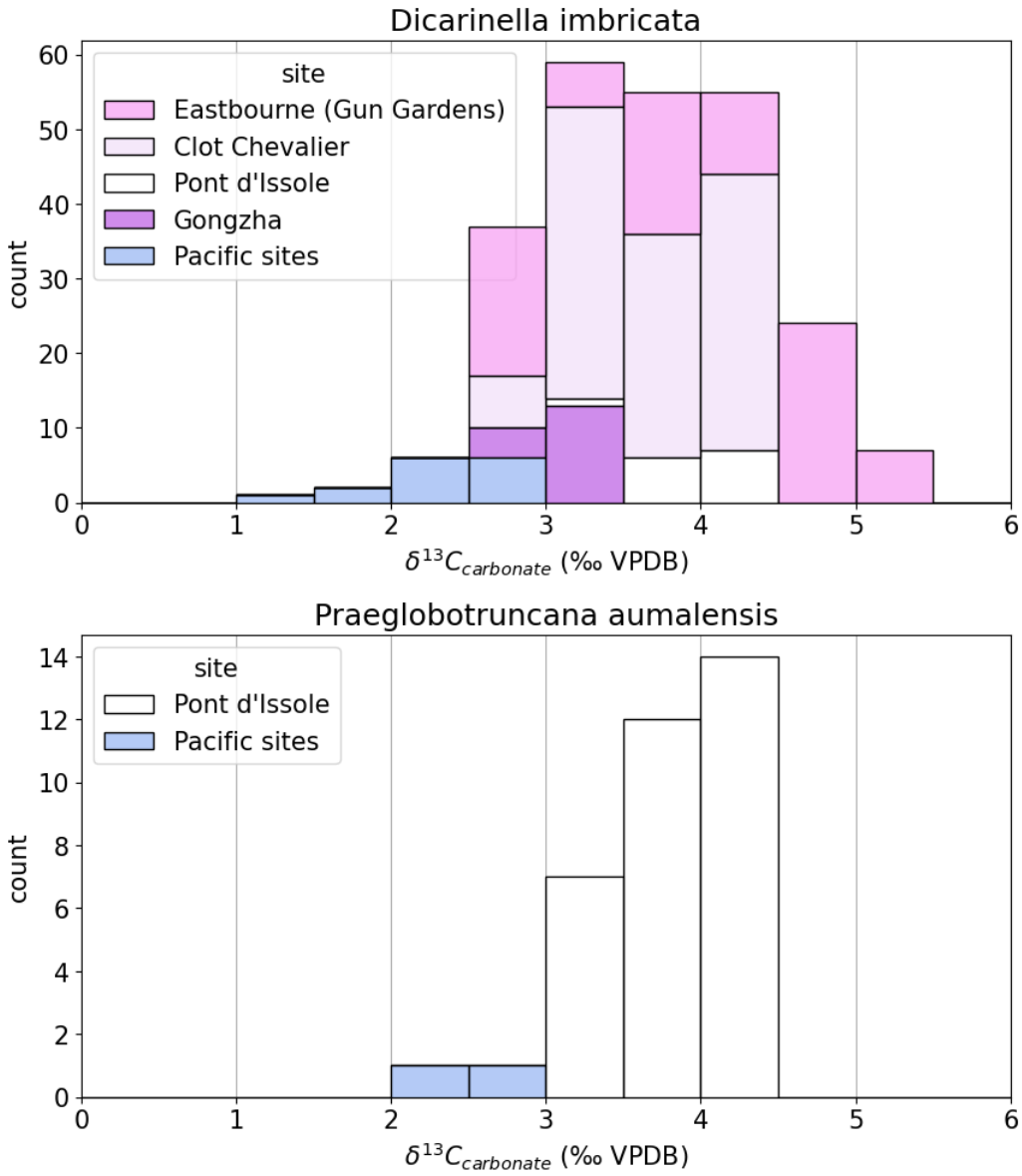
Dicarinella imbricata
site
Eastbourne (Gun Gardens)
Clot Chevalier
Pont d'Issole
Gongzha
Pacific sites
count
$\delta^{13}C_{carbonate}$ (‰ VPDB)
Praeglobotruncana aumalensis
site
Pont d'Issole
Pacific sites
count
$\delta^{13}C_{carbonate}$ (‰ VPDB)

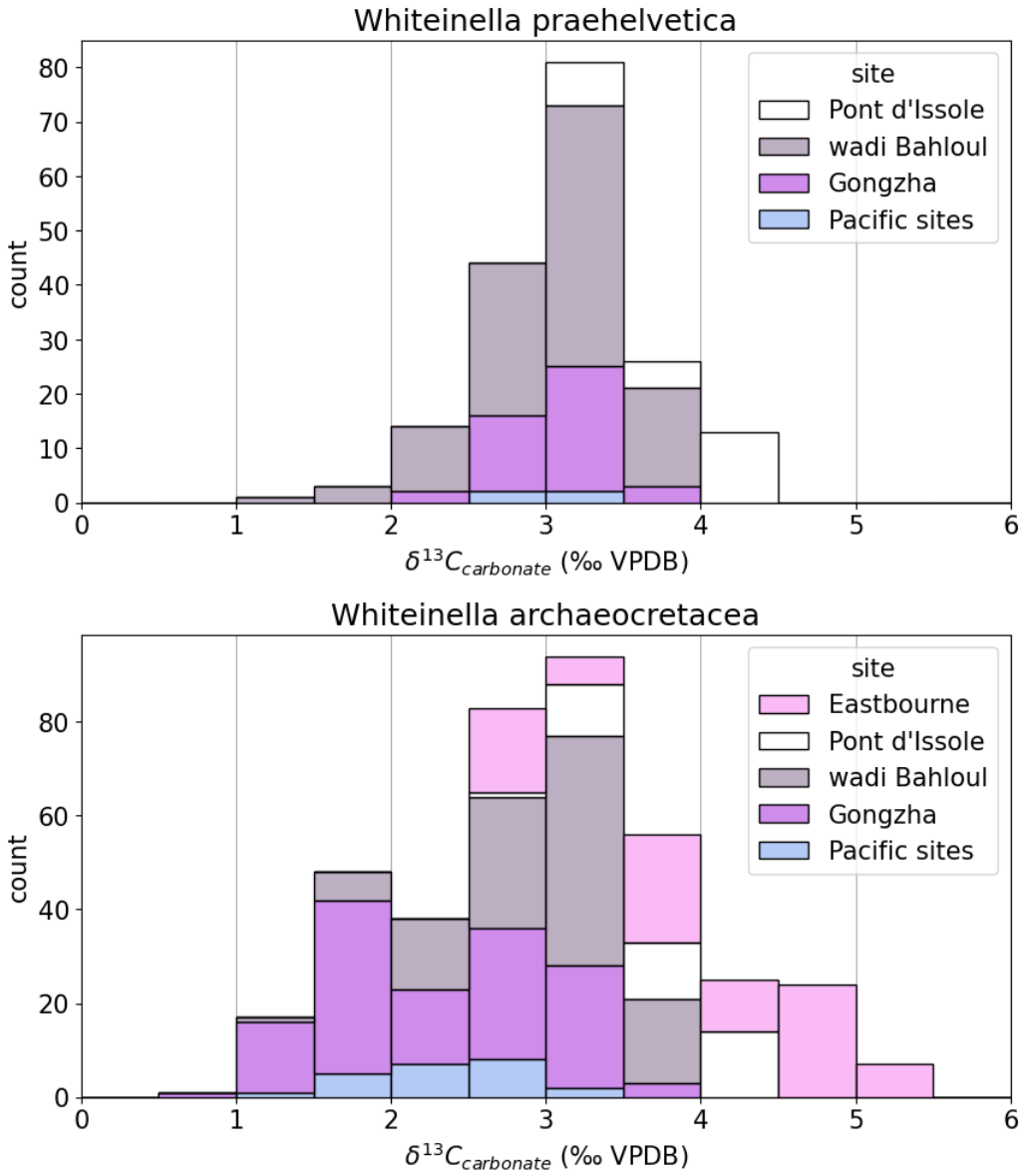
Whiteinella praehelvetica
site
Pont d'Issole
wadi Bahloul
Gongzha
Pacific sites
count
$\delta^{13}C_{carbonate}$ (‰ VPDB)
Whiteinella archaeocretacea
site
Eastbourne
Pont d'Issole
wadi Bahloul
Gongzha
Pacific sites
count
$\delta^{13}C_{carbonate}$ (‰ VPDB)

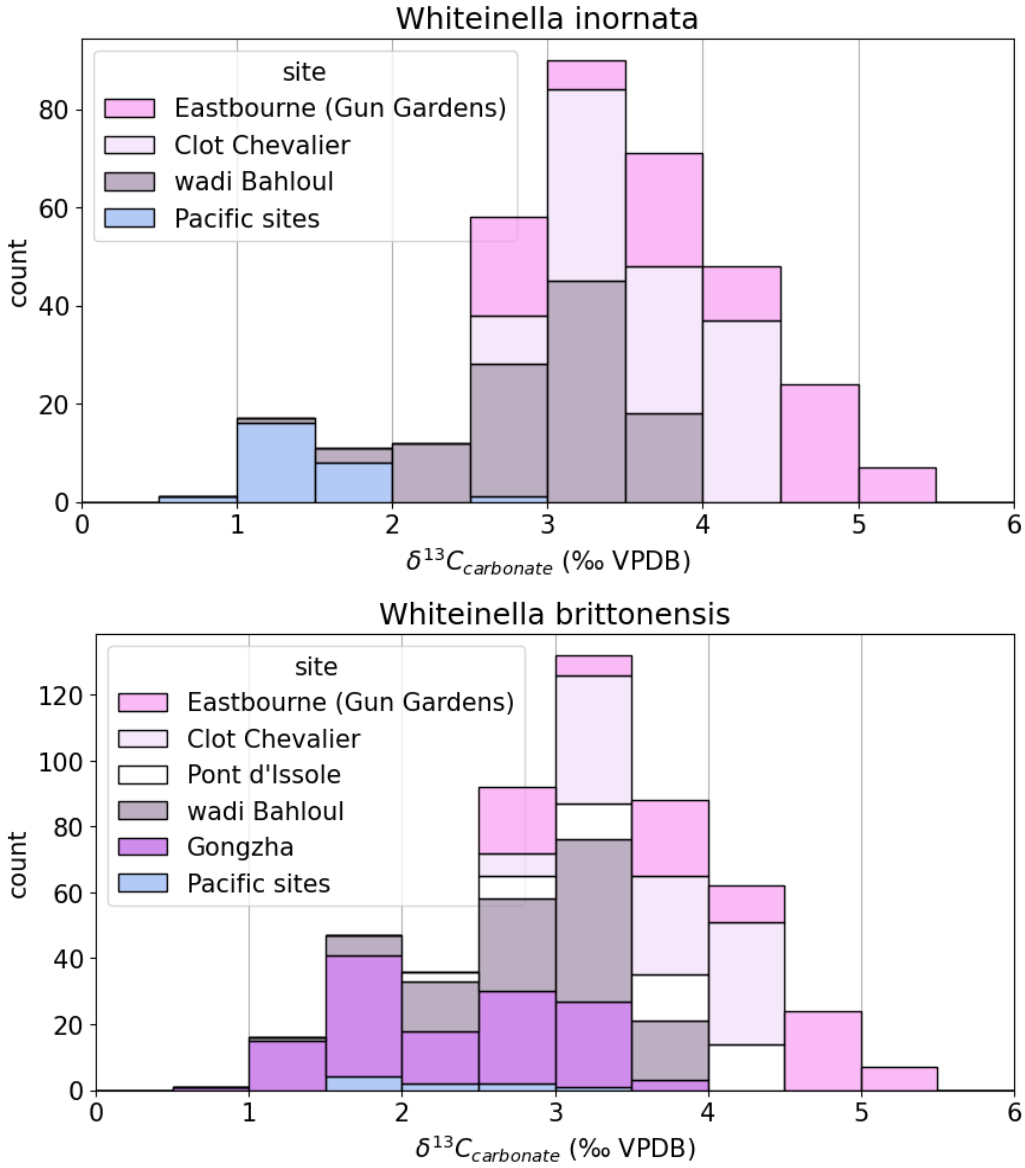
Whiteinella inornata
site
Eastbourne (Gun Gardens)
Clot Chevalier
wadi Bahloul
Pacific sites
count
$\delta^{13}C_{carbonate}$ (‰ VPDB)
Whiteinella brittonensis
site
Eastbourne (Gun Gardens)
Clot Chevalier
Pont d'Issole
wadi Bahloul
Gongzha
Pacific sites
count
$\delta^{13}C_{carbonate}$ (‰ VPDB)

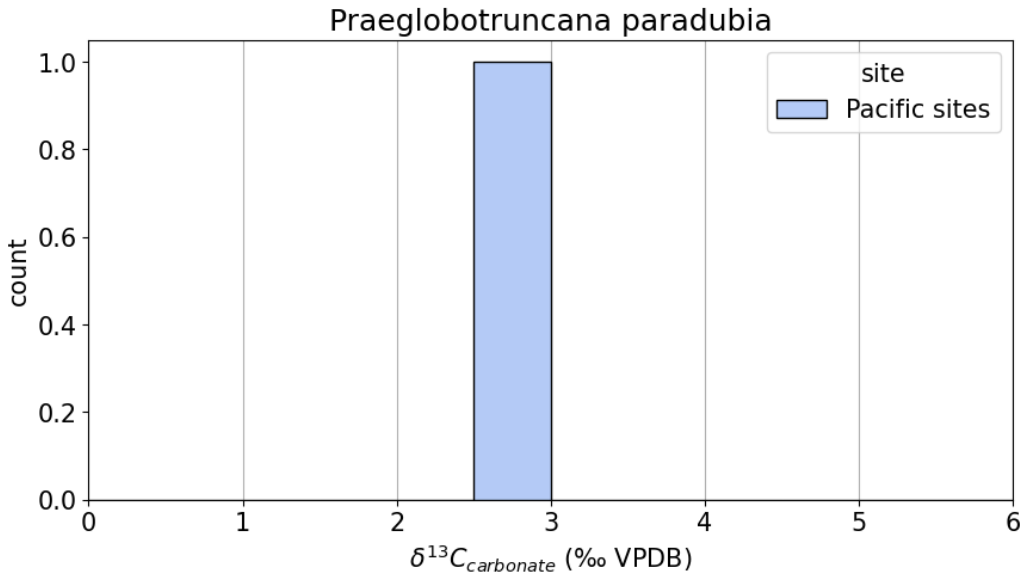
Praeglobotruncana paradubia
site
Pacific sites
count
0.0
0.2
0.4
0.6
0.8
1.0
0
1
2
3
4
5
6
$\delta^{13}C_{carbonate}$ (‰ VPDB)

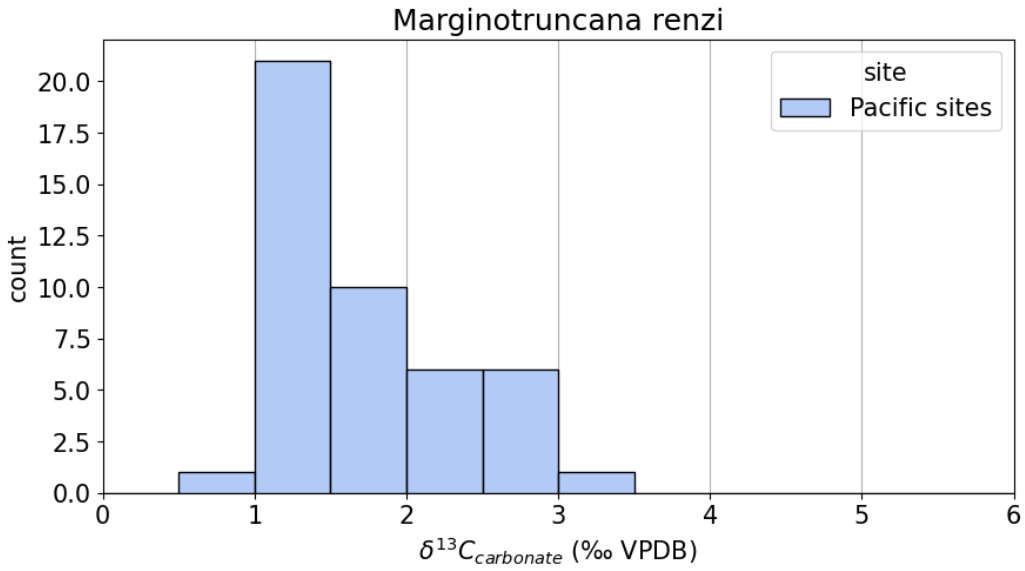
Marginotruncana renzi
site
Pacific sites
count
0.0
2.5
5.0
7.5
10.0
12.5
15.0
17.5
20.0
0
1
2
3
4
5
6
$\delta^{13}C_{carbonate}$ (‰ VPDB)

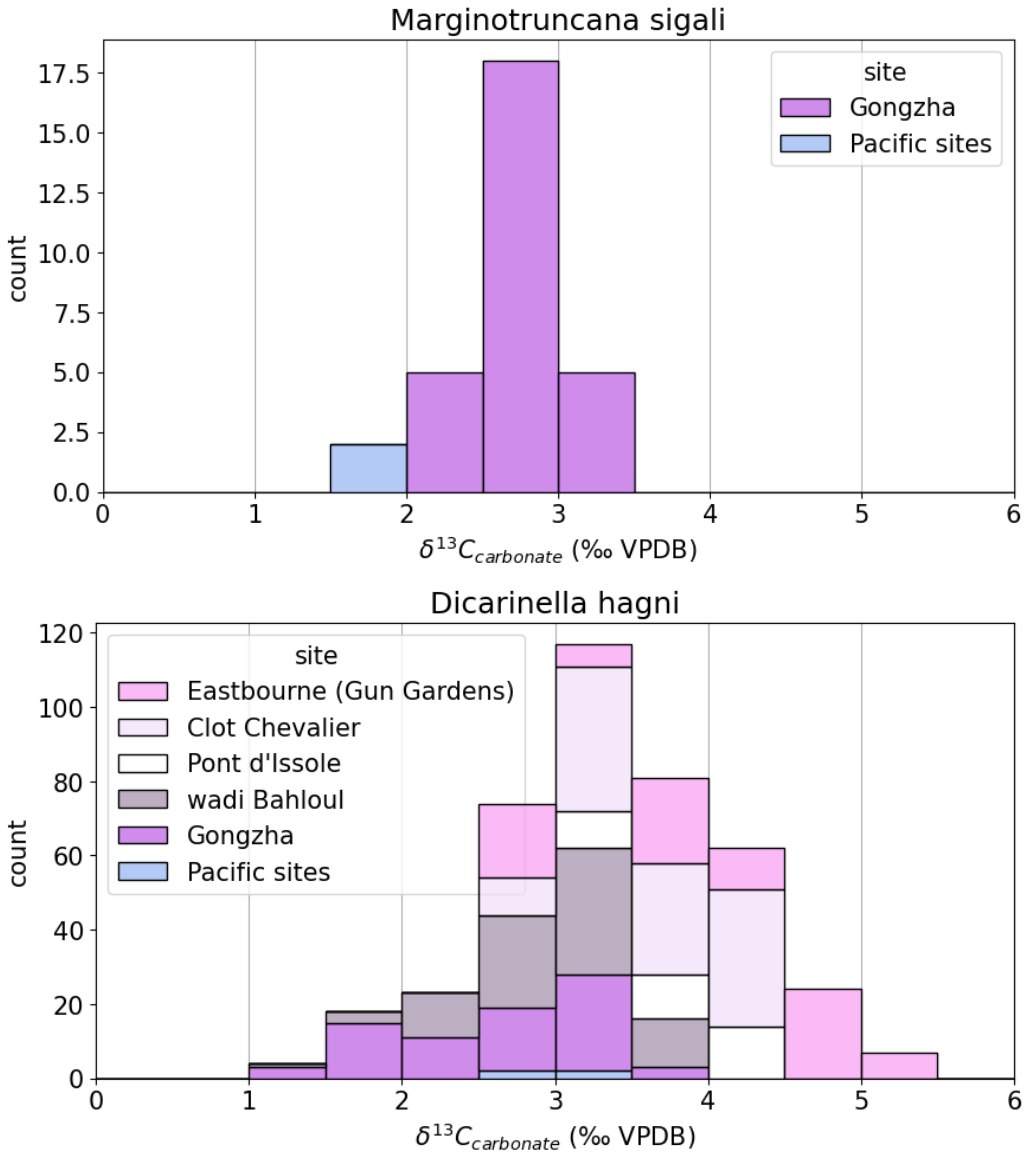
Marginotruncana sigali
site
Gongzha
Pacific sites
count
$\delta^{13}C_{carbonate}$ (‰ VPDB)
Dicarinella hagni
site
Eastbourne (Gun Gardens)
Clot Chevalier
Pont d'Issole
wadi Bahloul
Gongzha
Pacific sites
count
$\delta^{13}C_{carbonate}$ (‰ VPDB)

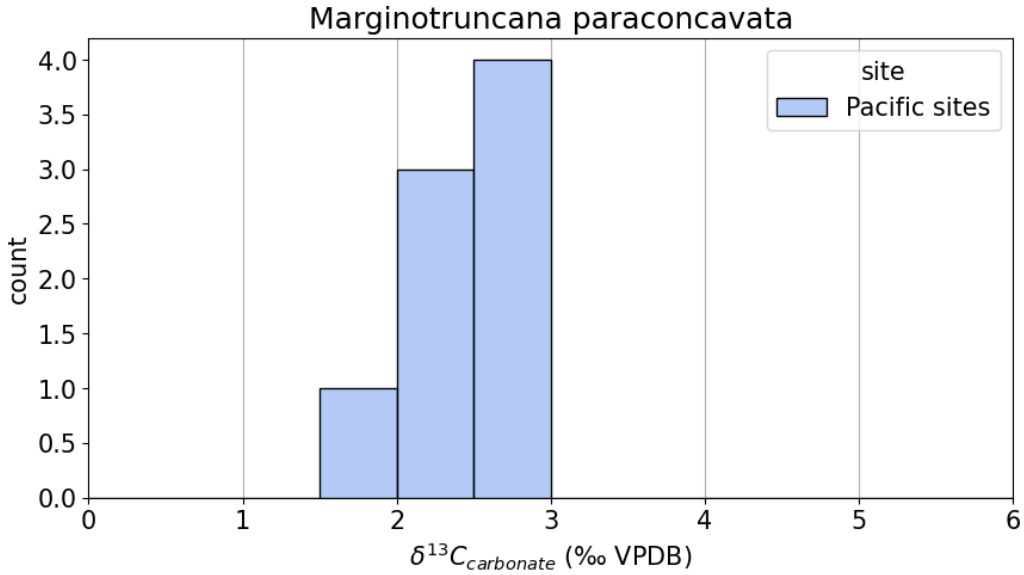
Marginotruncana paraconcavata
site
Pacific sites
count
0.0
0.5
1.0
1.5
2.0
2.5
3.0
3.5
4.0
0
1
2
3
4
5
6
$\delta^{13}C_{carbonate}$ (‰ VPDB)

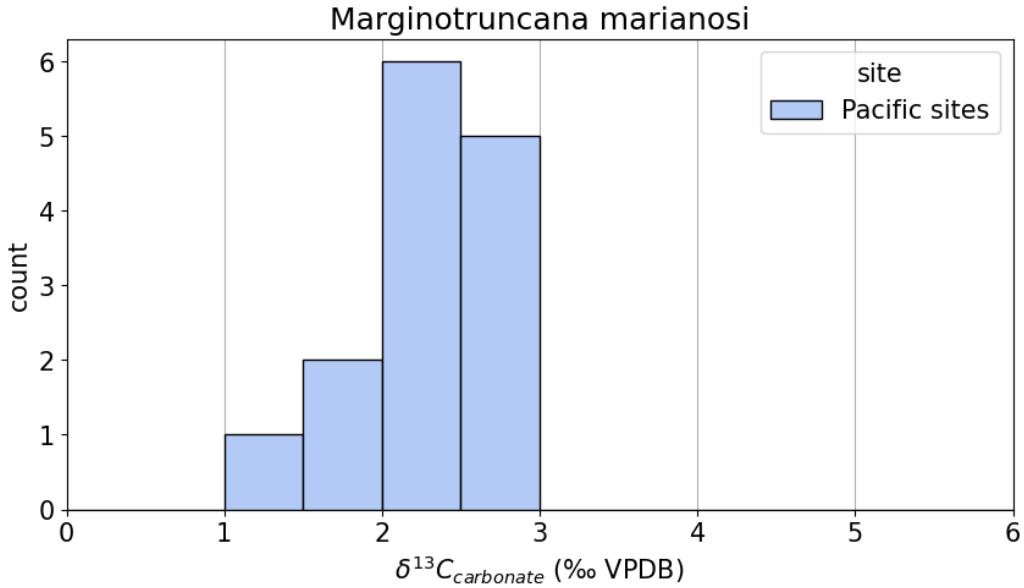
Marginotruncana marianosi
site
Pacific sites
count
0
1
2
3
4
5
6
0
1
2
3
4
5
6
$\delta^{13}C_{carbonate}$ (‰ VPDB)

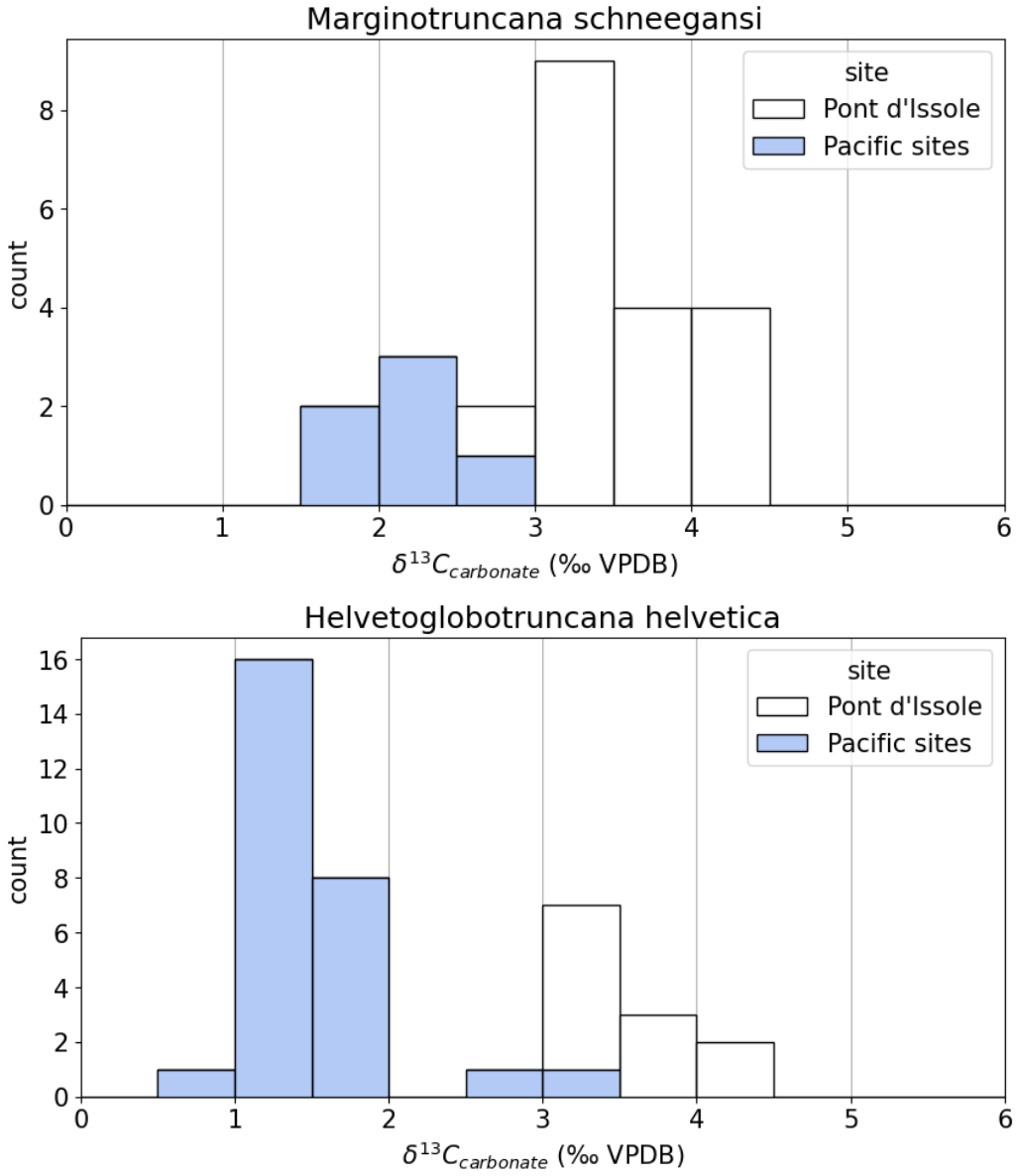
Marginotruncana schneegansi
site
Pont d'Issole
Pacific sites
count
$\delta^{13}C_{carbonate}$ (‰ VPDB)
Helvetoglobotruncana helvetica
site
Pont d'Issole
Pacific sites
count
$\delta^{13}C_{carbonate}$ (‰ VPDB)

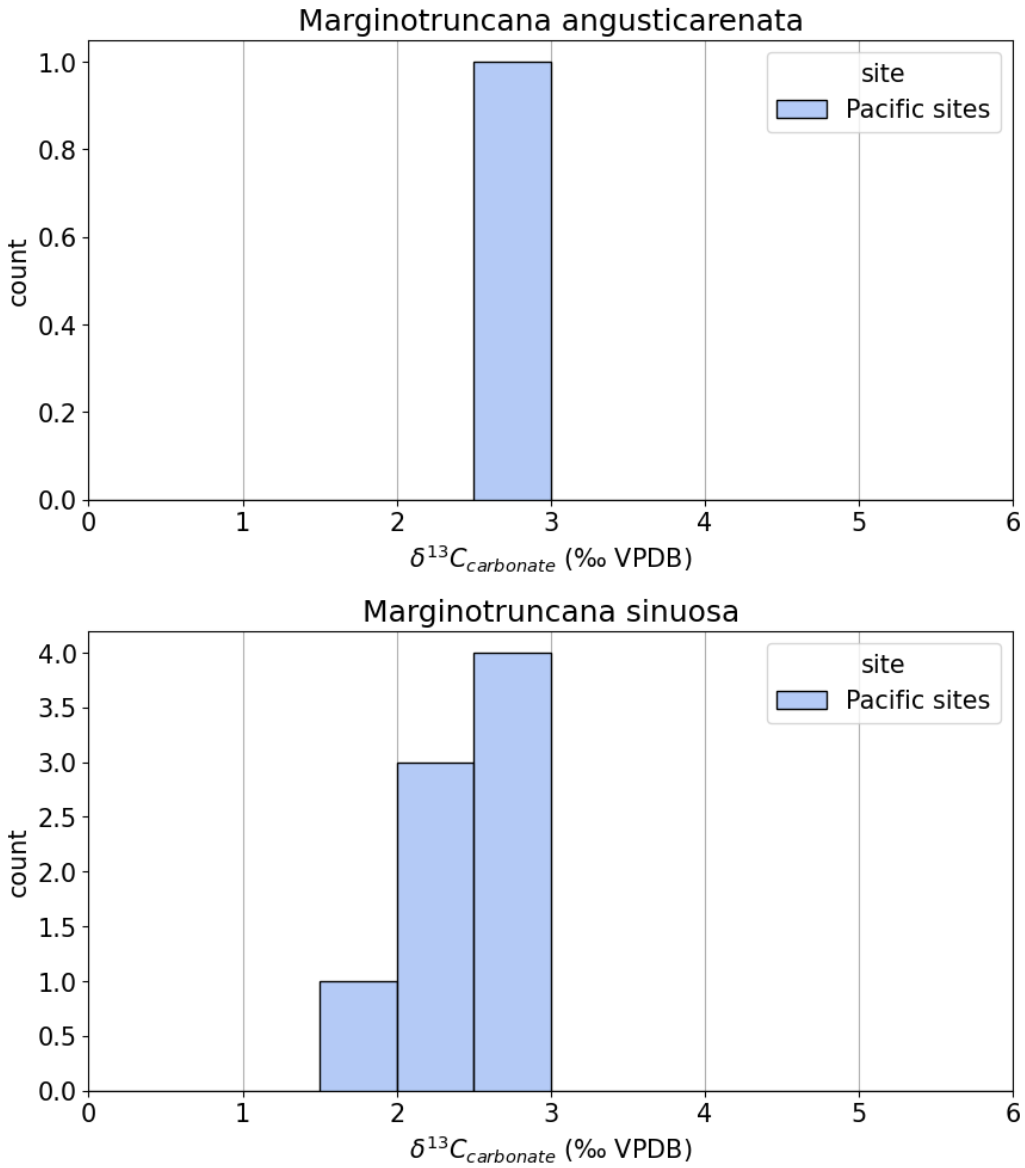
Marginotruncana angusticarenata
site
Pacific sites
count
0.0
0.2
0.4
0.6
0.8
1.0
0
1
2
3
4
5
6
$\delta^{13}C_{carbonate}$ (‰ VPDB)
Marginotruncana sinuosa
site
Pacific sites
count
0.0
0.5
1.0
1.5
2.0
2.5
3.0
3.5
4.0
0
1
2
3
4
5
6
$\delta^{13}C_{carbonate}$ (‰ VPDB)

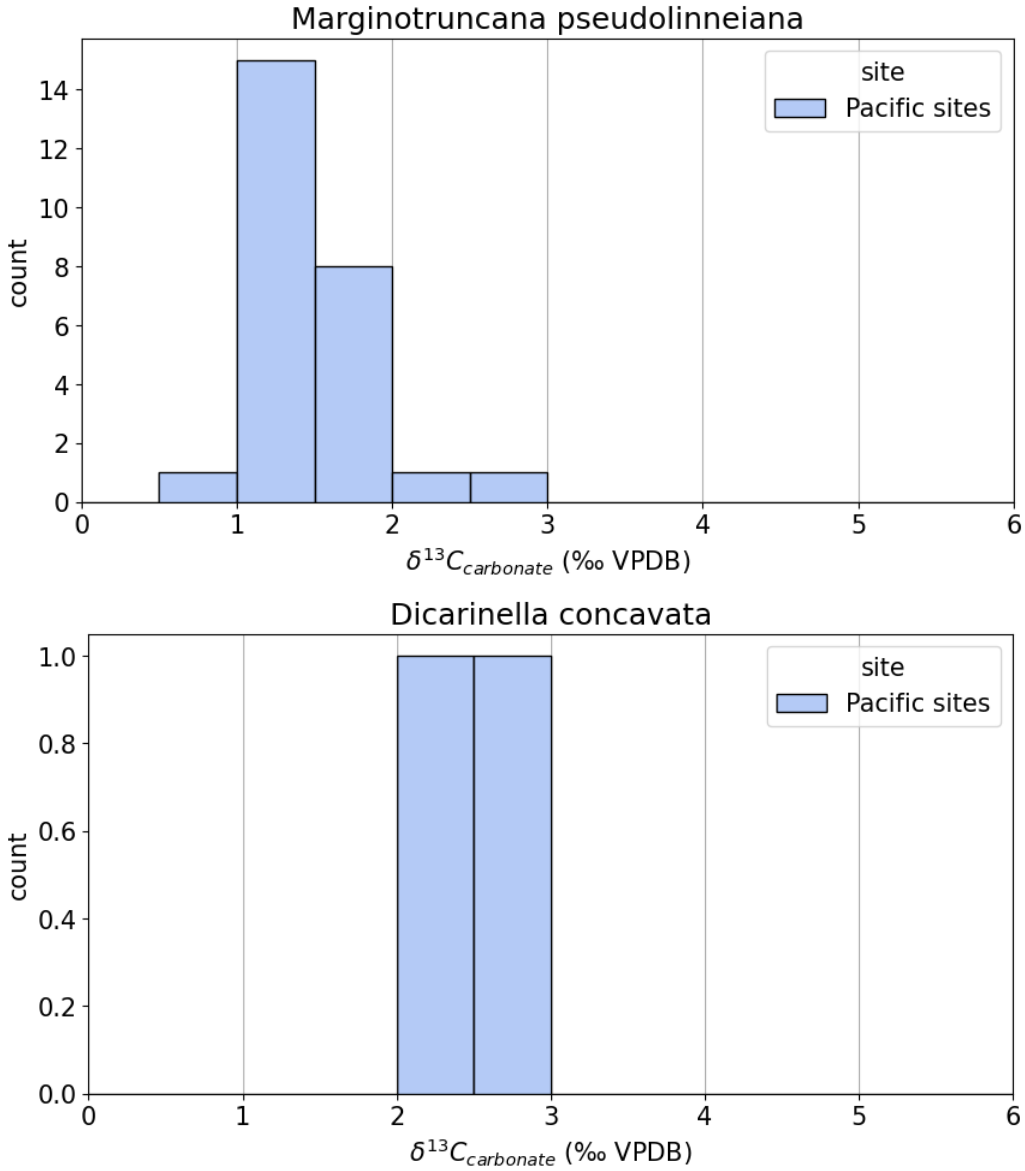
Marginotruncana pseudolinneiana
site
Pacific sites
count
0
2
4
6
8
10
12
14
0
1
2
3
4
5
6
$\delta^{13}C_{carbonate}$ (‰ VPDB)
Dicarinella concavata
site
Pacific sites
count
0.0
0.2
0.4
0.6
0.8
1.0
0
1
2
3
4
5
6
$\delta^{13}C_{carbonate}$ (‰ VPDB)

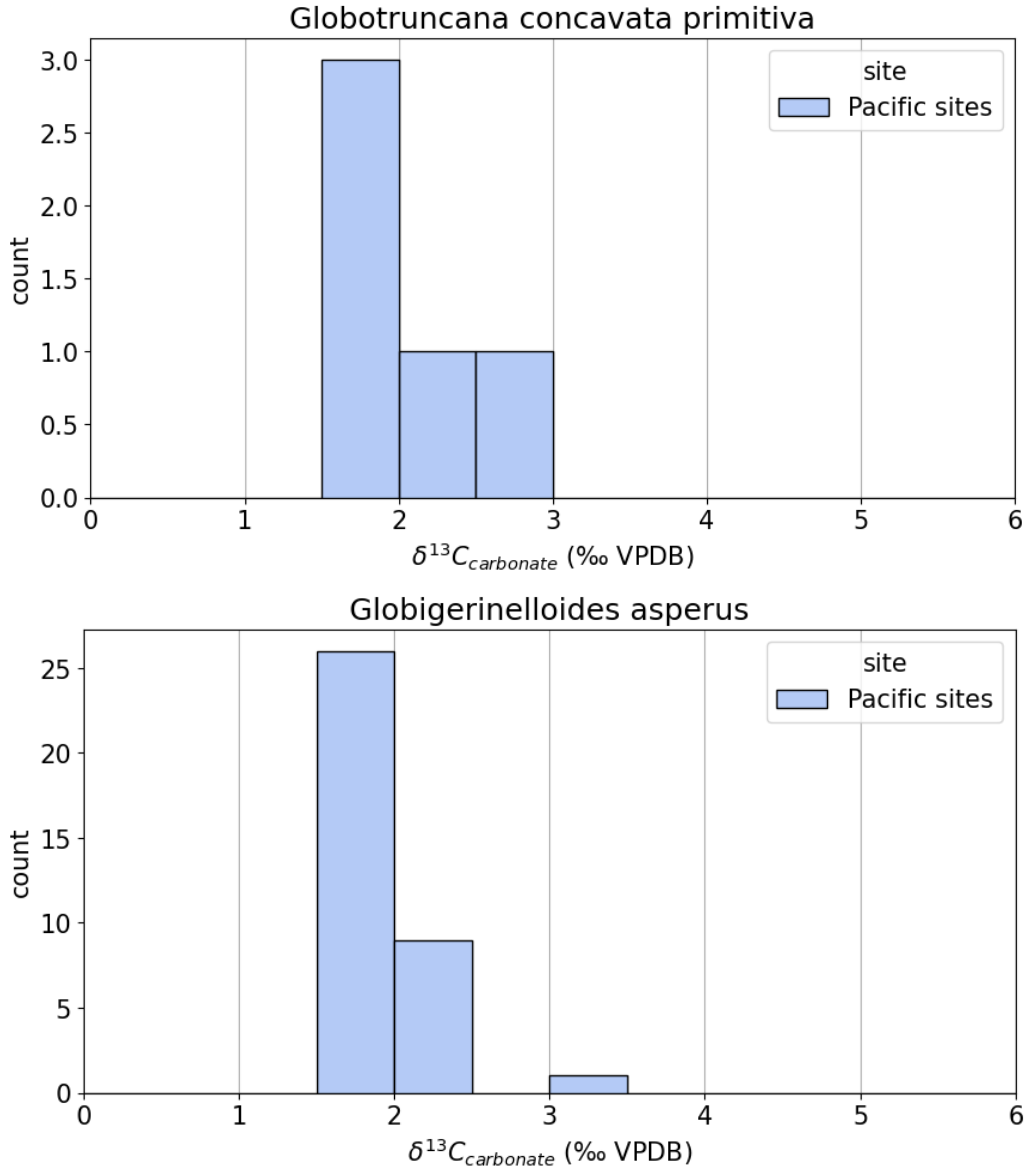
Globotruncana concavata primitiva
site
Pacific sites
count
3.0
2.5
2.0
1.5
1.0
0.5
0.0
0
1
2
3
4
5
6
$\delta^{13}C_{carbonate}$ (‰ VPDB)
Globigerinelloides asperus
site
Pacific sites
count
25
20
15
10
5
0
0
1
2
3
4
5
6
$\delta^{13}C_{carbonate}$ (‰ VPDB)

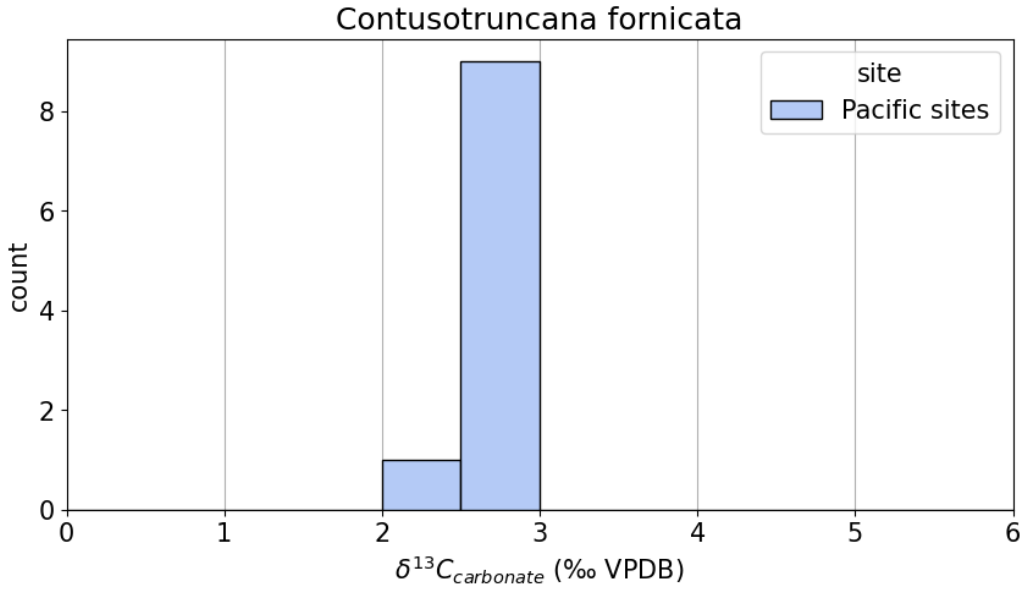
Contusotruncana fornicata
site
Pacific sites
count
0
2
4
6
8
0
1
2
3
4
5
6
$\delta^{13}C_{carbonate}$ (‰ VPDB)

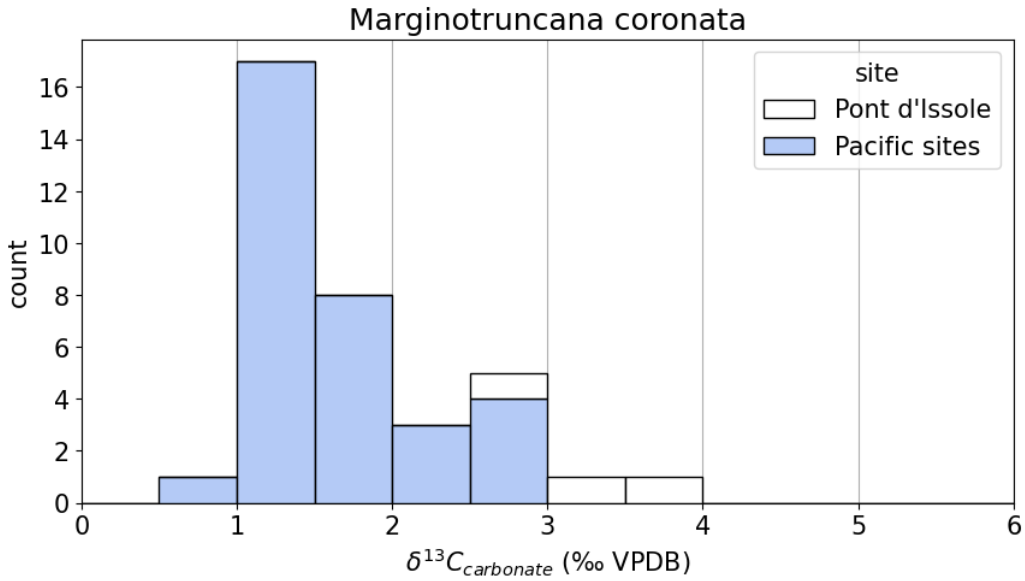
Marginotruncana coronata
site
Pont d'Issole
Pacific sites
count
0
2
4
6
8
10
12
14
16
0
1
2
3
4
5
6
$\delta^{13}C_{carbonate}$ (‰ VPDB)

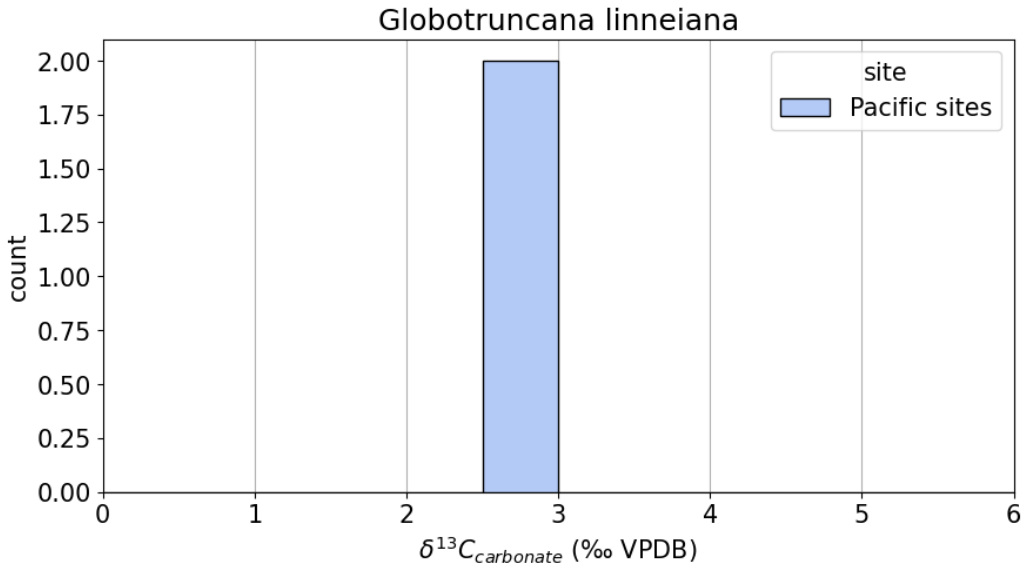
Globotruncana linneiana
site
Pacific sites
count
2.00
1.75
1.50
1.25
1.00
0.75
0.50
0.25
0.00
0
1
2
3
4
5
6
$\delta^{13}C_{carbonate}$ (‰ VPDB)

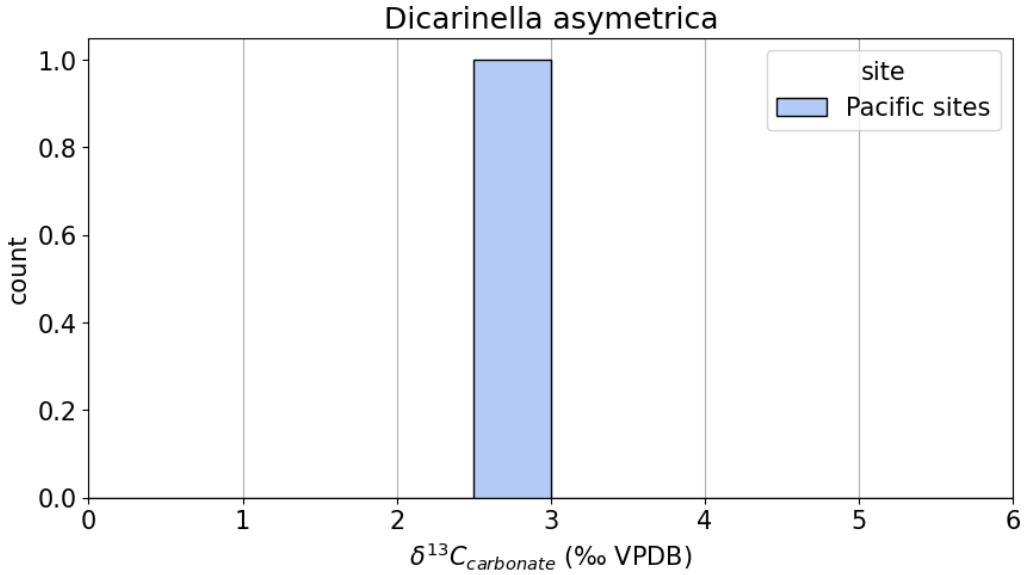
Dicarinella asymetrica
site
Pacific sites
count
1.0
0.8
0.6
0.4
0.2
0.0
0
1
2
3
4
5
6
$\delta^{13}C_{carbonate}$ (‰ VPDB)

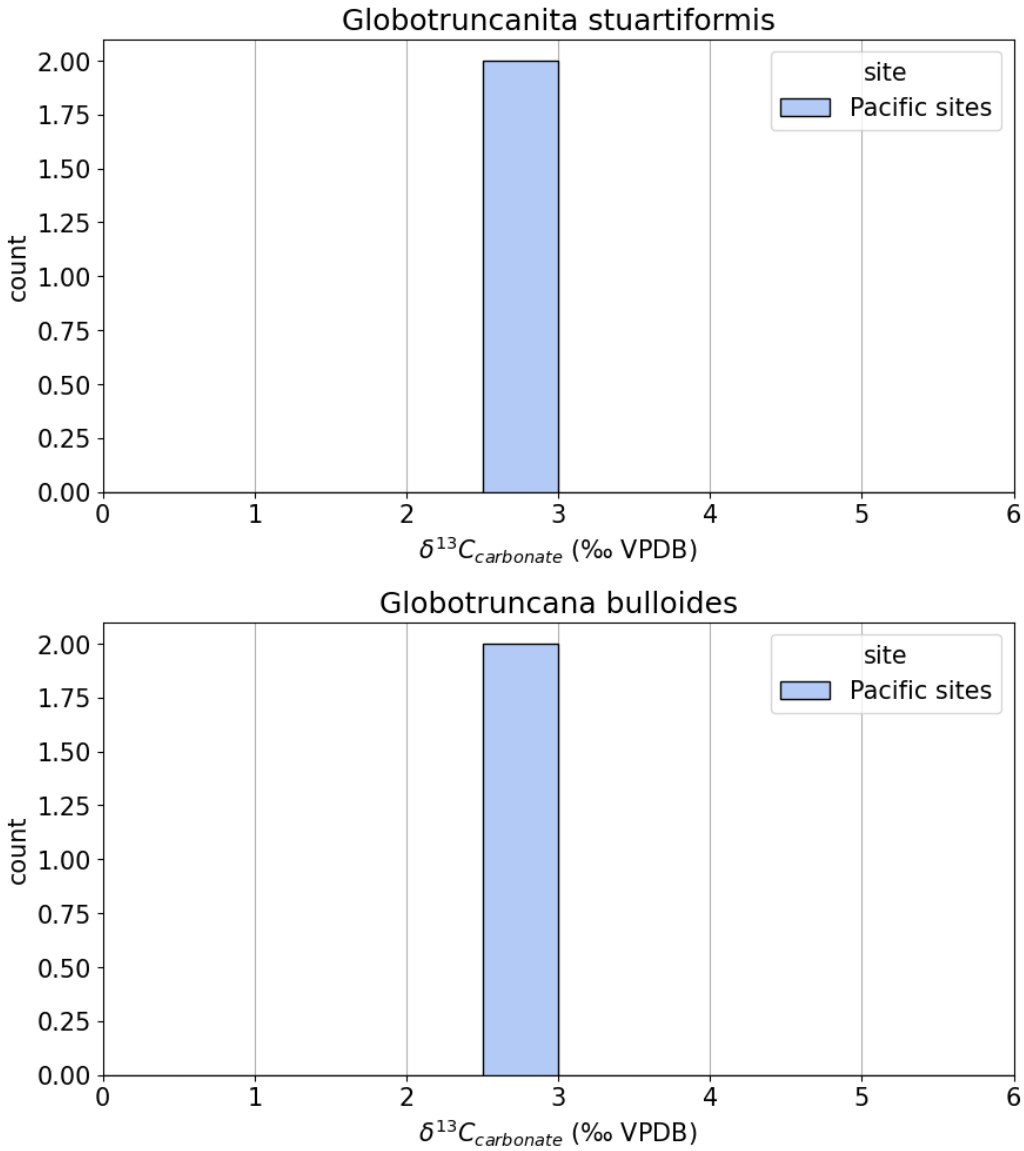
Globotruncanita stuartiformis
site
Pacific sites
count
2.00
1.75
1.50
1.25
1.00
0.75
0.50
0.25
0.00
0
1
2
3
4
5
6
$\delta^{13}C_{carbonate}$ (‰ VPDB)
Globotruncana bulloides
site
Pacific sites
count
2.00
1.75
1.50
1.25
1.00
0.75
0.50
0.25
0.00
0
1
2
3
4
5
6
$\delta^{13}C_{carbonate}$ (‰ VPDB)

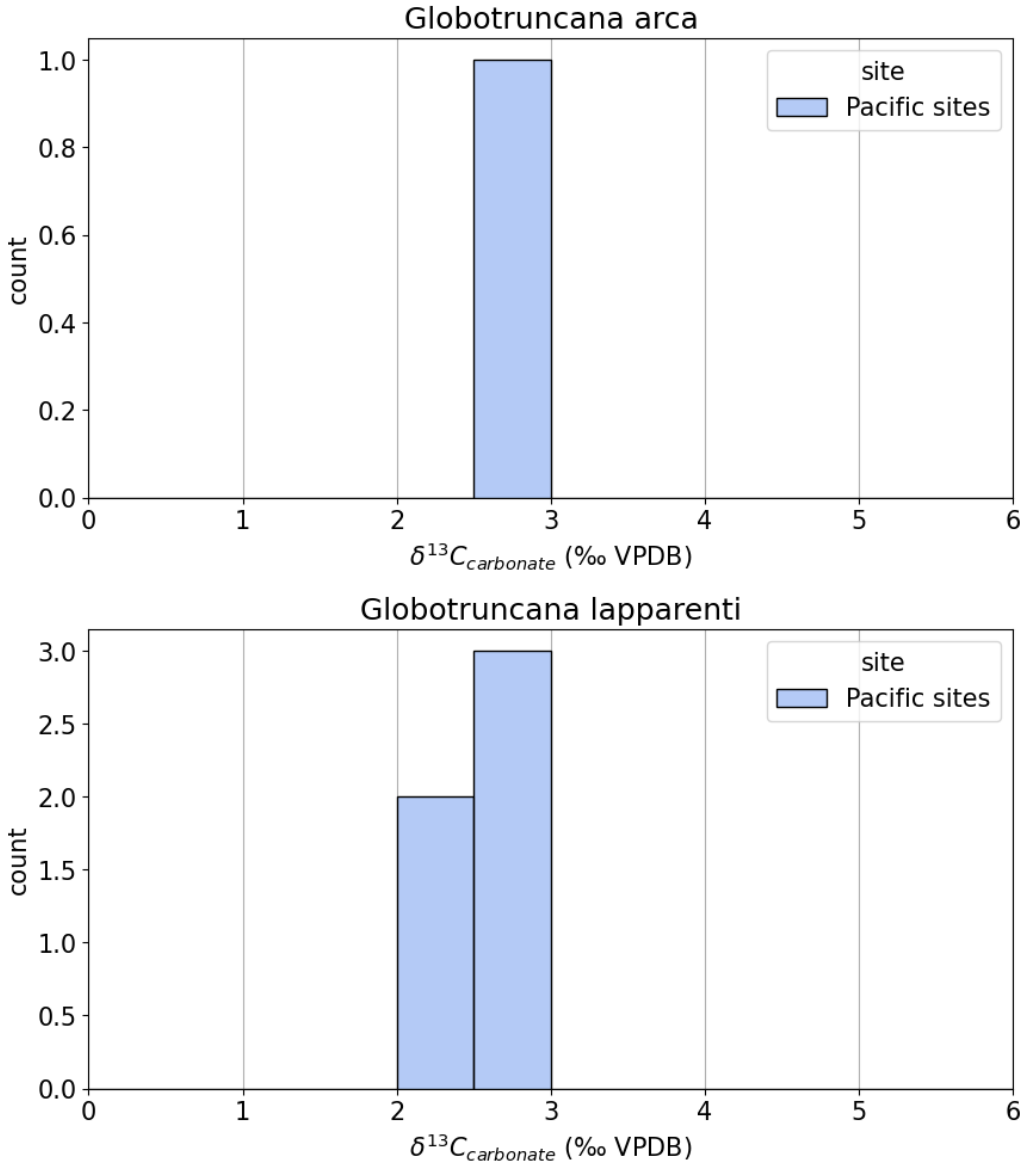
Globotruncana arca
site
Pacific sites
count
0.0
0.2
0.4
0.6
0.8
1.0
0
1
2
3
4
5
6
$\delta^{13}C_{carbonate}$ (‰ VPDB)
Globotruncana lapparenti
site
Pacific sites
count
0.0
0.5
1.0
1.5
2.0
2.5
3.0
0
1
2
3
4
5
6
$\delta^{13}C_{carbonate}$ (‰ VPDB)

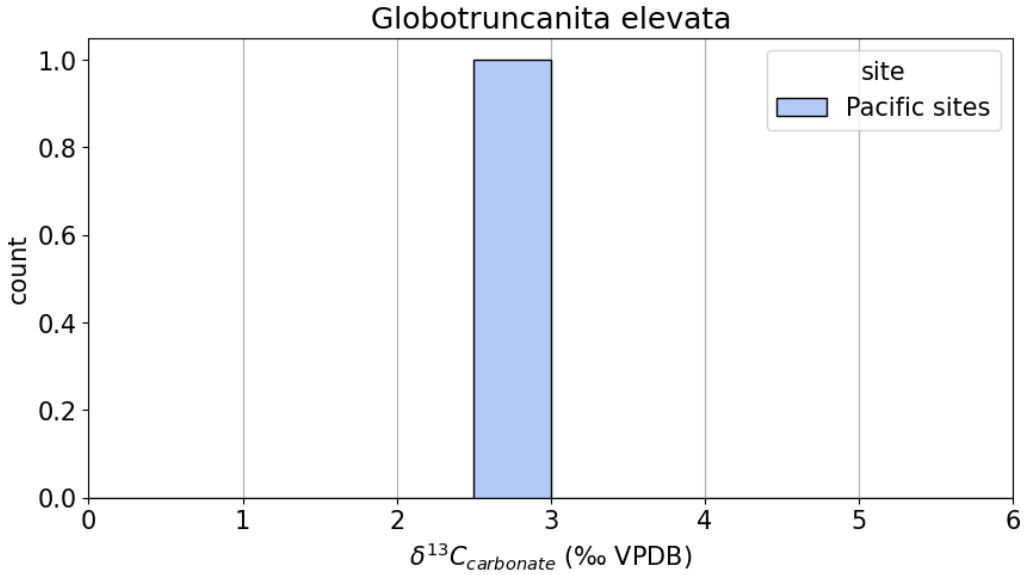
Globotruncanita elevata
site
Pacific sites
count
1.0
0.8
0.6
0.4
0.2
0.0
0
1
2
3
4
5
6
$\delta^{13}C_{carbonate}$ (‰ VPDB)

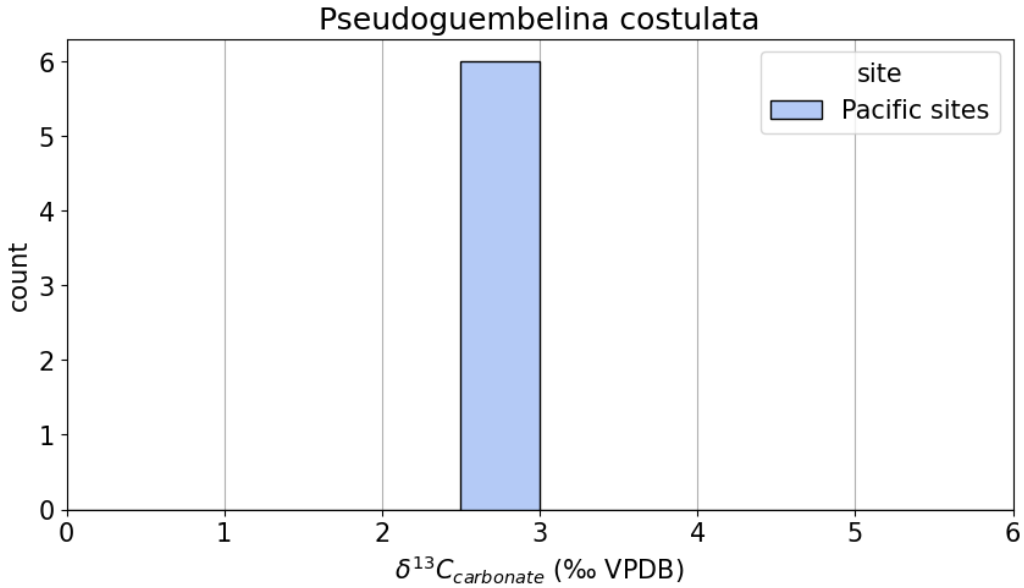
Pseudoguembelina costulata
site
Pacific sites
count
6
5
4
3
2
1
0
0
1
2
3
4
5
6
$\delta^{13}C_{carbonate}$ (‰ VPDB)

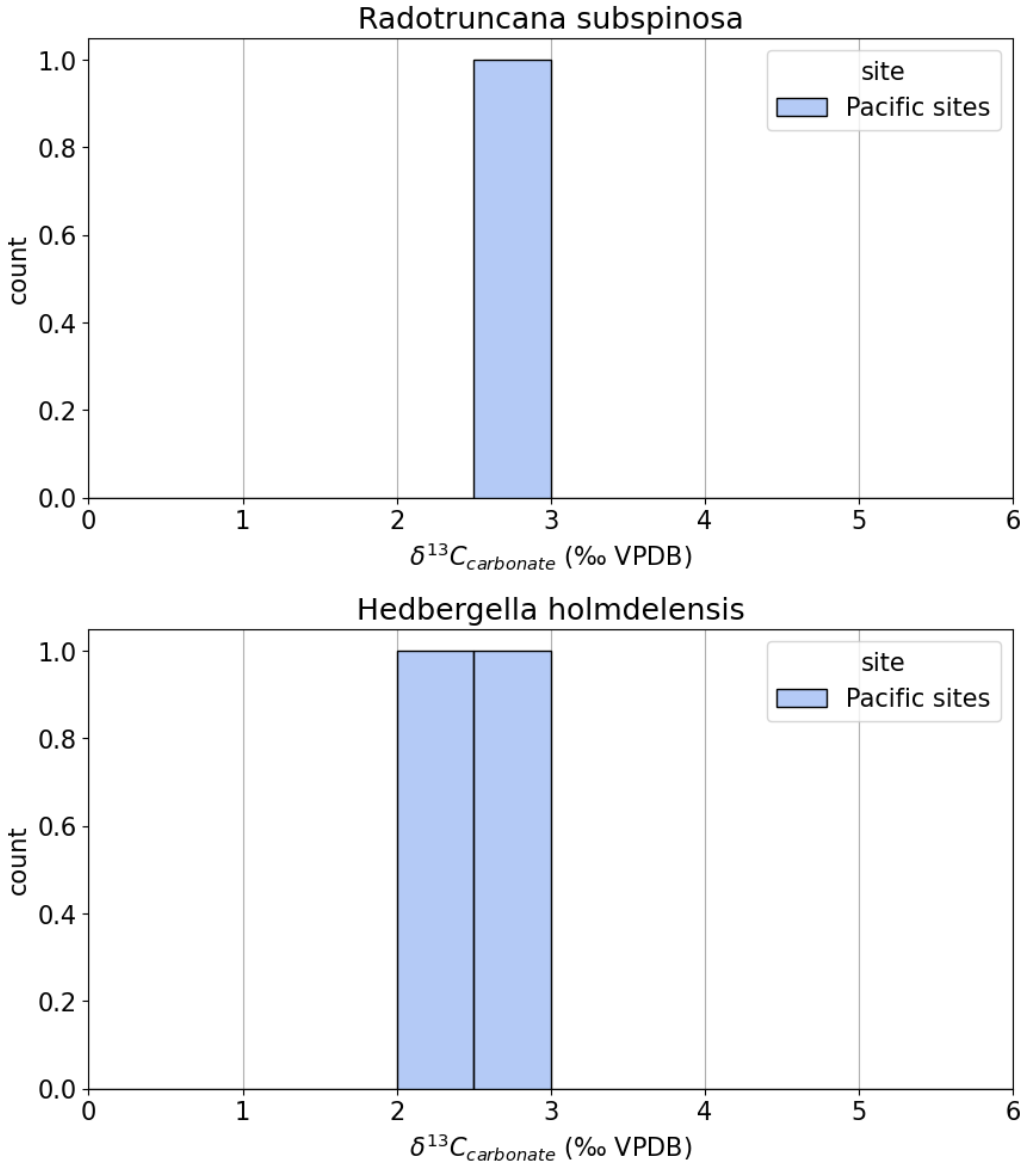
Radotruncana subspinosa
site
Pacific sites
count
0.0
0.2
0.4
0.6
0.8
1.0
0
1
2
3
4
5
6
$\delta^{13}C_{carbonate}$ (‰ VPDB)
Hedbergella holmdelensis
site
Pacific sites
count
0.0
0.2
0.4
0.6
0.8
1.0
0
1
2
3
4
5
6
$\delta^{13}C_{carbonate}$ (‰ VPDB)

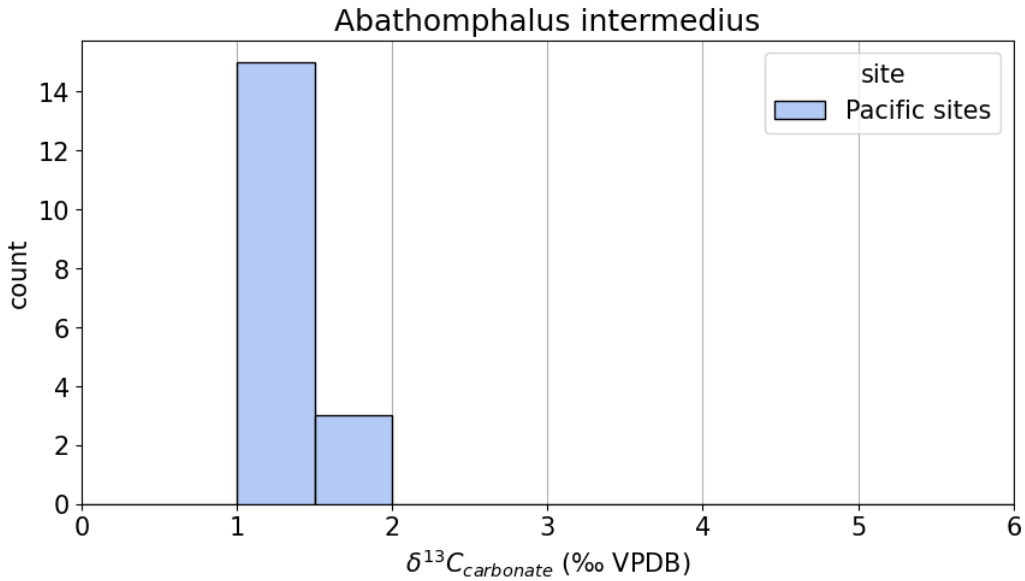
Abathomphalus intermedius
site
Pacific sites
count
0
2
4
6
8
10
12
14
0
1
2
3
4
5
6
$\delta^{13}C_{carbonate}$ (‰ VPDB)

Appendix A8: Evaluating microhabitat vital effects on benthic foraminiferal $\delta^{13}C_{carbonate}$ values at sites 62-463 and 32-305

The benthic foraminifera species with $\delta^{13}C_{carbonate}$ values reported in this thesis dwell in a range of sediment depths from the sediment-water interface to centimeters below it (0.5 cm to about 15 cm; Corliss, 1985). Specifically, 14 benthic foraminiferal $\delta^{13}C_{carbonate}$ values are measured in species dwelling mainly on top or within the top 0.5 cm of the sediment (5 *Globorotalites conicus*, 3 genus *Nuttallides* including 2 *Nuttallides truempyi*, 2 genus *Gavelinella*, 2 genus *Gyroidinoides*, and 2 genus *Osangularia*), 5 in species dwelling deeper in the sediment (5 genus *Praebulimina*), and 3 samples of unidentified "mixed" species do not have habitat noted (Widmark and Speijer, 1997; Erbacher et al., 1998; Dubicka et al., 2018; Wolfgring et al., 2022).

Microhabitat vital effects can lower benthic foraminiferal $\delta^{13}C_{carbonate}$ values relative to seawater $\delta^{13}C_{DIC}$ for foraminifera living in pore water with lowered $\delta^{13}C_{DIC}$ (Section 1.2.3; Friedrich et al., 2006; Hoogakker et al., 2024). In the modern mid-Pacific, the $\delta^{13}C_{DIC}$ of pore water can decrease by as much as 1‰ per centimeter below the sediment-water interface (McCorkle et al., 1985). Of the benthic foraminiferal samples reported here, 5 belong to a taxon of foraminifera thought to range from very shallow in the sediment to much deeper (*Praebulimina*; Dubicka et al., 2018). Their $\delta^{13}C_{carbonate}$ values could be significantly offset by this microhabitat effect, but it is unlikely that they have been, because they are consistently similar to $\delta^{13}C_{carbonate}$ values from other benthic foraminiferal taxa that dwell mainly on top or within the top 0.5 cm of the sediment.

Appendix A9: Evaluating the impact of aragonite vs. calcite proportion and species-specific vital effects on $\delta^{13}C_{carbonate}$ and $\delta^{18}O_{carbonate}$ values at 62-463 and 32-305

It is unlikely that differing proportions of aragonite vs. calcite in samples are responsible for the $\delta^{13}C_{carbonate}$ offsets between bulk and benthic foraminiferal samples. Bulk carbonate can contain biogenically and inorganically precipitated calcite and aragonite, while nannofossils and foraminifera have predominantly calcite shells (Milliman, 1993), and may therefore have lowered $\delta^{13}C_{carbonate}$ values relative to bulk carbonate. However, aragonite is expected to stabilize to calcite after its burial (Section 1.2.5), including when exposure of carbonate sediments to diagenetic fluid is low (Hashim and Kaczmarek, 2021). Even if aragonite persisted, benthic foraminifera do not generally contain a higher proportion of calcite than planktonic foraminifera (Blackmon and Todd, 1959). Therefore this effect would not explain why benthic foraminiferal $\delta^{13}C_{carbonate}$ values are much lower than planktonic foraminiferal and nannofossil $\delta^{13}C_{carbonate}$ values relative to bulk $\delta^{13}C_{carbonate}$ values.

Some of the taxa of benthic foraminifera considered here have documented vital effects that offset their $\delta^{13}C_{carbonate}$ values in a positive direction by $< 1‰$. For example, Katz et al. (2003) determine for the early Cenozoic that *Nuttallides truempyi* (composing 2 of the samples reported here) has $\delta^{13}C_{carbonate}$ 0.34‰ higher than *Cibicidoides*, whose $\delta^{13}C_{carbonate}$ value matches $\delta^{13}C_{DIC}$ depending on seawater carbonate chemistry (Schmittner et al., 2017; Nederbragt, 2023). Katz et al. (2003) also deter-

mine for the early Cenozoic that *Praebulimina* (composing 5 of the samples reported here) has $\delta^{13}C_{carbonate}$ 0.19‰ higher than *Nuttallides truempyi*. The literature therefore suggests that vital effects would raise benthic foraminiferal $\delta^{13}C_{carbonate}$ values relative to seawater $\delta^{13}C_{DIC}$ by 0.34-0.53‰ in the 8 samples of *Nuttallides truempyi* and *Praebulimina*. These vital effects would be expected to counteract the observed offset wherein bulk $\delta^{13}C_{carbonate}$ values are higher than benthic foraminiferal $\delta^{13}C_{carbonate}$ values, although slightly, since bulk samples likely contain benthic foraminiferal components. They cannot be responsible for the observed $\delta^{13}C_{carbonate}$ offsets between bulk and benthic foraminiferal samples.

Appendix A10: Interbasinal differences in $\delta^{13}C_{DIC}$ during the Cretaceous

Cramer et al. (2009) and Friedrich et al. (2012) (the authors of the two benthic foraminiferal $\delta^{13}C_{carbonate}$ and $\delta^{18}O_{carbonate}$ compilations) argued for interbasinal differences in $\delta^{13}C_{DIC}$ during the Cretaceous, notably between the North Atlantic and the Pacific. First, the temporal and spatial distribution of data in these compilations is arguably too sparse to draw this conclusion (Figure A.10). In the compilation of Cramer et al. (2009), Cretaceous $\delta^{13}C_{carbonate}$ data are available from 3 sites in the Pacific and 2 sites in the North Atlantic, and almost all data are from the end of the Cretaceous (after 80 Ma). The Friedrich et al. (2012) compilation covers more Cretaceous time (115-65 Ma) than the Cramer et al. (2009) compilation, but the geographical distribution of data remains sparse in this compilation, with only 2 sites in the Pacific and 4 sites in the North Atlantic (3 when Demerara Rise is omitted). 2-4 sites may not be representative of an entire ocean basin because local factors like those discussed in Section 5.1.1 may change their $\delta^{13}C_{carbonate}$.

Second, combining the two compilations makes the average interbasinal difference between the North Atlantic and the Pacific smaller. In the compilation of Friedrich et al. (2012), the North Atlantic has lower average Cretaceous $\delta^{13}C_{carbonate}$ than the Pacific by 0.85‰ due to Cenomanian-Santonian Demerara Rise $\delta^{13}C_{carbonate}$ values, which account for more than a third of all Cretaceous data in the compilation and are uniquely low (Figure 5.6). When Cenomanian-Santonian Demerara Rise $\delta^{13}C_{carbonate}$ values are omitted, average North Atlantic Cretaceous $\delta^{13}C_{carbonate}$ is 0.28‰ greater than average Pacific Cretaceous $\delta^{13}C_{carbonate}$ in the Friedrich et al. (2012) compilation. In the compilation of Cramer et al. (2009), the North Atlantic has lower average Cretaceous $\delta^{13}C_{carbonate}$ than the Pacific by 0.75‰. However, when the compilations

are combined, this difference is 0.34‰. If this does represent an interbasinal difference in $\delta^{13}C_{DIC}$, rather than an artifact of sparsity of data, the difference is a small one.